



Calhoun: The NPS Institutional Archive
DSpace Repository

Theses and Dissertations

1. Thesis and Dissertation Collection, all items

2010-12

Development of a nano-satellite
micro-coupling mechanism with
characterization of a shape memory alloy
interference joint

Crane, William M.

Monterey, California. Naval Postgraduate School

<http://hdl.handle.net/10945/5015>

This publication is a work of the U.S. Government as defined in Title 17, United States Code, Section 101. Copyright protection is not available for this work in the United States.

Downloaded from NPS Archive: Calhoun



<http://www.nps.edu/library>

Calhoun is the Naval Postgraduate School's public access digital repository for research materials and institutional publications created by the NPS community. Calhoun is named for Professor of Mathematics Guy K. Calhoun, NPS's first appointed -- and published -- scholarly author.

Dudley Knox Library / Naval Postgraduate School
411 Dyer Road / 1 University Circle
Monterey, California USA 93943



NAVAL POSTGRADUATE SCHOOL

MONTEREY, CALIFORNIA

THESIS

**DEVELOPMENT OF A NANO-SATELLITE MICRO-COUPLING
MECHANISM WITH CHARACTERIZATION OF A
SHAPE MEMORY ALLOY INTERFERENCE JOINT**

by

William Mike Crane

December 2010

Thesis Co-Advisors:

Marcello Romano
James Hansen Newman

Approved for public release; distribution is unlimited

THIS PAGE INTENTIONALLY LEFT BLANK

REPORT DOCUMENTATION PAGE			<i>Form Approved OMB No. 0704-0188</i>	
Public reporting burden for this collection of information is estimated to average 1 hour per response, including the time for reviewing instruction, searching existing data sources, gathering and maintaining the data needed, and completing and reviewing the collection of information. Send comments regarding this burden estimate or any other aspect of this collection of information, including suggestions for reducing this burden, to Washington headquarters Services, Directorate for Information Operations and Reports, 1215 Jefferson Davis Highway, Suite 1204, Arlington, VA 22202-4302, and to the Office of Management and Budget, Paperwork Reduction Project (0704-0188) Washington DC 20503.				
1. AGENCY USE ONLY (Leave blank)		2. REPORT DATE December 2010	3. REPORT TYPE AND DATES COVERED Master's Thesis	
4. TITLE AND SUBTITLE Development of a Nano-Satellite Micro-Coupling Mechanism with Characterization of a Shape Memory Alloy Interference Joint			5. FUNDING NUMBERS	
6. AUTHOR(S) CDR William M. Crane, USN				
7. PERFORMING ORGANIZATION NAME(S) AND ADDRESS(ES) Naval Postgraduate School Monterey, CA 93943-5000			8. PERFORMING ORGANIZATION REPORT NUMBER	
9. SPONSORING /MONITORING AGENCY NAME(S) AND ADDRESS(ES) N/A			10. SPONSORING/MONITORING AGENCY REPORT NUMBER	
11. SUPPLEMENTARY NOTES The views expressed in this thesis are those of the author and do not reflect the official policy or position of the Department of Defense or the U.S. Government. IRB Protocol number _____ N/A _____.				
12a. DISTRIBUTION / AVAILABILITY STATEMENT Approved for public release; Naval Postgraduate School Patent #12/878,760			12b. DISTRIBUTION CODE	
13. ABSTRACT (maximum 200 words) This thesis describes the design, development, and testing of an innovative nonexplosive actuator (NEA) micro-coupling device. The micro-coupling is obtained through the use of a nickel titanium (NiTi), shape memory alloy (SMA) cylindrical ring that is press-fit, in its detwinned martensitic phase, into a steel bushing, creating an interference joint. This SMA interference joint can subsequently decouple upon command, by heating the SMA cylindrical ring into its smaller austenitic memory shape, freeing it from its press-fit. The micro-coupling can be engineered to very small sizes, on the order of one cubic centimeter, and achieve coupling strengths in excess of 4,000 N (900 lbf). The SMA micro-coupling's concept validation, mechanization, and development into a device for satellite incorporation are explored by assembly and experimentation. Research on pseudoelastic material properties, analytical predictions, and tests of coupling strengths are examined to characterize the SMA micro-coupling. While the micro-coupling's characteristics are desirable for many applications, its small size, simple interface, and low-power zero-shock actuation are ideal for employment on nano-satellites to effectively increase space deployable actuation reliability by eliminating reliance on motors, clasps, latches, material fracture, or explosive devices.				
14. SUBJECT TERMS SMA, shape memory alloy, NiTi, nickel titanium, micro-coupling, press-fit, interference joint, spacecraft, deployable, zero-shock, NEA, nonexplosive actuator, martensitic, detwinned, memory shape, austenitic, nano-satellite.			15. NUMBER OF PAGES 211	
			16. PRICE CODE	
17. SECURITY CLASSIFICATION OF REPORT Unclassified	18. SECURITY CLASSIFICATION OF THIS PAGE Unclassified	19. SECURITY CLASSIFICATION OF ABSTRACT Unclassified	20. LIMITATION OF ABSTRACT UU	

THIS PAGE INTENTIONALLY LEFT BLANK

Approved for public release; distribution is unlimited

**DEVELOPMENT OF A NANO-SATELLITE MICRO-COUPPLING MECHANISM
WITH CHARACTERIZATION OF A SHAPE MEMORY ALLOY
INTERFERENCE JOINT**

William M. Crane
Commander, United States Navy
B.S., Norwich University MCV, 1995
Technology Management M.B.A., University of Washington, 2003

Submitted in partial fulfillment of the
requirements for the degree of

MASTER OF SCIENCE IN ASTRONAUTICAL ENGINEERING

from the

**NAVAL POSTGRADUATE SCHOOL
December 2010**

Author: William M. Crane

Approved by: Dr. Marcello Romano
Thesis Co-Advisor

Dr. James H. Newman
Thesis Co-Advisor

Dr. Knox T. Millsaps
Chairman, Department of Mechanical and Aerospace Engineering

THIS PAGE INTENTIONALLY LEFT BLANK

ABSTRACT

This thesis describes the design, development, and testing of an innovative nonexplosive actuator (NEA) micro-coupling device. The micro-coupling is obtained through the use of a nickel titanium (NiTi), shape memory alloy (SMA) cylindrical ring that is press-fit, in its detwinned martensitic phase, into a steel bushing, creating an interference joint. This SMA interference joint can subsequently decouple upon command, by heating the SMA cylindrical ring into its smaller austenitic memory shape, freeing it from its press-fit. The micro-coupling can be engineered to very small sizes, on the order of one cubic centimeter, and achieve coupling strengths in excess of 4,000 N (900 lbf). The SMA micro-coupling's concept validation, mechanization, and development into a device for satellite incorporation are explored by assembly and experimentation. Research on pseudoelastic material properties, analytical predictions, and tests of coupling strengths are examined to characterize the SMA micro-coupling. While the micro-coupling's characteristics are desirable for many applications, its small size, simple interface, and low-power zero-shock actuation are ideal for employment on nano-satellites to effectively increase space deployable actuation reliability by eliminating reliance on motors, clasps, latches, material fracture, or explosive devices.

THIS PAGE INTENTIONALLY LEFT BLANK

TABLE OF CONTENTS

I.	INTRODUCTION.....	1
A.	OBJECTIVE	1
B.	BACKGROUND	1
1.	Shape Memory Alloy	1
a.	<i>SMA Phases and Shape Memory Effect Hysteresis</i>	<i>2</i>
b.	<i>SMA Pseudoelasticity and Heat to Recover Process</i>	<i>3</i>
2.	Press-Fit Methods and Equations.....	4
C.	METHODOLOGY	7
1.	Conception of an SMA Interference Joint.....	7
2.	Applicable SMA Research	8
3.	SMA Interference Joint Characterization.....	10
4.	Design of a SMA Coupling Device.....	11
D.	COMPARABLE COUPLING DEVICES	13
1.	New Scale Technologies SQUIGGLE Motor.....	14
2.	TiNi Aerospace Pinpuller	15
3.	TiNi Aerospace Model FC2-16-31SR2 FRANGIBOLT	16
E.	ORIGINAL CONTRIBUTIONS	17
F.	THESIS ORGANIZATION.....	17
II.	MICRO-COUPLING DESIGN AND TEST	19
A.	NITI MICRO-COUPLING MECHANISM.....	19
1.	Concept Development and Requirements	19
2.	Press-Fit Considerations	20
3.	Interference Precision and Joint Strength Prediction.....	21
4.	Mechanization of the Micro-Coupling.....	24
B.	PRELIMINARY EXPERIMENTS	26
1.	Characterization of NiTi SMA Heat to Recover Hysteresis	26
2.	Press-Fit SMA Concept Validation	28
3.	Micro-Coupling Mechanism Powered Actuation	29
C.	MICRO-COUPLING MECHANISM LOAD TESTING	32
1.	Micro-Coupling Press-Fit Cradle.....	32
2.	Micro-Coupling Load Test Rig.....	34
D.	CONSOLIDATED TESTING CONCLUSIONS	36
III.	SINGLE MOTION ACTUATED SHAPE MEMORY ALLOY COUPLING (SMA²C).....	45
A.	ENGINEERING DESIGN UNIT	45
1.	SMA ² C Micro-Coupling Mechanism Components	45
2.	SMA ² C Device Design.....	49
B.	INTEGRATION OF THE SMA²C DEVICE INTO A NANO-SATELLITE.....	53
1.	TINYSCOPE Mission Overview	53
2.	TINYSCOPE Electrical Power System Overview	54

3.	SMA ² C Device Positioning for TINYScope	56
4.	Estimating SMA ² C Power Requirements for TINYScope	58
5.	SMA ² C Actuation Power Consumption Test	61
6.	Integrating SMA ² C Into TINYScope's Power Plan	64
IV.	CONCLUSIONS AND RECOMMENDATIONS.....	67
A.	SMA MICRO-COUPLING.....	67
1.	Synopsis.....	67
2.	Future Work.....	68
B.	SMA ² C DEVICE.....	70
1.	Synopsis.....	70
2.	Future Work.....	70
APPENDIX A.	NACL REPORT: SHAPE MEMORY ALLOY HTR AND HYSTERESIS VERIFICATION	71
APPENDIX B.	NACL REPORT: SHAPE MEMORY ALLOY MICRO- COUPLING CONCEPT VALIDATION	93
APPENDIX C.	NACL REPORT: MICRO-COUPLING ENGINEERING DESIGN UNIT LOAD BEARING CAPABILITY	117
APPENDIX D.	MICRO-COUPLING ACTIVE RELEASE MECHANISM PATENT PENDING #12/878,760.....	155
APPENDIX E.	SMA ² C ACTUATION PREDICTED POWER CONSUMPTION CALCULATIONS (SPACE)	185
APPENDIX F.	SMA ² C ACTUATION PREDICTED POWER CONSUMPTION CALCULATIONS (LABORATORY).....	187
	LIST OF REFERENCES	189
	INITIAL DISTRIBUTION LIST	191

LIST OF FIGURES

Figure 1.	Stress-Strain-Temperature Curves Exhibiting the Pseudoelasticity and HTR Process for a Typical NiTi SMA. From [1].	4
Figure 2.	Diagram Showing Hub and Shaft with Associated Press-Fit Dimensions	5
Figure 3.	Press-Fit Creation of an SMA Interference Joint/Micro-Coupling	8
Figure 4.	Monotonic Loading of a NiTi SMA at Given Constant Temperatures. From [1].	9
Figure 5.	Coupling Strength Test Data Sample from SMA Micro-Coupling Concept Validation.	11
Figure 6.	Original Concept Drawing from Early SMA Micro-Coupling Design	12
Figure 7.	SQ-100 Series SQUIGGLE Motors by New Scale Technologies	14
Figure 8.	TiNi Pinpuller by Aerospace Inc. (Units in Inches)	15
Figure 9.	FRANGIBOLT Model FC2-16-31SR2 by TiNi Aerospace Inc.	16
Figure 10.	SMA Micro-Coupling Mechanization. From [14].	25
Figure 11.	EDU SMA Heat to Recover and Shape Memory Effect Hysteresis Cycle	28
Figure 12.	Open Air Micro-Coupling Mechanism EDU Actuation Test Bench	30
Figure 13.	Open Air Micro-Coupling Mechanism EDU Actuation Temperatures and Power Consumption Data	31
Figure 14.	Component View of SMA ² C Press-Fit Cradle	33
Figure 15.	Component View of SMA ² C Micro-Coupling Load Test Rig	34
Figure 16.	Assembly and Operation of SMA ² C Micro-Coupling Load Test Rig	35
Figure 17.	Data Sample from SMA ² C Micro-Coupling Load Test	37
Figure 18.	SMA ² C Micro-Coupling Initial and Ultimate Strength Test Data with Predicted Strength Values	39
Figure 19.	Surface Features of SMA Micro-Coupling Load Test Specimens	40
Figure 20.	Initial SMA ² C Micro-Coupling Specimens Experiencing Possible Effects of Surface Oxidation	43
Figure 21.	SMA ² C Casehardened Steel Busing	46
Figure 22.	SMA ² C EDU Kapton Foil Heater Procured from Tayco Engineering Inc.	46
Figure 23.	SMA ² C EDU Micro-coupling	47
Figure 24.	TRA-Bond 2151 Epoxy Specifications	47
Figure 25.	SMA ² C EDU Micro-Coupling Retaining Bolt	48
Figure 26.	Component View of the SMA ² C Device	50
Figure 27.	Assembled Views of the SMA ² C Device	50
Figure 28.	SMA ² C Device EDU Hardware and Assembled Test Unit	51
Figure 29.	SMA ² C Device Actuation Sequence	52
Figure 30.	NPS TINYScope Configurations	53
Figure 31.	TINYScope's Power Equivalent Circuit. From [17].	54
Figure 32.	TINYScope Structural Design	55
Figure 33.	TINYScope Solar Array Design for SMA ² C Device Integration	56
Figure 34.	SMA ² C Device Placement in TINYScope	57

Figure 35.	SMA ² C Deployment of TINYScope's Solar Arrays.....	58
Figure 36.	EDU SMA ² C Device Actuation Power Consumption Test Bench.....	62
Figure 37.	EDU SMA ² C Device Actuation Temperatures and Power Consumption Data	63

LIST OF TABLES

Table 1.	Supplied NiTi SMA Cylindrical Ring Dimensions Used in the Micro-Coupling Mechanism Engineering Design Unit.....	20
Table 2.	Material Properties Used in Micro-Coupling Predicted Strength Calculations.....	22

THIS PAGE INTENTIONALLY LEFT BLANK

EXECUTIVE SUMMARY

The need to develop a nonexplosive actuator (NEA) coupling device specifically adaptable for nano-satellite applications has become evident, as many current NEA coupling devices possess complex interfaces, impart actuation shocks, or are too large for nano-satellites. The innovative idea of press-fitting a nickel titanium (NiTi) shape memory alloy (SMA) cylindrical ring into a hub, creating an interference joint that can be decoupled upon command by heating the SMA, yielded a micro-coupling mechanism that delivers the desired nano-satellite NEA characteristics of simplicity and small size. As with any coupling and release mechanism, especially those used in the demanding environment of outer space, quantitative characterization of the SMA micro-coupling's strength and operating characteristics allows understanding of its nominal usefulness and possible failure modes.

Validation of the SMA interference joint concept began with testing the complete heat-to-recover (HTR) and shape memory effect hysteresis cycles of NiTi SMA rings with the objective to provide insight into the design geometry required for the SMA micro-coupling mechanism. Testing results demonstrated cycling temperature of the SMA through its initial irreversible HTR yielded twice the reduction in available outer diameter as compared to the reversible shape memory effect hysteresis. These results supported using the detwinned martensitic state of SMA for press-fit with intent to decouple the interference joint by heating the SMA. Even with HTR ring diameter reductions, very precise design tolerances in construction of the micro-coupling would be required to produce high coupling strengths and release actuation reliability. Concept validation continued with testing the axial coupling strength of the SMA interference joint. Coupling strength characteristics were obtained by subjecting the micro-coupling to tensile machine tests, outputting force and displacement curves during imposed separation of the interference joint. Testing achieved substantial holding forces in excess of 500 lbf, but the process of SMA extraction revealed an unknown strength-compounding characteristic with several coupling strength peaks that eventually doubled the SMA interference joint's analytically predicted coupling capability. Follow-on

testing and research upon discovery of the strength-compounding characteristic suggested the SMA cylindrical ring experienced buckling upon forced extraction where normal forces inside the interference joint increased, thereby increasing the joint's strength. In addition, the extreme pressure at contact points between the SMA and hub, created during SMA interference joint assembly or forced removal of the SMA cylindrical ring, suggest there may be additional SMA geometry changes resulting from localized, pressure induced phase changes.

Completion of concept validation led to the design of an SMA micro-coupling mechanism engineering design unit (EDU). The mechanism's size was approximately one cubic centimeter and subjected to tensile tests achieving coupling strengths in excess of 4,000 N (900 lbf). Traditional press-fit equations used to predict the axial strength of the SMA interference joint, within propagated measurement error, appeared sufficient to predict the initial micro-coupling static friction strength, but insufficient to predict the micro-coupling's ultimate strength. Integration of the micro-coupling EDU into a zero-shock NEA for the field of nano-satellite technology produced a device named the Single Motion Actuated Shape Memory Alloy Coupling (SMA²C). The SMA²C device depends on the SMA micro-coupling to provide sufficient coupling strength and resist the environmental stresses imparted during satellite launch and orbit insertion. SMA²C device testing culminated in a powered actuation experiment followed by integration analysis into the nano-satellite project TINYScope. The powered actuation test of the SMA²C device, in a 96% vacuum at laboratory temperatures, modeled conditions without convection losses as in the space environment. The device was connected to a constant 10.0 Volt power supply and actuated within 80 seconds, consuming a total of 0.17 Watt-hours of energy. TINYScope integration analysis concluded a reduction in size of the SMA²C device would still exceed required coupling strengths for most nano-satellite applications and result in a new SMA²C device that would consume even less power and volume than the EDU.

LIST OF ACRONYMS AND ABBREVIATIONS

CTE	Coefficient of Thermal Expansion
EDU	Engineering Design Unit
EPS	Electrical Power System
HTR	Heat-to-Recover
NACL	Nano-satellite Advanced Concepts Laboratory
NEA	NonExplosive Actuator
NiTi	Nickel Titanium
NPS	Naval Postgraduate School
COTS	Commercial off the Shelf
SMA _s	Shape Memory Alloys
SMA ² C	Single Motion Actuated Shape Memory Alloy Coupling “SMACK”
TINYSCOPE	Tactical Imaging Nano-satellite Yielding Small-Cost Operations and Persistent Earth-coverage

THIS PAGE INTENTIONALLY LEFT BLANK

ACKNOWLEDGMENTS

The author would like to recognize:

Dr. Marcello Romano, Department of Mechanical and Aerospace Engineering and
Dr. James Newman, Space Systems Academic Group, Naval Postgraduate School

Both your insight and mentorship throughout the two-year process to conceive, design, and develop SMA²C were instrumental to the creation of this new technology. You enabled me to realize the dream of every engineer: to become an inventor and introduce a mechanism to industry that will enhance existing technology and enable new ones. You both are true pioneers of small satellite research.

Mr. Paul Oppenheimer, Naval Research Laboratory

Your contribution of research experience as a practicing engineer and creative imagination into the original design of the SMA micro-coupling was invaluable. I sincerely hope I have the good fortune to work with you again.

Mr. Tom Borden, Intrinsic Devices Inc.

Your initial consultation on the technical properties and applications of SMA rings were the seeds of innovation. I will always hold you and your company in the highest regard.

Mr. John Mobley and Glen Harrell, NPS Machine Shop

Your skill and experience enabled all the steps to make SMA²C a reality, from each of the test devices to the intricate parts of the engineering design unit. This thesis and invention would not have been possible without your mastery of metalworking.

Mr. David Rigmaiden and Jim Horning, NPS Small Satellite Laboratory

Your willingness to help students with technical questions and provide experienced advice on space systems paid many dividends to the development of SMA²C. Both of you are core to the quality and professionalism of the NPS astronautical program.

My wife, Denise, and daughter, Natalie

Your unwavering support and patience forged the keystone of my work while at the Naval Postgraduate School. Without both of you, this thesis and our first patent would have remained a dream instead of reality. You taught me through example that the measure of a person is not only his accomplishments in life, but how he loves his family.

THIS PAGE INTENTIONALLY LEFT BLANK

I. INTRODUCTION

A. OBJECTIVE

The genesis of this thesis' research, design, experimentation, and test was the desire to provide a very small, yet strong and reliable, micro-coupling device for application on nano-satellites. Existing coupling devices have complex interface designs or are too large for integration into nano-satellites, especially those of the CubeSat class.¹ The new nano-satellite coupling device should be constructed of very few parts and rely on a simple, single motion actuation, to minimize failure modes and effectively increase reliability. The micro-coupling should integrate into a nano-satellite's limited electrical bus using available power for actuation, and the micro-coupling's system volume should be on the order of one cubic centimeter. Additionally, the micro-coupling should exhibit characteristics of a nonexplosive actuator (NEA), imparting no actuation shock or debris, avoiding any potential damage to the nano-satellite due to its small size or the sensitivity of its payload.

B. BACKGROUND

1. Shape Memory Alloy

Shape memory alloys (SMAs) are part of a class of active materials that exhibit a mechanical change in response to a nonmechanical external input, such as a temperature change or exposure to a magnetic field or applied voltage. The mechanical response can manifest itself as a geometry change that is an order of magnitude greater (macroscopic) than a common materials' response (microscopic) to the same type of external input. Specifically, SMAs have the unique mechanical property that they will return to a memory shape when their temperature is increased. This mechanical change can be dramatic, given the particular geometric form of the SMA, such as a ring, wire, or working tool. With the amount of shape change observed in an SMA's mechanical response, one could assume plastic deformation of the metal alloy. In fact, SMAs can

¹ Nano-Satellite: 1-10 kg; CubeSat Class: 1 kg, 10 cm³.

take many recoverable shapes that can produce large amounts of mechanical work without experiencing plastic deformation.² The mechanical response is repeatable in the sense that the alloy's shape change is reversible with subsequent temperature cycling and application of stress.

Common SMAs have a composition of nickel and titanium. The alloy's makeup, defining the amount of nickel and titanium, controls the temperature at which the SMA changes shape, known as a phase change. There are other alloy combinations within the family of SMAs, but nickel titanium (NiTi) is the most studied alloy with a large number of commercial applications. Addition of other metals to NiTi, such as copper and lead, yield not only different material properties, but also different SMA mechanical response characteristics.

a. SMA Phases and Shape Memory Effect Hysteresis

SMA phases and their associated shapes are categorized into hot or cold states. Characterization of hot and cold can vary greatly, as transportation of some SMAs occur in liquid nitrogen because their hot state is room temperature, while other alloy compositions have to be heated in excess of 120 °C to reach their hot state. An SMA's hot state defines its austenitic phase. NiTi austenite has an atomic lattice organization where the crystal's orientation is cubic, having equal spacing between rows, achieving a compact form. An SMA's cold state defines its martensitic phase. NiTi martensite has an atomic lattice organization where the crystal's orientation is body centered tetragonal. The atoms can be thought of as having staggered spacing between rows; therefore, achieving a less compact form [1].

The repeatable mechanical response of cycling between martensitic and austenitic phases, induced by a shift in material temperature, defines a SMA's shape memory effect hysteresis. Initial application of external stress to the SMA programs its memory shape. The stress is stored as mechanical energy that manifests itself by the shift in atomic lattice organization (i.e., mechanical response capable of doing work)

² Plastic deformation of a metal or alloy occurs when applied stress is great enough to induce strain beyond the materials yield stress, resulting in a nonrecoverable permanent deformation.

associated with the phase/shape change of the SMA alloy. The area enclosed by the hysteresis stress-strain (σ/ϵ) curve remains constant, less the small amount of permanent strain change inherent to trained SMA experiencing multiple hysteric cycles [2]. There is a small amount of temperature energy absorbed and released during a zero-stress phase transformation just as in any metal's thermal expansion and contraction,³ but this latent heat of transformation is minimal and indicates the use of stored mechanical energy when the SMA changes phase [1].

b. SMA Pseudoelasticity and Heat to Recover Process

The cooler martensitic phase of NiTi SMA consists of two variants: twinned martensite and detwinned martensite. The twinned form exists as part of the hysteretic phase transition cycle, as described previously with cycling of temperature. The detwinned form exists when induced through mechanical deformation by applied stress (σ),⁴ see Figure 1. The creation of detwinned martensite is a constant temperature process that results in increased strain (ϵ) of the SMA (points B to C). The stress-induced deformation shifts the alloy's microstructure by aligning discrete martensitic crystals into a common orientation, thus creating detwinned martensite. A certain amount of isothermal de-straining occurs due to the elasticity of the material (points C to D) once the stress is removed.⁵ The effectively deformed detwinned martensite SMA's shape will remain permanent until the SMA is heated to austenite, relieving the stored stress, and returning the SMA to its memory shape (points D thru F). It is important to understand that the stress level for reorientation of martensitic crystals is lower than the permanent plastic yield stress of martensite. Both variants of martensite are within the elastic region of the NiTi alloy. The advantage of detwinned SMA is that the alloy experiences an increased strain upon phase transition to its austenitic phase; in essence, there is more stored mechanical energy available within detwinned martensite. An example of this increased strain is a detwinned SMA ring with an even larger diameter than that of its

³ Endothermic for martensite to austenite transformation. Exothermic for austenite to martensite transformation.

⁴ Note that the curve B-C-D lies on the σ/ϵ plane and that the curve B-D-E-F-A lies on the T/ϵ plane.

⁵ SMA rings are usually stored and shipped in this state (point D, detwinned martensite).

equivalent twinned martensitic phase, which is still recoverable with an increase in temperature. The hysteresis from detwinned martensite to austenite is not reversible with temperature change alone and describes the pseudoelasticity of an SMA. This one-way transformation delineates the heat-to-recover (HTR) process [3]. After the HTR process has occurred, the SMA hysteresis cycle will alternate with temperature between twinned martensite and austenite indefinitely, until an external stress is again applied to return the SMA to its deformed detwinned martensitic phase.⁶

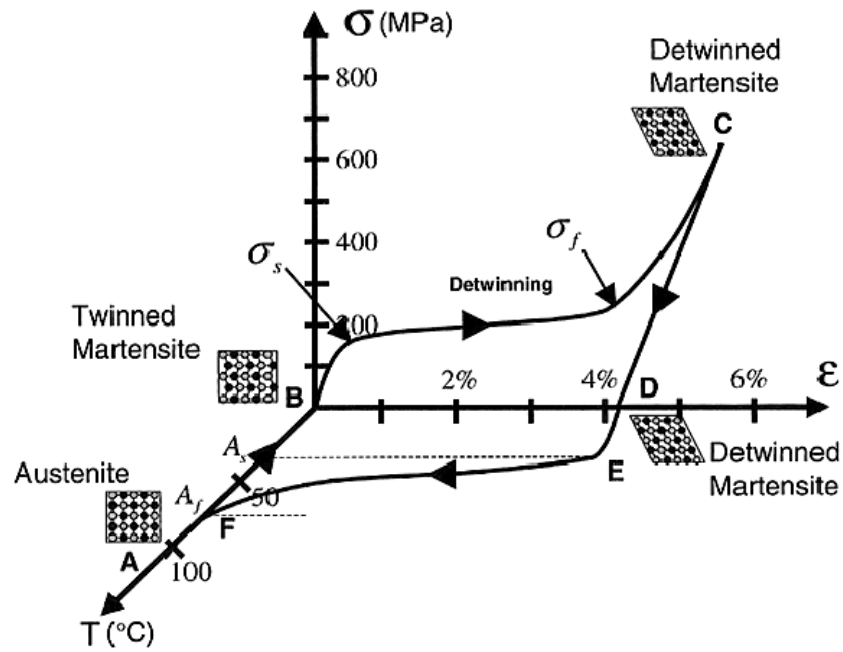


Figure 1. Stress-Strain-Temperature Curves Exhibiting the Pseudoelasticity and HTR Process for a Typical NiTi SMA. From [1].

2. Press-Fit Methods and Equations

The press-fit method is an assembly process commonly employed to connect a shaft and a hub together without the use of fasteners or adhesives. Typical applications of press-fitting include assembly of transmission gearing and bearing construction. The shaft's outer diameter is slightly larger than the hub's inner diameter resulting in an interference between the two parts, see Figure 2. The amount of pressure within an

⁶ The zero stress repeatable hysteresis cycle is not shown in Figure 1. It can be found in reference [1] or [2] in addition to Figure 11.

interference joint is dependent on the materials' moduli of elasticity, Poisson's ratio, and amount of interference [4]. The interference between the hub and shaft induce circumferential hoop stresses in each part that translate to radial normal forces. These normal forces, along with the materials' coefficient of static friction, produce a frictional force between the shaft and hub that governs the axial and torsional holding strength of the press-fit. The assembled shaft and hub interface is then defined as an interference joint. An increase in the interference typically results in a stronger interference joint, but too large of an interference can easily result in fracture or damage to the joined materials.

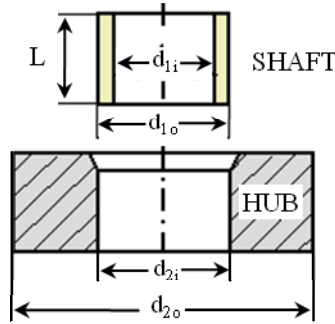


Figure 2. Diagram Showing Hub and Shaft with Associated Press-Fit Dimensions

In the press-fit process, either the shaft and hub can be forcefully pressed together at a common temperature or a shrink-fit can be done where the hub is heated to expand its inner diameter and the shaft cooled to contract its outer diameter. The differential temperatures take advantage of the respective material's coefficient of thermal expansion (CTE) and make it easier to insert the smaller part into the larger. The shaft and hub then stabilize at a common temperature creating a higher interference than what would have otherwise been possible. Press-fits, created by forcing the hub and shaft together at a common temperature, are only possible with interferences up to about one mil (one-thousandth of an inch is equal to one mil), while interferences above this magnitude require thermal treatment. Thermal expansion coefficients of metals are usually extremely small (ex: stainless 18-8 annealed steel has a CTE of 9.6×10^{-6} in/in $^{\circ}\text{F}$) [5], but can allow for interferences in excess of one mil for some metal types. Careful consideration of the press-fit material properties (ex: yield strength, ultimate strength, wall thickness) and maximum allowable interference enables the interference joint to be

created without either of the joined parts experiencing damage through material balling or stress induced fracture during the press-fit process.

Governing equations for a press-fit as described in [6] are:

p = Contact pressure or Interference Pressure

$$p = \frac{\Delta}{\frac{d_{1o}}{E_2} \left(\frac{d_{2o}^2 + d_{1o}^2}{d_{2o}^2 - d_{1o}^2} + \nu_2 \right) + \frac{d_{2i}}{E_1} \left(\frac{d_{2i}^2 + d_{1i}^2}{d_{2i}^2 - d_{1i}^2} - \nu_1 \right)} \quad (1.1)$$

δ_{1o} = Change of the outer radius of the inner member (shaft)

$$\delta_{1o} = -\frac{pd_{2i}}{2E_1} \left(\frac{d_{2i}^2 + d_{1i}^2}{d_{2i}^2 - d_{1i}^2} - \nu_1 \right) \quad (1.2)$$

δ_{2i} = Change of the inner radius of the outer member (hub)

$$\delta_{2i} = \frac{pd_{1o}}{2E_2} \left(\frac{d_{2o}^2 + d_{1o}^2}{d_{2o}^2 - d_{1o}^2} + \nu_2 \right) \quad (1.3)$$

σ_1 = Radial stress at the contact surface of the inner member (shaft)

$$\sigma_1 = -\frac{pd_{2i}^2}{d_{2i}^2 - d_{1i}^2} \left(1 - \frac{d_{1i}^2}{d_{2i}^2} \right) \quad (1.4)$$

σ_2 = Radial stress at the contact surface of the outer member (hub)

$$\sigma_2 = \frac{pd_{1o}^2}{d_{2o}^2 - d_{1o}^2} \left(1 - \frac{d_{2o}^2}{d_{1o}^2} \right) \quad (1.5)$$

T = Torque that the pressed interference joint will resist

$$T = \frac{\pi d^2}{4} \mu p L \quad (1.6)$$

F_n = Normal force (relative to the press-fit surface)

$$F_n = p \pi d L \quad (1.7)$$

F_μ = Frictional axial “holding” force of the interference joint

$$F_\mu = \mu F_n \quad (1.8)$$

E_1 = Elastic Modulus for the inner member (shaft)

E_2 = Elastic Modulus for the outer member (hub)

ν_1 = Poisson's Ratio for the inner member (shaft)

ν_2 = Poisson's Ratio for the outer member (hub)

μ = Coefficient of static friction at members interface

L = Contact length

d_{1o} = Outer diameter of the outer member (hub)

d_{1i} = Inner diameter of the outer member (hub)

d_{2o} = Outer diameter of the inner member (shaft)

d_{2i} = Inner diameter of the inner member (shaft)

Note: $r_i = 0$ for a solid member

d = Nominal interference diameter = $(d_{i,outer} - d_{o,inner})/2$

Δ = Calculated interference = $d_{i,outer} - d_{o,inner}$

C. METHODOLOGY

1. Conception of an SMA Interference Joint

The nano-satellite NEA concept solution derived itself from existing Naval Postgraduate School (NPS) Nano-satellite Advanced Concepts Laboratory (NACL) design research and experimentation with SMAs integrated into a nano-satellite docking interface. The pseudoelastic properties of SMA presented a unique material capable of changing shape upon command; therefore, becoming the working material for the micro-coupling. The micro-coupling's design was distinct from other SMA actuators in related fields by the method in which the SMA is used: press-fit in its detwinned martensitic phase creating an interference joint, coupling parts (deployables such as doors, solar panels, antennas, etc.) securely together until a commanded release. The SMA interference joint is, in itself, the micro-coupling, see Figure 3.

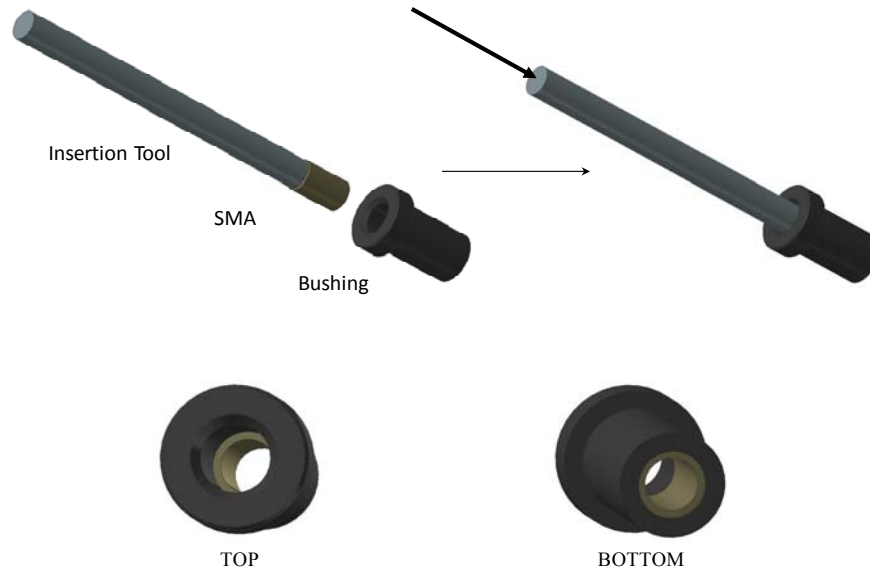


Figure 3. Press-Fit Creation of an SMA Interference Joint/Micro-Coupling

With the addition of a method to heat the SMA to its activation temperature, the interference joint becomes an NEA micro-coupling. This simple concept requires very few parts, and actuation occurs through a simple single motion operation that minimizes the total number of possible failure modes. Use of the micro-coupling could effectively improve the reliability of many coupling devices by eliminating their employment of motors, clasps, latches, material fracture, or explosive devices.

2. Applicable SMA Research

Since the conception of SMAs at the U.S. Naval Ordnance Laboratory in 1962 [2], a significant amount of research conducted on NiTi SMA was relevant in design of the proposed micro-coupling. Design considerations included SMA material properties affecting the press-fit process, material characteristics and interaction within the interference joint, and pseudoelastic properties of the SMA that enable its extraction from the interference joint upon heating. NiTi SMA material properties affecting micro-coupling design included:

- 1) SMA is more ductile in its martensitic phase, lending itself to an easier press-fit;
- 2) NiTi alloy's Poisson ratio varies from 0.33 for martensite to 0.30 for austenite, preferring the higher value for a stronger micro-coupling [1];
- 3) SMA modulus of elasticity is dependent on the alloy's composition and phase, resulting in a trade of micro-coupling strength with desired actuation temperature, see Figure 4. ;
- 4) Unconstrained recovery of the SMA (ϵ^t) is on the order of 6% upon HTR, providing insight into the SMA shaft's design geometry and allowable interference, see Figure 4.

Press-fitting a pseudo-elastic material to create an interference joint would hold a number of additional variables than those of traditional nonpseudoelastic interference joints. Research in related fields of pseudo-elastic materials and SMA rings pertained mostly to material wear durability and clamping applications.⁷ Although this research was unrelated to the concept of an SMA interference joint, it gave insight into the frictional properties of SMAs.

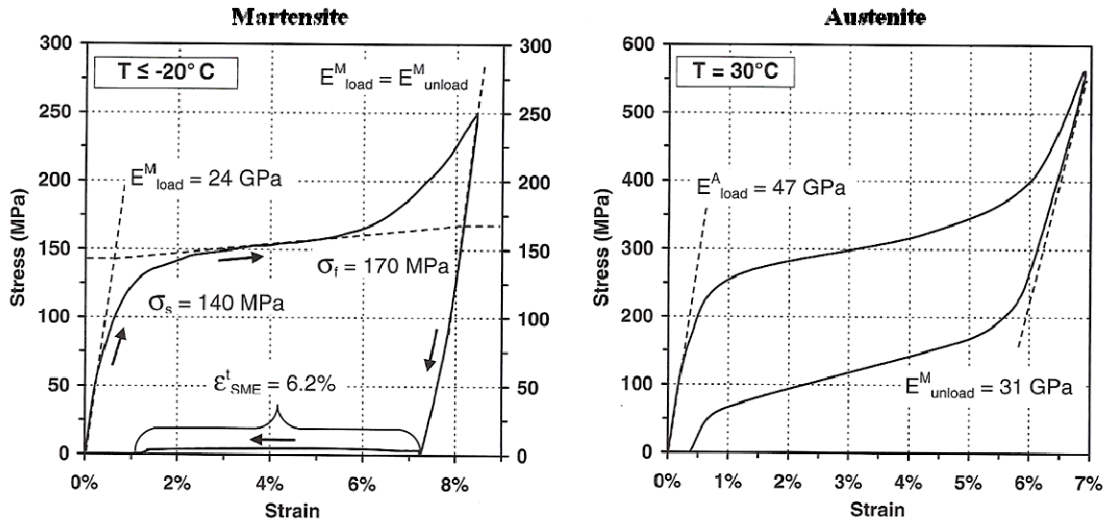


Figure 4. Monotonic Loading of a NiTi SMA at Given Constant Temperatures. From [1].

⁷ Press-fitting an SMA ring is contrary to current applications where the rings are used for clamping (i.e., hermetic sealing, shaft clamps, or electrical connectors).

The static and tribological behavior of NiTi is of particular importance as the SMA shaft/hub interface is where the micro-coupling derives its strength. Research conducted at the University of California Los Angeles found a change in the alloy's coefficient of friction occurs with an adjustment of applied pressure. Specifically, NiTi SMA used in high friction clamping interfaces, for loads large enough to form stressed induced martensite, the coefficient of friction between the two materials increases as the load increases [7]. This is contrary to nonpseudoelastic materials where frictional forces are directly proportional to the normal force applied and the coefficient of friction remains constant, see Equation 1.8. Additionally, the more intuitive case was confirmed where the coefficient of friction for the softer martensitic phase was greater than that of the harder austenite phase [8]. When comparing NiTi to stainless steel 304 for resistance to wear, research has determined that the detwinned martensitic phase is more wear resistant than the twinned martensitic or austenitic phase, and the pseudoelastic properties of the SMA strongly influence the frictional behavior of the alloy [9]. Finally, research on the physical geometry and material condition of press-fits demonstrate interference joints are the strongest in compressive loading, and controlled, consistent surface conditions of the materials being joined is very important in producing predictable joint strength [10].

3. SMA Interference Joint Characterization

Characterization of the SMA interference joint began with concept validation testing. This testing included two parts: precision measurement of the change in outer diameter of industry manufactured NiTi SMA rings during an unconstrained hysteresis cycle in order to develop micro-coupling design geometry, and forced separation of an SMA interference joint in order to determine the coupling capacity of the joint as a viable micro-coupling. The uniqueness of the SMA interference joint revealed itself during forced separation tests; wherein an unexpected increase in resistance to extraction followed the expected linear curve of coupling force vs. displacement, see Figure 5.

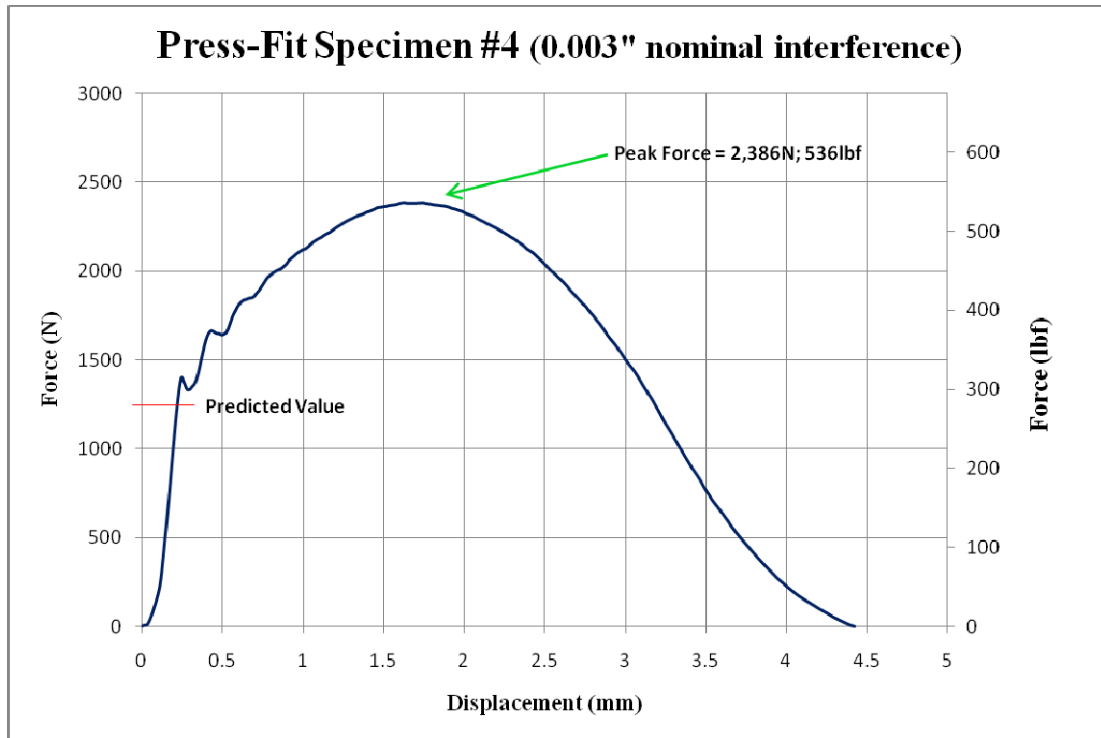


Figure 5. Coupling Strength Test Data Sample from SMA Micro-Coupling Concept Validation

The use of traditional press-fit axial holding strength equations adequately predicted the initial static friction coupling strength, but did not predict the stair stepped increase in axial coupling force; what will be referenced throughout this thesis as a strength-compounding characteristic of the SMA interference joint. The strength-compounding characteristic effectively doubled the predicted coupling strength of the SMA interference joint. These initial test results validated the concept of press-fitting an SMA ring into a hub to create a coupling mechanism, but also demonstrated the need to characterize the interactions between the SMA and hub in a forced decoupling scenario.⁸

4. Design of a SMA Coupling Device

Design and integration of the SMA micro-coupling into a fully functional NEA device that could be mounted on a nano-satellite began with consideration of how the SMA was to be press-fit. The SMA cylindrical ring could simply be press-fit directly

⁸ Appendices list detailed testing methods and results.

into the satellite's metallic frame leaving a portion of the cylinder exposed to attach the deployable. A foil heater or resistor could then be inserted into the SMA cylinder to heat and shrink the SMA, ultimately decoupling the deployable from the satellite's frame. The decision to put the SMA cylinder in compression superseded this design because applying tension to the SMA cylindrical ring would cause necking of the cylinder while under load. The SMA cylinder, while inside the interference joint, could possibly pull away from the walls of the joint, decreasing frictional holding forces and the overall strength of the joint. Conversely, an SMA cylinder under large compressive loads could buckle within the interference joint and increase the internal normal forces. An increase in normal force would result in larger frictional holding forces making a stronger SMA interference joint and micro-coupling. The original concept design for putting the SMA in compression called for the use of a bushing and retaining bolt, see Figure 6. The satellite deployable would easily attach to the retaining bolt, but a housing or mounting box would be required to fasten the bushing to the satellite bus. The micro-coupling's housing design could take many forms particular to its positioning on the satellite bus in addition to providing a means of integrating the micro-coupling's activation method into the satellites operating architecture.

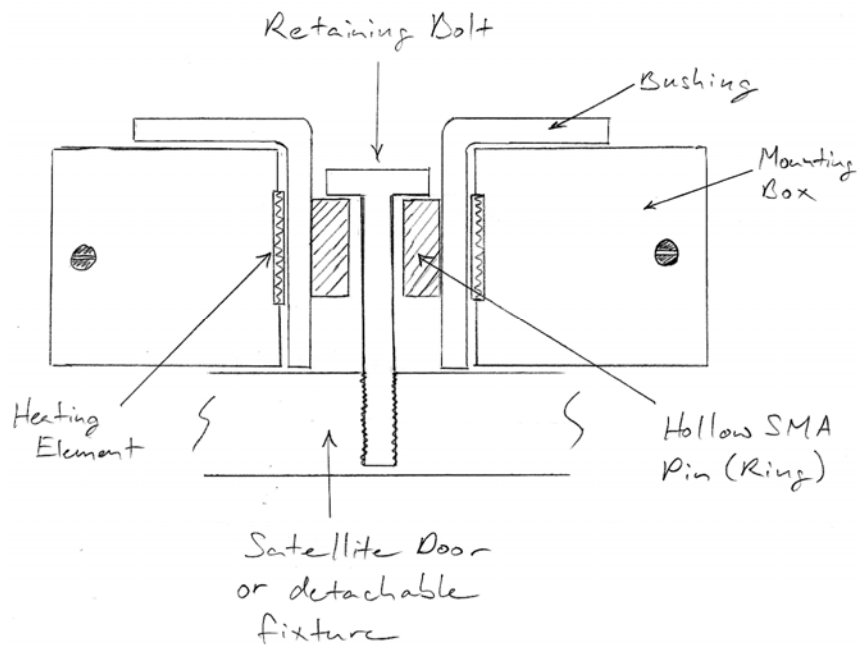


Figure 6. Original Concept Drawing from Early SMA Micro-Coupling Design

Any process for changing the temperature of the SMA would be a method of actuating the NEA: a heating element placed inside the SMA or around the exterior of the micro-coupling's hub; exposure of the device to an intense indirect heat source; or running a current directly through the SMA heating it via its own electrical resistance. Due to the extreme pressures within an interference joint, and the yet unknown characteristics of SMA within an interference joint, a simple casehardened steel bushing was used as the interference joint's hub. A nonconductive material, such as ceramic, would allow for direct electrical conduction of the SMA, but the brittleness of the ceramic and limited current available on nano-satellites precluded its use. Ultimately, avoiding complications during the decoupling process dictated the heating element's placement to be on the exterior of the steel bushing. If the heating element were placed internal to the SMA cylindrical ring, it would be subjected to large compressive forces during SMA HTR and possibly suffer a short circuit. A short circuit before obtaining complete HTR of the SMA would result in decoupling failure of the NEA micro-coupling device. In addition, placement of a heater and its associated electrical wiring within the path of the SMA during decoupling could cause inadvertent entanglement of the deployable.

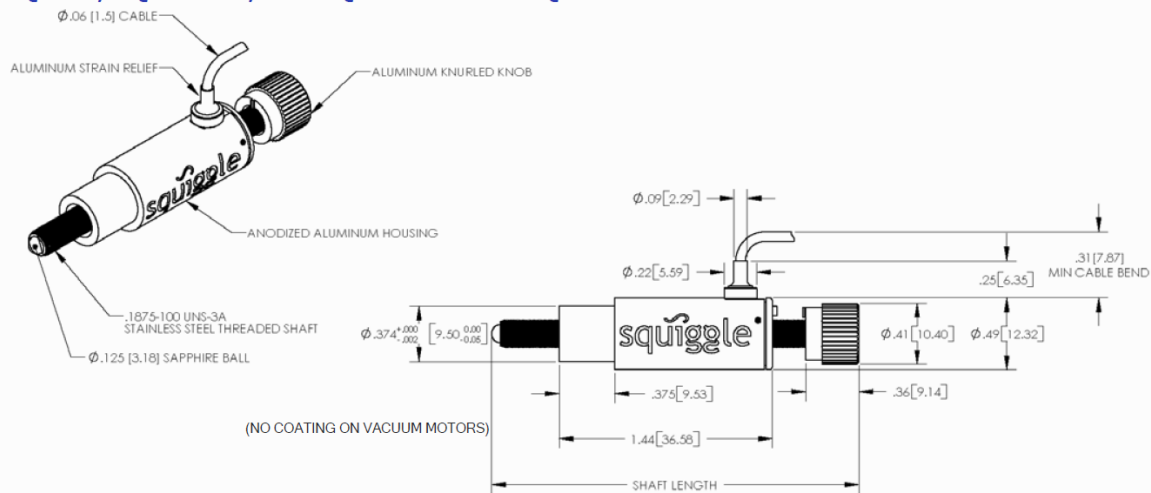
D. COMPARABLE COUPLING DEVICES

A coupling device has the ability to deploy or release connected parts upon command. Desirable characteristics of such a device include remaining secure under extreme forces, actuating reliably when commanded to decouple, and having small size so as not to impede upon the design of the coupled parts. Additionally, the characteristics of small mass and operating power would add versatility to the coupling device, allowing for a wider range of latch or fastener applications. Some coupling device designs may be impracticable in certain situations because of their interface design, complexity, or inability to scale to the size required. On the following pages are some examples of existing coupling devices.

1. New Scale Technologies SQUIGGLE Motor

The SQUIGGLE motor, developed by New Scale Technologies, consists of several piezoelectric ceramic actuators that change shape when electrically excited. These actuators are then attached to a threaded nut with a mating screw threaded inside that nut. Applying power to the actuators creates ultrasonic vibrations causing the nut to vibrate in an orbit. The nut's rotation then moves the threaded mating screw in-and-out with a linear motion. Once the mating screw is withdrawn, coupled components are released. A summary of the device's characteristics are in Figure 7.

SQ-100, SQ-100NM, and SQ-100V Series SQUIGGLE Motor



Specifications

SQ-100 Series Motor	
Housing Diameter	12.3 mm max.
- Mounting Diameter	9.5 mm
Housing Length	36.6 mm
Shaft Diameter/Thread	3/16" x 100 threads/in (4.76 mm x 0.25 mm lead)
Shaft Length	See Ordering Information
Stall Force	5 N
Resolution (typical)	20 nm (without encoder)
Start/Stop Time	0.2 ms
Speed Range	0.001 to 2 mm/s
Range of Motion	See Ordering Information
Off-Power Hold	Yes (self-locking threads)
Operating Temperature	-20 to 40 °C

Motor Ordering Information

Model	Travel/Shaft length ¹
SQ-115-C1	15 mm / 63 mm
SQ-115V-C1	15 mm / 63 mm
SQ-150-C1	50 mm / 103 mm

¹ Custom shaft length and range of motion on request.

² Vacuum motor operates to 10⁻⁷ Torr. Vacuum feed-throughs not included. Requirements: 3 wires, 30 gauge or greater, 200 V RMS.

Figure 7. SQ-100 Series SQUIGGLE Motors by New Scale Technologies

2. TiNi Aerospace Pinpuller

The TiNi Pinpuller, developed by Aerospace Inc., is a coupling device that retracts a pin upon command to decouple connected parts. The pin, when in the extended position, is under preload from a compression spring, see Figure 8. The pin remains locked in the extended position by means of a ball lock. This lock is made of a spring-loaded latch that drives an array of detent balls outward preventing the pin's retraction. Once actuated, the SMA element drives the latch upward causing the balls to roll inward allowing the pin to retract under the drive spring's force.

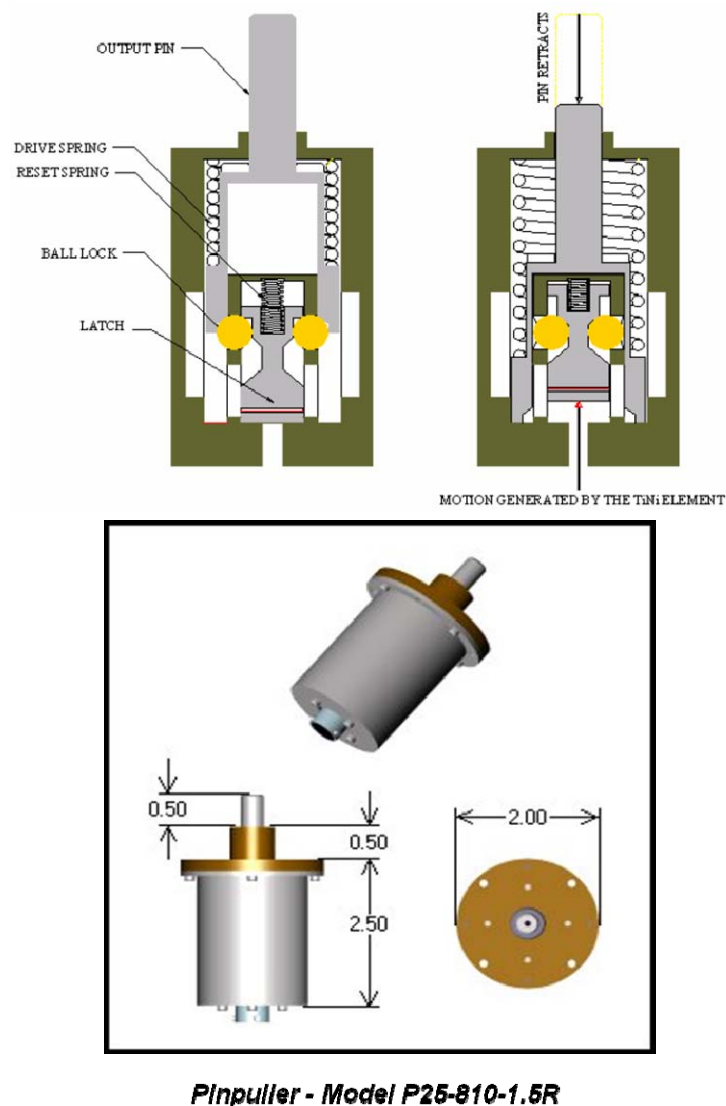


Figure 8. TiNi Pinpuller by Aerospace Inc. (Units in Inches)

3. TiNi Aerospace Model FC2-16-31SR2 FRANGIBOLT

Model FC2-16-31SR2 is the smallest FRANGIBOLT actuator produced by TiNi Aerospace with a design based upon an SMA cylinder that is heated to expand its length, as shown in Figure 9. A specially notched titanium fastener, provided by TiNi Aerospace, is then passed through the SMA cylinder and used to connect parts to be coupled. Once activated, the SMA's subsequent elongation fractures the titanium fastener at the notched weak point and decouples the previously coupled parts. The small volume and low power consumption of the coupling device makes it useful for many applications.

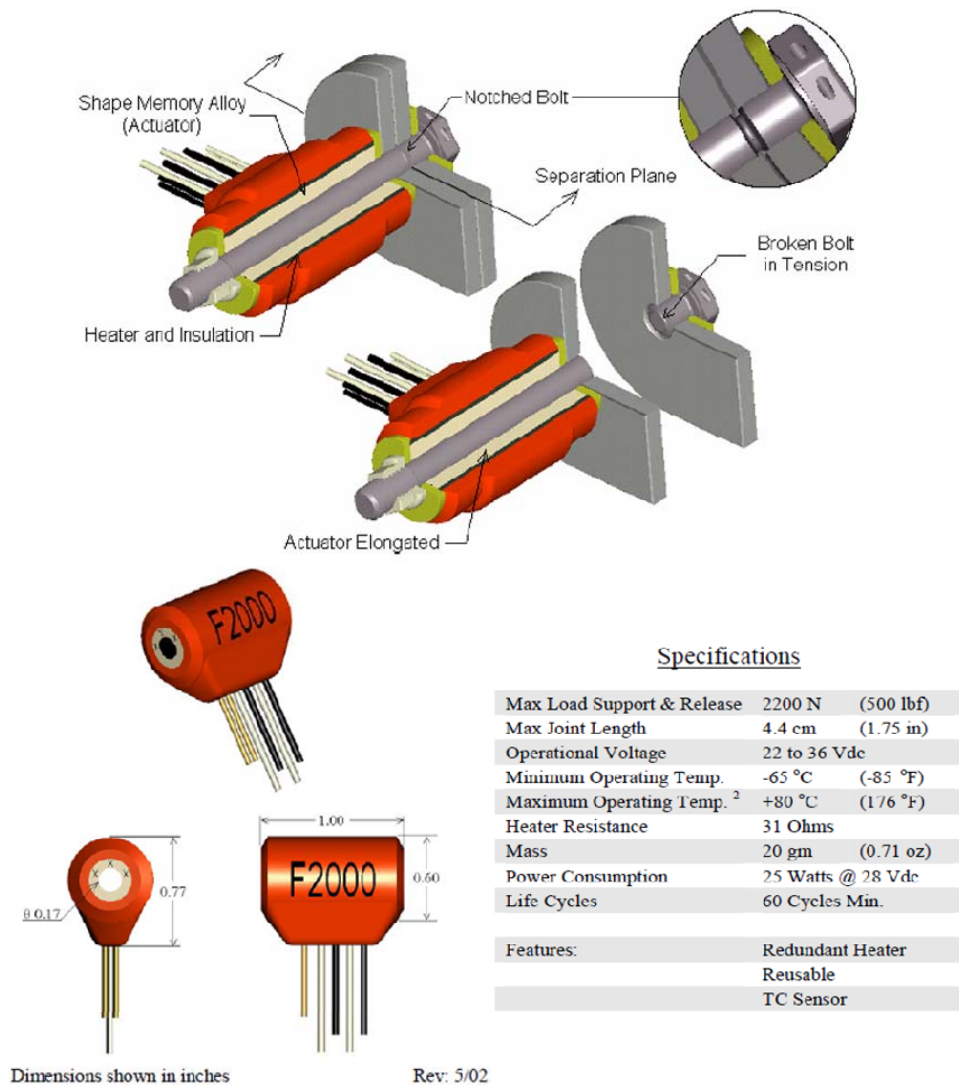


Figure 9. FRANGIBOLT Model FC2-16-31SR2 by TiNi Aerospace Inc.

E. ORIGINAL CONTRIBUTIONS

Concept, validation, design, and test of an SMA interference joint for use as a reliable NEA is the core contribution of this thesis. The SMA interference joint's fundamental development and initial exploration of application is original work by definition. Unique contributions to the related art of coupling devices and shape memory alloys are as follows:

- 1) A zero impact nonexplosive actuation device for nano-satellite applications.
- 2) An actively or passively releasable interference joint with high coupling strength.
- 3) A simple, low-failure mode, coupling mechanism for many applications in system design (i.e., safety devices, tamper locks, robotics, aeronautics, military, and spacecraft systems).
- 4) A method for characterization and analysis of SMAs under high-pressure interfaces.
- 5) A new concept for the application of detwinned martensitic SMA.

F. THESIS ORGANIZATION

Organization of this thesis divides into a main body and multiple supporting appendices. The body's organization is as follows:

Chapter I, Introduction: provides the reader a brief background on the related science of SMAs and interference joints within the context of the thesis' objective, the chronological development methodology of the micro-coupling, and comparable coupling devices within the related field;

Chapter II, Micro-coupling Mechanism Design and Test: describes the thought process behind the use of SMA in an interference joint, design considerations for making a reliable coupling mechanism, concept validation experiments, and testing of a micro-coupling engineering design unit (EDU).

Chapter III, Application of the Micro-coupling Mechanism: outlines the development of the first NEA EDU device using the micro-coupling mechanism followed by an initial investigation of the device's integration into a nano-satellite as a zero-shock NEA with the intent to mature the NEA device design.

Chapter IV, Conclusions and Recommendations: summarizes valid designs, current hypothesis, and guidance for future work relating to the thesis' objective.

Thesis appendices comprise NPS NACL test reports conducted in pursuit of this thesis, related micro-coupling patent as filed with the U.S. Patent and Trade Office, and the spreadsheets developed in support of communicating this thesis to the reader.

II. MICRO-COUPLING DESIGN AND TEST

A. NITI MICRO-COUPLING MECHANISM

1. Concept Development and Requirements

The objective to design a space-qualified “micro”-coupling implies the requirements of small size and adequate coupling strength to endure the rigors of launch and space environment. NiTi SMA comprised the working material of the micro-coupling’s SMA interference joint because of its well-defined pseudoelastic behavior with available phase transition temperatures suitable for use in the space environment. Detwinned martensite became the working phase of the SMA because it achieves a 5:3 greater unconstrained reduction in outer diameter as compared to twinned martensite.⁹ The additional diameter reduction afforded by the detwinned martensitic phase allowed for the use of a smaller SMA cylindrical ring, ultimately resulting in a smaller micro-coupling design. Constraints for the micro-coupling’s design included a derived requirement to support a 1 kg load under 20 times the force of gravity,¹⁰ a design safety factor of 2.0, and the SMA manufacturer’s available tooling for SMA ring production determining wall thickness, length, and standard diameter. The maximum outer diameter of the SMA cylindrical ring was chosen to leave a minimum of 0.003” (3 mils) clearance between itself, in the shrunken austenitic phase, and the steel hub it was press-fit into, ensuring decoupling of the interference joint upon HTR. Traditional interference joint equations determined baseline attainable coupling strength.¹¹ Manufacturer’s available tooling precluded strengthening the SMA cylindrical ring by increasing wall thickness; therefore, increasing the design length of the SMA cylindrical ring to increase contact surface area within the interference joint amplified coupling strength to meet loading

⁹The detwinned to twinned outer diameter reduction ratio was validated by running an engineering design unit SMA cylindrical ring through HTR and subsequent thermal cycling, see Appendix A.

¹⁰ A standard CubeSat deployable secured with the micro-coupling subject to extreme launch conditions.

¹¹ It was unknown at this stage if traditional interference joint strength equations would adequately characterize an SMA interference joint.

requirements. Finalized NiTi SMA cylindrical ring dimensions used in the micro-coupling mechanism EDU unit are listed in Table 1.

Table 1. Supplied NiTi SMA Cylindrical Ring Dimensions Used in the Micro-Coupling Mechanism Engineering Design Unit

Pre-HTR Detwinned Martensitic Phase		
Inner Diameter Range (in)	0.1565	0.1580
Outer Diameter Range (in)	0.2030	0.2045
Length Range (in)	0.3060	0.3080
Post-HTR Austenitic Phase		
Inner Diameter Range (in)	0.1470	0.1482
Outer Diameter Range (in)	0.1944	0.1960
“G” type Unilok SMA ring (AGE0156-0022-0312) as supplied by Intrinsic Devices Inc.		

2. Press-Fit Considerations

Traditional shrink-fit methods, using high temperatures to induce thermal expansion of the steel hub during the press-fit process, were not used. The high temperature of the hub would initiate SMA HTR phase change and negate the additional detwinned martensitic diameter reduction. This could reduce the reliability of successful decoupling and the available range of design interferences.

Preproduction testing at Intrinsic Devices Inc. precluded creating the micro-coupling interference joint by heating the SMA to facilitate insertion into the steel hub and then allowing it to cool and expand into the interference joint. Testing showed that the measured two-way recovery stress of a SMA rod’s expansion in length, when cooled from the austenitic phase to twinned martensitic phase, was about 5,000 psi when constrained, as would be the case for a shrink-fit. In contrast, a detwinned martensitic rod compressed by 2% in length, a magnitude adequate for a common temperature press-fit, experienced stresses up to 20,000 psi [11]. This led to a rough estimation that using a

detwinned martensitic SMA ring in a press-fit method would yield a four times smaller cross section, yet still achieve the same strength as the shrink-fit method.

The smaller geometry and stronger interference joint predictions resulted in conducting the micro-coupling press-fit process at room temperature using the characteristically more ductile detwinned martensitic phase of NiTi SMA. This co-temperature press-fit process ultimately reverses a portion of the manufacture's mechanical deformation of enlarging the ring's diameter when creating a detwinned martensite NiTi cylindrical ring,¹² but allows for the stored mechanical energy of deformation within the martensitic atomic structure to increase the strength of the interference joint. In addition, NiTi alloy has a higher coefficient of friction in its martensitic phase as compared to its austenitic phase [8]. This higher coefficient of friction translates to a stronger micro-coupling. Since martensitic NiTi SMA is a comparatively ductile material in relation to other metals, a larger interference can be chosen without damaging the hub and shaft during the press-fit process, see Figure 2. Extreme interferences produce pressures internal to the interference joint in excess of a GPa at the material's boundary while the pressure required to induce a phase change in NiTi SMA is approximately 700 MPa dependent on the alloy's blend [1]. This indicates a possibility of pressure induced phase change of the SMA during the press-fit process if one chooses too large an interference. Testing on subject SMA rings with interferences up to 5 mils never encountered this situation, but was a consideration in initial design and test.¹³

3. Interference Precision and Joint Strength Prediction

The unconstrained reduction in the SMA cylindrical ring's outer diameter along with press-fit assembly interference precision governs the geometry of the interference joint. The design goal in actuation of the micro-coupling was to avoid inadvertent re-engagement of the steel hub upon decoupling. Once the SMA shrinks via the HTR process and eventually enlarges again upon cooling to twinned martensite, this cooled

¹² Measurements taken from SMA rings after being extracted from their interference joints confirmed a reduction in diameter from original ring dimensions as received from the manufacturer.

¹³ See Appendix B and C.

diameter should not be large enough to re-engage the steel hub. Since SMA phase change is essentially a constant volume process, the SMA cylinder lengthens with associated reduction of its inner and outer diameters. The amount of SMA geometry change depends upon manufacturing techniques and prior annealing of the SMA alloy [9]. Exact manufacturing techniques of the SMA rings used for this thesis were unknown; therefore, testing determined the permanent HTR reduction in outer diameter for commercial-off-the-shelf (COTS) and EDU SMA rings.¹⁴ A maximum interference value of approximately 5 mils was possible for creation of the SMA interference joint to meet the aforementioned micro-coupling's design goals within the given dimensions and the associated HTR reduction found in Table 1.

The anticipated interference created between the casehardened steel hub and SMA cylindrical ring predicted micro-coupling interference joint strength following the press-fit equations in Section I, Part B2. Small deviations in the assembled interference, due to measurement precision or nonideal geometry of the assembled parts, influence the interference joint's predicted strength. The micro-coupling's predicted axial coupling strength will be affected by low precision measurements and geometry inaccuracies when these errors propagate from Equation 1.1 through to Equation 1.8 using the NiTi SMA characteristics noted in Table 2.

Table 2. Material Properties Used in Micro-Coupling Predicted Strength Calculations

	Elasticity (GPa)	Elasticity (x 10⁶ psi)	Poison's Ratio	Coefficient of Friction
High Carbon Steel [5]	207	30.015	0.29	0.13
NiTi SMA (Martensite) [12]	30	4.350	0.33	0.13

¹⁴ See Appendix A and Equation 2.1.

Propagation error traced through the press-fit equations by using average deviations [13], in the following manner:

1. Adding the micrometer's precision of 0.0001" (± 0.00005 ") to one standard deviation of the measured SMA diameter measurements defined Δd_o .¹⁵ Gauge pins measured the inner diameter of the steel hubs, with a precision of +0.00004" minus nothing, using one standard deviation calculated from the range of gauge from the largest pin that would fit into the steel hub to the smallest pin that would not. The gauge pins incremented by 0.0001" resulting in one standard deviation equal to 0.00007" defining Δd_i . Uncorrelated propagation error for the press-fit interference caused by measurement precision error and nonideal geometric shape was then calculated using Equation 2.1:

$$\Delta d = \sqrt{(\Delta d_o)^2 + (\Delta d_i)^2} \quad (2.1)$$

2. The uncorrelated propagation error in interference pressure (Δp) was calculated from an equation derived from Equation 1.1. The derivation employed average deviations based on the mathematical operations used on the individual variables within Equation 1.1. This derived equation and the interference error found in Equation 2.1, were scaled by the predicted interference pressure (p), resulting in Equation 2.2:

$$\Delta p = p \sqrt{\left(\frac{\Delta d \sqrt{2[(2\Delta d_o)^2 + (2\Delta d)^2]}}{\Delta} \right)^2 + \left(\frac{\Delta r \sqrt{2[(2\Delta d_i)^2 + (2\Delta d)^2]}}{\Delta} \right)^2} \quad (2.2)$$

3. The uncorrelated propagation error in predicted interference joint coupling force (ΔF_μ) was calculated from the propagated interference pressure error and, as before, the use of average deviations. The equation is derived based on the mathematical operations used on the individual variables within the predicted

¹⁵ The SMA rings are noncylindrical within a micrometer's precision.

interference-fit coupling force Equation 1.8 and then scaled by the predicted coupling force (F_{μ}), resulting in Equation 2.3:

$$\Delta F_{\mu} = F_{\mu} \sqrt{\left(\frac{\Delta p}{p}\right)^2 + \left(\frac{\Delta d}{\Delta}\right)^2} \quad (2.3)$$

Micro-coupling test results were compared to predicted coupling strengths by graphing the uncorrelated propagation error as error bars on the initial predicted coupling strength value for each interference type.¹⁶ These error bars revealed the extent of propagated prediction error attributed to the noncylindrical SMA rings and measurement tool precision, supporting the need for extreme precision and testing control standards.

4. Mechanization of the Micro-Coupling

The micro-coupling is an interference joint between an SMA cylindrical ring and a casehardened steel bushing, see Figure 10. The SMA cylindrical ring is press-fit into the bushing with a set interference value to create the desired coupling strength. The SMA is a “G” type nickel-titanium alloy provided by Intrinsic Devices, Inc. with HTR characteristics tailored to spacecraft application. The intent of the SMA’s high HTR onset temperature of 95 - 105 °C is to prevent unintentional SMA activation yet be low enough to be an obtainable temperature using a nano-satellite’s limited power while exposed to the extreme temperatures of the space environment. The press-fit SMA is held securely inside a steel bushing and a retaining bolt is then passed through the SMA ring, see Figure 10.1. The bolt’s head catches on the SMA cylindrical ring and cannot pass by the SMA interference joint, see Figure 10.2. The steel bushing attaches to the first part of a coupled pair and the retaining bolt is secured to the second.¹⁷ A resistive Kapton foil heater, placed around the exterior of the bushing in which the SMA cylindrical ring is press-fit, heats the micro-coupling and subsequently actuates the SMA. Heating the SMA enables the atomic transformation of the SMA, from its larger diameter martensitic phase, into its smaller diameter austenitic phase or memory shape, see

¹⁶ See Appendix B.

¹⁷ The coupled pair joined together by the micro-coupling is not shown in Figure 10.

Figure 10.3. Once heated, the SMA cylindrical ring shrinks, releases from its press-fit, and the SMA along with the retaining bolt slide out of the bushing releasing the coupled parts, see Figure 10.4.

Radial pressure and loading direction are important factors in design of interference joints when taken into account under actual service conditions; therefore, mechanization of the micro-coupling took advantage of putting the SMA cylindrical ring into compression. The SMA in compression would expect to see an increase in radial pressure as it tries to expand or buckle in the hub during forced extraction. Control of axial and radial surface roughness of the SMA and steel hub can achieve a higher measured coefficient of friction and ,therefore, a higher axial holding force [7]. In addition, geometrical accuracy and surface conditions within the interference joint are the two most important factors affecting the coefficient of friction [10]. Subsequent micro-coupling assembly required precise component measurement and a high level of test material preparation with associated handling controls to remove all surface contaminants and oils. All SMA cylindrical rings and steel hubs used to make the micro-coupling's interference joint were procured from outside vendors and mass-produced to maintain consistency between test specimens and reduce test data variability.

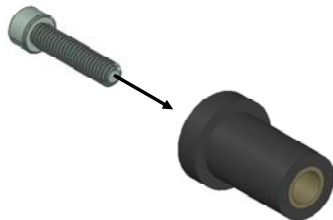


Figure 10.1



Figure 10.2

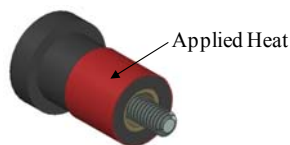


Figure 10.3

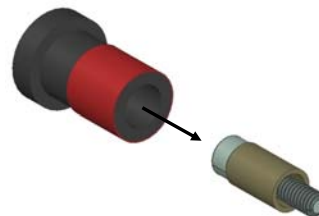


Figure 10.4

Figure 10. SMA Micro-Coupling Mechanization. From [14].

B. PRELIMINARY EXPERIMENTS

1. Characterization of NiTi SMA Heat to Recover Hysteresis

Hysteresis testing first began with COTS SMA rings obtained from Intrinsic Devices Inc. and then again with the SMA cylindrical rings specifically procured for the micro-coupling EDU. The test report is provided in its entirety in Appendix A. Excerpts from the executive summary follow:

COTS SMA Ring—Experiment objectives were to validate published HTR temperatures and SMA pseudoelastic properties as manufactured by Intrinsic Devices Inc. The purpose of this experiment was to provide insight into design tolerances required for development of the micro-coupling that utilizes SMA for actuation. Testing found the HTR change in outer dimension for the G type SMA ring to be 3.9%, a loss of 0.6% from the anticipated 4.5% outer diameter reduction. The change in inner diameter of the SMA ring upon HTR was found to be 7.5%, an excess of 1.5% from the published unconstrained HTR outer diameter reduction. A small reduction in outer diameter occurred prior to the published HTR temperature, but ultimate de-stressing of the SMA occurred at approximately 90 °C. Cycling the temperature of the SMA through its initial irreversible HTR produced a two-fold greater reduction in its outer diameter than the reduction produced when cycling the SMA through its reversible shape memory effect hysteresis. This supported using the detwinned martensitic state of the SMA for the press-fit process.

SMA Cylindrical Ring EDU—Experiment objectives were to validate HTR temperatures and pseudoelastic properties of the micro-coupling SMA cylindrical ring EDU, as procured from Intrinsic Devices Inc. The purpose of this experiment was to ensure adequate reduction of the outer diameter of the SMA to allow de-coupling from a steel hub with an inner diameter of 0.1990” before further testing and construction of the micro-coupling mechanism EDU. The HTR change in outer dimension for the G type EDU SMA was found to be 4.2% with a final austenitic outer diameter of 0.1955” ± 0.00005 ”, and the difference between the HTR process and repeatable hysteresis cycle can be clearly seen in Figure 11. Phase transition points, shown as capital letters,

represent the same shape memory effect as seen in Figure 1. The inner diameter of the SMA ring was measured and its smallest diameter was confirmed to be large enough to not engage the retaining bolt shaft.¹⁸ The same small reduction in outer diameter found with the COTS SMA ring occurred as the temperature increased to the published HTR temperature of 95 °C (0.27% reduction in OD prior to 95 °C; points D to E). This could indicate a propensity for the SMA interference joint to de-stress or creep when approaching phase change temperatures. Ultimate de-stressing of the SMA ring occurred at approximately 105 °C. Primary HTR resulted in a permanent 2.5% reduction in OD after cycling through 125 °C (published HTR temperature). The outer diameter reduction in the SMA cylindrical ring at austenitic temperatures would leave a delta of 0.0035” between the SMA and steel hub; therefore, the micro-coupling mechanism would achieve successful de-coupling upon SMA HTR. Once the stored stress within the SMA cylinder was released upon HTR, a new austenitic phase transition temperature of approximately 55 °C was established for the repeatable hysteresis. This lower transition temperature would be beneficial to the micro-coupling design in the event the SMA cylindrical ring reengaged the steel hub upon commanded release as less power would be required to re-shrink the SMA to its small austenitic diameter.

¹⁸ This ensured unconstrained recovery of the SMA cylindrical ring upon HTR. Unconstrained recovery yields a larger percentage of SMA shape change allowing for greater micro-coupling design interferences and the smallest possible final diameter of the SMA upon heating. See Appendix A.

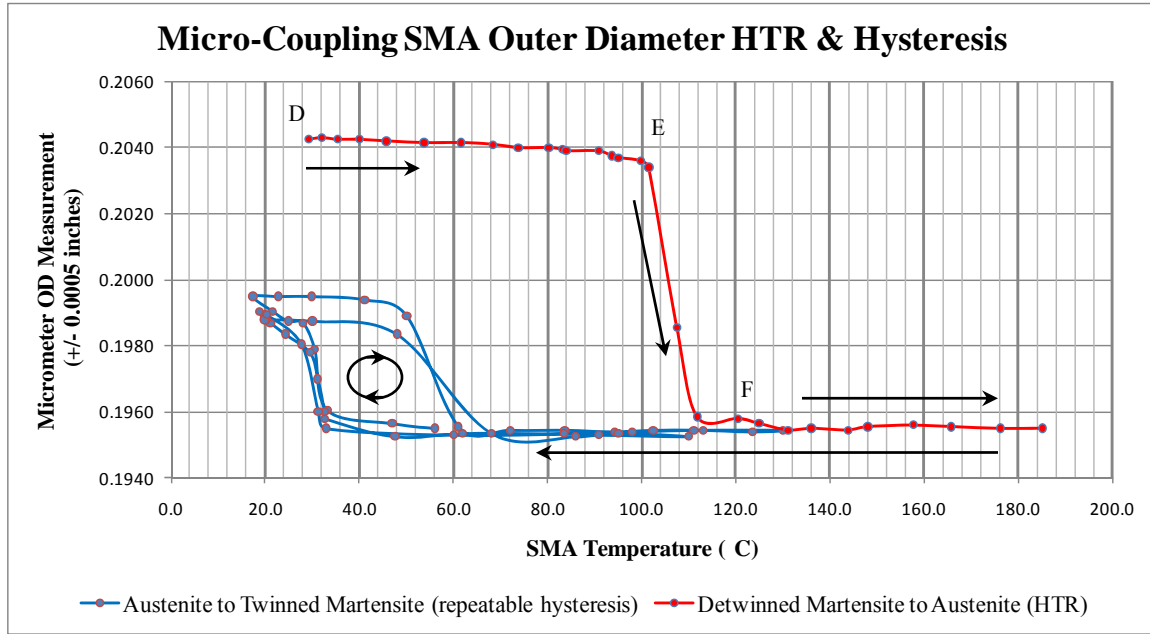


Figure 11. EDU SMA Heat to Recover and Shape Memory Effect Hysteresis Cycle

2. Press-Fit SMA Concept Validation

This experiment used COTS SMA rings obtained from Intrinsic Devices, Inc. The test report is provided in its entirety in Appendix B. Excerpts from the executive summary follow:

The primary experiment objective was to determine if an SMA interference joint, consisting of a detwinned martensitic NiTi SMA ring and stainless steel hub, could obtain sufficient axial coupling strength to be developed into a micro-coupling. Another objective was to determine if the press-fit process induced martensitic de-stressing or plastic deformation of the SMA cylindrical ring. Force and displacement curves were generated during the forced removal of the SMA from the interference joint by applying an axial force on the SMA cylindrical ring until it was pulled clear. Interference ranges of 0.0005" to 0.0030" were examined.

Achieving substantial holding forces in excess of 500 lbf validated the use of an SMA interference joint as the actuating mechanism for a coupling device. De-stressing of the SMA cylindrical ring was determined to be one half of the interference experienced by the SMA. The largest interference explored, 0.0030", yielded the largest

coupling strength and experienced several force peaks in resistance to extraction, see Figure 5. This led to a hypothesis that the SMA cylindrical ring experienced buckling upon forced extraction thereby increasing the normal forces inside the interference joint, subsequently increasing the interference joint's strength.

3. Micro-Coupling Mechanism Powered Actuation

A coupling mechanism's reliability in releasing a spacecraft's deployables ultimately determines the satellite's ability to achieve mission success; therefore, the micro-coupling's mechanization concept required validation to ensure decoupling of the SMA interference joint upon SMA activation. Micro-coupling actuation validation began with construction of a micro-coupling EDU.¹⁹ A desktop test bench, with associated power and data logging equipment, measured the micro-coupling temperatures and supplied the power required for actuation, see Figure 12. Three T-type thermocouples were attached to the micro-coupling with Kapton tape in the following locations:

- 1) Inside the SMA cylinder
- 2) Exterior of the Kapton foil heater
- 3) Head of the steel bushing

A laptop computer connected to an Omega HH147U USB data logger thermometer recorded all thermocouple-measured temperatures. Resistance of the Kapton foil heater measured $12.6\ \Omega$ at the power supply leads. The micro-coupling was suspended with a "helping-hand" armature by clamping the alligator clip around the base of the bushings brim. This suspension method was chosen to minimize conduction losses from contact with the steel bushing and to provide a stable platform to attach a weight to the micro-coupling. A 4-40 hex bolt was inserted into the micro-coupling to suspend a 0.273 kg mass. The mass delivered a 2.68 N preload to the micro-coupling and would drop free upon micro-coupling actuation.

¹⁹ The construction of the micro-coupling EDU was as described in Part III Section A1, less the outer diameter modification to the casehardened steel bushing.



Figure 12. Open Air Micro-Coupling Mechanism EDU Actuation Test Bench

Testing commenced with initiation of the temperature data logging software and application of 5.0 Volts across the heater's electrical leads. Initial current draw was 0.407 Amps and ultimately leveled off at 0.403 Amps. This particular test run was terminated before SMA actuation as the micro-coupling appeared to reach steady state at approximately 70 °C after a total of 430 seconds of applied power. Consequently, a second test run ensued at a higher voltage setting of 7.0 Volts. Initial current draw was 0.569 Amps and ultimately leveled off at 0.561 Amps. SMA actuation occurred at a measured temperature of approximately 80 °C after a total of 107 seconds of applied power, dropping the suspended mass to the tabletop. The micro-coupling had an average power draw of 3.94 Watts with a total power consumption of 0.116 Watt-hours before successful actuation. Micro-coupling temperature and supplied power profiles for the second test run are in Figure 13.

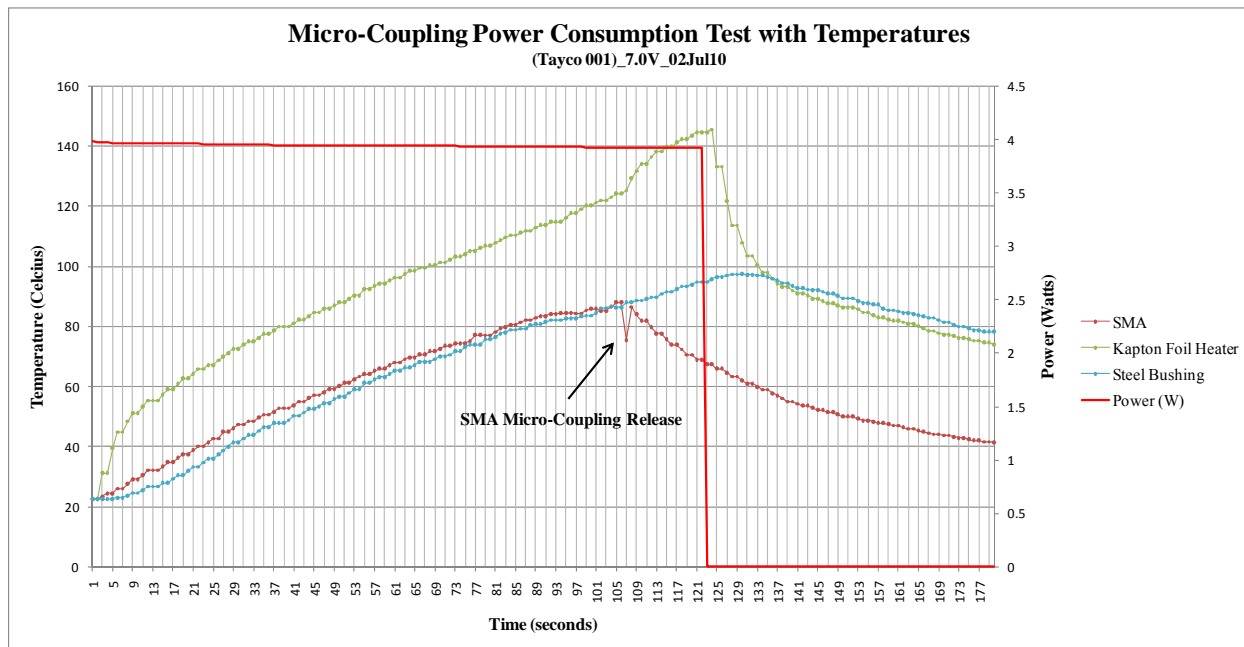


Figure 13. Open Air Micro-Coupling Mechanism EDU Actuation Temperatures and Power Consumption Data

Analysis of the thermocouple data revealed a temperature lag in the steel bushing as compared to the SMA and Kapton foil heater. This resulted from the placement of the bushing's thermocouple at the furthest conduction point, 0.332", from the foil heater's contact as compared to the shorter conduction path of 0.058" to the SMA through the

neck of the bushing. Possible reasons for the SMA actuating at the recorded value of 80 °C vs. the validated HTR temperature of 100 °C include:

- 1) The thermocouple reading a reduced temperature by not being in full contact with the SMA;
- 2) A SMA material property wherein there is a reduction of the alloy's HTR temperature while under extreme pressure [1], as would be experienced within the interference joint.

The experiment achieved its objective of validating the micro-coupling mechanization concept.

C. MICRO-COUPPLING MECHANISM LOAD TESTING

Validation of the concept and mechanization of the SMA micro-coupling, led to the requirement for a repeatable, controlled process of creating SMA interference joints and a standardized method for evaluating their coupling strength. The test report is provided in Appendix C. Excerpts from the test objective follow:

The threshold objective for the micro-coupling load test was to obtain the axial strength of the micro-coupling as designed for the Single Motion Actuated Shape Memory Alloy Coupling (SMA²C) device. The SMA²C micro-coupling was subjected to forceful extraction of the SMA from within the micro-coupling's interference joint producing force vs. displacement data. Additional testing goals included determining if the press-fit process induced martensitic de-stressing or plastic deformation of the SMA cylindrical ring, and if use of industry standard formulas for interference joint strength could predict the micro-coupling's strength within propagated measurement error.

1. Micro-Coupling Press-Fit Cradle

Design of the SMA²C press fit cradle allowed for a repeatable process of creating an SMA interference joint with a high degree of alignment accuracy. The cradle itself is constructed of 1¼" diameter type 304 stainless steel machined to use a circular tongue and groove for assembly alignment. A press-fit pin fits through the top of the assembly and holds the SMA cylindrical ring while the casehardened steel hub sits in an

appropriately dimensioned pocket in the assembly's bottom. The cradle's top and bottom are joined and placed on top of a load cell adaptor and load cell so the force used in the press-fit process can be recorded, see Figure 14.

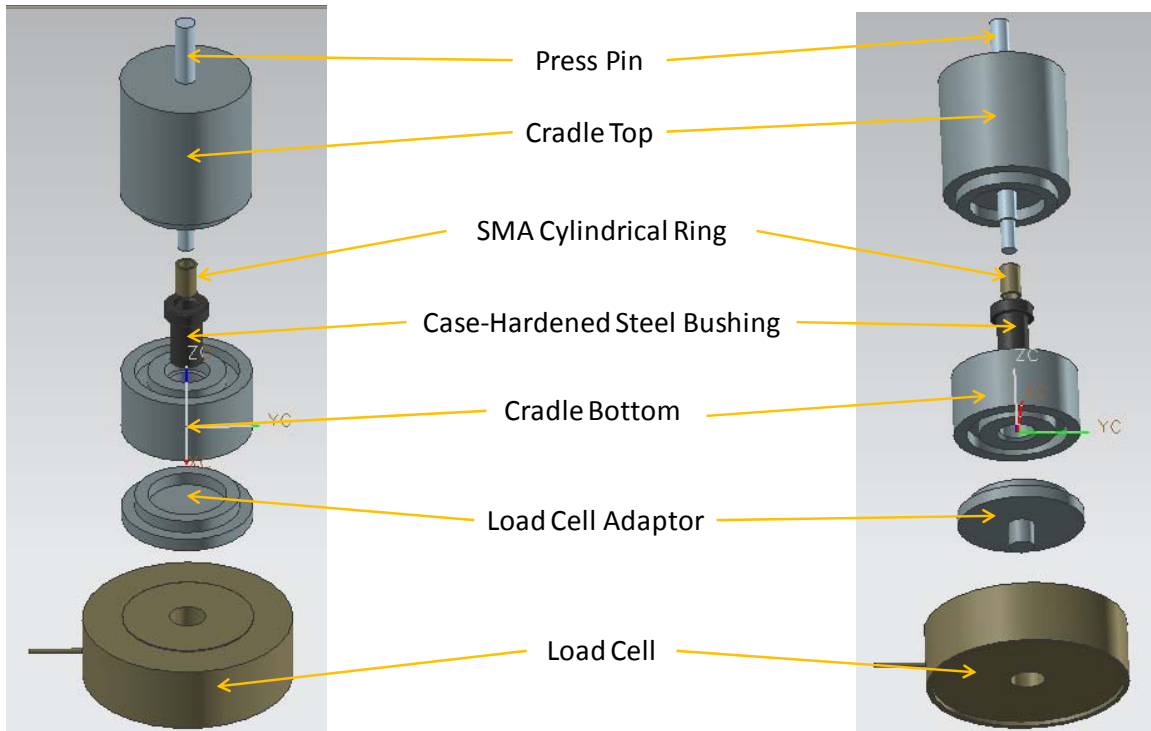


Figure 14. Component View of SMA²C Press-Fit Cradle

2. Micro-Coupling Load Test Rig

Design of the SMA²C micro-coupling load test rig allowed axial loading of the SMA interference joint. The test ring is constructed of 1¼" diameter type 304 stainless steel except for the rig bottom, constructed from 15-5 type Ph steel for additional strength at the 4-40 extraction hex bolt attachment point. An alignment slice holds the SMA²C micro-coupling in an appropriately dimensioned pocket allowing for attachment to the top of the test rig. The test rig top and bottom are joined using the extraction hex bolt and inserted into the tensile machine. Load cells record the force used to separate the SMA from the casehardened steel hub during the tensile test, see Figures 15 and 16.

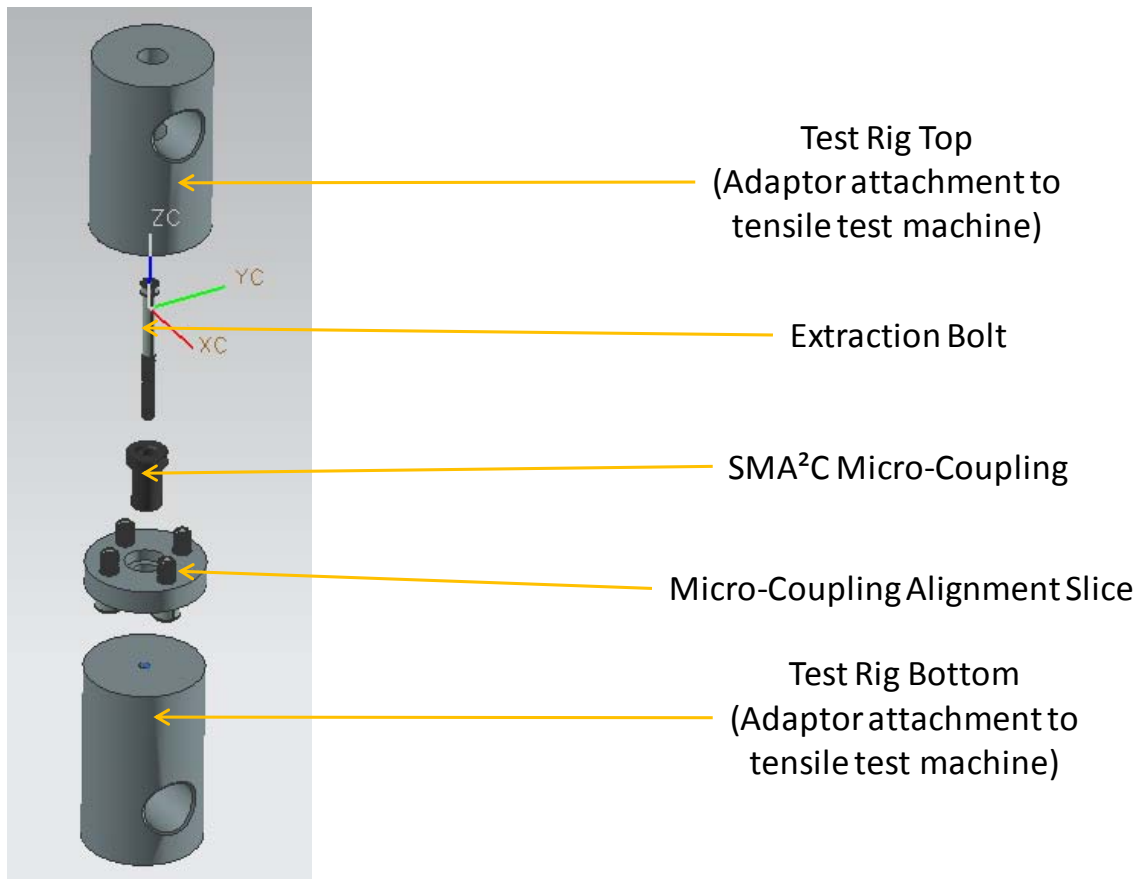


Figure 15. Component View of SMA²C Micro-Coupling Load Test Rig

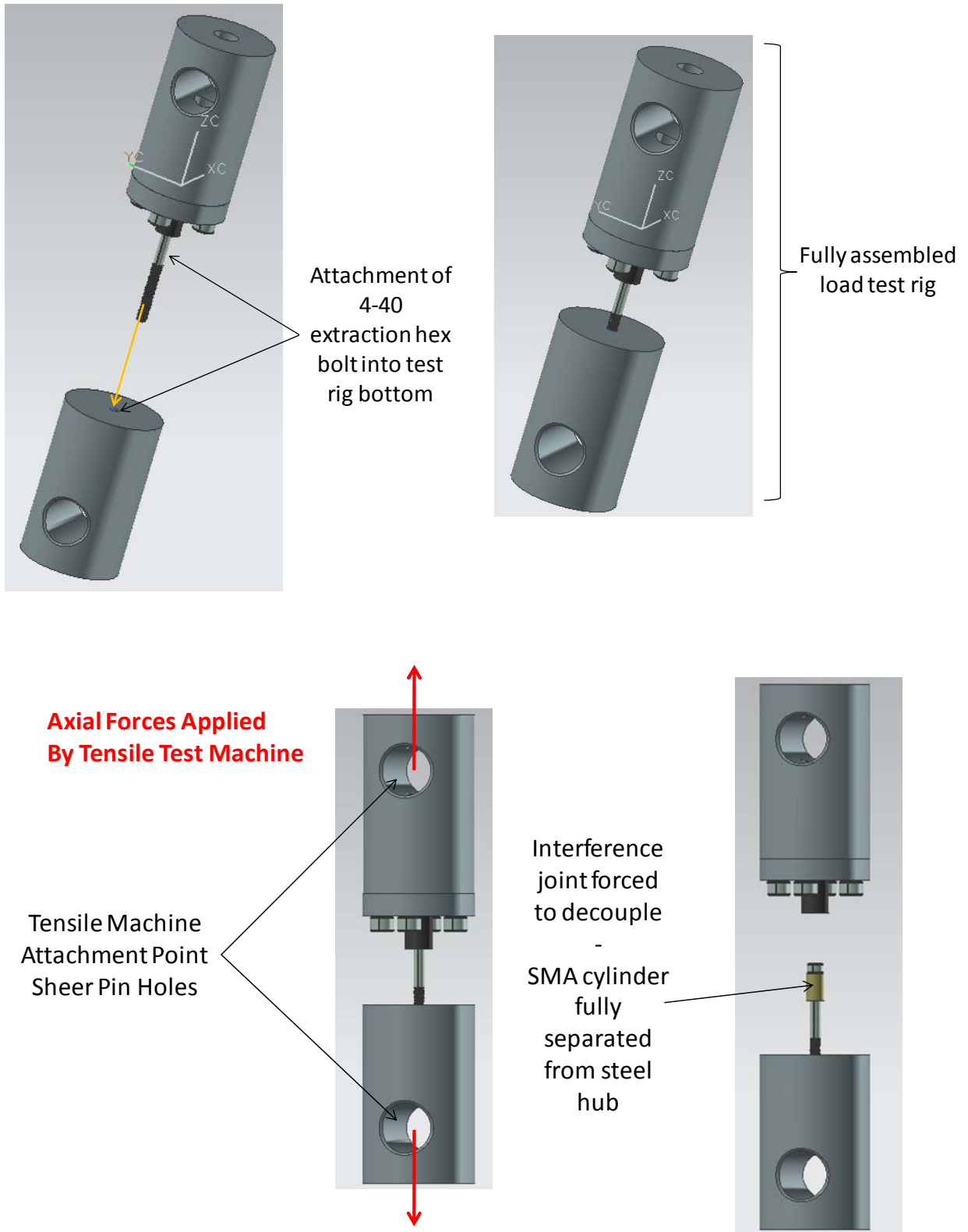


Figure 16. Assembly and Operation of SMA²C Micro-Coupling Load Test Rig

D. CONSOLIDATED TESTING CONCLUSIONS

Contrary to nonpseudoelastic materials with a constant static friction coefficient (μ_f), pseudoelastic NiTi μ_f increases as applied loading increases. This nonconstant μ_f characteristic, a product of the pseudoelastic nature of martensitic NiTi SMA, was discovered during stress induced phase transformation testing of the alloy to produce a large static friction coefficient μ_f [7].²⁰ This characteristic indicates mechanical friction rather than adhesive friction might be dominant without inducing plastic deformation in the SMA. Two geometry states internal to the micro-coupling SMA interference joint take advantage of this characteristic:

- 1) The imperfect geometry of the SMA cylindrical ring and the steel hub may induce pressure points or “hot spots” of localized pressures.
- 2) The design of the micro-coupling places the SMA in compression, possibly inducing buckling modes of the SMA cylinder, in the same manner as a column under excess loading.

These geometry states and μ_f characteristics of pseudoelastic materials lead to a probable situation where buckling induced by compressive extraction of the SMA creates pressure points that exceed the pressure induced phase change threshold of the SMA, forming localized phase changes. These phase changes would further alter the geometry of the SMA cylindrical ring within the interference joint, thereby increasing the normal forces and coupling strength of the joint. The buckling and pressure point geometry change events would continue to cascade and create the nonlinear increase in coupling intensity we see at critical interference values, see Figure 17. All micro-coupling test specimens exhibited an initial static friction peak before transitioning to a kinetic friction state. Subsequent static-to-kinetic friction transitions occurred as coupling strength increased.²¹ Ultimately, a smooth roll off in coupling strength took place due to decreasing interference joint surface area contact as the SMA separated from the steel hub.

²⁰ Extreme pressures can induce a constant temperature SMA phase change.

²¹ These transitions cannot be attributed to the extraction rate or function of the tensile test machine motor as the same transitions were observed during higher extraction rates. Extraction rates used were 1 mm/min and 3 mm/min as explained in Appendix C.

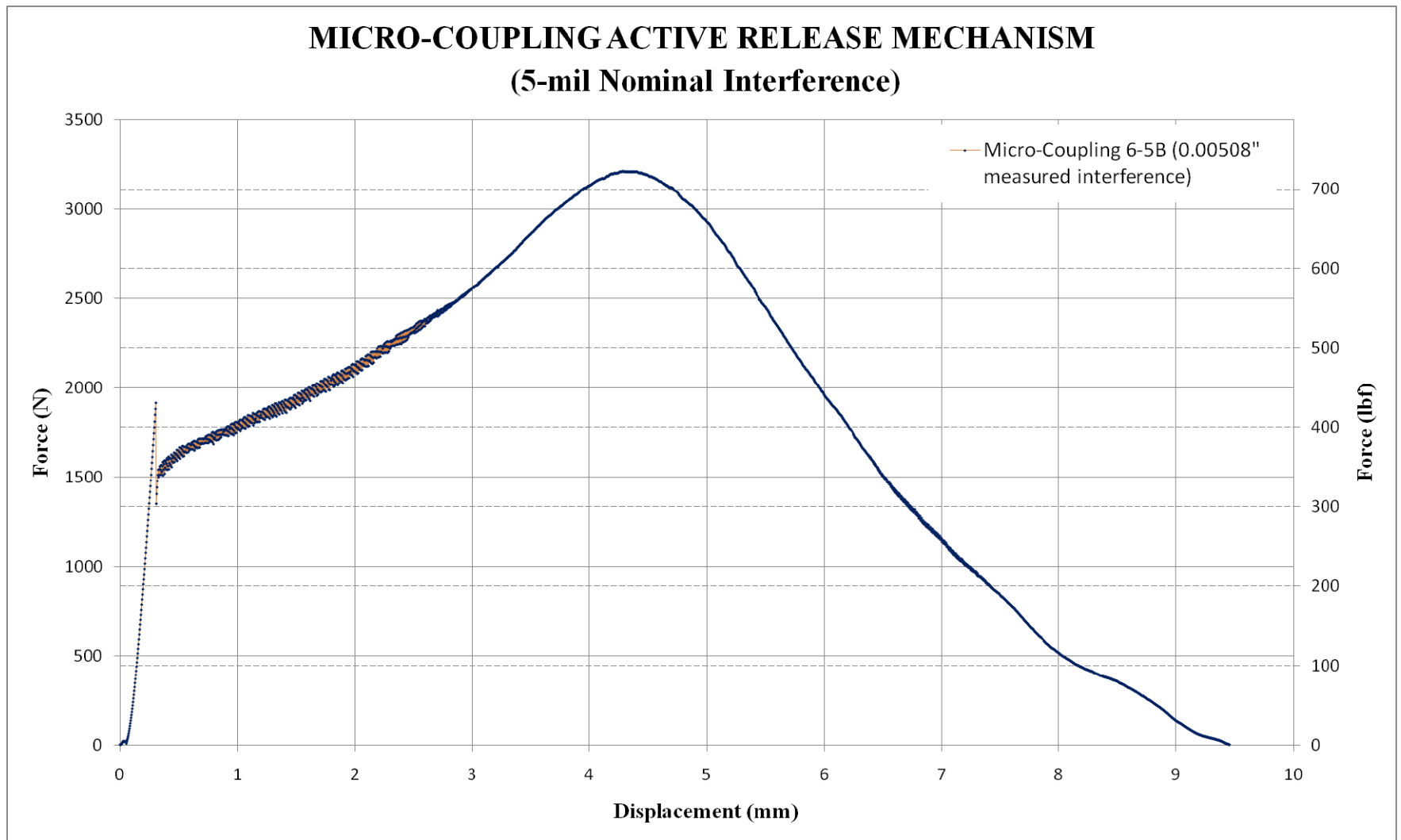


Figure 17. Data Sample from SMA²C Micro-Coupling Load Test

Traditional press-fit equations appear sufficient to predict the initial static friction micro-coupling strength for interferences less than 5 mils,²² but are insufficient to predict micro-coupling ultimate strength (i.e., the maximum extraction force required after overcoming initial static friction). The SMA extraction test results show that the 1 mil and 3 mil interferences yield the best strength-compounding characteristics for the micro-coupling, effectively doubling the predicted strength of the joint, but this characteristic diminishes at the 5 mil interference, see Figure 18. Initial static peak strengths of 140–457 lbf and ultimate strengths of 325–916 lbf were observed. Three mil nominal interference micro-couplings achieved the maximum coupling ability and there appeared to be no difference in the micro-coupling's axial strength dependant on the direction of the press-fit process (i.e., if the SMA cylindrical ring was press-fit into place beginning from the top or bottom of the steel bushing). There was no plastic deformation of the SMA or steel bushing beyond a visible surface texture change. Martensitic de-stressing was approximately 1-mil less than the nominal interference of the micro-coupling.

Post-test inspection of the SMA rings and casehardened steel hubs revealed visible contact spots and scratching down the long axis on the surface of the SMA. The steel hubs were less affected by the process, but did show a loss of surface texturing at SMA contact points. As the tested interference values increased, the contact spots and axial scratches grew in size and quantity, ultimately covering the entire outer circumference of the SMA ring at the tightest interference fit. Test specimens from validation and EDU testing that produced the greatest coupling strengths were examined under magnification, see Figure 19.

²² An example of the micro-coupling's initial static friction coupling strength can be seen just below 2,000 Newton and 1/4 mm displacement in Figure 17.

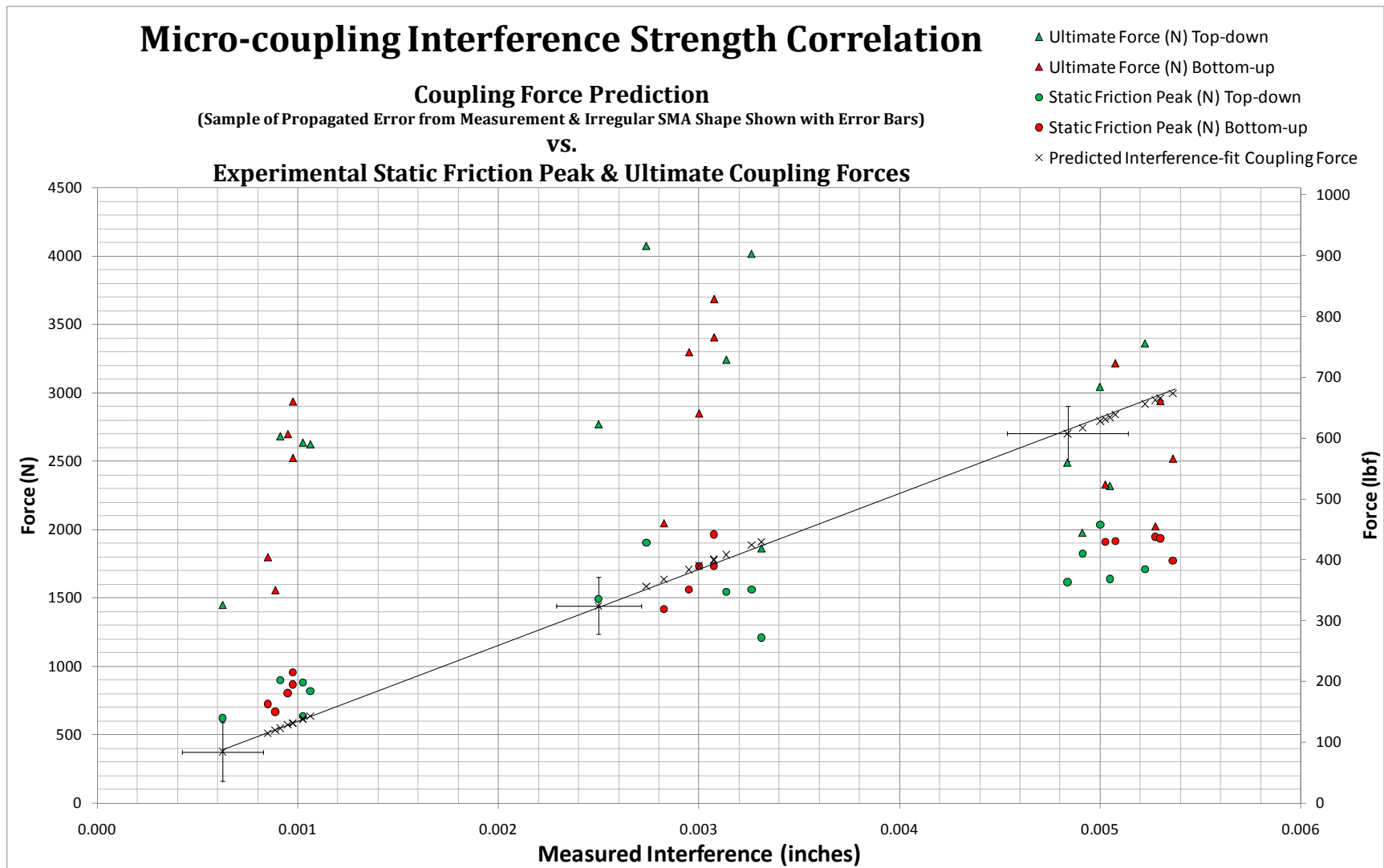
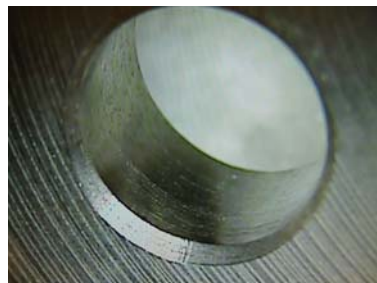


Figure 18. SMA²C Micro-Coupling Initial and Ultimate Strength Test Data with Predicted Strength Values

Validation SMA and Hub



EDU SMA and Hub



Figure 19.1 Test Specimen Samples Before Press-Fit

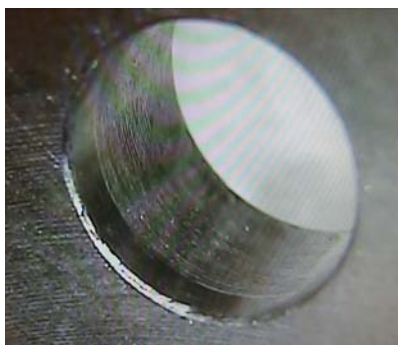


Figure 19.2 Test Specimen Samples After Forced Separation

Figure 19. Surface Features of SMA Micro-Coupling Load Test Specimens

Pseudo-elastic SMA interference joints hold a number of additional variables that traditional interference joints do not. Traditional interference joint strength is not only dependent on the interference pressure, but many other factors such as material hardness, elasticity, surface roughness, interface contaminants, temperature, humidity, and loading rates. All of these factors contribute to the final value of the coefficient of friction. Overall, geometrical accuracy and surface conditions within the interference joint are the two most important factors affecting the coefficient of friction [10]. If this statement holds true, the geometrical nonuniformities of the SMA cylinder may be helping the micro-coupling's ultimate strength.

A second school of thought states that frictional forces originate from two sources: the adhesion force created from the atomic interaction between two surfaces in contact, and the force needed to deform interacting asperities and their wear particles [9]. Choosing a bushing material that would enhance atomic adhesion and eliminate surface oxidation of the press-fit parts could significantly increase the strength of the micro-coupling. Surface oxidation of the casehardened steel, and to a lesser extent the NiTi SMA could significantly lessen the value of μ_f .

Axial surface roughness could be enhanced with etched axial grooves in the steel bushing to increase coupling strength with static friction values of 0.7 being obtainable [7]. However, it should be cautioned that implementing increased surface roughness in this manner, along with a nonideal off axis stress or preload of the SMA interference joint upon release, could cause binding in the micro-coupling mechanism as the SMA edges catch on the etched grooves. Current surface roughness of the interference joint design without modification, using forced compressive removal as a failure mode, still achieves more than adequate strength to be a viable micro-coupling design for many applications.

Uncertainties affecting the analysis of the results include the following, but are beyond the scope of this thesis to resolve:

- 1) Possible inaccuracy in the assumed coefficient of friction between the NiTi SMA and casehardened steel;

- 2) Actual vs. assumed surface area in contact between the SMA and steel hub due to nonideal geometry of press-fit parts for each explored interference;
- 3) The impact of possible SMA phase change due to excess pressures experienced at joint contact points during interference fit assembly or forced SMA removal;
- 4) Surface oxidation of both the SMA and casehardened steel bushing: It is hypothesized that the effect of surface oxidation on the casehardened steel bushing and TiNi SMA cylinder before their assembly into a micro-coupling resulted in inconsistent test data for the first micro-coupling EDU specimens, see Figure 20. Contrary to test specimens that were press-fit immediately following cleaning, a total of 15 days elapsed between cleaning and assembly of these initial samples. Three of the four initial test articles did not exhibit the SMA interference joint strength-compounding characteristic. In contrast, specimen 2B-5 did exhibit the strength-compounding characteristic, but suffered from large magnitude friction slips during forced extraction loading.

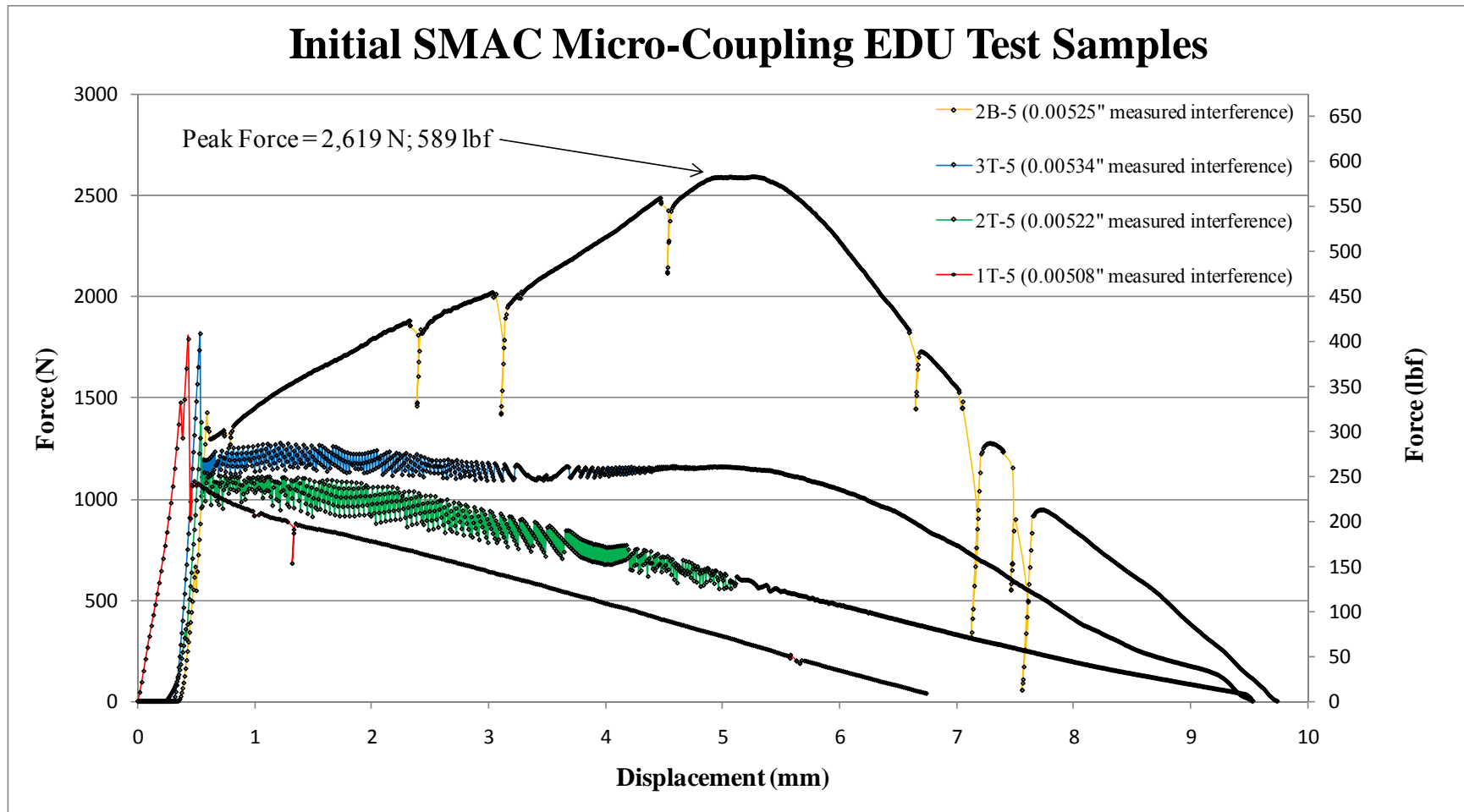


Figure 20. Initial SMA²C Micro-Coupling Specimens Experiencing Possible Effects of Surface Oxidation

THIS PAGE INTENTIONALLY LEFT BLANK

III. SINGLE MOTION ACTUATED SHAPE MEMORY ALLOY COUPLING (SMA²C)

A. ENGINEERING DESIGN UNIT

Nano-satellites need NEAs for the same purposes as those of larger satellites, but do not have equivalent power or volume available to allocate to these actuators. Therefore, successful integration of very small, reliable, low power consumption NEAs may be very useful for nano-satellites that require deployables such as solar arrays or communication antennas. The concept for such a device using the micro-coupling mechanism evolved into an NEA EDU called SMA²C. The SMA²C EDU would enable testing and design refinement to precede a prototype or proto-flight device and ultimate integration into a flight ready nano-satellite bus.

1. SMA²C Micro-Coupling Mechanism Components

In designing SMA²C, the SMA size and alloy properties could remain unchanged as initial micro-coupling development had the intended purpose of creating a micro-coupling for application in space. In addition, previously obtained test data would complement SMA²C EDU testing. The casehardened steel bushings were procured as COTS parts, see Figure 21. Modification of the bushing's outside diameter to measure 9/32" by removal of material using a lathe grinder, allowed for easier integration and assembly of the SMA²C device. Material removal also had the added benefit of reducing the thermal conductivity path to heat the SMA, and press-fit equations predicted only an 18 lbf reduction in the micro-coupling's strength resulting in negligible impact to its intended application. A Kapton foil heater was designed with a resistance of 13 Ohms and a surface area sized to match the length of the SMA cylinder, see Figure 22. The heater would wrap around the steel bushing and connect to the nano-satellite's electrical bus. The heater design objective was to keep the current draw below one ampere and yield a micro-coupling actuation time of less than one minute at worst case temperatures: starting at -45 °C and heating the SMA to 100 °C for complete HTR actuation.



Figure 21. SMA²C Casehardened Steel Busing

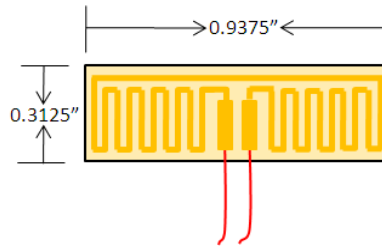


Figure 22. SMA²C EDU Kapton Foil Heater Procured from Tayco Engineering Inc.

Assembly of the SMA cylindrical ring, casehardened steel bushing, and Kapton foil heater creates the SMA²C EDU micro-coupling, see Figure 23. Thermally conductive epoxy, meeting NASA outgassing standards, secures the Kapton foil heater to the steel bushing, see Figure 24. Clamping or crimping methods used to secure the heater were avoided to preclude large conduction losses and the possibility of creating voids or “air bubbles” between the heater and bushing. These voids could forcefully expand in the vacuum of space, possibly resulting in heater damage or produce localized hot spots severe enough to burn out the heater during operation.

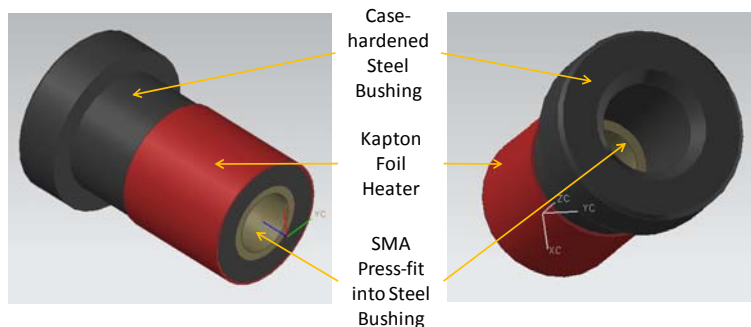


Figure 23. SMA²C EDU Micro-coupling

TRA-BOND 2151

THERMAL CONDUCTIVE ELECTRICAL INSULATING COMPOUND

TRA-BOND 2151 is a thixotropic (smooth paste) heat conductive epoxy system that passes the NASA Outgassing Specification. It is used for staking transistors, diodes, resistors, integrated circuits and other heat-sensitive components to printed circuit boards. This two-part adhesive develops strong, durable, high-impact bonds at room temperature which improve heat transfer while maintaining electrical insulation. TRA-BOND 2151 bonds readily to itself, and to metals, silica, steatite, alumina, sapphire and other ceramics, glass, plastics and many other materials, because its coefficient of thermal expansion provides a good match for those materials over a fairly wide temperature range. Fully cured TRA-BOND 2151 provides excellent resistance to salt solutions, mild acids and alkalis, and many other chemicals including petroleum solvents, lubricating oils, and alcohol. This adhesive complies with the requirements of NASA's Outgassing Specification.

PROPERTY		TYPICAL VALUES
Color		Blue
Specific gravity, mixed		2.300
Viscosity, cps, mixed	rv #7, 10 rpm @ 25°C	40,000
Thixotropic index	(5 rpm/50 rpm)	1.7
Operating temperature range, °C		-70 to 115
Hardness, Shore D		90
Mix ratio, pbw, Resin/Hardener		100/9.5
Thermal conductivity, W/M °K		9.50E-01
Lap shear, alum to alum, psi	2 hours @ 65°C	2,850
	24 hours @ 25°C	2,150
Lap shear, gold to gold, psi	4 hours @ 65°C	880
Glass transition (T _g), °C, ultimate		60.00
Coefficient of expansion, cm/cm/°C		2.60E-05
Impact, izod, ft. lbs/inch of notch		0.49
Tensile strength, psi	30 minutes @ 65°C	7,500
Volume resistivity, ohm-cm @ 25°C		2.10E+15
	ohm-cm @ 75°C	3.20E+13
Reactive solids contents, %		100
Outgassing, NASA		Passes

Figure 24. TRA-Bond 2151 Epoxy Specifications

A 4-40 socket cap screw, made of A286 Super Alloy meeting aerospace material specifications, became the retaining bolt inserted into the micro-coupling, mechanizing its actuation,²³ see Figure 25. Critical dimensions required for sizing of the retaining bolt were the head and shaft diameters. The head diameter had to be small enough to pass through the steel bushing yet large enough to catch over half of the SMA cylinder's top face within the interference joint. The shaft diameter had to be small enough to allow unconstrained recovery of the SMA cylindrical ring upon activation, yet strong enough to withstand the ultimate holding strength of the micro-coupling.

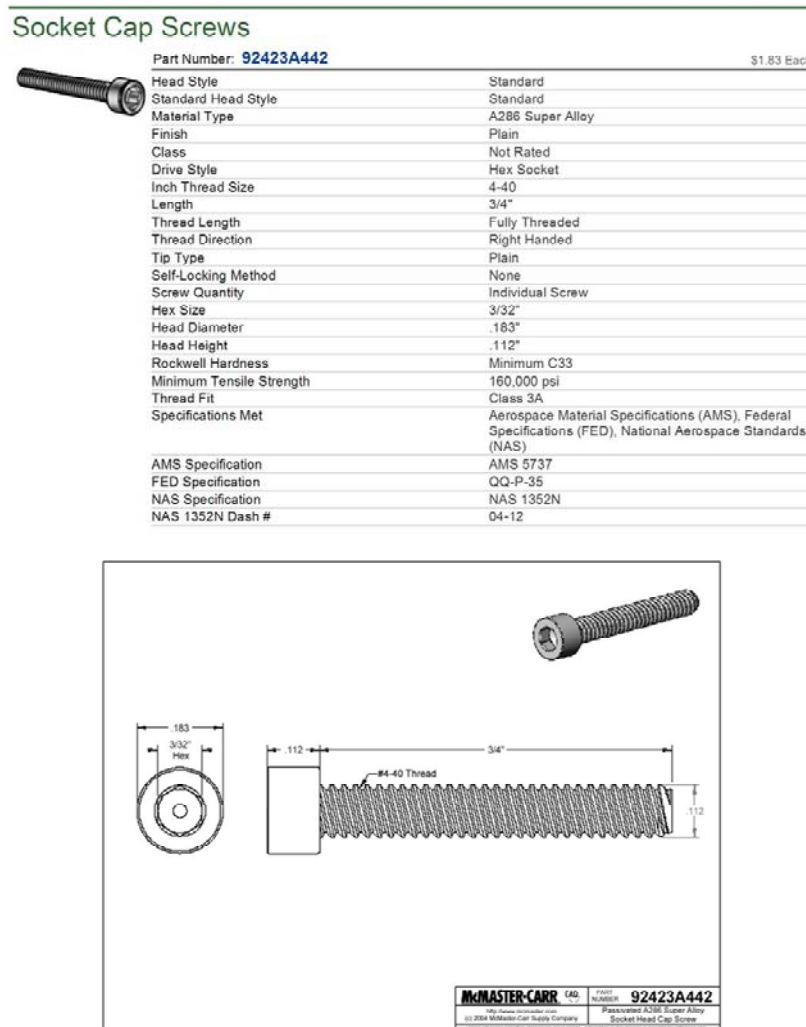


Figure 25. SMA²C EDU Micro-Coupling Retaining Bolt

²³ Mechanization as noted here is the process by which the SMA interference joint is made into a functioning mechanism, where a mechanism is a machine or part of a machine that performs a specific task.

2. SMA²C Device Design

The SMA²C device uses the micro-coupling mechanism with additional components to integrate into a host satellite, see Figure 26. The device's housing holds the micro-coupling and is designed to meet structural and volume requirements particular to the micro-coupling's placement within the host satellite. The SMA²C housing can take many forms and could even be integrated into the nano-satellite's own structure. The generic design of the SMA²C EDU encased the entire micro-coupling in 7075 T7351 aluminum, using NASA specifications [16], to enable structural continuity, and if mounted on the exterior of the satellite with appropriate application of paint or multi-layer insulation, prevent unintentional actuation of the micro-coupling from solar heating. In addition, the SMA²C EDU design enabled easy mounting for vibration testing and possible integration as a proto-flight subsystem. Thermally isolating the micro-coupling from the housing is of great importance because heat lost to the housing by thermal conduction would increase power requirements or even preclude SMA²C actuation. The generic design of the SMA²C EDU uses a Ultem 1000 polyetherimide washer to secure the micro-coupling in place and thermally isolate the micro-coupling from the aluminum housing. If desired, addition of a thermally resistive epoxy during installation of the polyetherimide washer would increase the EDU's rigidity and vibration tolerance. A spring sized to fit around the SMA²C micro-coupling attaches a pusher plate to the housing. This puts a small preload of approximately one-and-a-half pounds of force on the micro-coupling to aid in separation of the SMA and retaining bolt.

The micro-coupling mechanism assembled with the above described hardware (i.e., housing, thermal epoxy, polyetherimide thermal isolation washer, spring, and pusher plate), comprises the SMA²C device, see Figure 27. Photos of the SMA²C device EDU hardware and assembled test unit can be seen in Figure 28. Actuation of the assembled SMA²C device initiates by applying voltage across the Kapton foil heater's leads. The electrically resistive heater heats the steel bushing holding the SMA cylindrical ring. Once the SMA reaches HTR temperature, via thermal conduction through the steel bushing, the SMA shrinks and releases itself from the interference joint along with the holding bolt, see Figure 29.

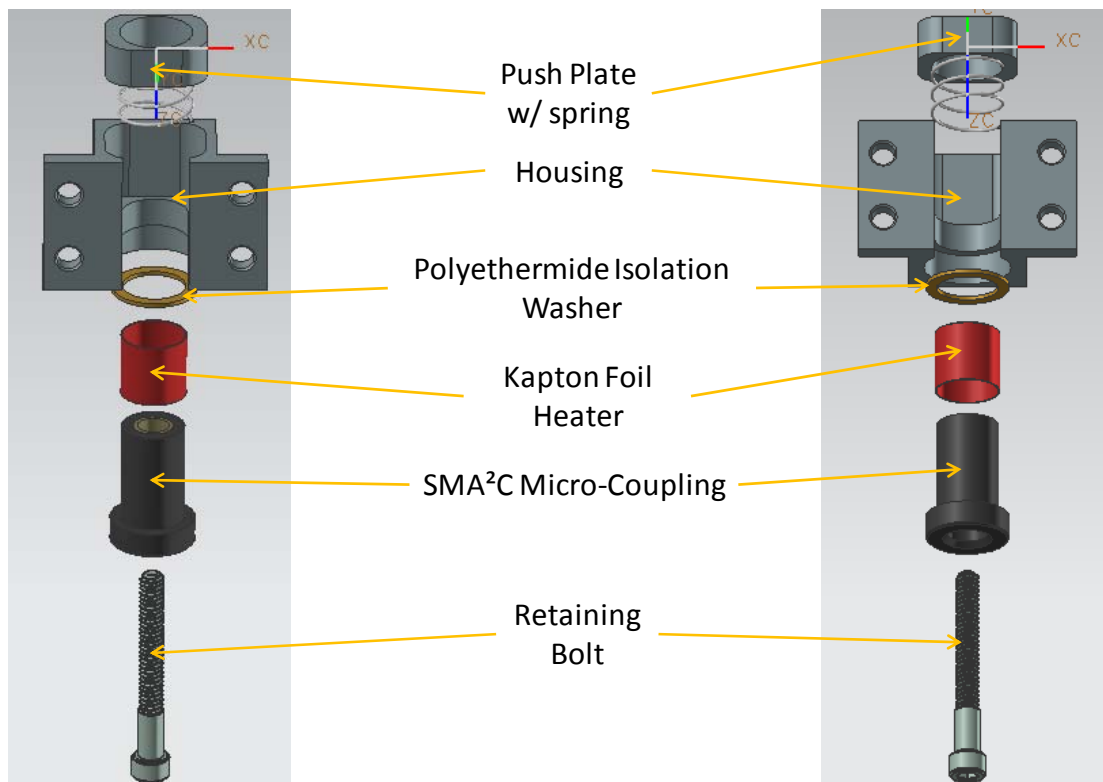


Figure 26. Component View of the SMA²C Device

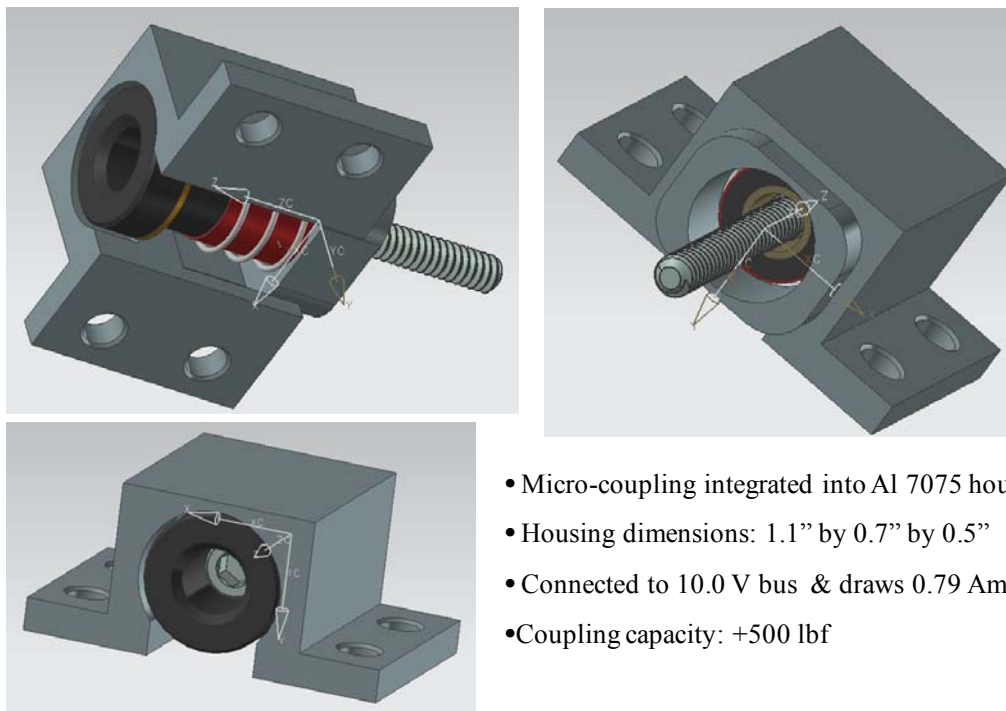


Figure 27. Assembled Views of the SMA²C Device

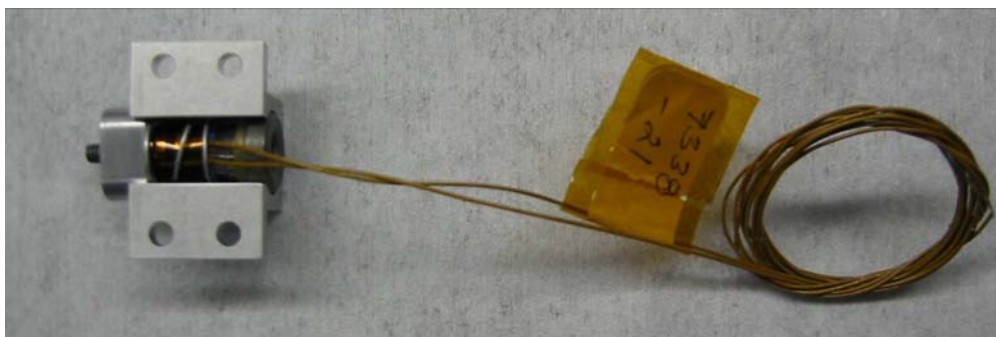


Figure 28. SMA²C Device EDU Hardware and Assembled Test Unit

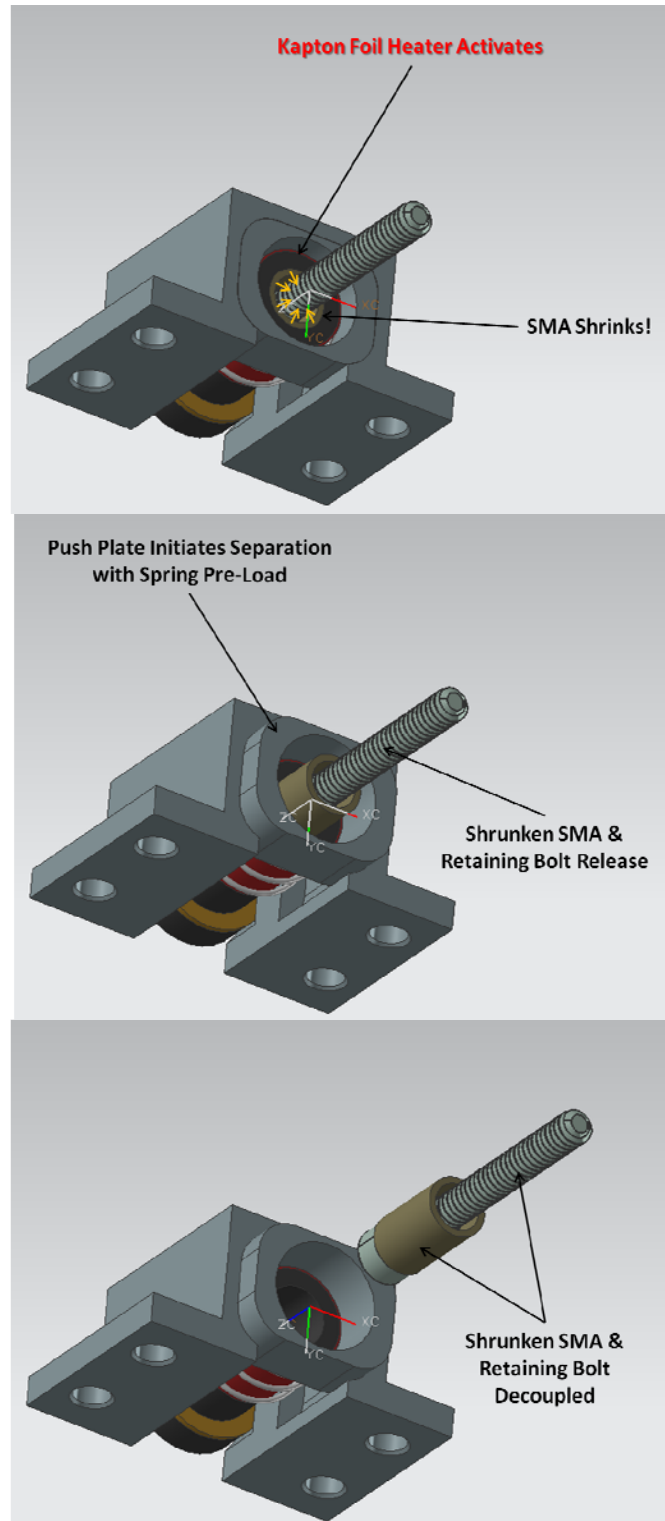


Figure 29. SMA²C Device Actuation Sequence

B. INTEGRATION OF THE SMA²C DEVICE INTO A NANO-SATELLITE

Preliminary investigation for implementing the SMA²C device included studying the integration of the EDU as a sub-system on a nano-satellite under development in the NACL known as the Tactical Imaging Nano-satellite Yielding Small-Cost Operations and Persistent Earth-coverage (TINYSCOPE). Actuation of the SMA²C device on orbit would deploy TINYSCOPE's solar arrays. Parameters explored included: TINYSCOPE solar array configuration with integration of the SMA²C device into TINYSCOPE's electrical power system (EPS), testing to determine the power required for successful actuation of the SMA²C micro-coupling, and integration of the SMA²C device into TINYSCOPE's power management plan.

1. TINYSCOPE Mission Overview

The mission of TINYSCOPE is to provide tactical imagery directly to war fighters using a small, relatively inexpensive nano-satellite, see Figure 30. Space-based imagers with high-resolution imagery are not readily available to small tactical units, as these field units do not generally require high-resolution imagery. Tactical units would however benefit from frequent access to lower resolution imagery. A constellation of TINYSCOPE satellites could provide near real-time quality imagery to its users.

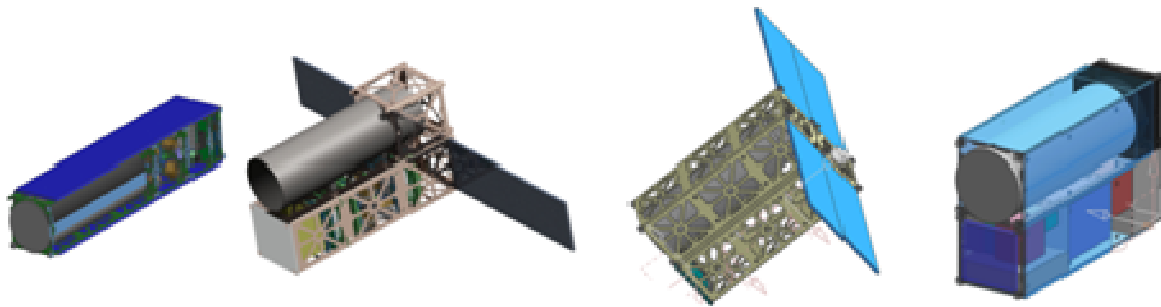


Figure 30. NPS TINYSCOPE Configurations

2. TINYSCOPE Electrical Power System Overview

Design constraints for TINYSCOPE include limited mass, volume, and power generation capabilities.²⁴ Power collection potential for CubeSat class satellites is limited due to their solar array size, lack of deployed array gimbals, or the small volume heat sink available to body mounted arrays affecting solar cell efficiency. TINYSCOPE's current configuration, using nongimbaled, deployed solar arrays and a nadir pointing payload, defines its power profile to be in a sun-soak orientation at all times other than when it is in an active imaging period or in eclipse.²⁵ Power storage potential is limited for TINYSCOPE's batteries due to reduced surface area availability for thermal dissipation. The EPS model for TINYSCOPE is predicated on a single orbit energy balance equation as simulated by a power equivalent circuit [17], see Figure 31. In this equation, the power collected during the satellite's daylight period provides all the power necessary to supply the loads during this period as well as fully charge the batteries from their use during eclipse, factoring in efficiencies in solar cells, electrical transmission, battery charge and discharge, and bus voltage conversion into a balanced cycle for each orbit.

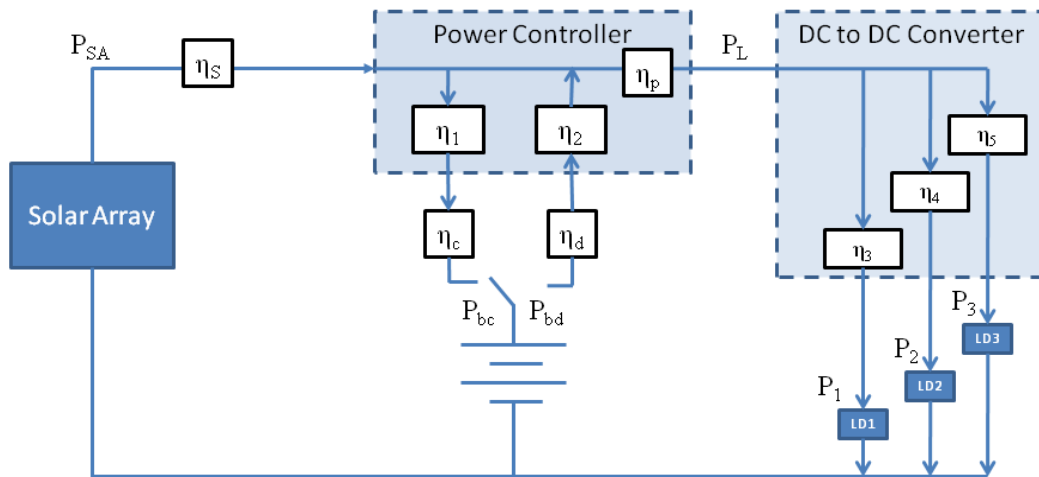


Figure 31. TINYSCOPE's Power Equivalent Circuit. From [17].

²⁴ TINYSCOPE is a six unit (6-U) CubeSat with 60 cm³ volume and 6 kg weight restrictions.

²⁵ Sun-soak orientation implies satellite positioning to drive the sun's angle of incidence on the solar arrays to zero.

TINYSCOPE's two larger sides of its six-cube configuration limit the size of the single fold deployment of its two arrays. The matured design has holes in the arrays to allow sun sensor and star tracker operation in contingency operations in the event the solar arrays do not deploy, see Figure 32. The absolute outer dimensions of the plus and minus X faces are 21.35 cm in width and 34.6 cm in height resulting in a total surface area for each solar array face of approximately 740 cm^2 ; doubling this for each array results in $1,480 \text{ cm}^2$.²⁶ A reduction in each solar panel's area occurs because of the openings required by the star tracker on the +X face and the sun sensor on the -X face, yielding approximately $1,450 \text{ cm}^2$. Adding cells on the -Z face with brings the total surface area available to place solar cells equal to about $1,650 \text{ cm}^2$.

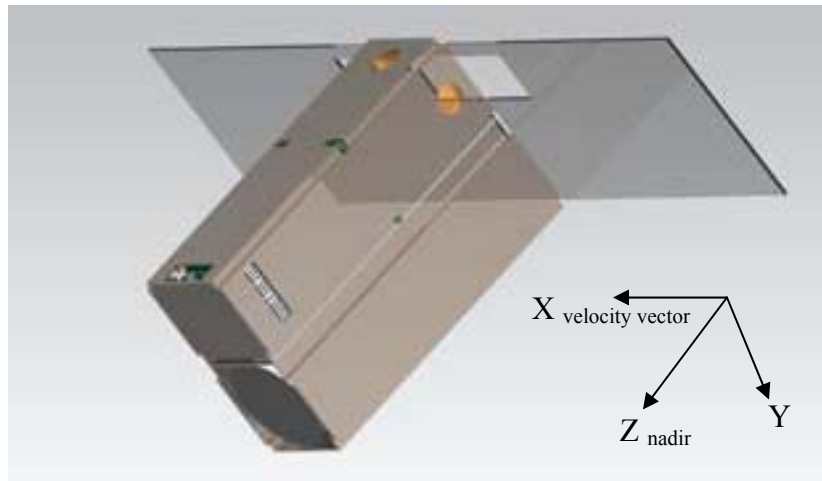


Figure 32. TINYSCOPE Structural Design

SMA²C device integration began with selection of Emcore's ATJM photovoltaic multi-junction cell for TINYSCOPE with an adjusted efficiency of 20.6%. The number of 30cm^2 solar cells required in series is determined by the level of voltage required by the power management system. The number of parallel strings of cells in series is dependent upon the overall current requirement of the entire satellite. Using a conservative packing factor of 80% to model the arrays, net current and voltage required by Simulink modeling using TINYSCOPE's Power Equivalent Circuit equaled 1.61

²⁶ The exact CubeSat form factor of 10 cm^3 is not used because the optic aperture uses the available space within the CubeSat launcher between the launch rails. This form factor results in the nonstandard dimensions of the solar arrays.

Amps and 17.3 Volts, respectively [17]. This requires a minimum of nine cells in series and four parallel strings, totaling 36 cells. The maximum number of cells with optimal redundancy would be laid out two strings per solar array panel. Another single string covering the -Z face and additional space on the solar panels would yield five strings of nine cells, see Figure 33. This configuration results in an optimal power output of approximately 31.4 Watts. In the contingency of a solar panel not deploying, the fifth string spanning both array panels and a portion of the -Z face would have to be isolated so as not to impact the other cell strings connected in parallel. TINYScope's current design uses the Ocean Server integrated battery and power control system operating on 14.4 Volt lithium-ion batteries, specially designed to work with the power control system, with a four series, three parallel configuration [17]. The 12-cell battery pack provides 6.6 Amp-hours or 95 Watt-hours of capacity supplying a 12 Volt primary and 5 Volt secondary electrical bus.

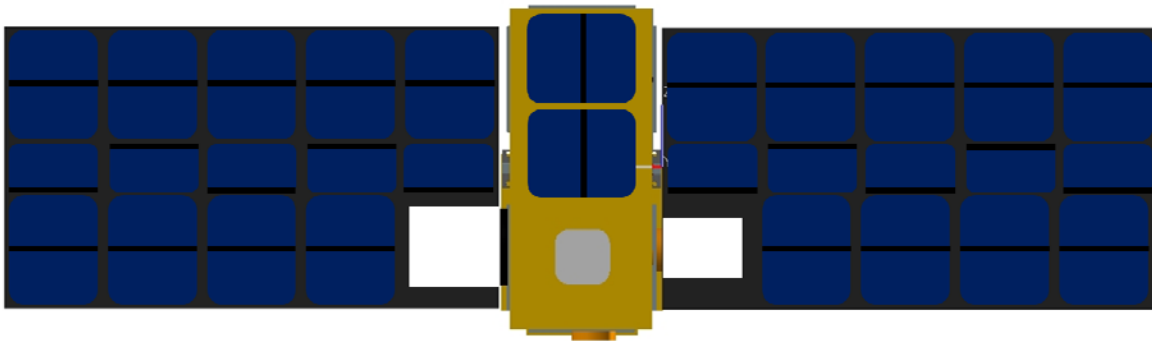


Figure 33. TINYScope Solar Array Design for SMA²C Device Integration

3. SMA²C Device Positioning for TINYScope

Placement of the SMA²C device on the nadir (+Z) side of the TINYScope bus opposing the solar array panel hinges enables deployment of both solar arrays. The SMA²C device can retain its EDU design and use 4-40 socket cap screws (not shown) to attach to TINYScope's structural bus, see Figure 34. The solar array panels have a torsion spring installed at their -Z hinge points that would apply a preload to the SMA²C device, so use of the pusher plate and spring may not be required for SMA²C integration into TINYScope.

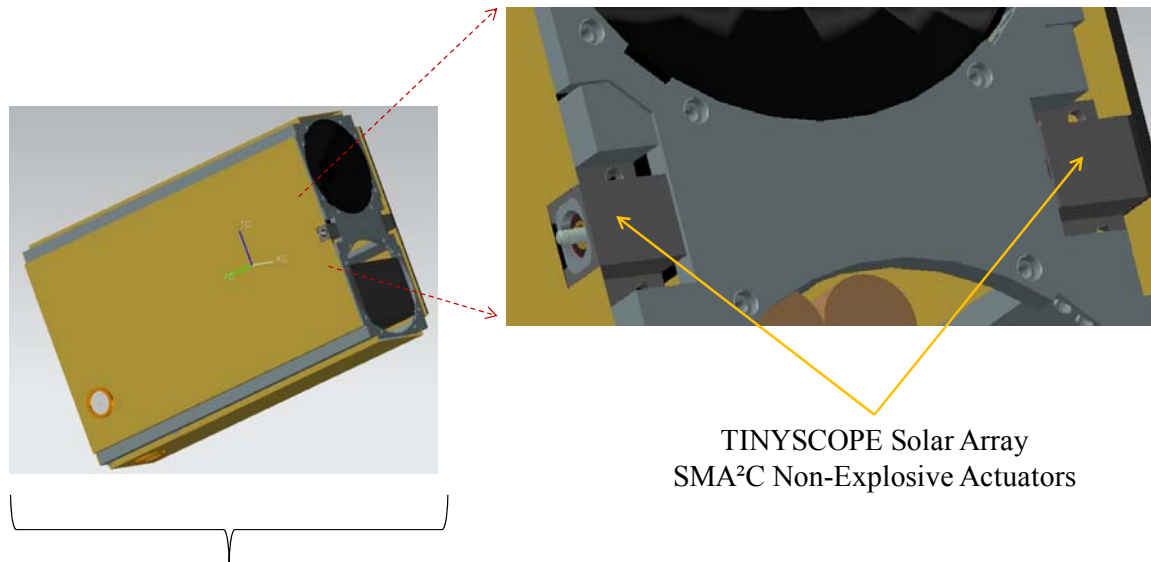


Figure 34. SMA²C Device Placement in TINYScope

Electrical connection of SMA²C is accomplished by connecting the Kapton foil heater leads directly to TINYScope's primary 12 Volt bus via an interconnect that switches power to the leads upon command. TINYScope's command and control unit initiates power to the SMA²C device while a micro-switch or single photovoltaic cell mounted under each stowed solar panel controls when to terminate power to the device. The micro-switch would show open upon solar array deployment or the light sensitive cell would be exposed to sunlight and command the interconnect supplying power to the SMA²C device to turn off. As a contingency, a preprogrammed maximum time required for SMA²C applied power would reside in a countdown timer that would discontinue power in the event of SMA²C failure. The countdown timer would avoid draining the batteries below maximum depth of discharge in the event of an array deployment malfunction. Solar array deployment sequencing follows SMA²C actuation as seen in Figure 35.²⁷

²⁷ Holes in the solar arrays for contingency operation of the sun sensor and star tracker are not shown in this figure.

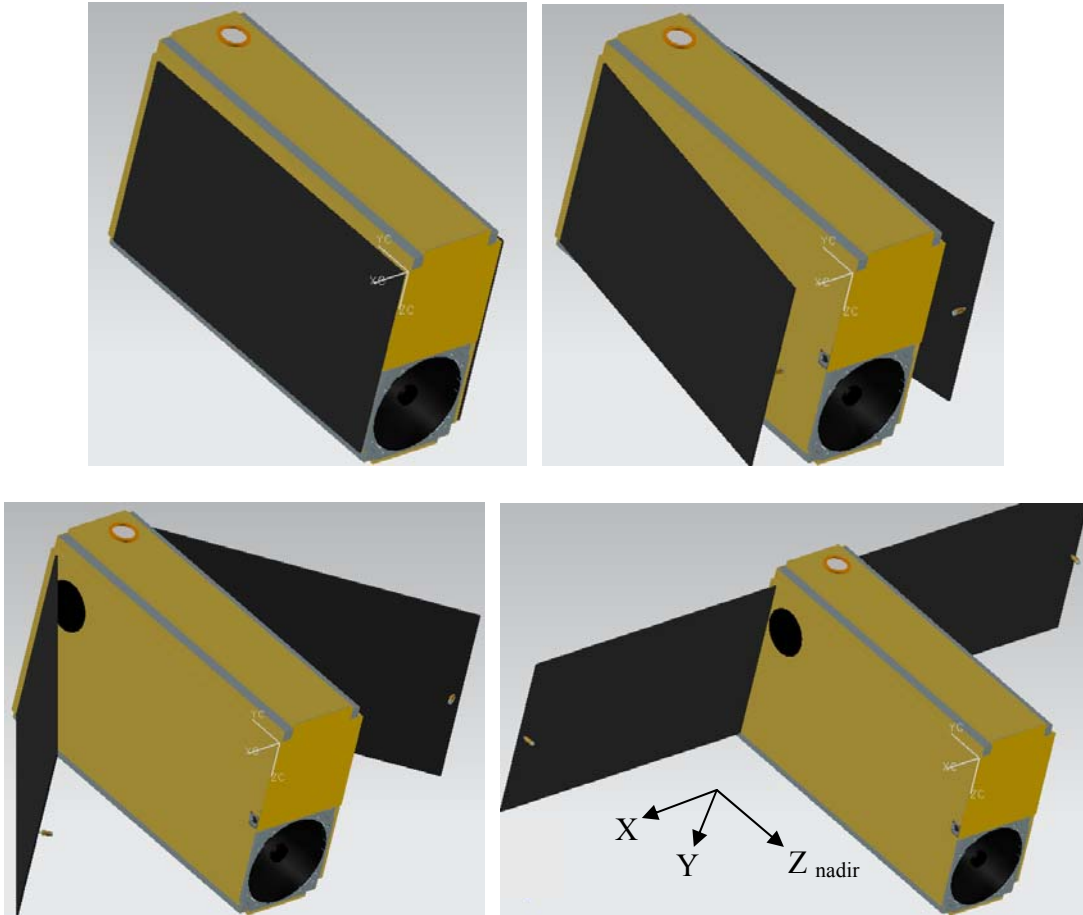


Figure 35. SMA²C Deployment of TINYSCOPE's Solar Arrays

4. Estimating SMA²C Power Requirements for TINYSCOPE

The SMA micro-coupling is at the heart of the SMA²C device, and the micro-coupling is activated by an increase in temperature; therefore, thermal interactions between the SMA²C housing and the micro-coupling it contains must be understood. The power required to bring the micro-coupling mechanism to HTR activation temperature is divided into two parts:

- 1) The power required to warm-up the micro-coupling to HTR temperature
- 2) The power necessary to overcome steady state conductive and radiation losses.²⁸

The sum of these two power requirements result in the total requisite power for SMA²C device actuation.

Power consumption estimates for the SMA²C device used a white paper published by MINCO on etched-foil heater power requirements [15]. Inserted in the following text are boxed excerpts from the white paper on conduction losses, radiation losses, and warm-up requirements. Appendices E and F show the associated calculation spreadsheets.

Conduction Losses: Area of conduction from the micro-coupling to the aluminum housing includes the under-side of the steel bushing's brim about its circumference, see Figure 23. The conductive loss path is through the polyetherimide washer under the bushing's brim. Conductive loss also occurs at the contact area between the retaining bolt and SMA cylindrical ring. Calculations assumed environmental conditions with a starting temperature of -45 °C and a finish temperature of 100 °C.

Conduction losses: Losses due to heat conduction through mounting hardware, insulation, and other material in contact with the heated part. Calculate separately for each conductive path.

Given the following:

K = Thermal conductivity of material from Table 1 (BTU•in/ft²/°F/hr)

A = Cross sectional area of material (ft²)

T_f = Heat sink temperature (°F)

T_a = Ambient temperature (°F)

L = Thickness of insulation = Length of conductive path (in)

$$P_{cd} = \text{Conduction loss (W)} = \frac{KA(T_f - T_a)}{3.412 L}$$

Steady state conductive losses resulted in a 3.445 Watt power requirement.

²⁸ The vacuum of space negates convection losses.

Radiation Losses: The entire exterior surface area of the steel bushing is subject to radiation losses.

Radiation Losses: Losses due to radiant transfer from the heat sink to surroundings. Ignore insulated surfaces.

Given the following:

ϵ = Emissivity of heat sink surface from Table 2

A = Area of exposed surface (ft²)

T_{fr} = Final absolute temperature (°R=°F+ 460)

T_{ar} = Absolute ambient temperature (°R=°F + 460)

$$P_r = \text{Radiation loss (W)} = \frac{\epsilon A (0.1713 \times 10^{-8}) (T_{fr}^4 - T_{ar}^4)}{3.412}$$

Steady state radiation losses resulted in a 0.388 Watt power requirement.

Warm-Up Power Required: An initial and ambient temperature equal to -45 °C was used to calculate the warm-up coefficient relating steady state losses to ambient temperature.

Calculate warm-up requirements. Calculate the power needed to bring the heat sink to temperature in the desired time.

Given the following:

m = Mass of material (lb)

C_p = Specific heat of material from Table 1 (BTU/lb/°F)

T_f = Final temperature of heat sink (°F)

T_i = Initial temperature of heat sink (°F)

T_a = Ambient temperature (°F)

t = Desired warm-up time (hr)

P_{sl} = Steady state loss (W) = $P_{cd} + P_r + P_{cv}$

$$H_w = \text{Warmup coefficient} = \frac{P_{sl}}{(T_f - T_a)}$$

$$P_w = \text{Warmup power (W)} = \frac{H_w (T_f - T_i)}{1 - \exp\left(\frac{-3.412 H_w t}{m C_p}\right)} + H_w (T_i - T_a)$$

A desired warm-up time of one minute resulted in a 7.324 Watt power requirement.

The measured resistance of the SMA²C's heater as procured from Tayco Inc. was 12.6 Ohms. Once attached to a 12 Volt bus, the Kapton foil resistive heater draws 0.952 Amps. Its available power at this voltage level is equal to 11.43 Watts. Taking this value and dividing the summed values of required warm-up power and steady state losses with a 10% margin over one minute equals 12.27 Watts, yielding an activation time of 64 seconds.²⁹

5. SMA²C Actuation Power Consumption Test

Objective: Determine the activation time and subsequent power consumption of the SMA²C device in a vacuum at laboratory temperatures.

Application: Integration of the SMA²C device EDU into TINYScope requires actual power consumption values for the NEA. These test values will determine what changes to the EDU need to transpire for a subsequent proto-flight SMA²C device design.

Test Description: Assembly of the SMA²C device EDU was as described in Section III Part A2 with the addition of a T-type thermocouple attached to the outer surface of the steel bushing just above the Kapton heater and below the polyetherimide ring. As shown in Figure 36, the device was then bolted to a one-foot long box aluminum bar with four 4-40 hex bolts. An additional 4-40 A286 Super Alloy socket cap screw dropped through the SMA²C device and secured in place with a nut and washer until the pusher plate was fully compressed. The measured preload force imparted by the pusher plate when fully compressed equaled 1.55 lbf. Power and thermocouple wires were ported through an access hole in the aluminum bar just under the SMA²C device in the same manner as intended for mounting on a nano-satellite. The aluminum bar and SMA²C device were placed inside a vacuum tube enclosure with electrical leads soldered to a multi-port electrical interface and thermocouple wires run across the o-ring and sealed with clay. An Omega HH147U type digital thermometer connected to the

²⁹ See Appendix E for calculations spreadsheet.

thermocouple and ported temperature data to a laptop for recording. The measured resistance across the wire leads connected to the HP E3615A power source equaled 12.6 Ohms.³⁰

The SMA²C device was supplied by a constant 10.0 Volt power source, not 12.0 Volts as if on TINYScope's primary electrical bus, because the Kapton heater's 30-gauge lead wires had a maximum current limit of 0.86 Amps.³¹ This change, along with a laboratory starting temperature of 18.7 °C, resulted in a predicted SMA²C actuation time of 61 seconds.³² A vacuum was drawn on the EDU equal to 29.5 in Hg. Then, the test setup was allowed to stabilize at room temperature after the associated temperature drop of approximately 1 degree Celsius. A video camera was set to record the test and any amperage change on the constant voltage power supply's digital readout. The test initiated with activation of the power supply, while the laptop computer recorded the SMA²C device's steel bushing temperature.

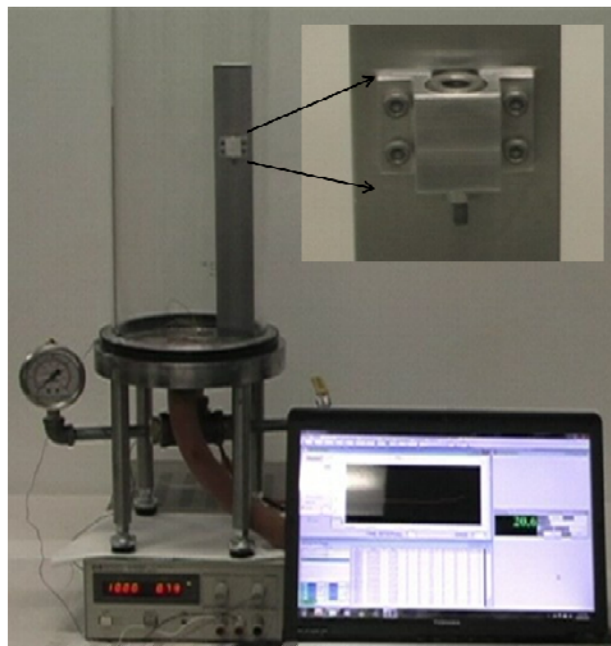


Figure 36. EDU SMA²C Device Actuation Power Consumption Test Bench

³⁰ The bias in the thermometer was measured at 0.2Ω.

³¹ The SMA²C EDU's design intended to connect to a 5.0 Volt bus; therefore, procurement of the Kapton heater had 30 gauge lead wires to accommodate tight assembly tolerances for device integration.

³² See Appendix F for calculations spreadsheet.

Test Results: The EDU SMA²C device decoupled after 80 seconds of applied power indicated by the SMA cylindrical ring, retaining bolt, washer, and nut dropping free to the bottom of the vacuum chamber. Total power consumed with an average draw of 7.74 Watts over the 80 seconds equaled 10.32 Watt-seconds or 0.172 Watt-hours, see Figure 37. The test proceeded as expected noting a slight sticking of the pusher plate upon release that lasted less than one second. Graphite lubrication of the outer rim of the pusher should circumvent this minor problem in future tests.

Test Conclusions: Additional conductive losses not accounted for in the analytical calculations could have contributed to the difference between the predicted 61 second actuation time and the 80 second actual actuation time. Recommendations to improve actuation time include using a larger gauge wire for the Kapton foil heater allowing a higher actuation voltage and current. Another improvement would be to reduce the size of the micro-coupling to match more closely the required holding force for TINYScope arrays, resulting in a more power efficient SMA²C device.

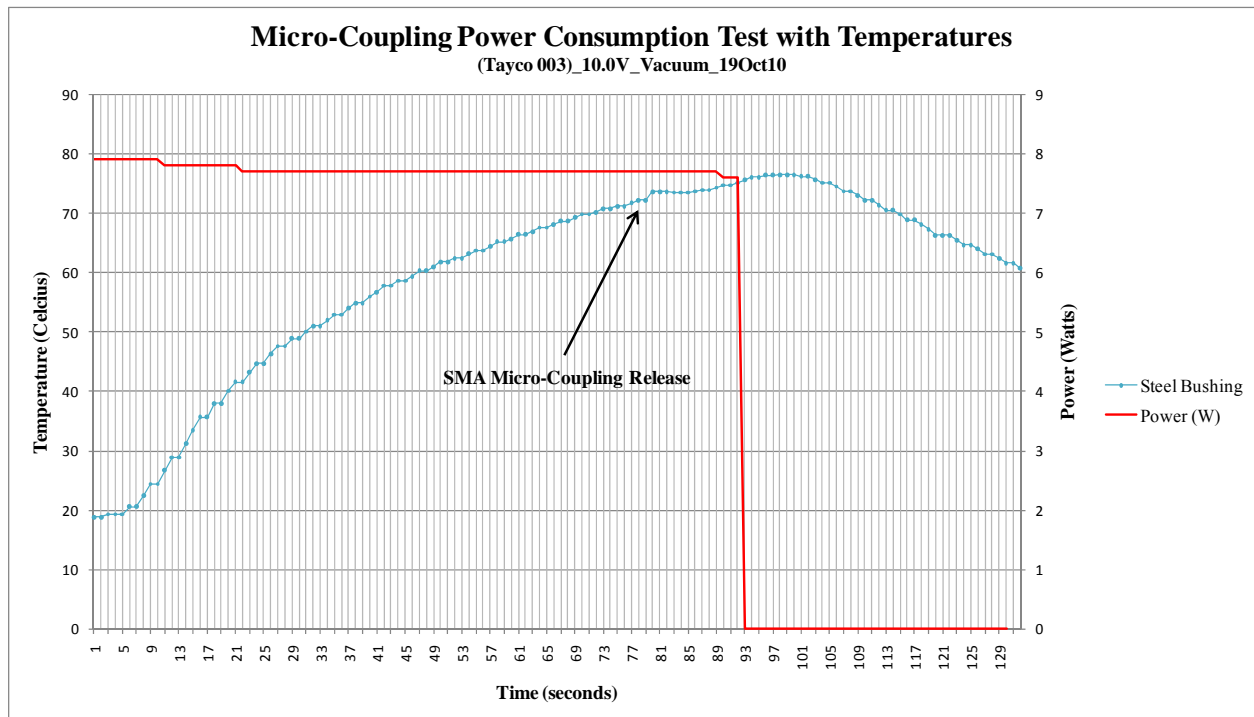


Figure 37. EDU SMA²C Device Actuation Temperatures and Power Consumption Data

6. Integrating SMA²C Into TINYScope's Power Plan

The primary function of TINYScope's solar arrays prior to their deployment is to recharge the batteries to full capacity, before attempting array deployment and prior to turning on the payload or any nonessential systems. Activation of SMA²C during this power critical phase should have the objective of using excess power available and not draw power from the charging batteries. Since the arrays have yet to deploy, only one panel can be oriented perpendicular to the sun vector. The batteries will charge if power from the single stowed solar array, properly oriented toward the sun, is greater than the power required by TINYScope in its pre-mission capable stowed configuration. A single exposed array's surface area is approximately 740 cm² using the worst case +X side with the larger hole allowing access to the star tracker. This panel will hold two strings of cells providing the proper bus voltage,³³ but at a reduced current of 0.9 Amps. This reduced amperage equates to a best-case 15.7 Watts power output from a single panel. The power required by TINYScope before array deployment is as follows [17]:

- C&DH, ADCS controller, IMU, star tracker, GPS, and sun sensor = 3.43 Watts
- Three reaction wheels at orientation/stabilization slew rate = 1.2 Watts
- Transceiver in sleep mode = 0.012 Watts
- Thermal control heaters on to prevent damage to the payload = 2.50 Watts

The total stowed configuration power requirements are 7.14 Watts leaving an excess of approximately 8.56 Watts to charge the battery or activate SMA²C. As generated power will be greater than consumed power, overall charge of the batteries will increase and allow TINYScope to recover from its eclipse period before solar array deployment.

An imposed integration constraint of SMA²C's actuation on TINYScope is avoiding any battery discharge before solar array deployment to preclude exacerbating a possible power critical situation. SMA²C's power draw on the 12 Volt primary electrical bus would be 11.43 Watts, in excess of the 8.56 Watts available. Although

³³ Supplied voltage is 17.3 Volts for the 12 Volt primary bus. The excess voltage margin is to ensure charging of the batteries as they will not charge below 12 Volts.

TINYSCOPE's EPS could supply this load, there would be a drain on the batteries when SMA²C was active.³⁴ A 10 Volt bus SMA²C actuation time of 93 seconds with a current draw of 0.79 Amps is within available daylight orbit time and available stowed configuration amperage for a single orbit.³⁵ SMA²C's power consumption of 7.9 Watts on a 10 Volt bus would be acceptable if conducted while TINYSCOPE was exposed to sunlight, leaving an excess of 0.6 Watts ensuring no battery charge is lost during SMA²C actuation; therefore, it is recommended that SMA²C be connected to a 10 Volt bus.

The above stowed array configuration power analysis assumed that TINYSCOPE had enough stored power upon reaching orbit to bring essential systems online and slew the spacecraft to a proper charging orientation. Further modeling should be conducted to plan for the possibility of an uncontrolled tumble of TINYSCOPE to better understand if a stowed array configuration would result in sufficient battery charging to maintain the 3.6 Watt-hours required to sustain minimum system function through eclipse. Initiation of the SMA²C device should not occur until essential TINYSCOPE stowed configuration systems are online and the ADCS can achieve the optimal (oriented) single solar panel production of 15.7 Watts.

³⁴ SMA²C connected to a 12 Volt electrical bus would draw 0.95 Amps and be in excess of the power supplied by a single solar panel. This situation is not desirable to ensure targeted battery depth of discharge is not exceeded and available battery charge/discharge cycles are not reduced.

³⁵ TINYSCOPE's designed sun-synchronous orbit insertion altitude is 500 km resulting in a 94.6 minute orbit with a 33 minute period of eclipse. Battery charge levels increase with the approximately 60 minute excess sunlight exposure time per orbit.

THIS PAGE INTENTIONALLY LEFT BLANK

IV. CONCLUSIONS AND RECOMMENDATIONS

A. SMA MICRO-COUPLING

The SMA micro-coupling shows great promise as a new type of zero-shock NEA. The present application of the invention relates generally to actively commanded release mechanisms that are secure under extreme forces, yet will reliably actuate to deploy or release connected parts of a device or machine when commanded. The constraints of small size, low operating power, and zero-shock actuation for many design situations make several existing actuators impracticable due both to their complexity and inability to scale to the size required. The SMA micro-coupling release mechanism presented in this thesis remains secure under extreme forces, actuates reliably when commanded to decouple, and has small size so as not to impede integration. Its characteristics of small mass and operating power adds versatility to the coupling device, allowing for a wider range of latch or fastener applications. In addition, the scale of the mechanism need not be limited to the micro class, but scaled up in size to meet many coupling needs. These features make the proposed mechanism useful for many applications in system design such as safety devices, tamper locks, robotics, aeronautics, military, and spacecraft systems.

1. Synopsis

NiTi SMA rings used in modern aeronautical clamping applications typically remain in an austenitic or memory shape for most of their useful design life after installation. The utility of SMA's more ductile martensitic phase, as explored in the medical field for wear durability, is also useful for a zero-shock NEA micro-coupling. The micro-coupling, made of a NiTi SMA cylindrical ring press-fit in its detwinned martensitic phase into a steel bushing, creates an interference joint. This joint can be subsequently decoupled upon command by heating the SMA into its smaller austenitic shape thereby freeing itself from the interference joint. The micro-coupling's size can be engineered to a form factor of approximately 1 cm^3 and achieve coupling strengths in excess of 4,000 N (900 lbf). While the micro-coupling's characteristics are desirable for

many applications, its small size and high strength are particularly relevant to nano-satellite design. The micro-coupling's small size results in a low actuation power requirement, and its design of very few parts with a simple single motion actuation minimizes the possible number of failure modes.

2. Future Work

This section lays out work that can be done to improve our theoretical understanding of the SMA micro-coupling's holding strength and to better know its operating characteristics. Several areas of interest are discussed, including the coefficient of friction between the SMA cylinder and hub, SMA pseudo-elastic properties within an interference joint, geometry design changes for an SMA interference joint, micro-coupling material selection, and the effects of aging on the SMA micro-coupling.

Coefficient of friction: Predicting the strength of the SMA interference joint is dependent on an accurate estimate of the coefficient of friction between the SMA cylinder and hub material interface. The press-fit process, environment, and material condition of the micro-coupling's parts require strict control in order to eliminate variability in the coefficient of friction for characterization of the SMA interference joint.³⁶ Manufacture and implementation of the micro-coupling mechanism in commercial applications necessitates an accurate coefficient of friction or a large enough sample of tested mechanisms to predict empirically the coupling strength.

Investigation of SMA pseudo-elastic properties within an interference joint: Analytical methods for accurately predicting the micro-coupling's strength should be investigated by determining the unique characteristics of SMA within an interference joint. The hypothesis of SMA pressure induced phase changes within the interference joint acting as a contributing factor to the strength of the micro-coupling requires validation. Understanding material interactions between the SMA shaft and hub at extreme pressures will lead to more predictable micro-coupling behavior and further methods of design and assembly to refine the micro-coupling's desirable characteristics.

³⁶ Controls for testing completed in this thesis were exacting, but need further refinement for extracting evidence to isolate variables to be controlled in design and assembly of the micro-coupling.

SMA cylindrical ring geometry impacts: Design of the SMA cylindrical ring, as manufactured for the SMA²C EDU, strived to achieve the smallest size with a HTR diameter reduction that guaranteed separation from the press-fit. Testing found that small interferences of one mil still achieved coupling strengths comparable to the larger five mil interferences. Therefore, use of a thicker walled SMA ring and a smaller press-fit interference could increase the strength of the SMA interference joint beyond that of just an increased interference, even though a thicker walled SMA cylinder yields less of a HTR diameter reduction. In addition, SMA cylinder geometry impacts induced buckling and micro-coupling mechanization, so one should confirm the compressive forces that induce SMA cylinder buckling for the chosen SMA geometry before assembly of the micro-coupling. This SMA cylinder characterization would validate the buckling action within the SMA interference joint as a contributing factor to the strength of the micro-coupling.

Micro-coupling material selection: Material for the hub of the micro-coupling should be investigated with the objectives to either produce a nonconductive hub that allows direct current resistive heating of the SMA to achieve HTR, or a hub created from a metal with the specific intent of inducing atomic cohesion with the SMA creating a stronger interference joint. Furthermore, testing of multiple micro-coupling lots resulted in slightly different strength curve responses dependant on the time between cleaning and assembly of the micro-coupling. This may have resulted from different amounts of surface oxidation forming on the casehardened steel hub affecting the test results. The micro-coupling interacting surfaces are airtight once assembled and not be prone to the effects of oxidation after assembly, but particular attention to surface oxidation and its effects on the micro-coupling should be investigated further.

Micro-coupling aging effects: The impact of prolonged exposure to extreme pressures on the material properties of detwinned martensite SMA and possible relaxation of its imparted hoop stress within an interference joint is unknown. It is recommended to create multiple test lots of micro-couplings over a period of time with exposure to expected space environmental conditions and note any disparity between coupling capability and micro-coupling age.

B. SMA²C DEVICE

1. Synopsis

The SMA²C device EDU was the first effort to design and apply the SMA micro-coupling as a zero-shock NEA for satellites. The intent of its rather generic design was to enable testing and integration to learn lessons for future design refinement. Simplicity of the SMA²C device is integral to its success as a coupling device and was the driving objective in its development and design. This device functioned successfully during its first test and should be an excellent starting point for future design iterations on the way to a fully certified flight unit.

2. Future Work

This section briefly suggests work that can be done to improve and validate the SMA²C device, such as reducing the size of the device and subjecting a proto-flight device to vibration and thermal testing.

Development of a 1/4 scale SMA²C device: The coupling strengths achieved by the SMA²C EDU were greater than those required for most nano-satellite applications. A smaller SMA²C device matching the required coupling strength would capitalize on a lower integration footprint and reduced actuation power requirement.

Vibration and environmentally controlled vacuum testing: Assembly of the SMA²C device currently uses NASA approved materials and epoxies, but the polyetherimide ring that thermally isolates and holds the micro-coupling in place, is not permanently secured and simply fits into place with tight assembly tolerances. The SMA²C device assembly methods have not been proven to withstand the vibrations experienced during launch or the extreme temperature variations of the space environment; therefore, vibration and thermally controlled vacuum chamber tests are required for the SMA²C device to check for integrity after exposure to operational conditions. Lessons learned from these tests may necessitate SMA²C EDU design changes.

APPENDIX A. NACL REPORT: SHAPE MEMORY ALLOY HTR AND HYSTERESIS VERIFICATION



NACL Test Report #SMA²C-1
Date of Testing: 15 MAY 2009
Date of Report: 26 MAY 2009
Addendum Update: 15 APR 2010

NAVAL POSTGRADUATE SCHOOL NANO-SATELLITE ADVANCED CONCEPTS LABORATORY TEST REPORT

Performed by:
LCDR William Crane

Testing Performed for:
Single Motion Actuated Shape Memory Alloy Coupling (SMA²C)

Verification of “G” type Shape Memory Alloy Ring Heat to Recover
Published Temperatures and Outer Diameter Reduction

Signatures of Certifying Individuals

Dr. Marcello Romano
NPS Professor, MAE & Space Systems Academic Group

Dr. James Newman
NPS Professor, Space Systems Academic Group

Reviewer Signatures

LCDR William M. Crane
NPS 591 Class 2010 & SMA²C Developer

Mr. Paul Oppenheimer
NPS 591 Class 2009 & SMA²C Co-developer

Contents

Section 1 - Overview	2
Section 2 – Test Item	4
Section 3 - Testing.....	5
Section 4 – Data Analysis & Calculations	9
Section 5 – Findings and Conclusions	10
Engineering Design Unit SMA Test Addendum	16

Section 1 - Overview

1.1 Testing Purpose and Scope

Objective – Validate published Heat-To-Recover (HTR) temperatures and SMA pseudoelastic properties of a “G” type Unilok® Shape Memory Alloy (SMA) ring (AGE0210-0049-0157), as manufactured by Intrinsic Devices Incorporated. The purpose of this test is to provide insight into design tolerances required for a micro-coupling mechanism that utilizes Shape Memory Alloy for actuation.

Threshold: Confirm the published unconstrained HTR outer diameter dimension reduction of 4.5% (tolerance of ± 0.0001 inches) upon heating the SMA to its austenitic phase temperature.

Goal: Obtain threshold data in addition to obtaining inner diameter measurements during HTR (tolerance of ± 0.001 inches). Secondly, define dimension characteristics of the SMA for a complete HTR hysteresis during a heat-cool-reheat cycle. This incorporates the irreversible de-stressing of the de-twinned martensitic phase on the initial heating to the austenite phase, subsequent cooling below 25 °C to the twinned martensitic phase, and heating back to its complete austenitic phase at 160 °C.

1.2 Executive Summary

Both primary “threshold” and secondary “goal” objectives were met within measurement tolerances. The HTR change in outer diameter for the G type SMA ring was found to be 3.9%. A loss of 0.6% from anticipated outer diameter reduction. Inner diameter of the SMA ring upon HTR was found to be 7.5%; an excess of 1.5% from the published unconstrained HTR outer diameter reduction. The cause for this difference is most likely due to the reorientation process the SMA undergoes during HTR. During SMA phase change the volume of material essentially remains constant, so as a ring shrinks the length and thickness will increase to maintain the same volume. Particularly, the thickness increase results in a larger inner diameter change as opposed to outer diameter change resulting in the final shrunk SMA outer diameter to be less than expected.

A small reduction in outer diameter was found to occur prior to the published HTR temperature, but ultimate de-stressing of the SMA occurred at approximately 90 °C. The initial small reduction in outer diameter indicates a possible propensity of the SMA to de-stressing creep when approaching phase change temperatures.

Cycling temperature of the SMA through its initial irreversible HTR, yielded twice the reduction in available outer diameter as compared to the reversible pseudoelastic phase cycling. This supports using the detwinned martensitic state of the SMA for press-fit applications.

1.3 Test Applicability Abstract

The Single Motion Actuated Shape Memory Alloy Coupling (SMA²C) device is dependent on a micro-coupling mechanism for operation. The micro-coupling mechanism itself is a SMA based interference joint. Precise design tolerances and construction of the micro-coupling yield its strength characteristics and subsequent release actuation reliability. Adequate foreknowledge of the amount of contraction the SMA will have upon heating is essential to determine interference limits available for the press-fit process, achievable coupling strength, and adequate clearance between the SMA and hub to ensure the ring will come free from the interference fit upon command.

Current manufacturing methods and published data for SMA rings are focused on inner diameter tolerances before and after heat-to-recover (HTR) actuation because this particular metric is the most important for most if not all SMA ring applications. Clamping force and inner diameter change parameters are not nearly as relevant as the outer diameter change and available hoop stress of the SMA ring for the micro-coupling's construction.

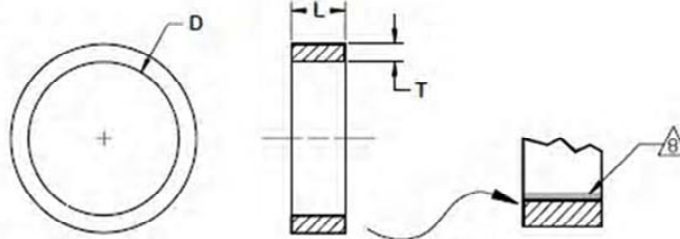
The size of SMA ring to be used in SMA²C has an outer diameter of 0.2". This equates to a change in outer diameter of -0.0078" once the test result of 3.9% HTR change is applied, resulting in a final diameter of 0.1922". This final diameter allows for a theoretical maximum press fit interference of 0.003" (& a measurement & manufacturing error of +/- 0.0005") leaving conservatively, an additional 0.003" for ultimate release of the SMA from its press fit upon HTR activation.

Section 2 – Test Item

2.1 Part Description & Properties

INTRINSIC

UniLok[®] Heat Shrinkable Rings



Product Description	D Minimum Supplied	D Maximum Recovered	T Supplied	L Supplied	Minimum Substrate Diameter	ΔD Increase on Cooling	Nominal Clamping Force at 160°C (lbs)
	0.210	0.200	.047 / .051	.152 / .162	0.2040	0.0037	1950

NOTES:

- 1 Ring material: NiTi, Intrinsic Alloy G
- 2 On the first heating cycle, the ring will begin to shrink in diameter at 95°C to 115°C (203°F to 239°F). Once in contact with the substrate, the ring will build clamping force linearly with increasing temperature, reaching the "Nominal Clamping Force" at 160°C (320°F).
- 3 This is the nominal radial clamping force for design purposes, equal to the ring-to-substrate contact area times the contact pressure. The actual force applied by a ring is a function of installation method, substrate material and geometry, and operating temperatures. The force decreases with decreasing temperature and decreasing substrate diameter. Testing is required to qualify performance in specific applications.
- 4 To insure consistent clamping force, the substrate should have the dimensions and rigidity to hold the installed ring diameter to this size or larger.
- 5 The ring will relax its grip if cooled below 25°C (77°F).

- expanding in diameter by the amount ΔD .
- 6 The ring will re-grip when heated above 75°C (167°F) reaching maximum clamping force at 120°C (248°F). The clamping force achieved will be less than the initial clamping force if a smaller substrate is substituted for the original one. If one ring will be used to clamp multiple substrates, contact Intrinsic Devices for design assistance.
- 7 If operating temperatures exceed 275°C (530°F) stress relaxation may occur depending on the time at temperature.
- 8 "I" and "J" suffix rings have an insulating coating on the ring ID which is .0005" to .005" thick and may extend onto the end faces of the ring. Only ID coating is assured on "I" rings. The coating will extend at least halfway from the ID to the OD on the end faces of "J" rings. Coating adds to dimensions T & L. D is unchanged. Coating is used when installing rings by direct electrical resistance heating.
- 9 Dimensions are in inches.

UniLok[®] is a registered trademark of Intrinsic Devices, Inc.

Product Document

**UniLok, Rectangular Section,
105°C Recovery, English Units**

Drawing ID	Date	Rev.	Page
PD AGE	8/15/06	G	1 of 1

Intrinsic Devices, Inc.

2353 Third Street
San Francisco, CA 94107-3108
tel: 415 252-5902 fax: 415 252-1624

intrinsicdevices.com

CAGE Code 08CE6

Section 3 - Testing

3.1 Test Description

Method - Observation and measurement of inner and outer diameters of a shape memory alloy ring at given temperatures during initial HTR cycle and subsequent re-heat SMA phase change cycle.

3.2 HTR Diameter Test

Number of Items Tested – One “G” type Unilok® SMA ring (AGE0210-0049-0157)

Location: NPS Small Satellite Laboratory

Equipment:

- One “G” type Unilok® Shape Memory Alloy ring (AGE0210-0049-0157)
- Hot Plate with calibrated digital temperature readout
- Aluminum block pedestal (allows separation of SMA from heating surface for measurement tool access)
- Thermocouple
- Kapton tape and scissors
- Source for ambient temperature readings
- Heat resistant tweezers / needle nose pliers
- Micrometer
- Gauge pins (0.001” steps from 0.210 to 0.200)
- Wristwatch
- Personal Protective Equipment (PPE)
 - Gloves, long sleeve shirt & safety glasses
- Camera (if desired)

Procedure (*Intermediate results annotated in italics*):

1. Zeroize micrometer and measure outer diameter of all gage pins to specified tolerances.
2. Measure outer diameter & inner diameter of “G” type Unilok® SMA ring; record data.
(*see Table 3.2*)
3. Compare the ambient temperature read from the thermocouple to an alternate device measuring the ambient temperature of the lab in close proximity to the hot plate; record data.
a. Ambient: 18.9 °C Thermocouple: 18.8 °C
4. Place the thermocouple on the face of the hot plate and run the hot plate temperature from ambient to 160 °C checking the calibration and rate of temperature change of the hot plate; record data. (*see Table 3.1*)
5. Attach the thermocouple to a flat face of the SMA ring to be tested.
6. Place aluminum block pedestal on hot plate in a position to allow easy access for concurrent micrometer measurements and thermometer temperature readings of SMA ring.
7. Place the SMA ring flat onto the aluminum block pedestal (at room temperature) and measure initial outer diameter & ID of the SMA ring practicing techniques to avoid removing the SMA ring from the heat source while measurements are being conducted; record data.

Page 5 of 21

(see Section 4.1)

8. Begin 'SMA Heat To Recover Test'
 - a. Record data as listed in SMA Heat To Recover Test table.
 - b. Temperature increments to be input into the hot plate (once reached SMA dimensions are to be recorded):

Testing point	Description
1.	Ambient
2.	95 °C Range of published HTR phase change start
3.	105 °C Range of published HTR phase change end
4.	125 °C Intermediate measurement
5.	145 °C Published 'unconstrained' HTR phase completion
6.	160 °C Published HTR phase completion
7.	95 °C Cooling Intermediate measurement
8.	25 °C Reversion of SMA to twinned-martensitic form
Note: This temperature may have to be achieved by placing the SMA and thermocouple in a cooled environment.	
9.	Optional step: (5 °C Ensure SMA twinned-martensitic formation)
10.	Ambient
11.	75 °C Published re-heat HTR phase change start
12.	105 °C Published re-heat 'unconstrained' HTR phase completion
13.	125 °C Intermediate measurement
14.	160 °C Targeted HTR heating cycle temperature

- Record all data (Table 3.2).
- Return all testing items and mark SMA ring to be permanently identifiable as to having been cycled through HTR temperatures and de-stressed.

3.3 Test Results:

Hot Plate Calibration Test (Table 3.1)

Time (PST)	Hot Plate Setting (°C)	Hot Plate Temperature (°C)	Thermocouple temperature (°C)	Delta (°C)
1001	50	50	48.3	1.7
1004	60	65	66.9	-1.9
1005	70	71	71.3	-0.3
1006	80	83	82.7	0.3
1007	90	90	88.8	1.2
1009	100	100	99.3	0.7
1010	110	110	110.0	0
1011	120	120	119.7	0.3
1012	130	130	127.2	2.8
1013	140	140	140.0	0
1015	150	151	150.0	1
1017	160	160	158.1	1.9

Note: Calibration was conducted on 08 May 2009.

SMA Heat To Recover Test (Table 3.2)

Testing Point Number	Time (PST)	Ambient Temperature (°C)	Hot Plate Temperature (°C)	SMA Temperature (°C)	Micrometer OUTER DIAMETER Measurement (inches)	Gauge Pin ID Measurement (inches)
1	1015	18.9	19	19.8	0.3125	0.212
	1020	-	-	45.0	0.3125	0.212
	1026	-	-	70.0	0.3120	0.211
	1030	-	-	85.0	0.3118	0.211
2	1035	19.1	143	96.1	0.3115	0.210
3	1040	18.8	165	106.2	0.3015	0.199
4	1045	19.1	189	125.7	0.3005	0.197
5	1049	19.6	205	145.9	0.3002	0.196
6	1055	19.8	224	160.8	0.3002	0.196
7	1101	19.4	N/A	83.2	0.3002	0.197
8	1106	18.5	N/A	24.2	0.3060	0.204
	1107	18.5	-	20.0	0.3063	0.204
9	1114	18.4	-*	15.6	0.3068	-
10	1117	18.9	N/A	20.1	0.3068	0.204
11	-**	-	-	76.0	0.3000	-
12	-**	-	-	-	-	-
13	1121	18.8	167	140	0.3000	0.196
14	1129	18.8	230	162.7	0.3000	0.196

* A -10 °C decrease from published temperature for twinned martensitic SMA was deemed sufficient for beginning second HTR cycle.

** SMA Temperature rise was too rapid to accurately measure intermediate testing points due to temperature gradient control of the aluminum block pedestal holding residual heat.

Section 4 – Data Analysis & Calculations

4.1 Calculated HTR Values

4.5% reduction in SMA outer diameter & inner diameter dimensions (inches) upon HTR:

	<u>Initial dimensions</u>	<u>Reduction Value</u>	<u>Final dimensions</u>
Outer Diameter:	0.312" ±0.0005	0.0140" (calculated)	0.298" ±0.0005
Inner Diameter:	0.210" ±0.001	0.010" (published)	0.200" ±0.001

4.2 Calculated Coefficient of Thermal Expansion for NiTi SMA

These values are for comparing relative diameter change due to the material's coefficient of thermal expansion vs. the diameter change caused by SMA pseudoelastic phase change. Theoretically, the thermal expansion of the SMA should be subtracted from the material's contraction due to phase change, both induced by an increase in temperature.

Note: The volume of SMA ring does not change appreciably during HTR. A published 0.01" increase in length is experienced by a "G" type Unilok® SMA ring (AGE0210-0049-0157) upon HTR.

Coefficient of Thermal Expansion NiTi (50/50% composition) Martensite:

$$6.0 \times 10^{-6}/^{\circ}\text{C} \quad (3.33 \times 10^{-6}/^{\circ}\text{F})$$

Coefficient of Thermal Expansion NiTi (50/50% composition) Austenite:

$$11.0 \times 10^{-6}/^{\circ}\text{C} \quad (6.1 \times 10^{-6}/^{\circ}\text{F})$$

	<u>Delta Temperature</u>		<u>Associated Thermal Expansion of SMA ring</u>	
Baseline Outer Diameter ----->			7.9375mm	0.31250in
Freezing:	0°C	32°F	0.0mm	0.0in
Martensite finish:	15°C	59°F	0.000714mm	0.000028in
Room temp:	20°C	68°F	0.000953mm	0.000038in
Martensite start:	55°C	131°F	0.002619mm	0.000103in
Re-baseline Outer Diameter ----->			7.9413mm	0.31265in
Austenite start:	80°C	176°F	0.00381mm	0.000150in
Austenite finish:	89°C	192°F	0.00460mm	0.000331in
HTR bottom range:	95°C	203°F	0.00512mm	0.000352in
HTR top range:	115°C	239°F	0.006867mm	0.000420in
Final testing temp:	160°C	320°F	0.010798mm	0.000575in

COE values are minimal compared to the 0.0140" expected outer diameter reduction. If the above numbers are added to the expected reduction, the final calculated outer diameter should be approximately: 0.0134". Testing resulted in a final outer diameter of 0.0123".

Section 5 – Findings and Conclusions

The initial irreversible HTR phase change for the G type SMA ring resulted in an outer diameter reduction of 3.9% vs. the anticipated 4.5% outer diameter reduction (see Figure 1). In addition, a small reduction in outer diameter was found to occur prior to the published HTR temperature indicating a possible propensity to prematurely de-stress when approaching phase change temperatures. Inner diameter of the SMA ring upon HTR was found to be 7.5%; an excess of 1.5% from the published unconstrained HTR inner diameter reduction. Ultimate de-stressing of the SMA ring occurred at approximately 90 °C.

Test results show a smaller reduction in the outer diameter than the inner diameter. This will ultimately lead to the need for very precise manufacturing and measurement tolerances for the SMA²C micro-coupling. The cause for this difference is most likely due to the reorientation process the SMA undergoes during HTR and phase change with a constant volume of material. As a ring shrinks, the length and thickness will increase to maintain the same volume. The thickness increase resulted in a larger inner diameter reduction as opposed to outer diameter reduction. A way to get more outer diameter reduction would be to make the inner diameter larger by decreasing the wall thickness, but this would ultimately impact the strength of the SMA ring.

Note: This test was conducted with a single Off-The-Shelf (OTS) SMA ring and the data recorded in this report should be handled as a single data point, manufacturer tolerance verification; thereby understanding that additional testing is needed for more substantiated findings and conclusions.

Appendix

NACL Test Report #SMA²C-1
Date of Testing: 15 MAY 2009
Date of Report: 26 MAY 2009

Supporting Graphs & Diagrams

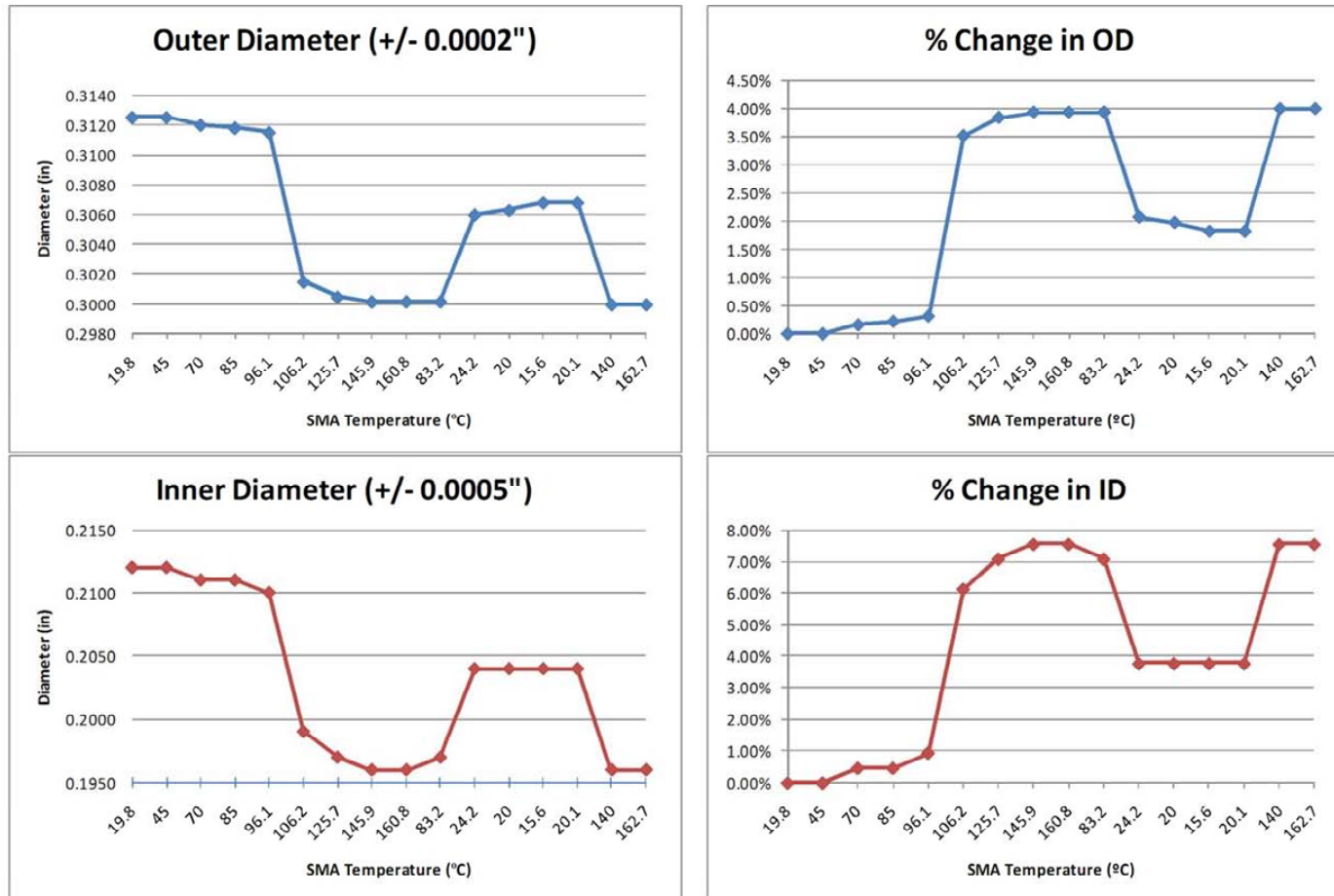


Figure A1 Outer and Inner Diameter Measurements for "G" Type SMA Ring
(Initial HTR & one additional HTR cycle with associated % dimension change)

Page 11 of 21

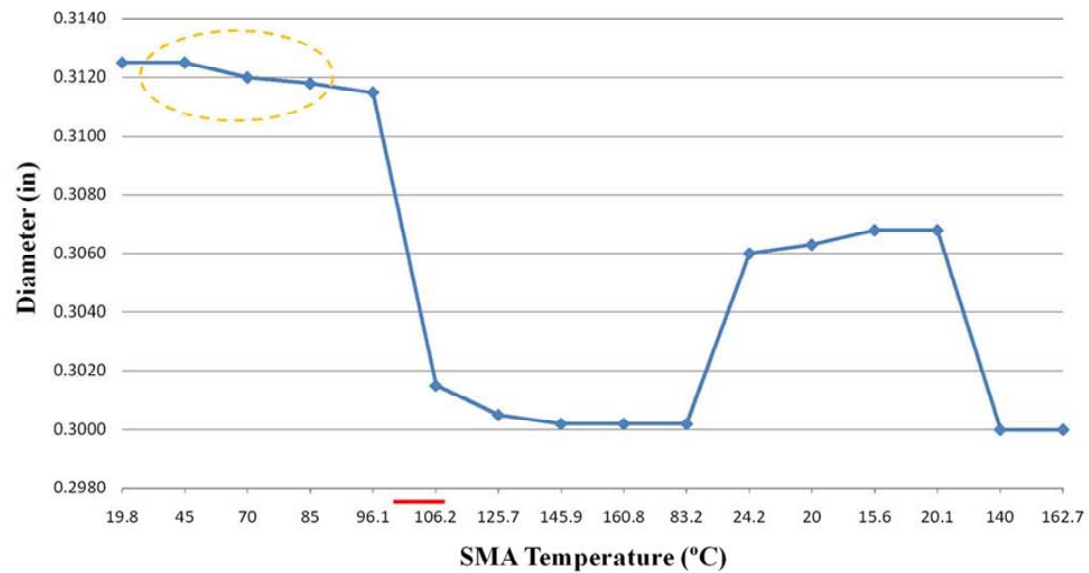
Test Equipment and Instrumentation

<u>Instrument or Equipment</u>	<u>Manufacturer</u>	<u>Model</u>	<u>Serial Number</u>	<u>Calibration Date</u>
Micrometer	Mitutoyo	0-1" +/-0.00005	293-832	Unknown
Thermocouple	OMEGA	SAI-K	-	-
Electronic Hot Plate	Automated Products Inc.	GF-SL	APS-GF-SL0712244	08May09 (+/- 1.5°C)
Thermometer	FLUKE	52 J/K Thermometer	4490235	15May09 (+/- 0.05°C)
Gauge Pins	Fowler	0.061-0.250"	USN 026039	15May09 (+/- 0.00005")

Additional Figures and Tables

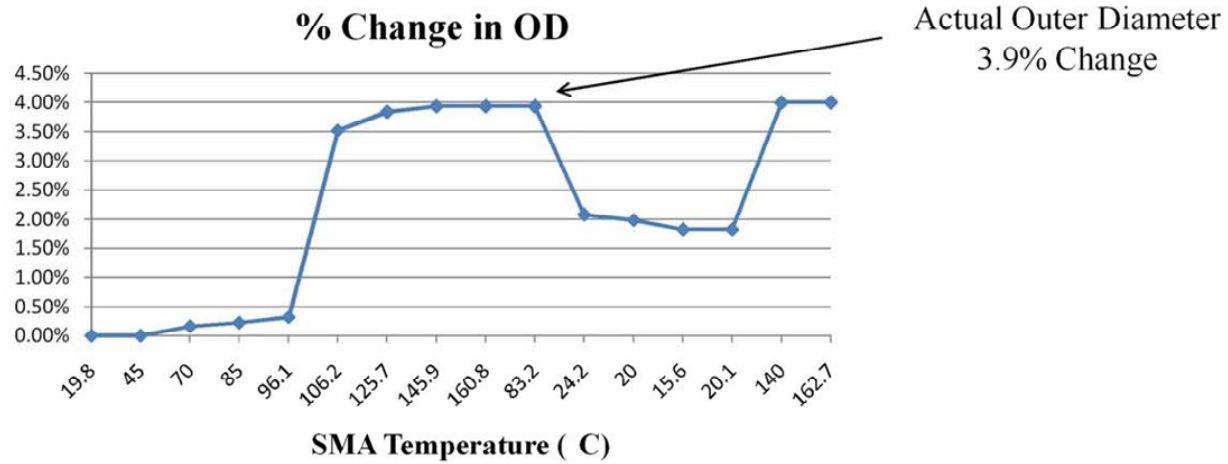
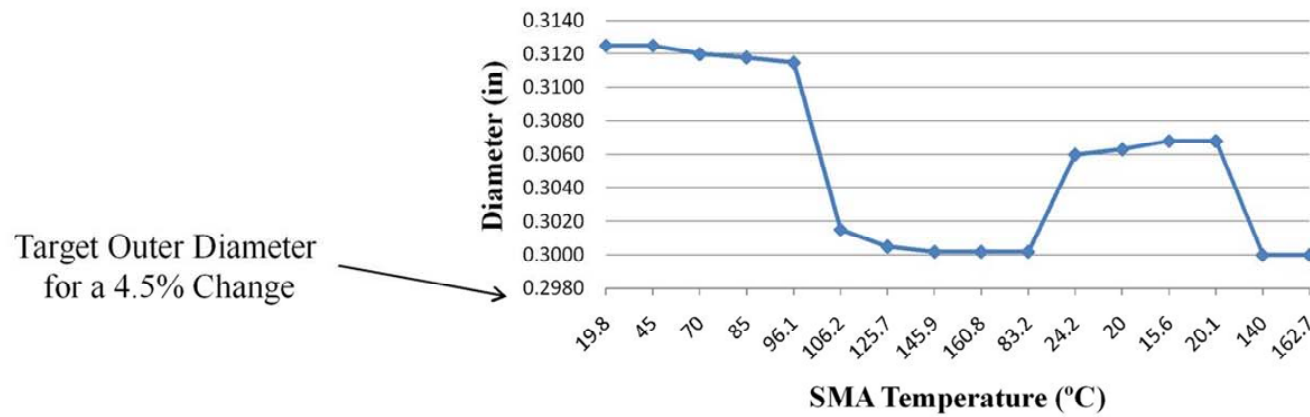
SMA HTR Initiation

Outer Diameter (+/- 0.0002")



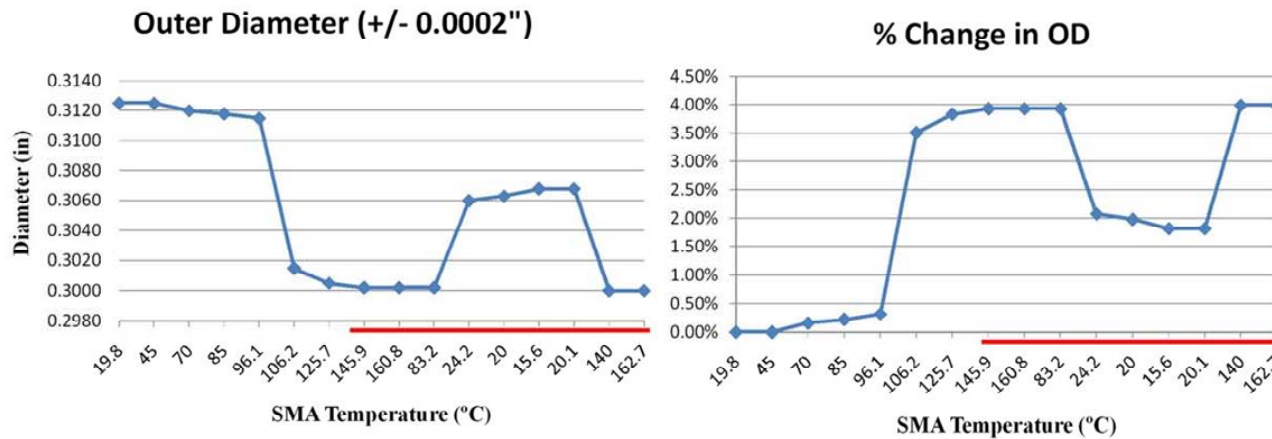
Conclusion: Possible de-stressing prior to HTR temperatures (annotated by red line) equal to a 0.25% reduction in OD prior to 95 °C (circled in yellow).

Outer Diameter (+/- 0.0002")



Post HTR SMA Hysteresis

(Temperatures annotated by red line)



Conclusions: Permanent 2.1% reduction in OD upon reaching 125 °C (Heat To Recover).
1.8% change in OD for subsequent SMA reversible heat/re-heat cycles.

Engineering Design Unit SMA Test Addendum

Objective – Validate published Heat-To-Recover (HTR) temperatures and pseudoelastic properties of the SMA²C micro-coupling Engineering Design Unit (EDU) SMA cylindrical ring, as manufactured by Intrinsic Devices Incorporated. The purpose of this test is to ensure adequate reduction of the outer diameter of the EDU SMA ring to allow removal from a steel hub upon HTR activation. Commanded release for the SMA²C device depends upon the SMA micro-coupling mechanism that utilizes the “G” type SMA for actuation. Proper SMA hysteresis needs to be ensured before further construction of the EDU device.

Threshold and goals for this test addendum are the same as those of the original test.

Test Item – See below and next page:

Supplier Specifications for EDU SMA Ring (inches)

Supplied Dimensions:

Inner Diameter	.1565 / .1580
Outer Diameter	.2030 / .2045
Length	.3060 / .3080

Recovered Dimensions:

Inner Diameter	.1470 / .1482
Outer Diameter	.1944 / .1960

(Typical outer diameter taper on SMA ring = +/- 0.0005)

Method - Measurement of the change in outer diameter of a shape memory alloy cylindrical ring for use in the SMA²C micro-coupling mechanism during initial HTR and subsequent re-heat pseudoelastic SMA phase change cycle. Equipment and procedural steps are the same as original test.

Data - See following pages

Findings and Conclusion – The HTR change in outer dimension for the G type SMA ring was found to be 4.2% with a final austenitic outer diameter of 0.1955” ±0.00005”. Inner diameter of the SMA ring was measured but of no concern to the construction of the EDU micro-coupling mechanism. The same small reduction in outer diameter occurred as temperature increased to the published HTR temperature of 95 °C (0.27% reduction in OD prior to 95 °C). This could indicate a possible propensity of the SMA to de-stress or “creep” while in the micro-coupling when approaching phase change temperatures. Ultimate de-stressing of the SMA ring did not occur until approximately 105 °C. Primary HTR resulted in a permanent 2.5% reduction in OD upon reaching 125 °C (Heat To Recover). Cycling temperature of the SMA after HTR resulted in a 1.7% change in OD for subsequent SMA reversible heat/re-heat cycles.

Outer diameter reduction in the SMA cylindrical ring would leave a delta of 0.0035” between the SMA and the case hardened steel hub with inner diameter of 0.1990”; therefore, the micro-coupling mechanism would achieve a successful commanded de-coupling upon SMA HTR activation.

Engineering Design Unit SMA Cylindrical Ring:

- “G” type Unilok® SMA ring (AGE0156-0022-0312)

INTRINSIC

UniLok® Material Properties

Nominal Properties for All Alloys

Melting Point	1300°C (2370°F)
Thermal Conductivity	0.18 W/cm·°C (10.4 BTU/hr·ft·°F)
Specific Heat	0.2 cal/g·°C (0.2 BTU/lb·°F)
Coefficient of Thermal Expansion	11x10 ⁻⁶ /°C (6.1x10 ⁻⁶ /°F)
Poisson's Ratio	0.33
Electrical Resistivity	90x10 ⁻⁶ ohm-cm (35x10 ⁻⁶ ohm-in)
Magnetic?	No
Magnetic Permeability	<1.002
Magnetic Susceptibility	3x10 ⁶ emu/g
Corrosion	Similar to 300 series stainless steel. For specific compatibility data, consult Intrinsic Devices.

Austenitic Mechanical Properties

Yield Strength	415MPa (60kpsi)
Ultimate Tensile Strength	800MPa (115kpsi)
Elongation to Failure	25%
Young's Modulus in Tension	75GPa (11x10 ⁶ psi)
Hardness	65 Ra

Alloy Specific Properties

Composition (wt%)	Ti 45, Ni 55
Density	6.5g/cm ³ (0.235 lb/in ³)

Note: All properties given are nominals for initial design purposes. Testing is required to qualify performance in specific applications. Always test for adequate clamping force at the minimum operating temperature of the assembly.

UniLok® is a registered trademark of Intrinsic Devices, Inc.

Intrinsic Devices, Inc.
2353 Third Street
San Francisco, CA 94107-3108
tel: 415) 252-0902 fax: 415) 252-1624
<http://www.intrinsicdevices.com/>

Product Document
Material Properties

Drawing ID	Rev.	Date	Page
PD 005	F	9/19/03	1 of 1

TEST REPORT NOTE: Modulus of elasticity for NiTi, Intrinsic Alloy G in its detwinned martensitic state as provided by the manufacturer is 5,000 ksi (34.475 GPa).

Page 17 of 21

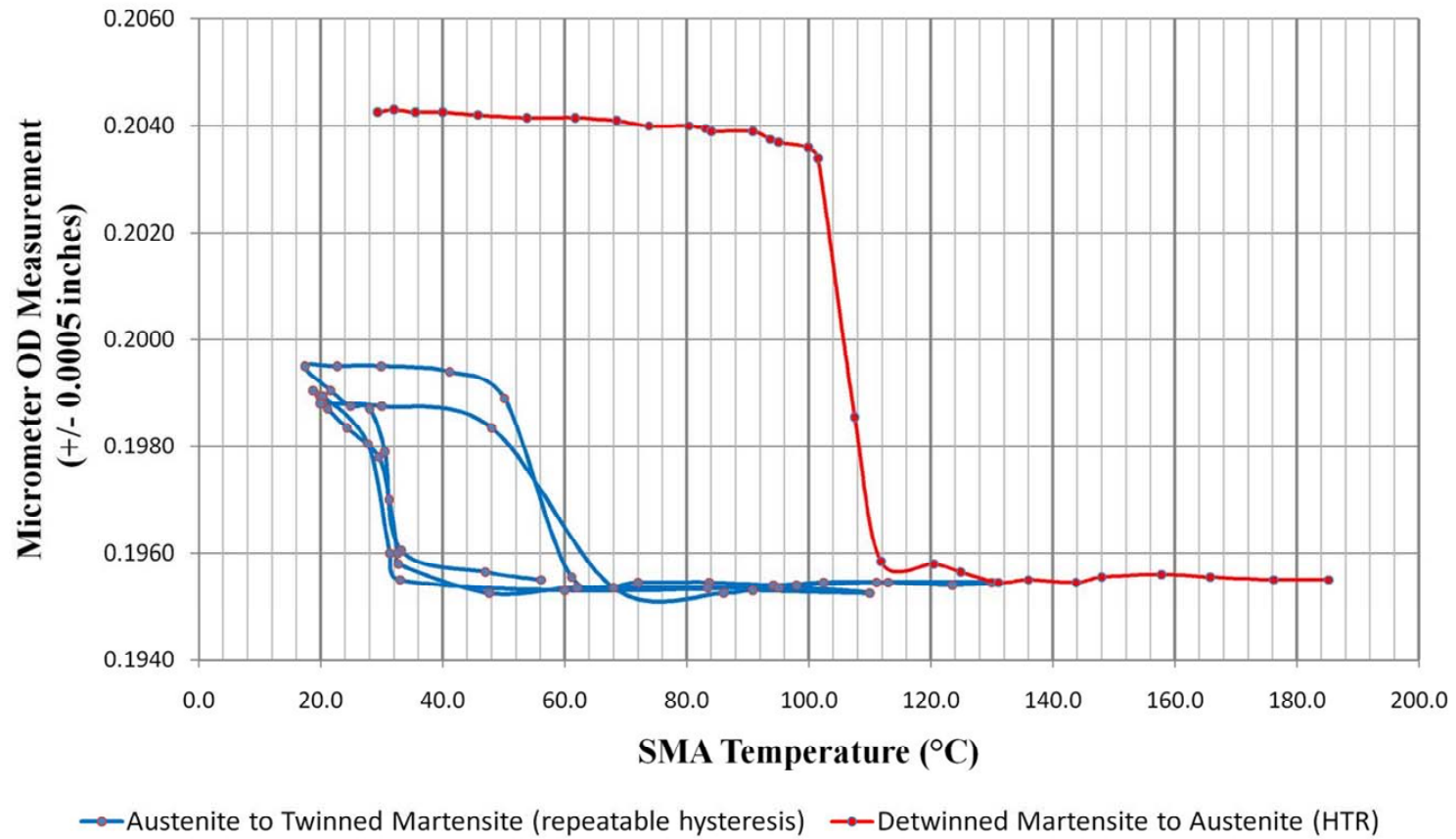
Testing Point	Time (PST)	Ambient Temperature (°C)	Hot Plate Temperature (°C)	SMA Temperature (°C)	Micrometer OD Measurement (inches)	Gauge Pin ID Measurement (inches)	OD % Change	ID % Change
1	0925	18.8	33	29.3	0.20425	0.157	0.00%	0.00%
2	0928	-	40	32.0	0.20430	0.157	-0.02%	0.00%
3	0930	-	47	35.5	0.20425	0.157	0.00%	0.00%
4	0933	-	52	40.0	0.20425	0.157	0.00%	0.00%
5	0935	-	61	45.8	0.20420	0.157	0.02%	0.00%
6	0937	-	70	53.8	0.20415	0.157	0.05%	0.00%
7	0941	-	79	61.7	0.20415	0.157	0.05%	0.00%
8	0944	-	90	68.5	0.20410	0.157	0.07%	0.00%
9	0946	-	99	73.8	0.20400	0.157	0.12%	0.00%
10	0949	-	109	80.3	0.20400	0.157	0.12%	0.00%
11	0950	-	111	83.1	0.20395	0.157	0.15%	0.00%
12	0951	-	120	84.0	0.20390	0.157	0.17%	0.00%
13	0953	-	124	90.8	0.20390	0.157	0.17%	0.00%
14	0954	-	133	93.7	0.20375	0.157	0.24%	0.00%
15	0956	-	141	95.0	0.20370	0.157	0.27%	0.00%
16	0957	-	139	99.9	0.20360	0.156	0.32%	0.64%
17	0959	-	141	101.5	0.20340	0.156	0.42%	0.64%
18	1001	-	158	107.5	0.19855	0.148	2.79%	5.73%
19	1003	-	164	111.8	0.19585	0.147	4.11%	6.37%
20	1004	-	169	120.5	0.19580	0.147	4.14%	6.37%
21	1005	-	168	124.9	0.19565	0.147	4.21%	6.37%
22	1006	-	167	131.1	0.19545	0.147	4.31%	6.37%
23	1008	-	171	136.0	0.19550	0.147	4.28%	6.37%
24	1010	-	180	143.8	0.19545	0.147	4.31%	6.37%
25	1012	-	189	148.0	0.19555	0.147	4.26%	6.37%
26	1014	-	197	157.8	0.19560	0.147	4.24%	6.37%
27	1017	-	208	165.8	0.19555	0.147	4.26%	6.37%
28	1018	-	214	176.2	0.19550	0.147	4.28%	6.37%
29	1023	-	230	185.2	0.19550	0.147	4.28%	6.37%
30*	-	-	-	56.1	0.19550	-	4.28%	-
31	-	-	-	47.0	0.19595	-	4.06%	-
32	-	-	-	39.2	0.19625	-	3.92%	-
33	-	-	-	35.5	0.19790	-	3.11%	-
34	-	-	-	30.0	0.19870	-	2.72%	-
35	-	-	-	24.9	0.19875	-	2.69%	-
36	-	-	-	21.6	0.19905	-	2.55%	-

* Circuit breaker in lab blew. SMA removed from hot plate to cool rapidly.

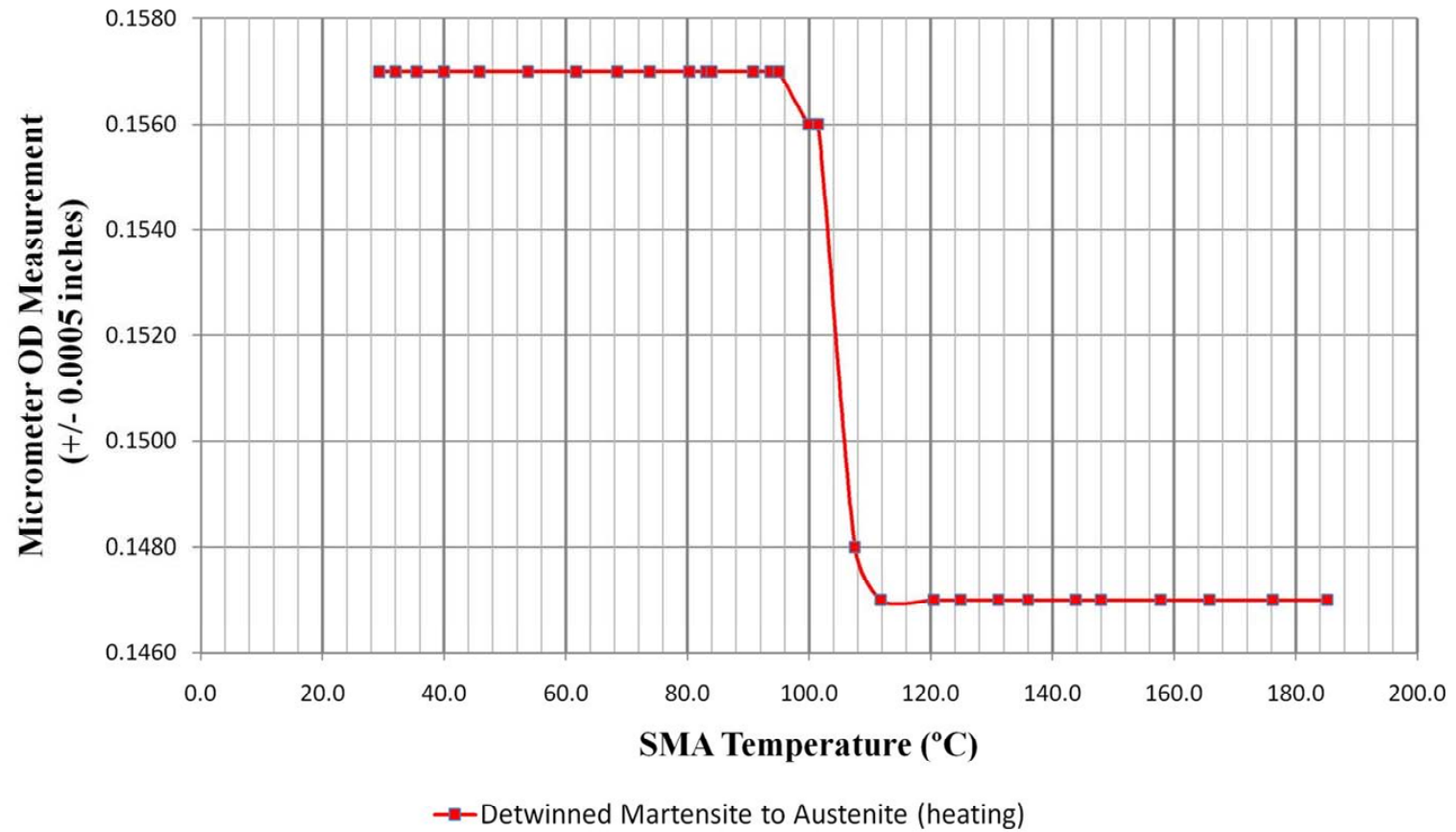
New Data: 23 Sept 2010 using same SMA cylindrical ring

Testing Point	Ambient Temperature (°C)	Hot Plate Temperature (°C)	SMA Temperature (°C)	Micrometer OD Measurement (inches)	OD % Change
1	17.8	-	17.4	0.19950	2.33%
2	-	-	22.7	0.19950	2.33%
3	-	-	29.9	0.19950	2.33%
4	-	-	41.1	0.19940	2.37%
5	-	-	50.1	0.19890	2.62%
6	-	-	61.1	0.19555	4.26%
7	-	-	72.0	0.19545	4.31%
8	-	-	83.7	0.19545	4.31%
9	-	-	94.2	0.19540	4.33%
10	-	-	102.4	0.19545	4.31%
11	-	-	113.0	0.19545	4.31%
12	-	-	123.5	0.19540	4.33%
13	-	-	130.0	0.19545	4.31%
14	-	-	111.1	0.19545	4.31%
15	-	-	98.0	0.19540	4.33%
16	-	-	83.4	0.19535	4.36%
17	-	-	62.0	0.19535	4.36%
18	-	-	47.6	0.19525	4.41%
19	-	-	32.7	0.19580	4.14%
20	-	-	32.6	0.19600	4.04%
21	-	-	31.2	0.19700	3.55%
22	-	-	29.5	0.19780	3.16%
23	-	-	24.3	0.19835	2.89%
24	-	-	21.1	0.19870	2.72%
25	-	-	20.2	0.19880	2.67%
26	-	-	19.8	0.19895	2.59%
27	-	-	19.9	0.19880	2.67%
28	-	-	30.0	0.19875	2.69%
29	-	-	48.0	0.19835	2.89%
30*	-	-	68.0	0.19535	4.36%
31	-	-	86.0	0.19525	4.41%
32	-	-	90.8	0.19530	4.38%
33	-	-	110.0	0.19525	4.41%
34	-	-	95.0	0.19535	4.36%
35	-	-	60.0	0.19530	4.38%
36	-	-	33.0	0.19550	4.28%
37	-	-	31.3	0.19600	4.04%
38	-	-	27.7	0.19805	3.04%
39	-	-	20.3	0.19895	2.59%
40	-	-	18.7	0.19905	2.55%

Micro-Coupling SMA Outer Diameter HTR & Hysteresis



SMA Ring Inner Diameter HTR



THIS PAGE INTENTIONALLY LEFT BLANK

APPENDIX B. NACL REPORT: SHAPE MEMORY ALLOY MICRO-COUPPLING CONCEPT VALIDATION



NACL Test Report #SMA²C-2
Date of Testing: 20 JUL 2009
Date of Report: 07 OCT 2009

NAVAL POSTGRADUATE SCHOOL NANO-SATELLITE ADVANCED CONCEPTS LABORATORY TEST REPORT

Performed by:
LCDR William Crane

Testing Performed for:
Single Motion Actuated Shape Memory Alloy Coupling (SMA²C)

Micro-Coupling Concept Validation of a Press-Fit Detwinned
Martensitic Shape Memory Alloy Ring to Provide Calculated Load
Bearing Capability

Signatures of Certifying Individuals

Dr. Marcello Romano
NPS Professor, MAE & Space Systems Academic Group

Dr. James Newman
NPS Professor, Space Systems Academic Group

Reviewer Signatures

LCDR William M. Crane
NPS 591 Class 2010 & SMA²C Developer

Mr. Paul Oppenheimer
NPS 591 Class 2009 & SMA²C Co-developer

Contents

Section 1 - Overview	2
Section 2 - Test Item	4
Section 3 - Testing	5
Section 4 - Data Analysis & Calculations	9
Section 5 - Findings and Conclusions	16

Section 1 - Overview

1.1 Testing Purpose and Scope

Objective – Obtain the axial coupling strength of an interference joint consisting of a detwinned martensitic Nickel Titanium (NiTi) Shape Memory Alloy (SMA) cylindrical ring press-fit into a stainless steel hub.

Threshold: Validate the Single Motion Actuated Shape Memory Alloy Coupling (SMA²C) concept by obtaining force & displacement curves during the intentional separation of a SMA interference joint by applying axial force on the SMA cylindrical ring until it is pulled clear from the press-fit.

(Interference Range: 0.0005” to 0.0030”)

Goal: Obtain the threshold objective in addition to determining if the press-fit process induced martensitic de-stressing or plastic deformation of the SMA cylindrical ring. Validate the use of standard interference joint formulas to predict the axial strength of the SMA²C interference joint within propagated measurement error.

1.2 Executive Summary

Use of SMA as the actuating material in a coupling device, such as the SMA²C device, was proven by the substantial holding forces achieved (in excess of 500 lbf). De-stressing of the SMA cylindrical ring was observed in approximate proportion to ½ of the interference experienced by the SMA within the interference joint. The largest interference explored (0.003”) yielded the greatest axial coupling strength and experienced several coupling force peaks in resistance to forced SMA extraction. A hypothesis is that the SMA cylindrical ring experienced buckling upon forced extraction increasing the normal forces internal to the joint thereby increasing the strength of the SMA interference joint.

Press-fitting detwinned martensitic SMA, rather than traditional metals or alloys, increases the number of material reaction and interaction variables to the forces encountered within interference joints. This test utilized industry standard press-fit equations for prediction of axial coupling forces and achieved an accurate prediction within measurement error for the limited number of tests performed. It is important to note that even if the standard press-fit equations have applicability for nominal SMA interference joints, the equations fail to explore the impact of de-stressing the detwinned martensitic SMA and also the possible geometry changes of the SMA cylindrical ring (buckling and stress induced phase change) upon forceful removal from the press-fit.

Outstanding variables that remain are:

- Possible inaccuracy in the assumed coefficient of friction between the nickel titanium shape memory alloy and stainless steel;

- Actual vs. assumed surface area in contact between the SMA and stainless steel hub for each explored interference;

- The impact of possible SMA phase change due to excess pressures experienced at joint contact points during interference fit assembly or during forced SMA removal from the stainless steel hub.

1.3 Test Applicability Abstract

The “SMA²C” device (Single Motion Actuated Shape Memory Alloy Coupling) is dependent on a press-fit SMA cylindrical ring providing sufficient coupling strength to resist being forcefully removed. This coupling force is obtained by frictional forces generated when the SMA is press-fit into a metallic bushing creating an interference joint. To be a reliable coupling mechanism, the interference between the two parts has to be within precise tolerances. If the press-fit interference is too little, not enough friction is created to supply the needed coupling strength. If the press-fit interference is too large, de-stressing or phase change of the martensitic SMA could occur and subsequently reduce coupling strength. In addition, excess interference could disable the SMA’s ability to free itself from the press-fit upon heating and therefore defeat the designed purpose of the coupling mechanism to release itself upon command (see Figure 1.1). In order to substantiate the SMA²C device SMA interference joint concept, existing commercial-off-the-shelf “G” type SMA rings produced by Intrinsic Devices Inc., were used to compare analytical calculations with test data in an attempt to validate assumptions and formulas to predict interference joint axial coupling strength.

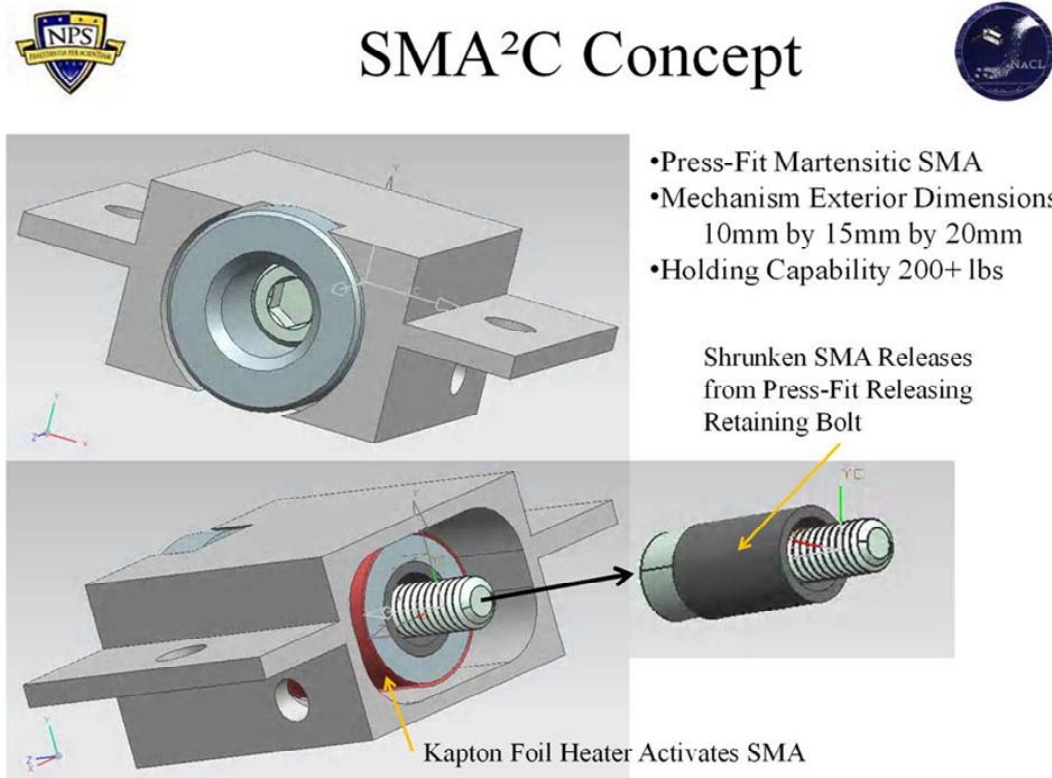


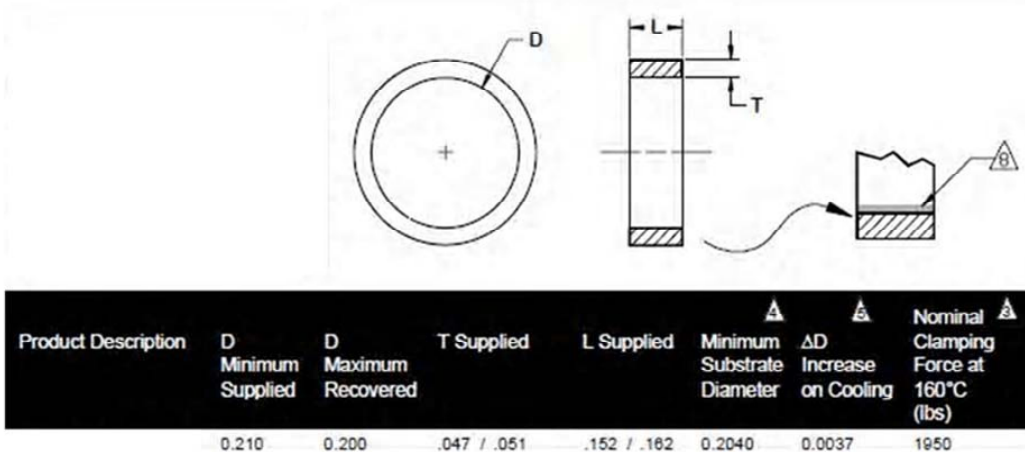
Figure 1.1 Single Motion Actuated Shape Memory Alloy Coupling (SMA²C) device showing the release of a press-fit shape memory alloy cylindrical ring upon command

Section 2 – Test Item

2.1 Part Description & Properties

INTRINSIC

UniLok® Heat Shrinkable Rings



TEST REPORT NOTE: Modulus of elasticity for NiTi, Intrinsic Alloy G in its detwinned martensitic state as provided by the manufacturer is approximately 5,000 ksi (34.475 GPa).

NOTES:

- 1 Ring material: NiTi, Intrinsic Alloy G
- 2 On the first heating cycle, the ring will begin to shrink in diameter at 95°C to 115°C (203°F to 239°F). Once in contact with the substrate, the ring will build clamping force linearly with increasing temperature, reaching the "Nominal Clamping Force" at 160°C (320°F).
- 3 This is the nominal radial clamping force for design purposes, equal to the ring-to-substrate contact area times the contact pressure. The actual force applied by a ring is a function of installation method, substrate material and geometry, and operating temperatures. The force decreases with decreasing temperature and decreasing substrate diameter. Testing is required to qualify performance in specific applications.
- 4 To insure consistent clamping force, the substrate should have the dimensions and rigidity to hold the installed ring diameter to this size or larger.
- 5 The ring will relax its grip if cooled below 25°C (77°F).

expanding in diameter by the amount ΔD .

- 6 The ring will re-grip when heated above 75°C (167°F) reaching maximum clamping force at 120°C (248°F). The clamping force achieved will be less than the initial clamping force if a smaller substrate is substituted for the original one. If one ring will be used to clamp multiple substrates, contact Intrinsic Devices for design assistance.
- 7 If operating temperatures exceed 275°C (530°F) stress relaxation may occur depending on the time at temperature.

- 8 "I" and "J" suffix rings have an insulating coating on the ring ID which is .0005" to .005" thick and may extend onto the end faces of the ring. Only ID coating is assured on "I" rings. The coating will extend at least halfway from the ID to the OD on the end faces of "J" rings. Coating adds to dimensions T & L. D is unchanged. Coating is used when installing rings by direct electrical resistance heating.
- 9 Dimensions are in inches.

UniLok® is a registered trademark of Intrinsic Devices, Inc.

Product Document

UniLok, Rectangular Section,
105°C Recovery, English Units

Intrinsic Devices, Inc.

2353 Third Street
San Francisco, CA 94107-3108
tel: 415 252-5902 fax: 415 252-1624

intrinsicdevices.com

CAGE Code 08CE6

Drawing ID	Date	Rev.	Page
PD AGE	8/15/06	G	1 of 1

Section 3 - Testing

3.1 Test Description

Method - Observation and measurement of increasing axial loads used to remove a press-fit SMA cylindrical ring from a stainless steel hub.

SMA rings are measured with a micrometer and stainless steel press-fit hubs are measured with gauge pins to determine the interference fit obtained by the joining of the two parts within measurement precision. The 'SMA²C tensile test rig' (see Figures 3.1-3.3) mounts the press-fit SMA into a tensile test machine that measures applied force and subsequent displacement of the interference joint. SMA rings are again measured with a micrometer post-test to determine the amount of de-stressing experienced during the interference joint assembly process and subsequent forced removal by the tensile test machine.

3.2 Press-Fit SMA Tensile Load Test

Number of Items to be tested: Four "G" type Unilok® SMA rings
(AGE0210-0049-0157)

Location: NPS Machine Laboratory

Equipment:

- Four "G" type Unilok® Shape Memory Alloy ring (AGE0210-0049-0157)
- Micrometer (+/- 0.00005")
- Gauge pins (0.001" steps from 0.309 to 0.312; - 0.0005")
- SMA²C Tensile Test Rig
- Tensile Test Machine (+/- 0.5% of applied force; Newtons)
- Acetone and Isopropyl Alcohol (99%)
- Oil free (clean room) swabs and latex gloves (powder free)
- Clean room pads (cleaning patches)
- Tweezers
- Personal Protective Equipment (PPE)
 - Gloves, long sleeve shirt & safety glasses
- Video camera (if desired)

Procedure:

1. Measure the outer diameter of the SMA cylindrical rings with a micrometer at multiple points by rotating the ring 60-90° every measurement; record data in Table 3.1.
2. Measure the inner diameter of the press-fit hubs using gauge pins; record data in Table 3.1 and etch measurement onto hub.
3. Prepare press-fit steel hubs and SMA cylindrical rings by cleaning in acetone and then isopropyl alcohol giving special attention to the outside surface of the SMA and the inside surface of the hub where the interference joint is to be created. (Clean tweezers to be oil free)

4. Match specific SMA rings to each steel hub and place in separate oil free bags with appropriate identification markings.
5. Clean press-fit vice (arbor press) and place an oil free mat at base of vice fixture. Use oil free gloves or tweezers to manipulate SMA and hubs into position. Apply a small amount of alcohol for lubrication and press-fit SMA cylindrical rings into steel hubs using a smooth application of force.
 - Note: A special press-fit pin was manufactured, with dimensions particular to the test item described in section 2, to hold and guide the SMA ring into the steel hub.
6. Allow the isopropyl alcohol to evaporate and place the assembled press-fit joint back into its particular oil free bag.
7. Construct the SMA²C tensile test rig as described below and conduct tensile test for each press-fit joint; record data in Table 3.1.
8. Once the SMA cylindrical ring is free, Measure the outer diameter of the SMA cylindrical rings with a micrometer at multiple points by rotating the ring 60-90° every measurement; record data in Table 3.1.

3.3 Test Results:

Table 3.1 Press-Fit SMA Tensile Load Test Data

Press-Fit SMA Test Number	Measured Inner Diameter of Stainless Steel Press-Fit Hole (+/- 0.00075 inches)	Measured Outer Diameter of SMA Ring Pre Test (+/- 0.00005 inches)	Calculated Press-Fit Interference (+/- inches)	Maximum Holding Force Measured During Test (N & lbf)	Measured Outer Diameter of SMA Ring Post Test (inches) Relative Error (%)	Calculated Reduction (+/- 0.00007 inches)
1	0.3115	0.3125 (0.3120-0.3130)	0.0010 (+/- 0.00093)	220N 50lbf	0.3123 (0.12%)	0.00028
2	0.3110	0.3121 (0.3119-0.3122)	0.0011 (+/- 0.00078)	695N 156lbf	0.3117 (0.06%)	0.00035
3	0.3100	0.3125 (0.3123-0.3127)	0.0025 (+/- 0.00079)	885N 199lbf	0.3113 (0.04%)	0.00128
4	0.3090	0.3126 (0.3124-0.3128)	0.0036 (+/- 0.00079)	2,386N 536lbf	0.3110 (0.05%)	0.00162

Note: The range given in parenthesis for SMA ring diameter are the bounds of micrometer readings obtained from multiple outer diameter measurements (i.e. range is due to non-circular rings). Subsequent calculated interference values and their respective measurement error are affected by this variance.

SMA²C tensile test rig:

The design of the SMA²C tensile test rig allows axial loading of the interference joint made between the SMA cylindrical ring and the stainless steel hub (see Figure 3.1). This is accomplished by first press-fitting the SMA ring into the steel hub, within a measured interference, and then attaching the hub to the top of the SMA²C tensile test rig with four 1/8" hex bolts until snug. The test rig top and hub combination are then attached to the bottom of the test rig by means of a single 1/8" hex bolt dropped through a top access hole in the test rig until the head of the bolt catches the SMA cylindrical ring (see Figure 3.2). An Allen wrench is inserted through the top access hole and used to screw the hex bolt loosely into the test rig bottom (see Figure 3.3).

Note: Care must be taken not to thread the center hex bolt too much as to make contact between the hub and tensile rig bottom. This would add a preload to the press-fit joint.

The entire SMA²C tensile test rig (top, hub & bottom) is now assembled and inserted into the tensile test machine with shear pins.

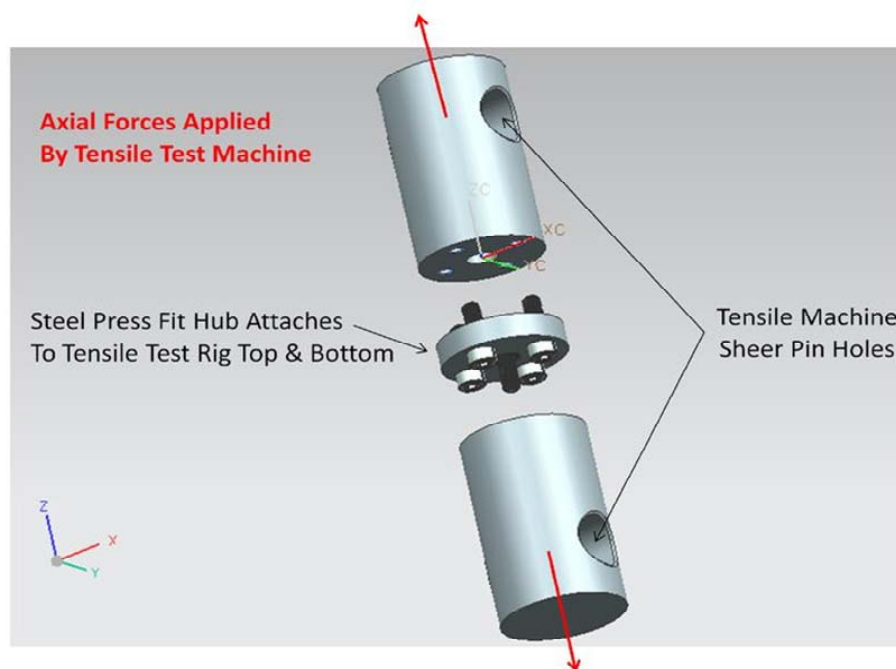


Figure 3.1 Concept View of SMA²C Tensile Test Rig Configuration and Applied Loading

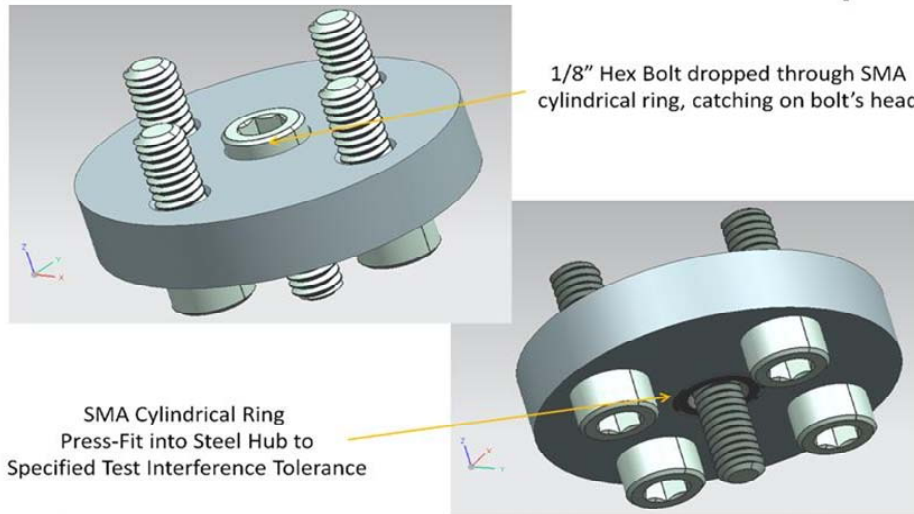


Figure 3.2 Close up View of Steel Hub and SMA Cylindrical Ring Interference Joint with Holding Bolts Present

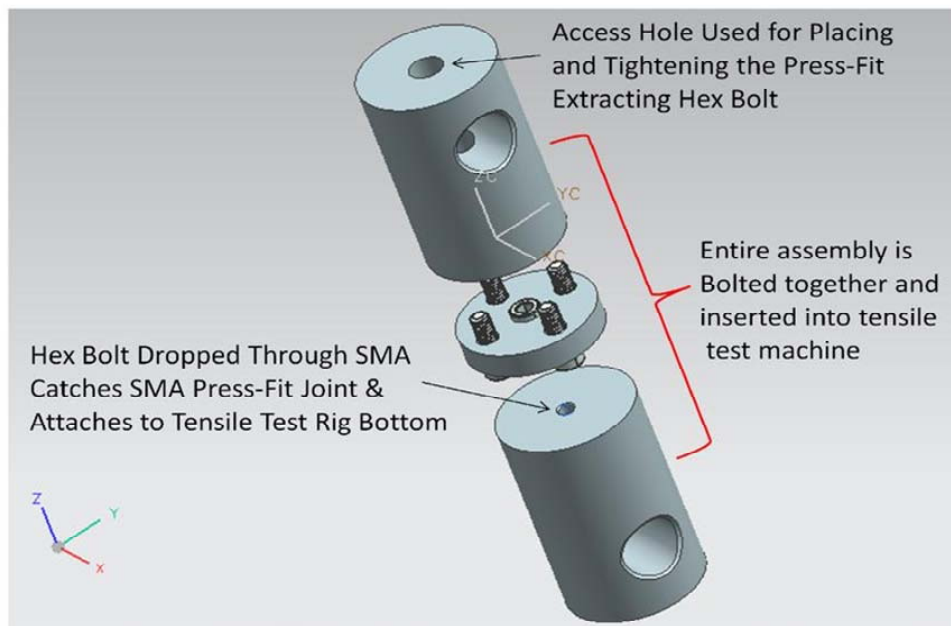


Figure 3.3 View of SMA²C Tensile Test Rig and Extracting Hex Bolt Threaded Hole

Section 4 – Data Analysis & Calculations

4.1 Predicted Interference Joint Coupling Force Values

Test Sample #	Desired Interference	Predicted Coupling Force	
1	0.0005" ±0.00005"	210 N	47.2 lbf
2	0.001" ±0.00005"	430 N	96.7 lbf
3	0.002" ±0.00005"	850 N	191.1 lbf
4	0.003" ±0.00005"	1,280 N	287.6 lbf

The interference generated from the press-fit between the SMA outer diameter and the hub inner diameter creates high contact pressures on the SMA-hub interface. This normal pressure (force/area perpendicular to the shaft axis of the SMA cylindrical ring), along with an estimated coefficient of friction of the mating materials, is used to calculate the coupling capability. The equations for contact pressure, frictional force, and torque transmission are:

Variables:

E_1 = Elastic Modulus for the inner member (SMA cylindrical ring)

E_2 = Elastic Modulus for the outer member (Stainless steel hub)

ν_1 = Poisson's Ratio for the inner member

ν_2 = Poisson's Ratio for the outer member

μ = Coefficient of static friction at the interface of the members.

L = Contact length

r = Nominal radius at the interference, common radius

r_o = Outer radius of the outer member

r_i = Inner radius of the inner member (note $r_i = 0$ for a solid member)

p = Contact pressure, Interference Pressure

$$p = \frac{\delta}{\frac{r}{E_2} \left(\frac{r_o^2 + r^2}{r_o^2 - r^2} + \nu_2 \right) + \frac{r}{E_1} \left(\frac{r^2 + r_i^2}{r^2 - r_i^2} - \nu_1 \right)}$$

δ = Radial Interference

$$\delta = \frac{pr}{E_2} \left(\frac{r_o^2 + r^2}{r_o^2 - r^2} + \nu_2 \right) + \frac{pr}{E_1} \left(\frac{r^2 + r_i^2}{r^2 - r_i^2} - \nu_1 \right)$$

δ_i = Change of the outer radius of the SMA cylindrical ring

$$\delta_i = -\frac{pr}{E_1} \left(\frac{r^2 + r_i^2}{r^2 - r_i^2} - \nu_1 \right)$$

δ_o = Change of the inner radius of the stainless steel hub

$$\delta_o = \frac{pr}{E_2} \left(\frac{r_o^2 + r^2}{r_o^2 - r^2} + \nu_2 \right)$$

σ_i = Tangential stress at the contact (outer) surface of the SMA cylindrical ring

$$\sigma_i = -p \left(\frac{r^2 + r_i^2}{r^2 - r_i^2} \right) \quad \text{Note: This is shown as } d_i \sigma_t \text{ in the press-fit calculator below.}$$

σ_o = Tangential stress at the inner (contact) surface of the stainless steel hub

$$\sigma_o = p \left(\frac{r_o^2 + r^2}{r_o^2 - r^2} \right) \quad \text{Note: This is shown as } d_o \sigma_t \text{ in the press-fit calculator below.}$$

T = Torque that the pressed joint will resist

$$T = 2\pi r^2 \mu p L$$

F_n = Normal Force (relative to the press fit surface)

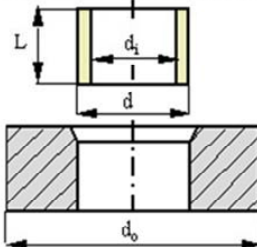
$$F_n = p 2\pi r L$$

F_μ = Frictional "Holding" Force of the SMA cylindrical ring

$$F_\mu = \mu F_n$$

Interference Fit Internal Pressure and Frictional Coupling Force Predictions

Credit: Tribology-abc.com calculators



1)

d_i	5.3340	mm	L	3.8608	mm	E_i	34.475	GPa	ν_i	0.33
d	7.9375	mm	$\delta^{(1)}$	0.0127	mm	E_o	210	GPa	ν_o	0.30
d_o	12.700	mm	$\mu^{(2)}$	0.11						

(Default value bronze bushing, steel hub)

Interference pressure p 20.13 MPa

Friction force F 0.21 kN

Transmission torque T 0.85 Nm

Stresses	ring i		ring o	
	d_i	d	d	d_o
σ_t	-73.4 MPa	-53.27 MPa	45.93 MPa	25.6 MPa
σ_r	0 MPa	-20.13 MPa	-20.13 MPa	0 MPa
σ_e	73.4 MPa	46.59 MPa	58.64 MPa	25.8 MPa

2)

d_i	5.3340	mm	L	3.8608	mm	E_i	34.475	GPa	ν_i	0.33
d	7.9375	mm	$\delta^{(1)}$	0.0254	mm	E_o	210	GPa	ν_o	0.30
d_o	12.700	mm	$\mu^{(2)}$	0.11						

(Default value bronze bushing, steel hub)

Interference pressure p 40.25 MPa

Friction force F 0.43 kN

Transmission torque T 1.69 Nm

Stresses	ring i		ring o	
	d_i	d	d	d_o
σ_t	-146.79 MPa	-106.54 MPa	91.86 MPa	51.6 MPa
σ_r	0 MPa	-40.25 MPa	-40.25 MPa	0 MPa
σ_e	146.79 MPa	93.18 MPa	117.28 MPa	51.6 MPa

3)

d_i	5.3340	mm	L	3.8608	mm	E_i	34.475	GPa	ν_i	0.33
d	7.9375	mm	$\delta^{(1)}$	0.0508	mm	E_o	210	GPa	ν_o	0.30
d_o	12.700	mm	$\mu^{(2)}$	0.11						
<input type="button" value="Solve"/> <input type="button" value="Reset"/> <input type="button" value="Print"/> (Default value bronze bushing, steel hub)										
Interference pressure p									80.5	MPa
Friction force F									0.85	kN
Transmission torque T									3.38	Nm

Stresses	ring i		ring o					
	d_i	d	d	d_o				
σ_t	-293.59	MPa	-213.08	MPa	183.71	MPa	103.21	MPa
σ_r	0	MPa	-80.5	MPa	-80.5	MPa	0	MPa
σ_e	293.59	MPa	186.36	MPa	234.57	MPa	103.21	MPa

4)

d_i	5.3340	mm	L	3.8608	mm	E_i	34.475	GPa	ν_i	0.33
d	7.9375	mm	$\delta^{(1)}$	0.0762	mm	E_o	210	GPa	ν_o	0.30
d_o	12.700	mm	$\mu^{(2)}$	0.11						
<input type="button" value="Solve"/> <input type="button" value="Reset"/> <input type="button" value="Print"/> (Default value bronze bushing, steel hub)										
Interference pressure p									120.76	MPa
Friction force F									1.28	kN
Transmission torque T									5.08	Nm

Stresses	ring i		ring o					
	d_i	d	d	d_o				
σ_t	-440.38	MPa	-319.62	MPa	275.57	MPa	154.81	MPa
σ_r	0	MPa	-120.76	MPa	-120.76	MPa	0	MPa
σ_e	440.38	MPa	279.54	MPa	351.85	MPa	154.81	MPa

Note: Only axial forces were tested to validate the calculated values above.

4.2 Predicted vs. Experimental Data with Propagated Measurement Error

Predicted coupling force is based upon the anticipated interference created between the stainless steel hub and SMA cylindrical ring. Very small changes in the interference (defined as $\delta = r_o - r_i$) on the order of 0.0001" have a dramatic impact on the resulting coupling force; therefore measurement precision of both the stainless steel hub and SMA cylindrical ring play an important role as their resulting measurement error propagates through the press-fit equations found in section four effecting our predicted coupling force $F_\mu = \mu p 2\pi r L$.

Error propagation was found by using the standard deviation of the measurement variance for each variable in the press-fit equations starting with the interference error:

$$\Delta r = \sqrt{(\Delta r_o)^2 + (\Delta r_i)^2}$$

It is important to note here that the SMA cylindrical rings were found to be non-circular. This non-uniform shape was included in the values for Δr_o compounding the interference error.

Next, the interference pressure error is created from the interference error scaled by the predicted interference pressure:

$$\Delta p = p \sqrt{\left(\frac{\Delta r \sqrt{2[(2\Delta r_o)^2 + (2\Delta r)^2]}}{\delta} \right)^2 + \left(\frac{\Delta r \sqrt{2[(2\Delta r_i)^2 + (2\Delta r)^2]}}{\delta} \right)^2}$$

Finally, the coupling force error is created by the interference pressure error scaled by the predicted coupling force:

$$\Delta F_\mu = F_\mu \sqrt{\left(\frac{\Delta p}{p} \right)^2 + \left(\frac{\Delta r}{\delta} \right)^2}$$

A summary of the recorded measurement values and their precision can be found in the appendix.

The press-fit equations found in section four yield a static friction coupling force, so once the interference fit begins extraction, the coefficient of static friction is replaced by a lower kinetic friction value. This friction coefficient transition leads to an initial peak in coupling force at the beginning of the test as seen in the experimental data (Figures A1 & A3). This static friction-coupling peak is termed as the experimental coupling force "static peak". The smooth roll off in resistance to extraction with increasing displacement observed during the tests was caused by a decrease in interference joint surface area in contact as the SMA separated from the steel hub.

As can be seen in Figures A2 & A4, the static peak is not always the maximum experimental coupling force obtained. For this reason, a comparison of the predicted coupling force and the integrated average of the interference joint extraction data are conducted. The experimental static peak and integrated average coupling values are shown along with the predicted coupling values in Figure 4.1. Error bars on the predicted values show the extent of prediction error attributed to the non-circular SMA rings and measurement tool tolerances.

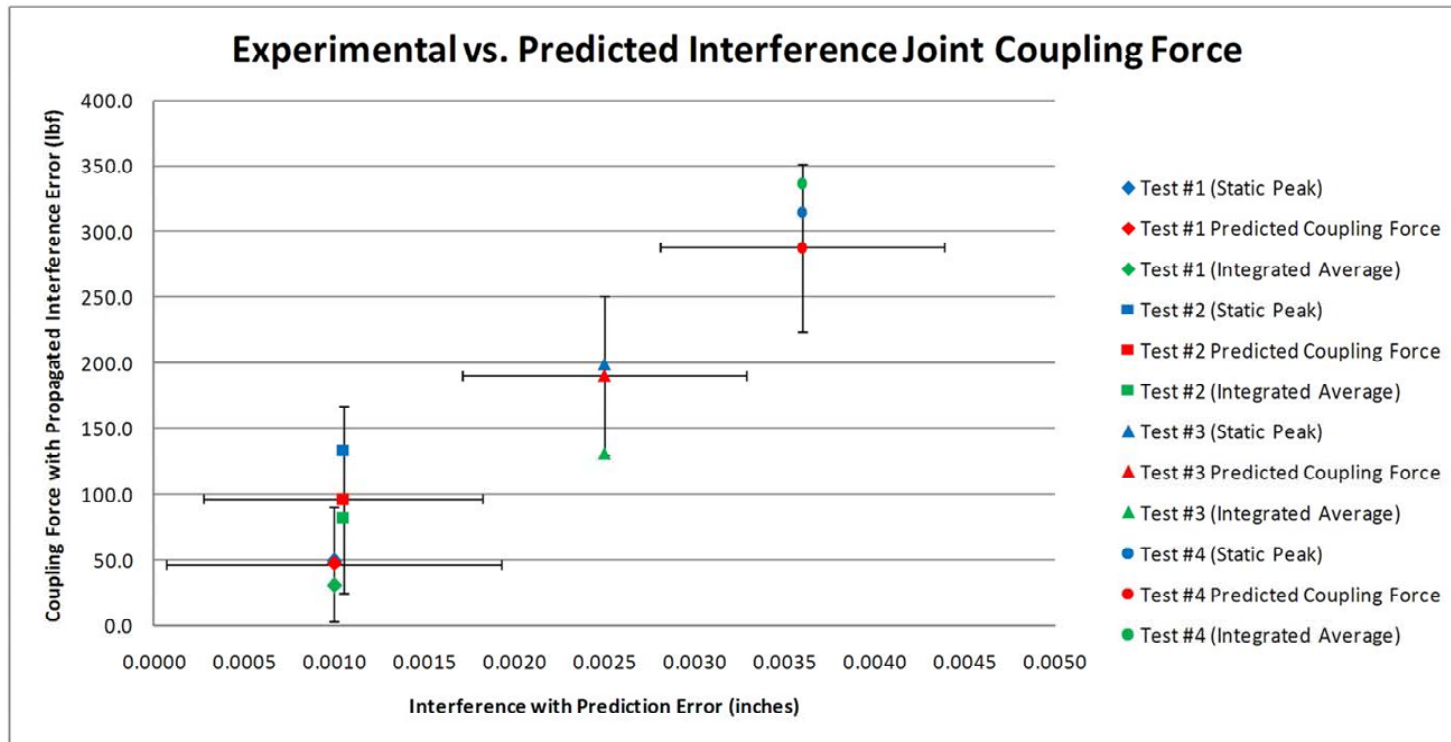


Figure 4.1 Comparison of Predicted and Experimental Data for Interference Joint Coupling Forces.
Note: An additional graph of the above data is presented in the appendix.

4.3 Post-Test Correlation Between SMA Outer Diameter and Tested Interference

The outer diameter of the SMA cylindrical ring was measured post-test to determine the extent of de-stressing imparted upon the detwinned martensitic SMA from both the press-fit and interference joint removal process. Greater fidelity of post-test data measurements resulted in a relative error for each SMA ring (see Table 3.1) for the recorded measurements. Although measurement error from the pre-test calculated interference was large relative to the desired interference, a correlation between the post-test SMA outer diameter and the tested nominal interference can be seen in Figure 4.2.

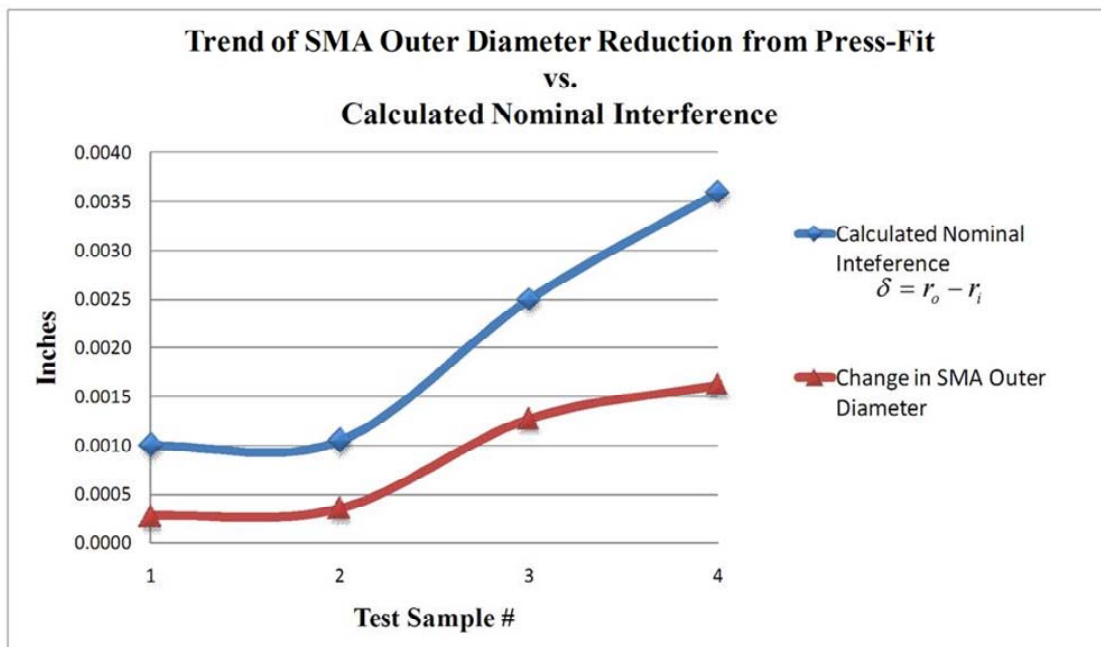


Figure 4.2 SMA Post-Test Reduced Diameter and Tested Interference Comparison

Section 5 – Findings and Conclusions

The interference joint created by press-fitting SMA into a steel hub achieved significant axial strength confirming the concept is viable for coupling mechanisms. Overlaying of the force/displacement curves (see Figure A5) shows a linear resistance response to press-fit removal before a peak in applied force. This would equate to a change from static to kinetic friction as the press-fit joint begins to be removed from the stainless steel hub. The largest interference fit explored (0.003") yielded the strongest interference joint that experienced several force peaks in resistance to extraction (see Figure A4). It is hypothesized that the cylindrical SMA ring experienced buckling upon forceful removal from its press-fit. This buckling would result in increased normal pressures at interference joint contacts as the stainless steel hub resists the SMA change in geometry. Increased normal forces would directly increase the axial coupling capability of the interference joint.

De-stressing of the detwinned SMA cylindrical ring was found to be in approximate proportion to $\frac{1}{2}$ of the calculated interference. This leads to the conclusion that a complete phase change of the detwinned SMA cylindrical ring for any of the explored interference values did not occur. If there would have been a complete phase change in the detwinned SMA due to acute pressures induced by extraction or excessive interference fit, the SMA ring would be permanently deformed as stable twinned martensite after the test (Note: normal SMA phase change from martensite to austenite is caused by an increase in temperature). The maximum outer diameter for SMA rings used in this test in the twinned martensitic phase was 0.2977". The smallest post-test extracted SMA cylindrical ring outer diameter was measured at 0.3108".

Inspection of the SMA rings and stainless steel hubs after test revealed visible contact spots and scratching down the long axis surface of the SMA. As the interference fits increased, the contact spots and scratches grew in size and quantity ultimately covering the entire outer circumference of the SMA ring at the tightest interference fit. The stainless steel hubs were less effected by the process, but did show a loss of luster at contact points.

This test utilized proven interference fit equations for non-shape memory alloy metals. Comparison of analytical predictions and experimental test data have shown the traditional interference fit equations give an adequate estimation of static axial coupling capability for press-fit shape memory alloys within the limited test cases. Inaccuracies in the predicted coupling values occurred due to measurement tolerances, but could have additional sources as follows:

Inaccuracy in the chosen coefficient of friction between the nickel titanium shape memory alloy and the stainless steel hub;

Actual surface area in contact for each explored interference fit;

Possible SMA phase change localized at interference fit contact points due to excessive localized pressures experienced during the press-fit process or forced removal from the stainless steel hub.

Appendix

Supporting Graphs & Diagrams

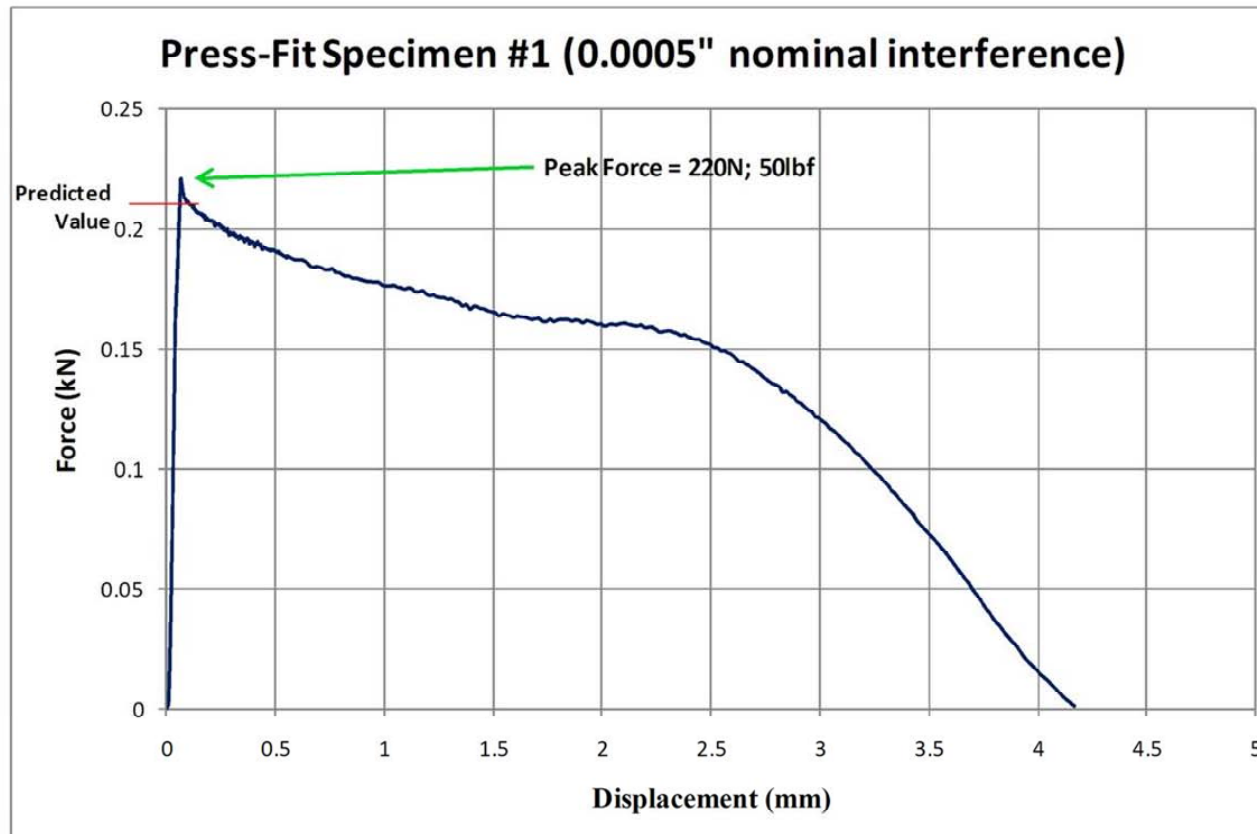


Figure A1 SMA Press-Fit Removal Force vs. Displacement for a 0.0005" Nominal Interference

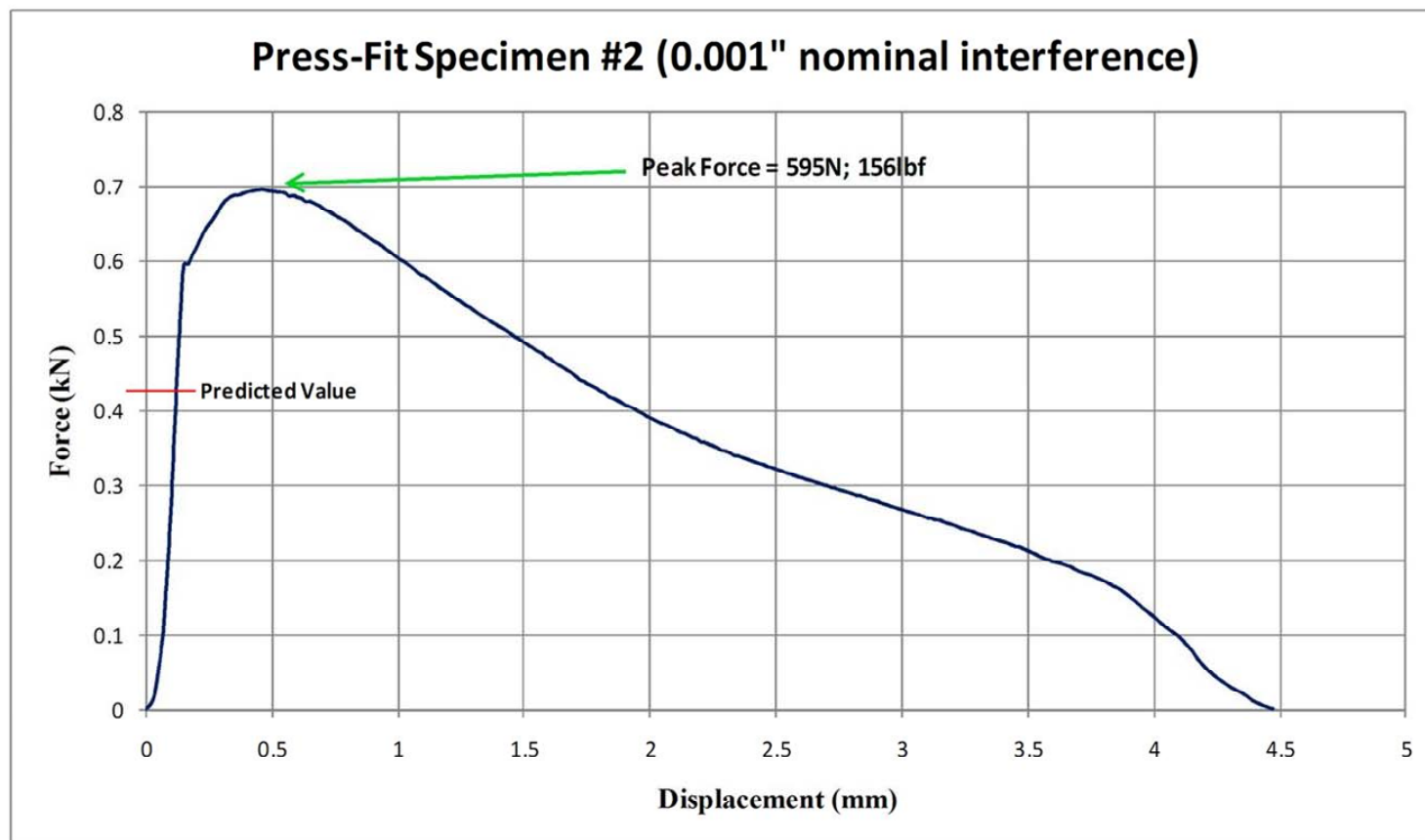


Figure A2 SMA Press-Fit Removal Force vs. Displacement for a 0.001" Nominal Interference

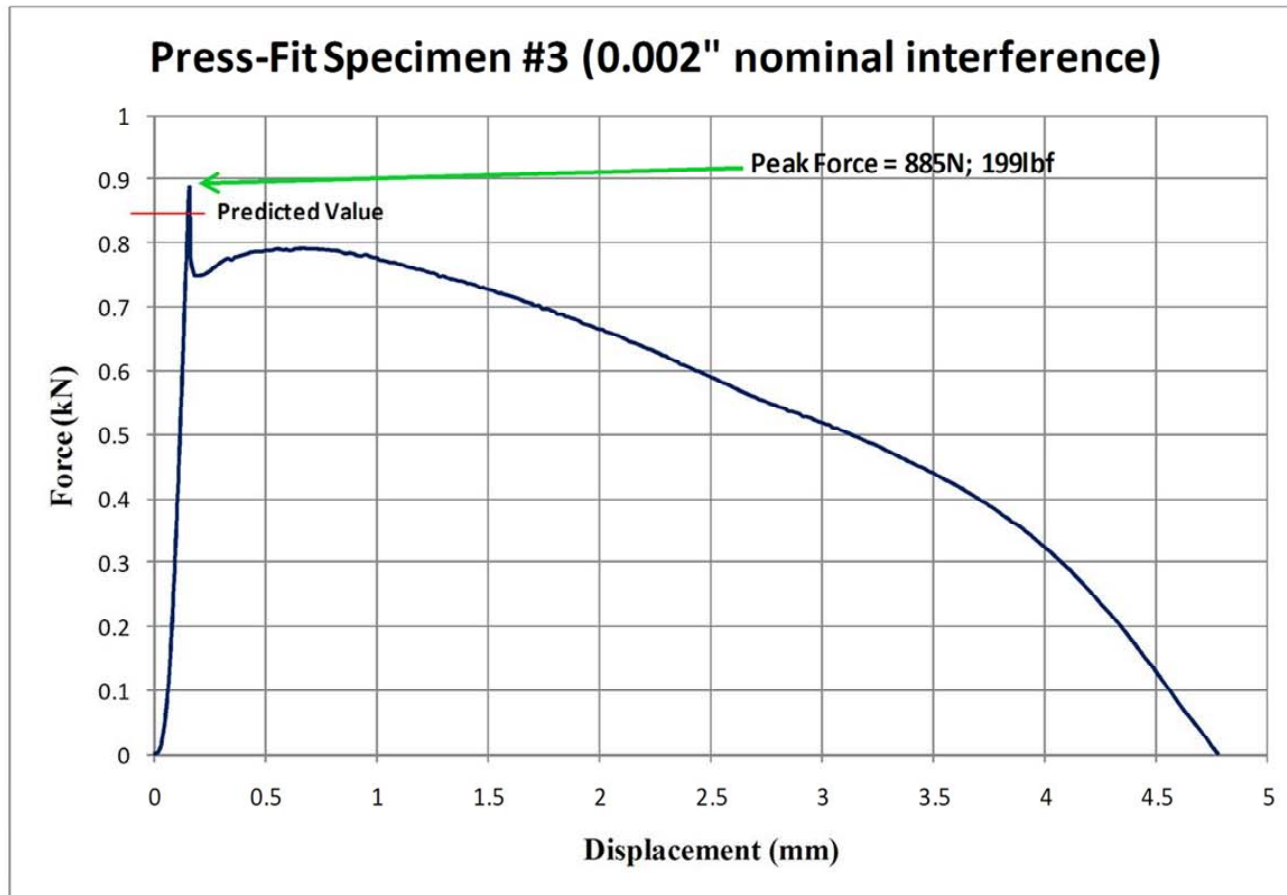


Figure A3 SMA Press-Fit Removal Force vs. Displacement for a 0.002" Nominal Interference

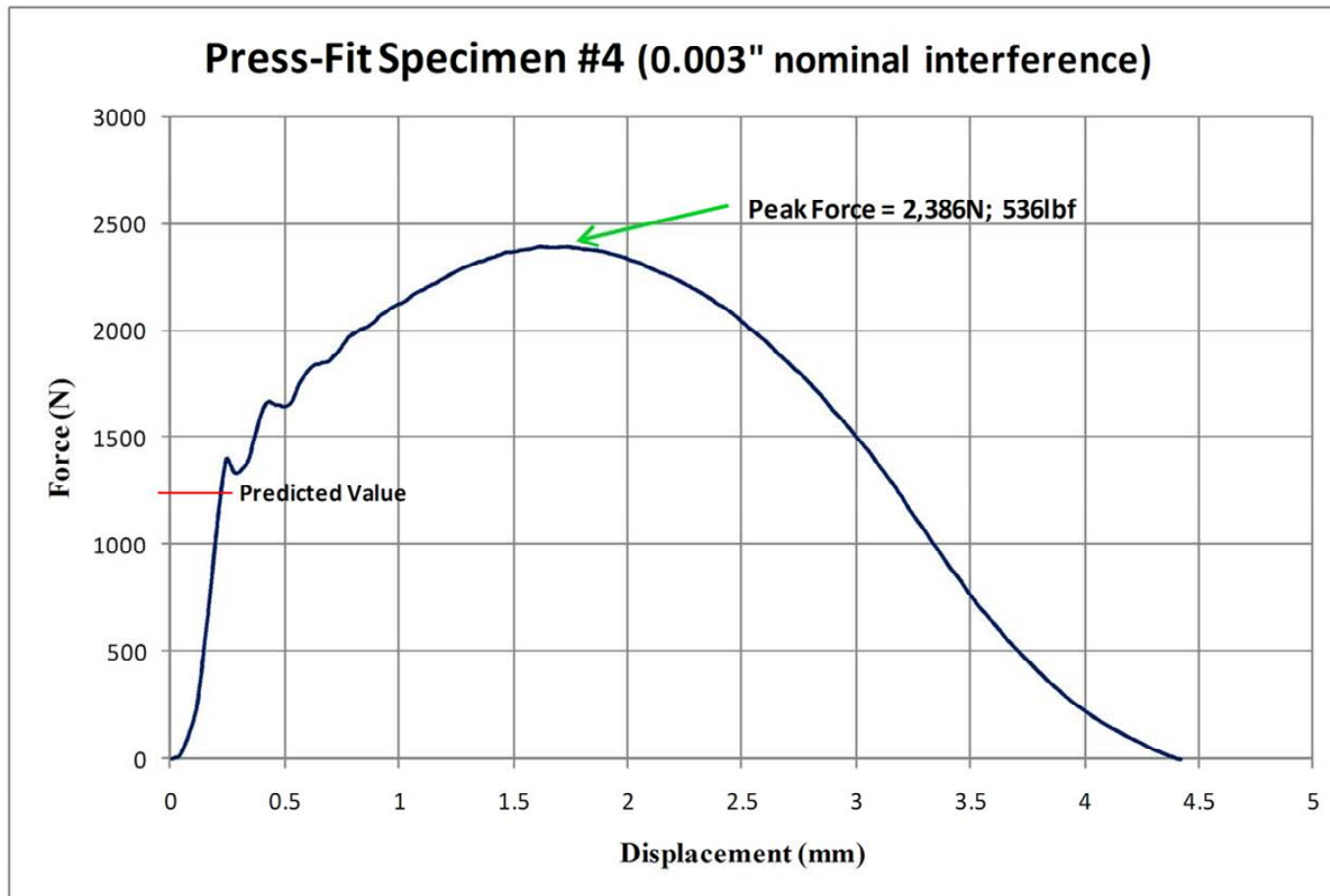


Figure A4 SMA Press-Fit Removal Force vs. Displacement for a 0.003" Nominal Interference

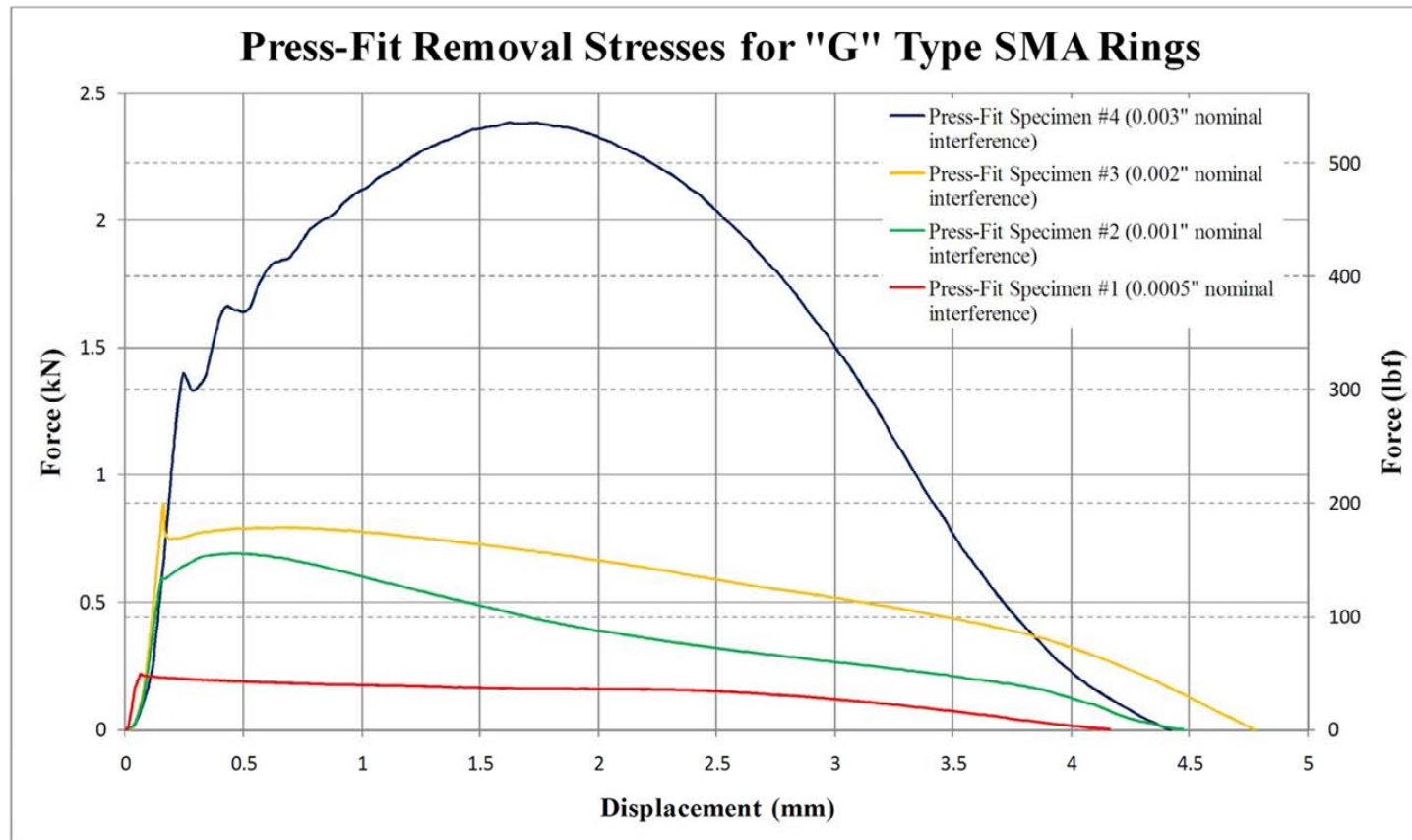
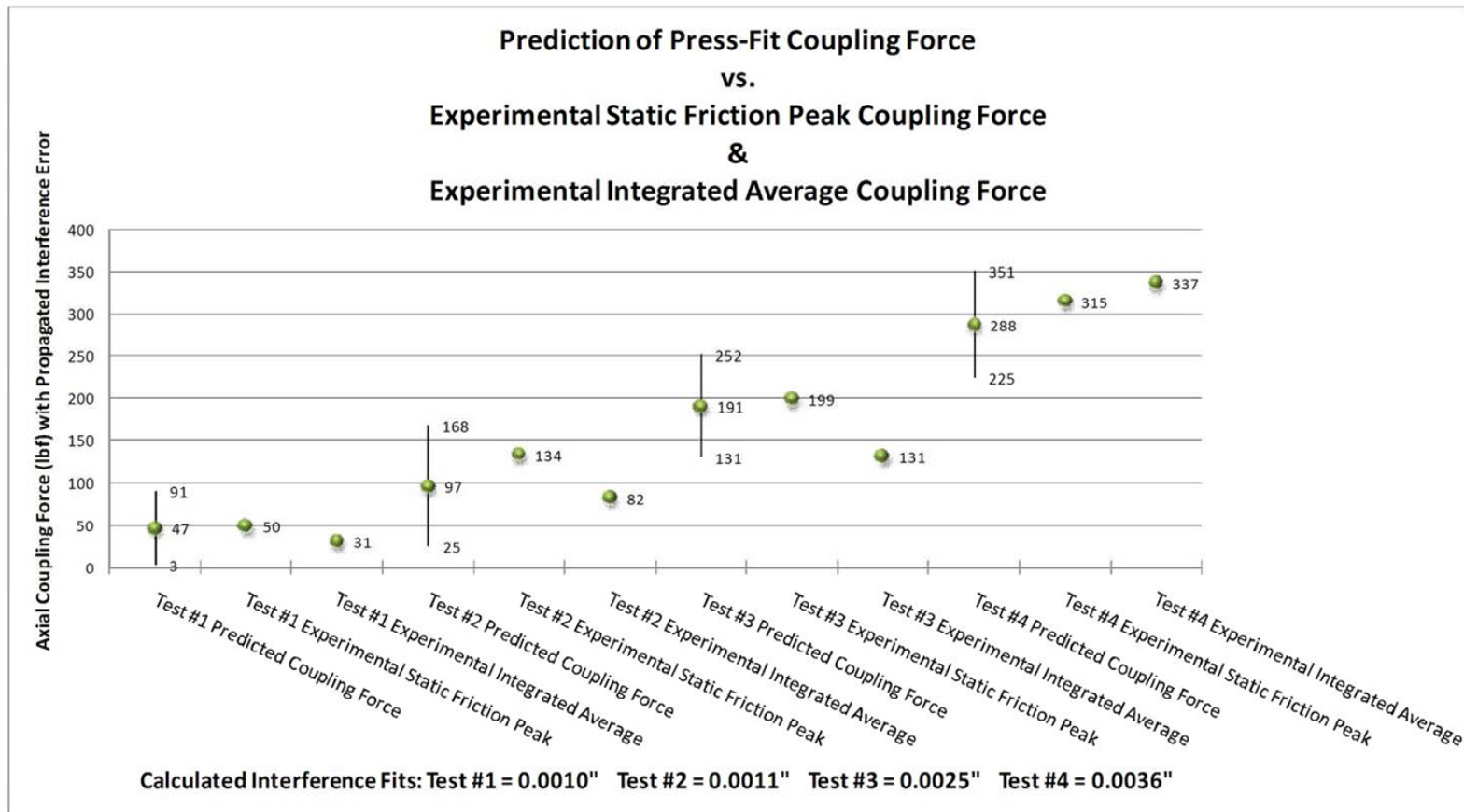


Figure A5 SMA Press-Fit Removal Tests Overlay View

Additional Graphs



Test Equipment and Instrumentation

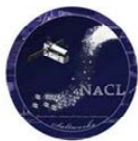
Instrument or Equipment	Manufacturer	Model	Serial Number	Calibration Date
Micrometer	Mitutoyo	0-1" +/-0.00005	293-832	Unknown
Gauge Pins	Fowler	0.061-0.250"	USN 026039	15May09 (+/- 0.00005")
Tensile Machine Load Cell	Instron	8500 (2518-103)	uk193 USN 62271A4547	24 June 09

Measured Values with Associated Tolerances

<u>Pre-Interference Fit</u>					
	Stainless Steel Hubs			Tolerance	
Test #	Reamed Diameter (+0.0002") r_o	Gauge Pin Inserted (- 0.0005")	0.00075	median	
1	0.3115	0.311 (loose fit)		0.3115	
2	0.3110	0.311 (very tight fit)		0.3110	
3	0.3100	0.310 (tight fit)		0.3100	
4	0.3090	0.309 (easy fit)		0.3090	
	SMA Rings			Tolerance	Non-circular
Test #	4 point Micrometer Measured Diameter (+/- 0.00005") r_i		0.00005	median	SMA Ring Δ
1	0.3120 - 0.3130			0.31250	0.00050
2	0.3119 - 0.3122			0.31205	0.00015
3	0.3123 - 0.3127			0.31250	0.00020
4	0.3124 - 0.3128			0.31260	0.00020

<u>Post-Interference Fit</u>							
Test #	SMA Rings 4 point Micrometer Measured Diameter (+/- 0.00005")	mean	median	variance	σ	Relative Error	Change in SMA Outer Diameter (inches)
1	0.3118						
	0.3120						
	0.3125						
	0.3126	0.3122	0.3123	1.49167E-07	0.00039	0.12%	0.00028
2	0.3115						
	0.3118						
	0.3119						
	0.3116	0.3117	0.3117	3.33333E-08	0.00018	0.06%	0.00035
3	0.3112						
	0.3111						
	0.3114						
	0.3112	0.3112	0.3112	1.58333E-08	0.00013	0.04%	0.00128
4	0.3112						
	0.3108						
	0.3109						
	0.3110	0.3110	0.3110	2.91667E-08	0.00017	0.05%	0.00162

APPENDIX C. NACL REPORT: MICRO-COUPLING ENGINEERING DESIGN UNIT LOAD BEARING CAPABILITY



NACL Test Report #SMA²C-3

Date of Testing: 09 JUL 2010

Date of Report: 23 JUL 2010

NAVAL POSTGRADUATE SCHOOL NANO-SATELLITE ADVANCED CONCEPTS LABORATORY TEST REPORT

Performed by:
CDR William Crane

Testing Performed for:
Single Motion Actuated Shape Memory Alloy Coupling (SMA²C)

Micro-Coupling Engineering Design Unit Load Capability

Signature of Certifying Individuals

Dr. Marcello Romano
NPS Professor, MAE & Space Systems Academic Group

Dr. James Newman
NPS Professor, Space Systems Academic Group

Reviewer Signatures

CDR William M. Crane
NPS 591 Class 2010 & SMA²C Developer

Mr. Paul Oppenheimer
Naval Research Laboratory/SMA²C Co-developer

Contents

Section 1 - Overview	2
Section 2 - Test Items	4
Section 3 - Testing	8
Section 4 - Data Analysis & Results	18
Section 5 - Findings and Conclusions	28

Section 1 - Overview

1.1 Testing Purpose and Scope

Objective – Obtain the axial coupling strength of the NiTi Shape Memory Alloy (SMA) interference joint as designed for the Single Motion Actuated Shape Memory Alloy Coupling (SMA²C) using prototype hardware.

Threshold: Validate the Engineering Design Unit (EDU) design geometry of the SMA²C micro-coupling by obtaining force vs. displacement data during the forceful extraction of the SMA from the micro-coupling's interference joint.

Goal: Obtain the threshold objective in addition to determining if the press-fit process induced martensitic de-stressing or plastic deformation of the SMA cylindrical ring. Determine if industry standard formulas for interference joint strength or force recorded during the micro-coupling press-fit creation process are valid to predict the expected micro-coupling's strength within propagated measurement error.

1.2 Executive Summary

Threshold and goal objectives were met. Traditional press-fit equations appear sufficient to yield initial static friction micro-coupling strength, but are insufficient to predict micro-coupling ultimate strength. The expected initial static friction peak can be seen in Figure 4.1 and experimental data found in the appendix. Unexpected static to kinetic friction transitions are found after the initial static friction peak in addition to an increasing coupling strength as the SMA is extracted. Ultimately, a smooth roll off in resistance with continued extraction was observed due to decreasing interference joint surface area contact as the SMA separated from the steel hub. Initial static peak strengths of 140-457 lbf and ultimate strengths of 325-916 lbf were achieved. Maximum coupling forces were achieved by the 3-mil interference micro-couplings.

There appeared to be no difference if the micro-coupling was created by a top-down or bottom-up press-fit direction, and the coefficient of friction is not constant between the two materials used in the interference joint (this is confirmed through testing done on pseudoelastic SMA for medical applications by other research institutions). There was no plastic deformation of the SMA beyond a visible surface texture change. Martensitic de-stressing can be seen to be approximately 1-mil less than the nominal interference by the elasticity of the SMA characterized by a slight "spring-back" upon being freed from the interference joint.

The pseudoelastic properties of SMA within an interference joint yielded exciting results: Test data plots are accentuated by static to kinetic friction "vibrations," but are not believed to be the cause of increasing coupling strength upon SMA forced removal. The SMA interference joint's ultimate strength, induced by atomic interactions between the SMA and case hardened steel materials, are purely hypothetical at the level of testing conducted, but the combination of SMA over-pressurization phase change and column buckling of the SMA cylinder within the interference joint are believed to be the contributing factors that manifested the unique test data collected. More testing is needed for any definitive SMA interference joint material interaction conclusions and accurate predictions of SMA²C micro-coupling ultimate strength.

1.3 Test Applicability Abstract

The SMA²C device is dependent on a press-fit SMA cylindrical ring to create a coupling mechanism that will provide sufficient coupling strength to resist being forcefully removed under adverse loading, and maintain enough allowable SMA geometry change upon commanded phase change activation of the coupling mechanism to ensure successful de-coupling (see Figure 1.1).

Coupling strength is obtained by frictional forces generated when the SMA is press-fit into a metallic bushing creating an interference joint. To be a reliable coupling mechanism, the interference between the two parts has to be within precise tolerances:

If the press-fit interference is too little, not enough friction is created to supply the needed coupling strength;

If the press-fit interference is too large, de-stressing or phase change of the martensitic SMA could occur and subsequently reduce coupling strength. Excess interference could disable the SMA's ability to free itself from the press-fit upon heating and therefore defeat the designed purpose of the coupling mechanism to release itself upon command.

If the press-fit interference is not measured to precise tolerances, prediction of the coupling mechanism's strength could be overestimated leading to premature loading failure.

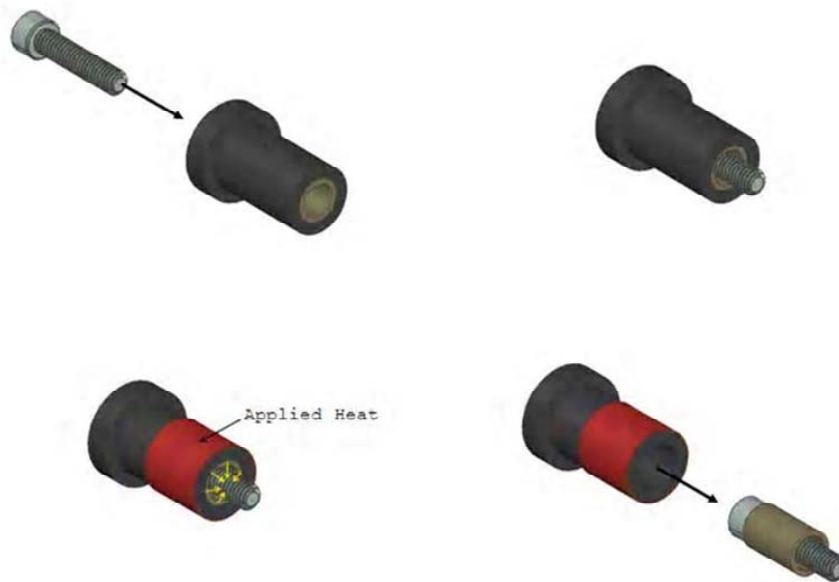


Figure 1.1 SMA²C micro-coupling concept illustrating the release of a press-fit shape memory alloy cylindrical ring upon commanded release by use of an applied heat source.

Section 2 – Test Items

2.1 Part Descriptions & Properties

- 1) “G” type Unilok® SMA ring (AGE0156-0022-0312)

INTRINSIC

UniLok® Material Properties

Nominal Properties for All Alloys

Melting Point	1300°C (2370°F)
Thermal Conductivity	0.18 W/cm·°C (10.4 BTU/hr·ft·°F)
Specific Heat	0.2 cal/g·°C (0.2 BTU/lb·°F)
Coefficient of Thermal Expansion	11x10 ⁻⁶ /°C (6.1x10 ⁻⁶ /°F)
Poisson's Ratio	0.33
Electrical Resistivity	90x10 ⁻⁶ ohm-cm (35x10 ⁻⁶ ohm-in)
Magnetic?	No
Magnetic Permeability	<1.002
Magnetic Susceptibility	3x10 ⁶ emu/g
Corrosion	Similar to 300 series stainless steel. For specific compatibility data, consult Intrinsic Devices.

Austenitic Mechanical Properties

Yield Strength	415MPa (60kpsi)
Ultimate Tensile Strength	800MPa (115kpsi)
Elongation to Failure	25%
Young's Modulus in Tension	75GPa (11x10 ⁶ psi)
Hardness	65 Ra

Alloy Specific Properties

Composition (wt%)	Ti 45, Ni 55
Density	6.5g/cm ³ (0.235 lb/in ³)

Note: All properties given are nominals for initial design purposes. Testing is required to qualify performance in specific applications. Always test for adequate clamping force at the minimum operating temperature of the assembly.

UniLok® is a registered trademark of Intrinsic Devices, Inc.

Intrinsic Devices, Inc.
2353 Third Street
San Francisco, CA 94107-3108
tel: 415) 252-5902 fax: 415) 252-1624
<http://www.intrinsicdevices.com/>

Product Document
Material Properties

Drawing ID	Rev.	Date	Page
PD 005	E	9/19/03	1 of 1

TEST REPORT NOTE: Modulus of elasticity for martensitic NiTi SMA is 30 GPa as referenced in: *Shape Memory Alloys Modeling and Engineering Applications*; Editor Dimitris C. Lagoudas, Department of Aerospace Engineering Texas A&M; Published by Springer Science + Business Media, LLC © 2008.

Supplier Specifications for EDU SMA Ring

Supplied Dimensions (inches):

Inner Diameter .1565 / .1580
Outer Diameter .2030 / .2045
Length .3060 / .3080

Recovered Dimensions (inches):

Inner Diameter .1470 / .1482
Outer Diameter .1944 / .1960
(Typical outer diameter taper on SMA ring = +/- 0.0005)

2) Casehardened Steel Hubs

(as procured from McMaster Carr)

Inner Diameter 0.1990"



Part Number: 8492A026

Type	Press-Fit Drill Bushings with Head
Material	Steel
Steel Material Type	Case-Hardened Steel
Wire Gauge Drill Size	#8 (.1990")
System of Measurement	Inch
Inside Diameter	.199"
Inside Diameter Tolerance	+ .0001" to + .0004"
Outside Diameter	5/16"
Outside Diameter Tolerance	+ .0013" to + .0016"
Length	1/2"
Length Tolerance	± .015"
Head Diameter	27/64"
Head Thickness	1/8"
Rockwell Hardness	C61-C65
Specifications Met	American National Standards Institute (ANSI)

Inner Diameter 0.2010"



Part Number: 8492A101

Type	Press-Fit Drill Bushings with Head
Material	Steel
Steel Material Type	Case-Hardened Steel
Wire Gauge Drill Size	#7 (.201")
System of Measurement	Inch
Inside Diameter	.201"
Inside Diameter Tolerance	+ .0001" to + .0004"
Outside Diameter	3/8"
Outside Diameter Tolerance	+ .0013" to + .0016"
Length	1/2"
Length Tolerance	± .015"
Head Diameter	1/2"
Head Thickness	3/32"
Rockwell Hardness	C61-C65
Specifications Met	American National Standards Institute (ANSI)

Inner Diameter 0.2031"



Part Number: 8492A173

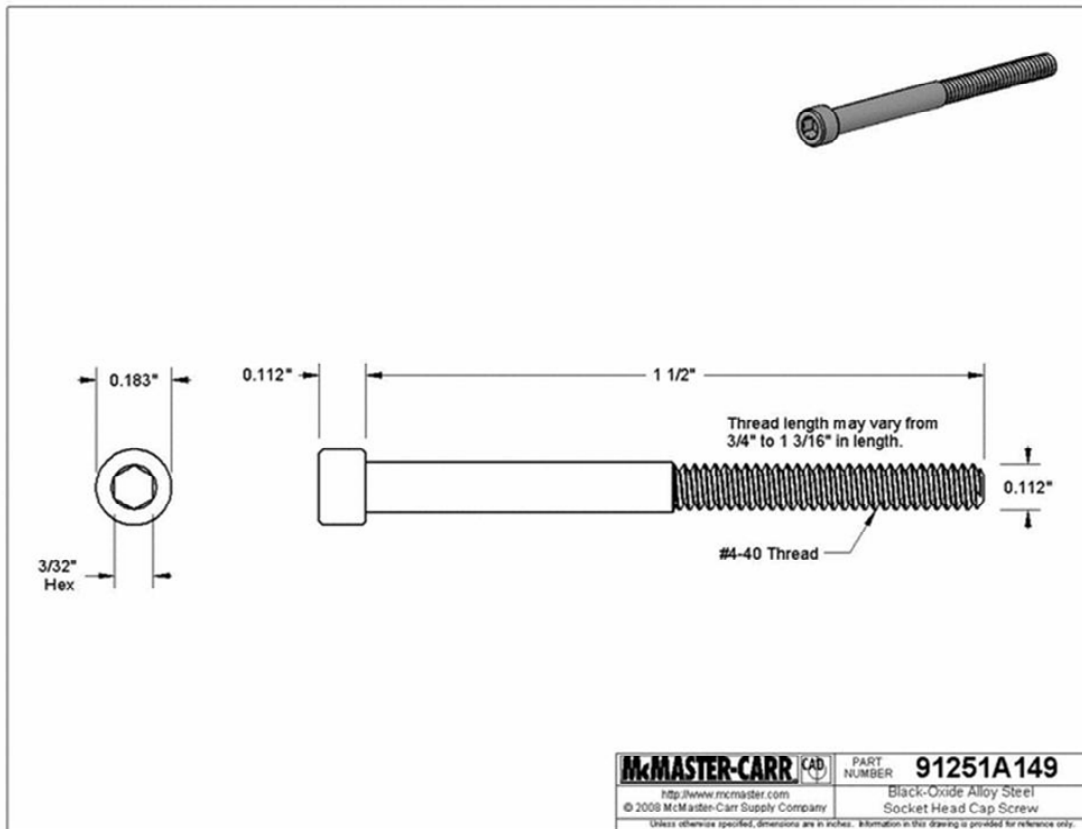
Type	Press-Fit Drill Bushings with Head
Material	Steel
Steel Material Type	Case-Hardened Steel
Fractional Drill Size	13/64" (.2031")
System of Measurement	Inch
Inside Diameter	.2031"
Inside Diameter Tolerance	+.0001" to +.0004"
Outside Diameter	1/2"
Outside Diameter Tolerance	+.0014" to +.0016"
Length	1/2"
Length Tolerance	±.015"
Head Diameter	39/64"
Head Thickness	7/32"
Rockwell Hardness	C61-C65
Specifications Met	American National Standards Institute (ANSI)

3) Socket Cap Screws



Part Number: 91251A149

Head Style	Standard
Standard Head Style	Standard
Material Type	Steel
Finish	Black-Oxide
Class	Not Rated
Drive Style	Hex Socket
Inch Thread Size	4-40
Length	1-1/2"
Thread Length	Partially Threaded
Thread Direction	Right Handed
Tip Type	Plain
Self-Locking Method	None
Screw Quantity	Individual Screw
Hex Size	3/32"
Head Diameter	.183"
Head Height	.112"
Rockwell Hardness	Minimum C39
Minimum Tensile Strength	180,000 psi
Thread Fit	Class 3A
Specifications Met	American Society for Testing and Materials (ASTM)
ASTM Specification	ASTM A574



Section 3 - Testing

3.1 Test Description

Method - Observation and measurement of axial loads using a tensile test machine to forcefully remove an interference joint consisting of a press-fit SMA cylindrical ring from a casehardened steel hub.

SMA cylindrical rings are measured using a micrometer with a 90° rotation between measurements at each end resulting in four total cross-diameter values. This method measures the amount of circular precision and taper in each cylindrical ring. Inner diameters of the casehardened steel hubs are measured using gauge pins to determine manufacturing accuracy with high precision. The difference between the SMA cylindrical ring outer diameter and the casehardened steel hub inner diameter yields the interference obtained, within measurement precision, when the two parts are joined. The method for press fitting the SMA into the steel hub uses a 'SMA²C press-fit cradle assembly' (see Figure 3.1) to align the two parts with a high degree of accuracy while enabling repeatability of the interference joint creation process. (It should be noted that the SMA cylindrical rings and steel hubs are mass-produced and have not been altered to reduce the possibility of data skewing induced by non-repeatable part modification.) A load cell is placed in series with the press-fit cradle to measure the maximum force used in creation of the interference joint.

The 'SMA²C coupling load test rig' (see Figure 3.6) mounts the SMA interference joint into a tensile test machine aligning the joint axially to measure the applied force and displacement of the interference joint during forced removal. The rate of displacement for the tensile machine is set to 1 mm/min to reduce the possibility of frictional heating that could induce a phase change in the SMA. The design of the SMA²C micro-coupling puts the SMA in compression vice tension while being forcefully removed. This design takes advantage of increasing frictional coefficients during forced removal due to the larger normal forces created by buckling and deformation of the SMA cylinder in compression vice necking in a pure tension situation. SMA cylindrical rings are again measured after forced removal to determine the amount of de-stressing the 'detwinned' martensitic SMA experienced during joint assembly and subsequent forced removal. The casehardened steel hubs are also measured after forced removal to determine if any plastic deformation occurred.

Thirty micro-coupling SMA interference joint specimens will constitute the sample set for this test; ten specimens at each of three nominal interference lots: 0.001", 0.003" & 0.005". Half of each interference lot (five specimens) will be created by pressing the SMA from the top of the bushing down, and the second half, created by pressing the SMA from the bottom of the bushing up. This change in press-fit direction is done to expose any resulting coupling strength characteristics that may be caused by the direction in which the press-fit process is conducted.

3.2 SMA & Case-Hardened Steel Hub Press-Fit Process

Number of Items to be created: 30 SMA²C Prototype Shape Memory Alloy Micro-Coupling Interference Joints

Location: NPS Machine Laboratory

Equipment:

- 30 “G” type Unilok® SMA rings (AGE0156-0022-0312)
- Micrometer (+/- 0.00005”)
- 10 casehardened steel bushings (0.1990”)
- 10 casehardened steel bushings (0.2010”)
- 10 casehardened steel bushings (0.2031”)
- Gauge pins (0.0001” steps from 0.1980” to 0.2045”; +0.00004”)
- Acetone and Isopropyl Alcohol (99%)
- Oil free (clean room) swabs and latex gloves (powder free)
- Clean room pads (cleaning patches)
- Tweezers
- Personal Protective Equipment (PPE)
 - Gloves, long sleeve shirt & safety glasses
- SMA²C Press-Fit Cradle (see Figure 3.1)
- Hand Press
- 1 ¼” Load Cell with data display and connected computer for data capture
- Video camera (if desired)

Procedure:

1. Measure the outer diameter of a SMA cylindrical ring with a micrometer (clean contact points and tare the digital readout) at two cross diameter points by rotating the ring 90° between measurements at both ends; record data in Table 4.1.
2. Measure the inner diameter of the casehardened steel hub using gauge pins. Note the ambient temperature and record data in Table 4.1.
3. Prepare steel hub and SMA cylindrical ring by cleaning in acetone and then isopropyl alcohol giving special attention to the outside surface of the SMA and the inside surface of the hub where the interference joint is to be created.
4. Re-measure the SMA cylinder to find the tapered end of the SMA cylinder (if any) and mark with permanent marker (dot on top of cylinder, not on contact face) to note which end to press into the steel hub first.
5. Match the SMA cylindrical ring to the steel hub by assigning a specimen number and placing both parts in separate oil free bags with appropriate identification markings.

6. Proceed to machine laboratory with prepared parts and assemble the SMA²C press-fit cradle with cleaned SMA and steel hub as shown in figures 3.1 thru 3.4. Use oil free gloves or tweezers to manipulate SMA and hubs into position. SMA should be placed to have the marked tapered end entering the steel busing first for ease of press-fit. Half of each interference type lot of 10 samples is to be created by pressing the SMA from the top of the bushing down, and the remaining half created by pressing the SMA from the bottom of the bushing up.
7. Align the press-fit cradle onto the load cell adaptor and load cell so they fit snugly in series. Place the assembly on a hard surface at the base of the arbor press.
8. Apply 99% isopropyl alcohol liberally at the SMA/hub interface before cradle's final assembly for lubrication.
9. Initiate load cell data recording with appropriate part number in the file title.
10. Press-fit the SMA cylindrical ring into the steel hub with a smooth application of force from the arbor press onto the press-fit cradle's pin protruding from the top of the assembly; record peak press-fit force displayed on load cell readout in Table 4.1.
11. Disassemble the press-fit cradle and remove the micro-coupling SMA/steel bushing interference joint. Allow the excess isopropyl alcohol to evaporate, write the specimen number on the outside of the steel bushing with a permanent marker and place the assembled SMA interference joint back into its labeled oil free bag.

SMA²C press-fit cradle:

The design of the SMA²C press fit cradle allows for a repeatable process of creating an interference joint with a high degree of alignment accuracy. The cradle itself is constructed of 1 1/4" diameter type 304 stainless steel machined to use a circular tongue and groove for assembly alignment. A press-fit pin holds the SMA cylindrical ring and fits through the top of the assembly while the casehardened steel hub is held in an appropriately dimensioned pocket in the assembly's bottom. The two halves are joined and placed on top of a load cell adaptor and load cell so the forces used in the press-fit process can be recorded (see Figures 3.1 thru 3.5).

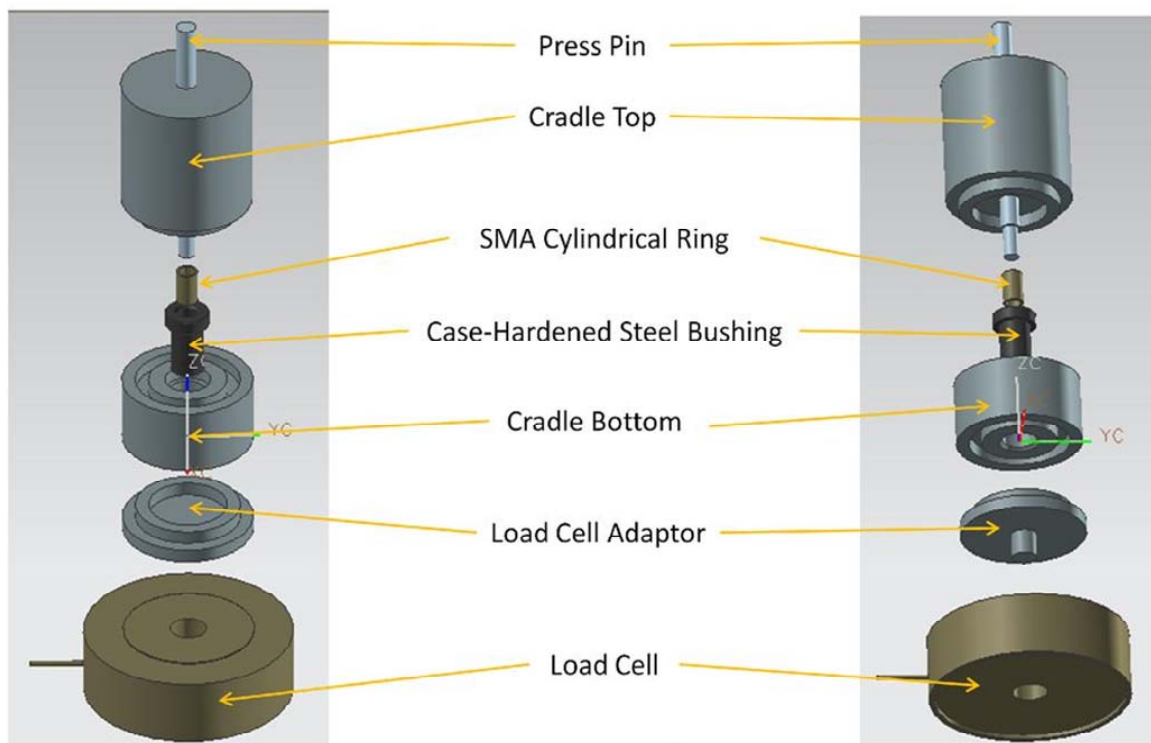
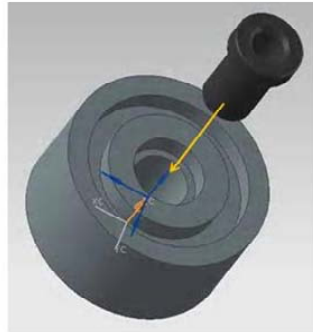
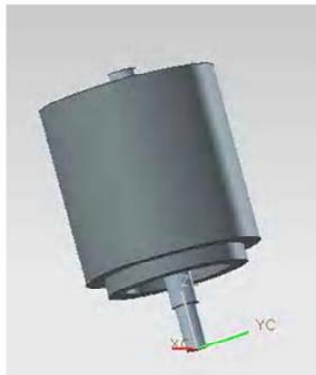


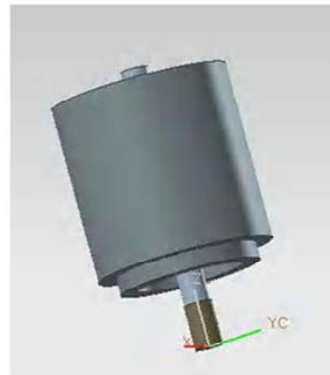
Figure 3.1 Component View of SMA²C Press-Fit Cradle



Place Hardened Steel Bushing
 Into Cradle Bottom



Place Press Pin Into Cradle Top



Place Press SMA On Tip of Press Pin

Figure 3.2 Placement of Steel Bushing and SMA Ring into Cradle Assembly

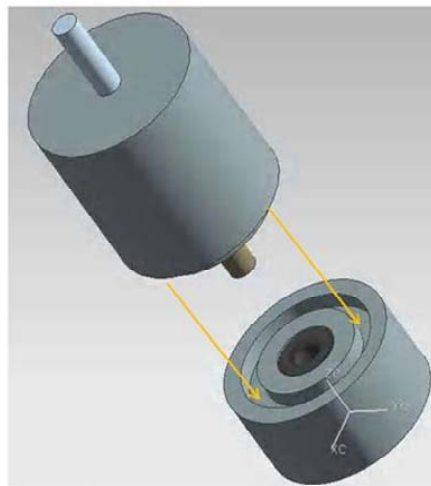
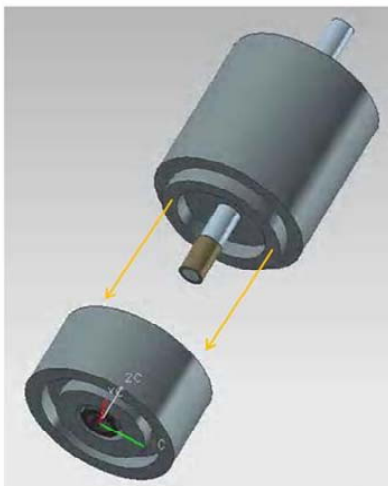


Figure 3.3 Press-Fit Cradle Top and Bottom Assembly

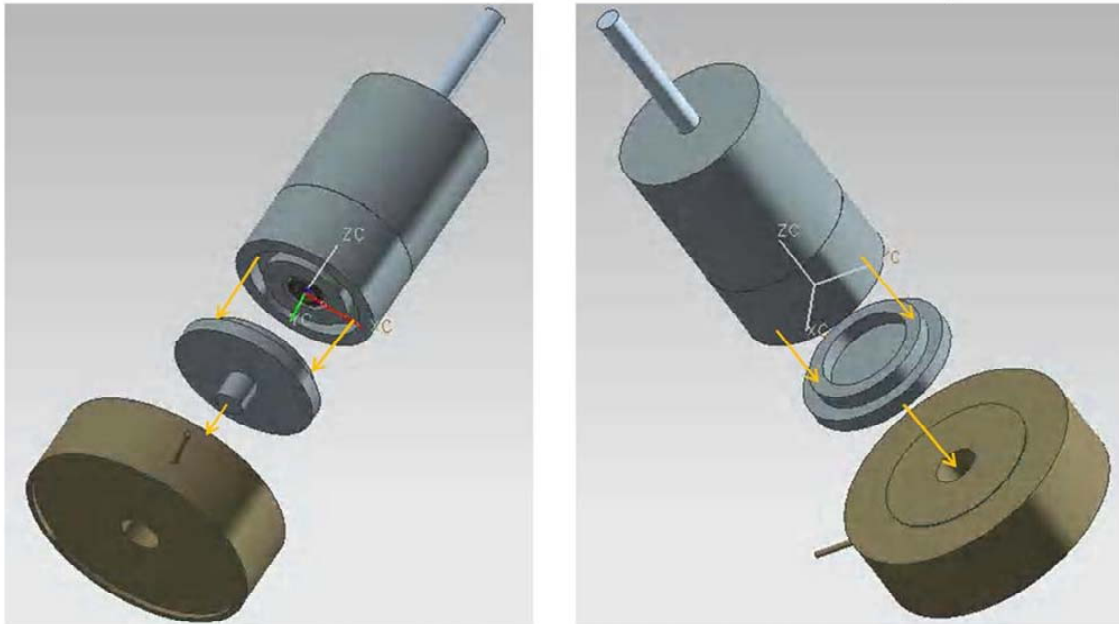


Figure 3.4 Load Cell and Load Cell Adaptor Attachment

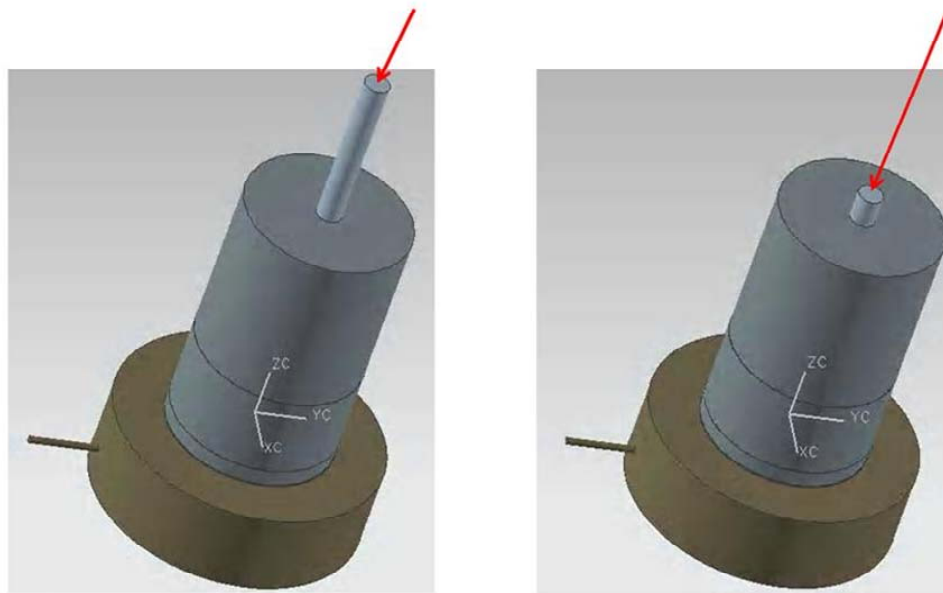


Figure 3.5 Creation of Interference Joint by Forcing Push Pin Full Stroke

3.3 Interference Joint Coupling Strength Test

Number of Items to be tested: 30 SMA²C Prototype Shape Memory Alloy Micro-Coupling Interference Joints

Location: NPS Machine Laboratory

Equipment:

30 SMA²C Micro-couplings
Micrometer (+/- 0.00005")
Gauge pins (0.0001" steps from 0.1980" to 0.2045"; +0.00004")
SMA²C Tensile Test Rig (see Figure 3.6)
Tensile Test Machine (+/- 0.5% of applied force; Newtons)
Personal Protective Equipment (PPE)
 - Gloves, long sleeve shirt & safety glasses
Video camera (if desired)

Procedure:

1. Assemble the SMA²C micro-coupling load test rig by placing a micro-coupling test specimen into its appropriately sized alignment slice and attach the alignment slice to the test rig top with four 8-32 hex screws (see Figure 3.7).
2. Drop the 4-40 hex "extraction" bolt down through the test rig top access hole until its head catches the press-fit SMA (see Figure 3.8).
3. Attach both the top and bottom test rig sections to the tensile test machine. Bring both halves together slowly until the extraction hex bolt can be screwed into the test rig bottom with an Allen wrench inserted through the top access hole in the test rig top. Note: care must be taken not to tighten hex bolt beyond contact pressure to avoid preloading to the press-fit joint (see Figure 3.9).
4. Tensile machine should be set to a progression rate of 1 mm per minute and a data capture rate of one sample every 0.2 seconds.
5. Once all parts are secure, conduct tensile test for each press-fit joint (see Figure 3.10). Record data in Table 4.2.
6. Once the interference joint has completely separated and the SMA cylindrical ring is free, mark the bottom of the extracted SMA with permanent marker to note the side that was facing down during extraction. Put the micro-coupling test sample parts back into their respective labeled oil-free bag.
7. Measure the outer diameter of the SMA cylindrical rings and the inner diameter of the steel hubs in the same manner as before (clean micrometer contact points and tare its digital readout). Note the ambient temperature and record data in Table 4.2.

SMA²C micro-coupling load test rig:

The design of the SMA²C micro-coupling load test rig allows axial loading of the interference joint made between the SMA cylindrical ring and the casehardened steel hub. The test rig is constructed of 1 1/4" diameter type 304 stainless steel with exception to the rig bottom that is constructed from 15-5Ph steel for additional strength at the 4-40 extraction hex bolt attachment point. An alignment slice holds the micro-coupling interference joint in an appropriately dimensioned pocket allowing for attachment to the top and bottom of the test rig. The two halves of the test rig are inserted into the tensile machine and joined via the extraction hex bolt. The tensile test is executed and load cells record the forces used to extract the SMA from the case-hardened steel hub (see Figures 3.6 thru 3.10).

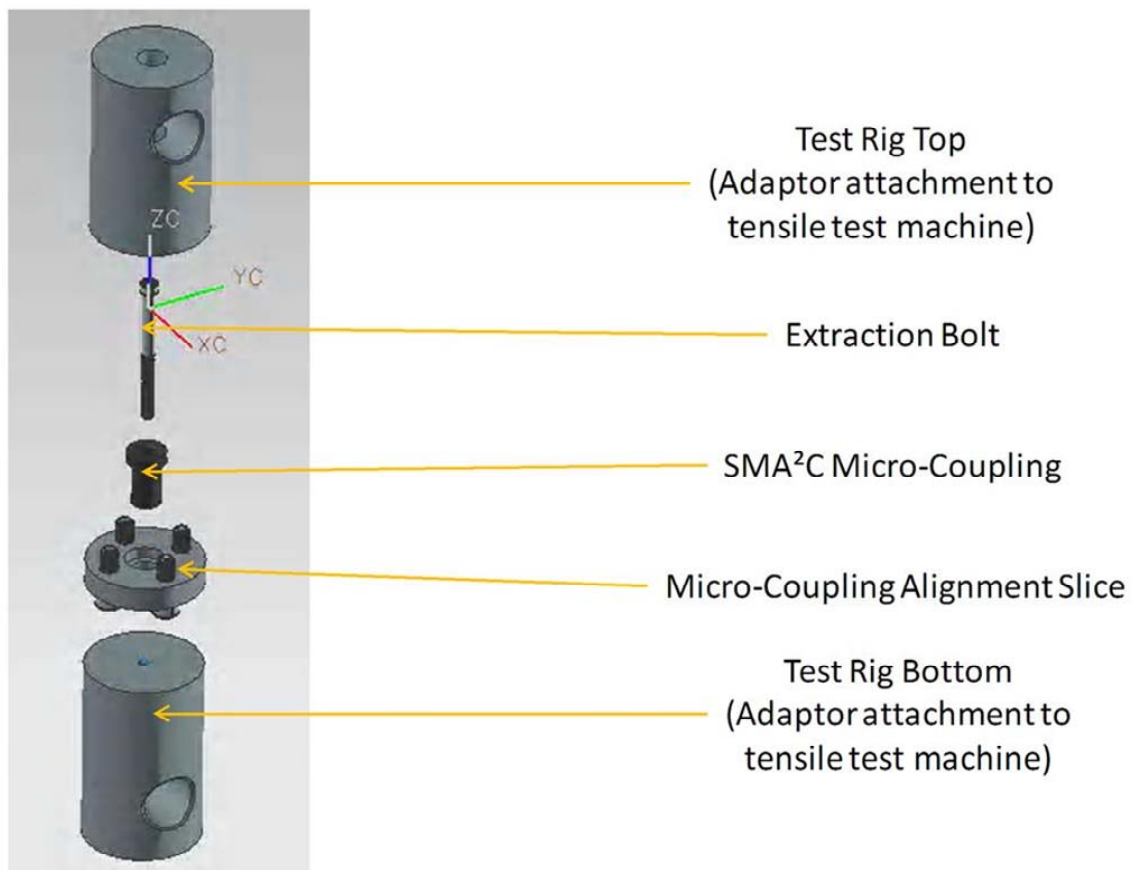


Figure 3.6 SMA²C Micro-Coupling Load Test Rig Assembly Components

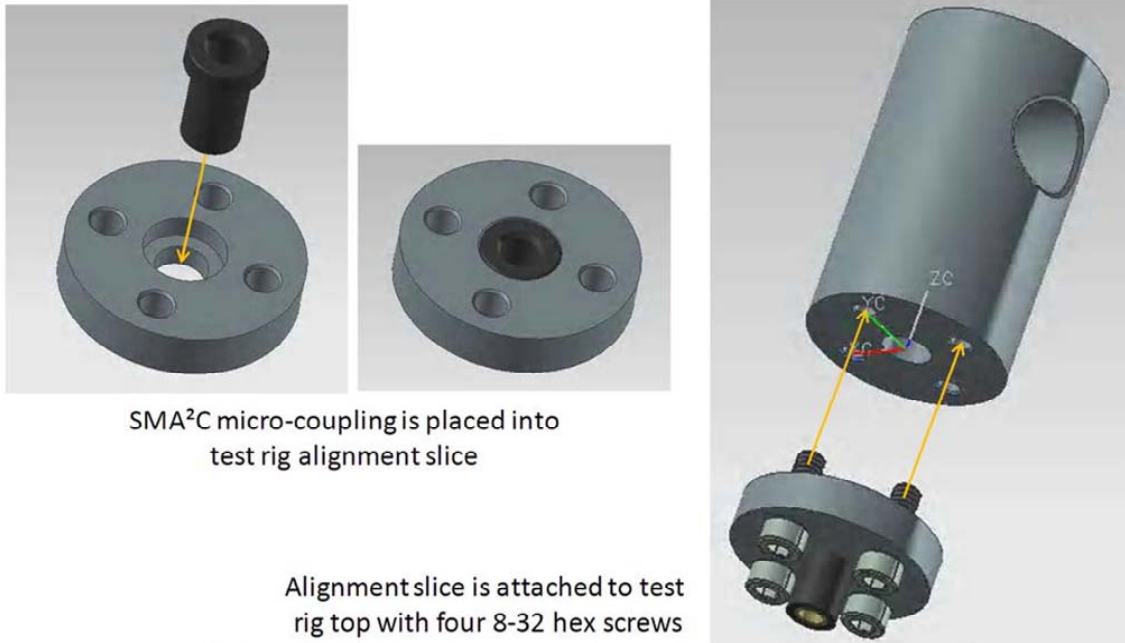


Figure 3.7 Micro-Coupling Insertion and Attachment of the Alignment Slice



Figure 3.8 SMA²C Micro-Coupling Load Test Rig Upper Assembly with Extracting Hex Bolt Insertion

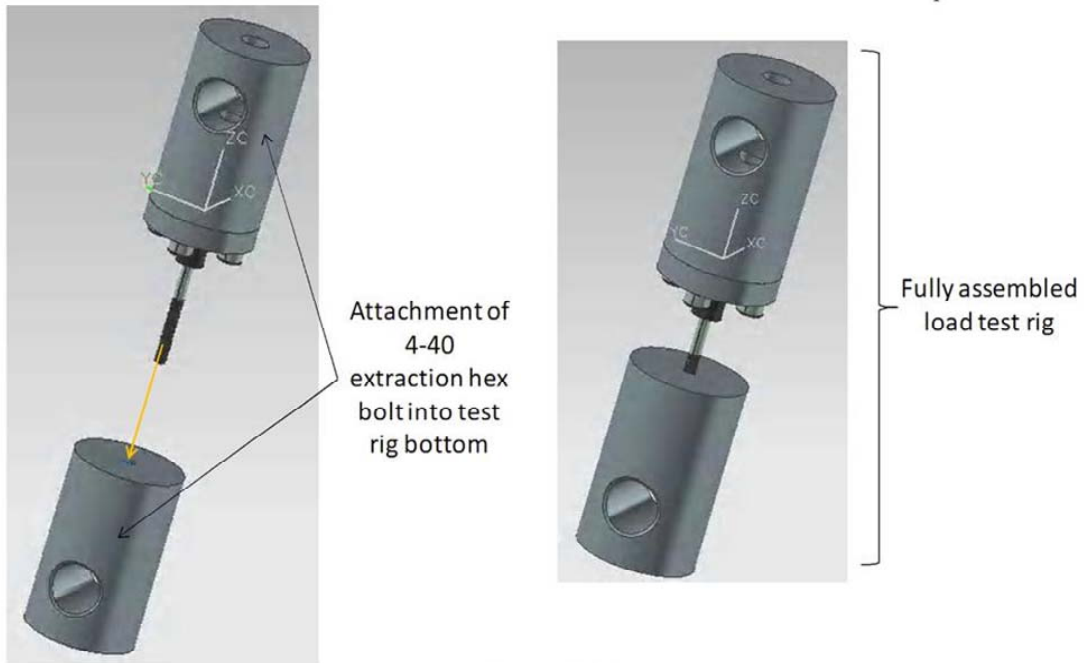


Figure 3.9
 Joining of Top and Bottom of SMA²C Micro-Coupling Load Test Rig

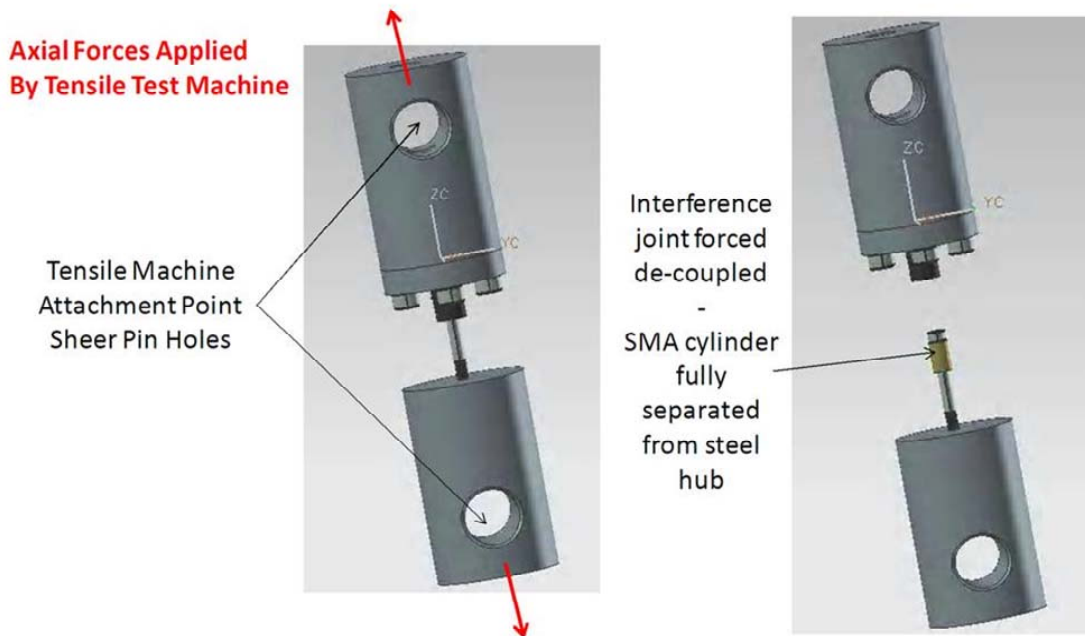


Figure 3.10 Insertion of the SMA²C Micro-Coupling Load Test Rig into Tensile Test Machine &
 Forced Removal of Press-Fit Shape Memory Alloy

Section 4 – Data Analysis & Results

4.1 Predicted Interference Joint Coupling Force Values

Test Lot #	Desired Nominal Interference	Predicted Coupling Force	
1-1 to 10-1	0.001" ±0.00005"	630 N	142 lbf
1-3 to 10-3	0.003" ±0.00005"	1,870 N	420 lbf
1-5 to 10-5	0.005" ±0.00005"	3,050 N	686 lbf

The interference generated from the press-fit creates high contact pressures on the SMA-steel hub interface. This normal pressure (force/area perpendicular to the shaft axis of the SMA cylindrical ring), along with an estimated coefficient of friction of the mating materials (0.13), is used to calculate the coupling capability. The equations for contact pressure, frictional force and torque transmission are:

Variables:

E_1 = Elastic Modulus for the inner member (SMA cylindrical ring)
 E_2 = Elastic Modulus for the outer member (Stainless steel hub)
 ν_1 = Poisson's Ratio for the inner member
 ν_2 = Poisson's Ratio for the outer member
 μ = Coefficient of static friction at the interface of the members.
 L = Contact length
 r = Nominal radius at the interference, common radius
 r_o = Outer radius of the outer member
 r_i = Inner radius of the inner member (note $r_i = 0$ for a solid member)
 p = Contact pressure, Interference Pressure

$$p = \frac{\delta}{\frac{r}{E_2} \left(\frac{r_o^2 + r^2}{r_o^2 - r^2} + \nu_2 \right) + \frac{r}{E_1} \left(\frac{r^2 + r_i^2}{r^2 - r_i^2} - \nu_1 \right)}$$

δ = Radial Interference

$$\delta = \frac{pr}{E_2} \left(\frac{r_o^2 + r^2}{r_o^2 - r^2} + \nu_2 \right) + \frac{pr}{E_1} \left(\frac{r^2 + r_i^2}{r^2 - r_i^2} - \nu_1 \right)$$

δ_i = Change of the outer radius of the SMA cylindrical ring

$$\delta_i = -\frac{pr}{E_1} \left(\frac{r^2 + r_i^2}{r^2 - r_i^2} - \nu_1 \right)$$

δ_o = Change of the inner radius of the stainless steel hub

$$\delta_o = \frac{pr}{E_2} \left(\frac{r_o^2 + r^2}{r_o^2 - r^2} + \nu_2 \right)$$

σ_i = Tangential stress at the contact (outer) surface of the SMA cylindrical ring

$$\sigma_i = -p \left(\frac{r^2 + r_i^2}{r^2 - r_i^2} \right) \quad \text{Note: This is shown as } d_i \sigma_t \text{ in the press-fit calculator below.}$$

σ_o = Tangential stress at the inner (contact) surface of the stainless steel hub

$$\sigma_o = p \left(\frac{r_o^2 + r^2}{r_o^2 - r^2} \right) \quad \text{Note: This is shown as } d_o \sigma_t \text{ in the press-fit calculator below.}$$

T = Torque that the pressed joint will resist

$$T = 2\pi r^2 \mu p L$$

F_n = Normal Force (relative to the press fit surface)

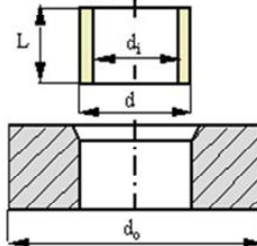
$$F_n = p 2\pi r L$$

F_μ = Frictional "Holding" Force of the SMA cylindrical ring

$$F_\mu = \mu F_n$$

Interference Fit Internal Pressure and Frictional Coupling Force Predictions

Credit: Tribology-abc.com calculators



Interference

0.001":

d_i	3.9942	mm	L	7.7978	mm	E_i	30	GPa	ν_i	0.33
d	5.1892	mm	$\delta^{(1)}$	0.0254	mm	E_o	207	GPa	ν_o	0.29
d_o	12.7	mm	$\mu^{(2)}$	0.13						

(Default value bronze bushing, steel hub)

Interference pressure p 38.42 MPa

Friction force F 0.63 kN

Transmission torque T 1.65 Nm

Stresses	ring i		ring o	
	d_i	d	d	d_o
σ_t	-188.52 MPa	-150.11 MPa	53.81 MPa	15.4 MPa
σ_r	0 MPa	-38.42 MPa	-38.42 MPa	0 MPa

0.003":

d_i	3.9942	mm	L	7.7978	mm	E_i	30	GPa	ν_i	0.33
d	5.1892	mm	$\delta^{(1)}$	0.0762	mm	E_o	207	GPa	ν_o	0.29
d_o	9.525	mm	$\mu^{(2)}$	0.13						

(Default value bronze bushing, steel hub)

Interference pressure p 113.34 MPa

Friction force F 1.87 kN

Transmission torque T 4.86 Nm

Stresses	ring i		ring o	
	d_i	d	d	d_o
σ_t	-556.22 MPa	-442.88 MPa	209.02 MPa	95.68 MPa
σ_r	0 MPa	-113.34 MPa	-113.34 MPa	0 MPa

0.005":

d_i	3.9942	mm	L	7.7978	mm	E_i	30	GPa	ν_i	0.33
d	5.1892	mm	$\delta^{(1)}$	0.127	mm	E_o	207	GPa	ν_o	0.29
d_o	7.9375	mm	$\mu^{(2)}$	0.13						

Solve Reset Print (Default value bronze bushing, steel hub)

Interference pressure p 184.44 MPa

Friction force F 3.05 kN

Transmission torque T 7.91 Nm

Stresses	ring i		ring o	
	d_i	d	d	d_o
σ_t	-905.14 MPa	-720.7 MPa	459.78 MPa	275.34 MPa
σ_r	0 MPa	-184.44 MPa	-184.44 MPa	0 MPa

Note: Micro-coupling interference joints were tested axially to validate frictional forces. Torsional forces were not tested or validated.

4.2 Experimental vs. Predicted Data with Propagated Measurement Error

Predicted coupling force is based upon the anticipated interference created between the case hardened steel hub and SMA cylindrical ring. Very small changes in the interference (defined as $\delta = r_o - r_i$) on the order of 0.0001" will have a dramatic impact on the generated coupling force. The imperfect geometric cylindrical shape of the SMA along with measurement precision of the steel hub's inner diameter and the SMA cylindrical ring's outer diameter, play an important role in the micro-coupling's predicted strength. The resulting geometry and measurement error propagates through the traditional press-fit equations discussed in section 4.1 effecting our predicted interference force $F_\mu = \mu p 2\pi r L$ leading to our micro-coupling's strength.

SMA geometry and micrometer precision error propagation was traced by using one standard deviation calculated from the recorded SMA diameter measurements, as the SMA cylindrical rings are non-circular within the micrometer's precision. The non-uniform cylindrical shape's standard deviation was added to the micrometer's precision of 0.0001" (± 0.00005 "). This delta sum was accounted for by Δr_o .

Gauge pin precision error propagation was traced by using one standard deviation calculated from the range of gauge from the largest pin that would fit into the steel hub to the smallest pin that would not. The gauge pin precision of +0.00004" minus nothing and incremented by 0.0001" resulted in one standard deviation equal to 0.00007". This delta was accounted for by Δr_i .

Interference-fit uncorrelated propagation of geometric shape and measurement error was calculated by:

$$\Delta r = \sqrt{(\Delta r_o)^2 + (\Delta r_i)^2}$$

Next, the uncorrelated propagated interference pressure error (Δp) was calculated from the interference error and the use of average deviations. The equation was derived based on the mathematical operations used on the individual variables within the interference pressure equation (as given in section 4.1) and scaled by the predicted interference pressure (p):

$$\Delta p = p \sqrt{\left(\frac{\Delta r \sqrt{2[(2\Delta r_o)^2 + (2\Delta r)^2]}}{\delta} \right)^2 + \left(\frac{\Delta r \sqrt{2[(2\Delta r_i)^2 + (2\Delta r)^2]}}{\delta} \right)^2}$$

Finally, the interference-fit uncorrelated propagation error in predicted holding force (ΔF_μ) was calculated from the interference pressure error and, as before, the use of average deviations. The equation was derived based on the mathematical operations used on the individual variables within the predicted interference-fit coupling force equation $F_\mu = \mu p 2\pi r L$ and scaled by the predicted coupling force (F_μ):

$$\Delta F_\mu = F_\mu \sqrt{\left(\frac{\Delta p}{p} \right)^2 + \left(\frac{\Delta r}{\delta} \right)^2}$$

Note: A summary of the recorded measurement values can be found in section 4.4.

Micro-coupling interference-fit uncorrelated propagation error in predicted coupling strength is shown as error bars on the initial predicted coupling strength value for each interference type (see Figure 4.1). These error bars show the extent of propagated prediction error attributed to the non-circular SMA rings and measurement tool precision.

Test Specimen Numbering Code:

- 1st position – Specimen number within respective lot.
(Lots are divided according to nominal interference in thousandths of an inch.)
- 2nd position - Nominal interference in mills.
- 3rd position - Press-fit direction.
(T = SMA inserted from bushing's top brim and pressed downward)
(B = SMA inserted from bushing's bottom and pressed upward)

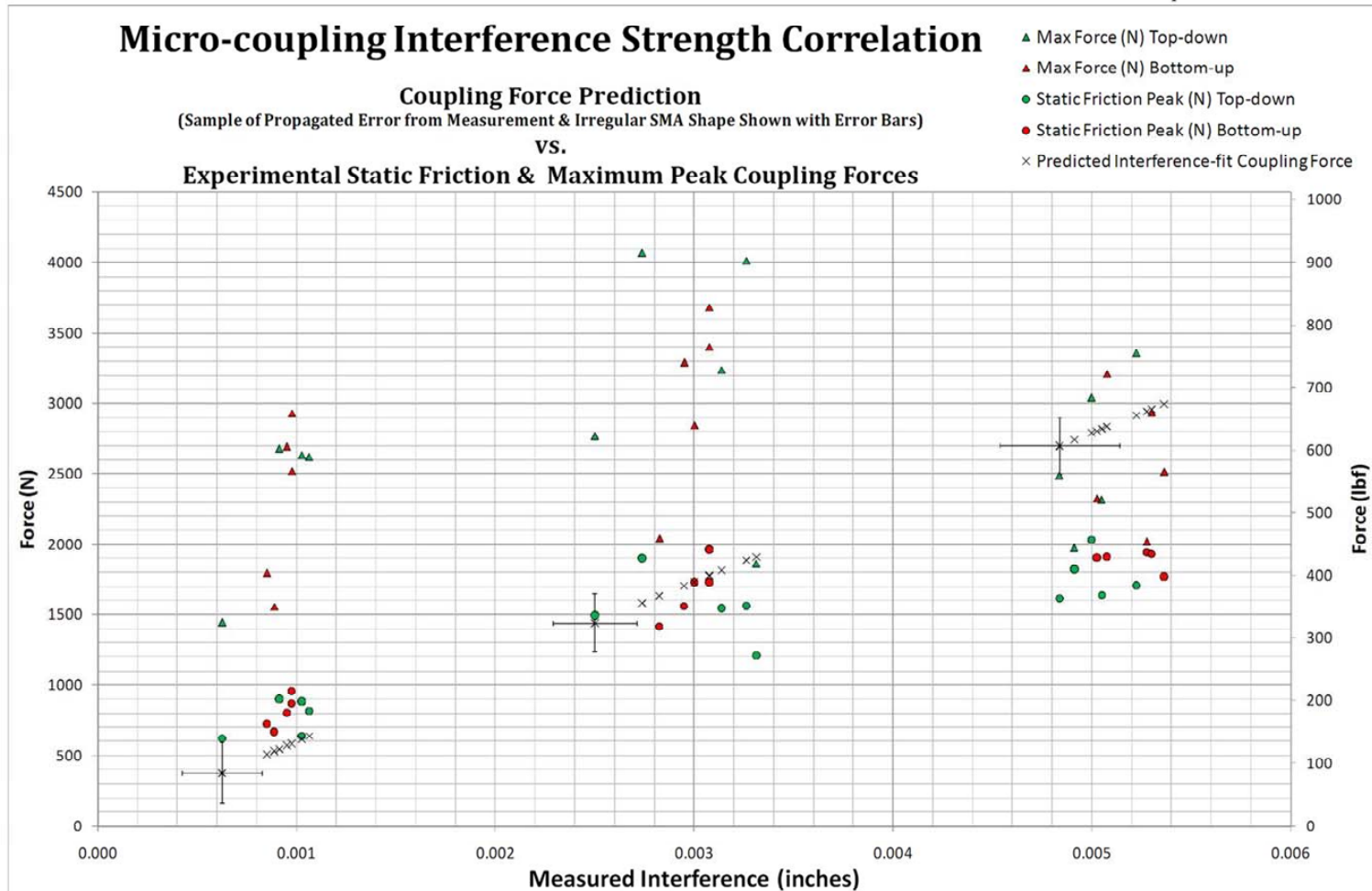


Figure 4.1 Comparison of Predicted and Experimental Data for Interference Joint Coupling Forces.

4.3 Correlation Between Post Test SMA Outer Diameter Change and Interference Used

The outer diameter of the SMA cylindrical rings and the inner diameter of the steel hubs were measured post-test to determine the extent of de-stressing imparted upon the detwinned martensitic SMA and if any plastic deformation was imparted on the steel hub from the press-fit creation and interference joint removal process:

Case hardened steel hubs: It should be noted that 15 days passed between tensile tests and post-test measurement. Visible oxidation of the steel hub's inner surface was found and contributed to the inability to insert the same pre-test gauge pin. No significant change in steel hub measurement was found, but visible surface markings were present (see Table 4.3).

SMA cylindrical rings: A correlation between the post-test SMA outer diameter and the tested nominal interference can be seen in Figure 4.2. SMA diameter change is found by taking the difference between pre & post-test average diameters. SMA spring-back is calculated by taking the post-test diameter and subtracting pre-test diameter less measured interference.

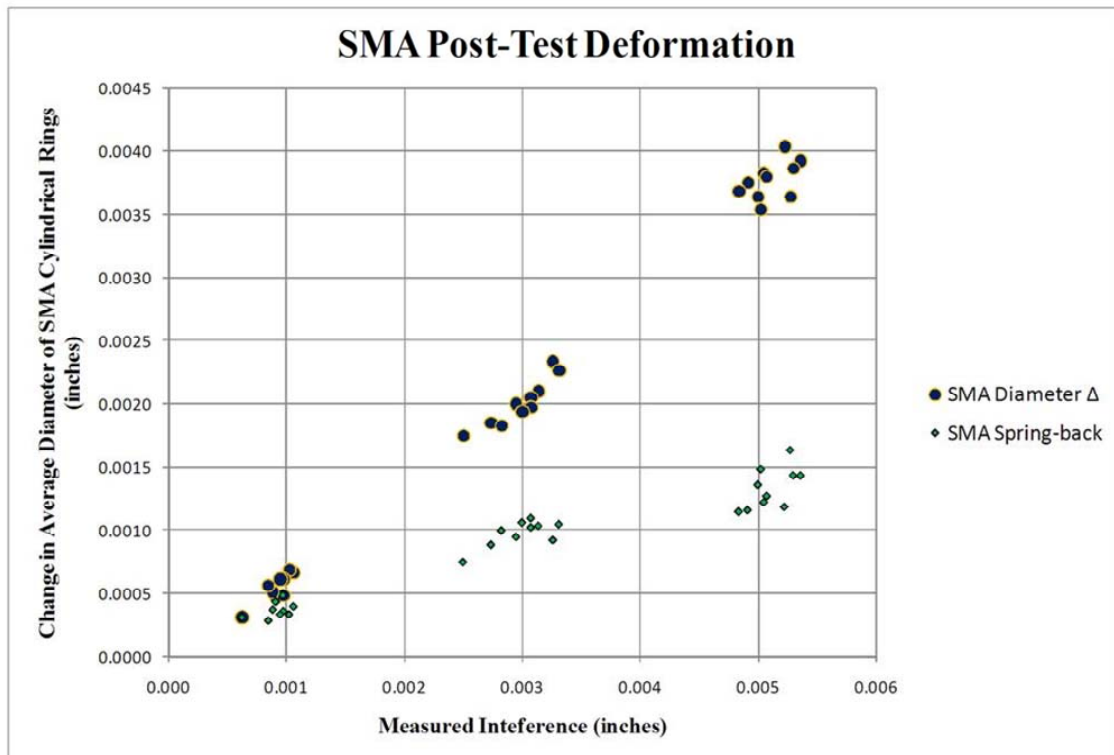


Figure 4.2 SMA & Steel Hub Post-Test Diameter Measurement Comparison

4.4 Tabulated Test Results:

Table 4.1 Micro-coupling Measurement and Press-Fit Creation Data

Press-Fit SMA Test Number	Inner Diameter of Case-Hardened Steel Hub* (inches) <i>Note: largest gauge pin inserted</i>	SMA Cylindrical Ring Average Outer Diameter (inches) <i>Calculated from four cross diameter measurements</i>	SMA Cylindrical Ring Measurement Standard Deviation	SMA Cylindrical Ring Measurement Relative Error (%)	Measured Interference (inches)	Maximum Force Used During Press-Fit Process (lbf)
1-1T	0.2033	0.20433	0.000225	0.16%	0.00103	514.2
2-1T	0.2032	0.20426	0.000170	0.13%	0.00106	370.6
3-1T	0.2032	0.20423	0.000104	0.10%	0.00103	149.3*
4-1T	0.2033	0.20393	0.000144	0.12%	0.00063	246.3
5-1T	0.2032	0.20411	0.000180	0.14%	0.00091	338.5
6-1B	0.2032	0.20418	0.000166	0.13%	0.00098	128.9*
7-1B	0.2032	0.20409	0.000304	0.20%	0.00089	206.2
8-1B	0.2032	0.20418	0.000119	0.11%	0.00098	458.5
9-1B	0.2034	0.20435	0.000265	0.18%	0.00095	15.3*
10-1B	0.2032	0.20405	0.000183	0.14%	0.00085	99.7*
1-3T	0.2011	0.20424	0.000085	0.09%	0.00314	359.8
2-3T	0.2011	0.20436	0.000103	0.10%	0.00326	371.8
3-3T	0.2010	0.20350	0.000212	0.15%	0.00250	117.5*
4-3T	0.2009	0.20421	0.000118	0.11%	0.00331	413.2
5-3T	0.2011	0.20384	0.000256	0.17%	0.00274	108.6*
6-3B	0.2011	0.20405	0.000173	0.13%	0.00295	381.8
7-3B	0.2011	0.20393	0.000150	0.12%	0.00283	187.7*
8-3B	0.2012	0.20428	0.000144	0.12%	0.00307	52.1*
9-3B	0.2010	0.20408	0.000104	0.10%	0.00307	516.4
10-3B	0.2011	0.20410	0.000041	0.07%	0.00300	34.3*
1-5T	0.1991	0.20410	0.000178	0.14%	0.00500	158.7*
2-5T	0.1991	0.20401	0.000175	0.13%	0.00491	288.4*
3-5T	0.1991	0.20415	0.000178	0.14%	0.00505	382.6
4-5T	0.1991	0.20394	0.000170	0.13%	0.00484	337.4
5-5T	0.1991	0.20433	0.000287	0.19%	0.00523	818.3
6-5B	0.1992	0.20428	0.000155	0.13%	0.00508	308.3
7-5B	0.1991	0.20413	0.000266	0.18%	0.00503	356.7
8-5B	0.1991	0.20446	0.000287	0.19%	0.00536	597.4
9-5B	0.1991	0.20438	0.000166	0.13%	0.00528	297.5*
10-5B	0.1991	0.20440	0.000248	0.17%	0.00530	331.2

Ambient temperature for gauge pin measurements: 69 °F

* Due to the slow data sampling rate of the load cell (1 sample/sec), peak force was likely missed.

Table 4.2 Press-Fit SMA Tensile Load Test Data

Press-Fit SMA Test Number	Static Friction Peak (lbf)	Maximum Recorded Coupling Strength (lbf)	Interference-fit uncorrelated propagation of measurement error (inches) Δr	Interference-fit uncorrelated propagation of measurement error in calculated pressure (lbf/in ²) Δp	Interference-fit uncorrelated propagation of measurement error in holding force (lbf) ΔF_{μ}	Predicted Interference-fit Coupling Force (lbf) F_{μ}
1-1T	142.8	Test Interrupted	0.00033	2.866	48.6	138
2-1T	184.3	589.9	0.00028	2.011	48.5	143
3-1T	198.4	592.6	0.00022	1.202	48.5	138
4-1T	139.5	325.6	0.00025	1.671	48.6	84
5-1T	202.2	603.0	0.00029	2.147	48.5	123
6-1B	215.0	659.8	0.00027	1.952	48.5	131
7-1B	150.0	350.2	0.00041	4.338	48.5	119
8-1B	195.1	567.0	0.00023	1.365	48.5	131
9-1B	180.8	606.3	0.00037	3.568	48.7	128
10-1B	162.9	404.2	0.00029	2.189	48.5	114
1-3T	347.5	728.7	0.00020	0.985	46.8	408
2-3T	351.1	902.8	0.00021	1.157	46.8	424
3-3T	335.8	622.6	0.00032	2.564	46.7	324
4-3T	272.0	418.7	0.00023	1.312	46.7	429
5-3T	427.8	915.9	0.00036	3.305	46.8	356
6-3B	350.9	740.7	0.00028	1.995	46.8	384
7-3B	318.9	460.1	0.00026	1.691	46.8	367
8-3B	441.5	765.1	0.00025	1.622	46.9	401
9-3B	389.3	828.0	0.00022	1.166	46.8	399
10-3B	389.4	640.2	0.00016	0.620	46.8	390
1-5T	457.3	684.0	0.00029	1.999	45.2	628
2-5T	409.9	444.4	0.00028	1.960	45.2	617
3-5T	368.5	521.3	0.00029	1.999	45.2	634
4-5T	363.0	559.7	0.00028	1.896	45.2	607
5-5T	384.3	755.4	0.00039	3.767	45.2	656
6-5B	430.2	722.4	0.00026	1.709	45.3	638
7-5B	428.9	523.5	0.00037	3.381	45.2	631
8-5B	398.5	566.0	0.00039	3.759	45.2	674
9-5B	437.6	454.7	0.00027	1.838	45.2	662
10-5B	435.0	660.4	0.00036	3.070	45.2	666

Ambient temperature of machine lab during test: 70 °F

Table 4.3 Post-Test Sample Deformation Measurements and Correlation

Press-Fit SMA Test Number	Post Test Inner Diameter of Case-Hardened Steel Hub (inches) <i>Note: smallest gauge pin inserted</i>	Case-Hardened Steel Hub Calculated Diameter Change* (inches)	Post Test Average Outer Diameter of SMA Ring (inches) <i>four cross diameter measurements, both ends</i>	Outer Diameter of SMA Ring Calculated Reduction (inches)
1-1T	0.2033	0.0000	SMA Lost during test	SMA Lost during test
2-1T	0.2032	-0.0001	0.20360	0.00066
3-1T	0.2032	-0.0001	0.20354	0.00069
4-1T	0.2033	0.0000	0.20361	0.00031
5-1T	0.2032	-0.0001	0.20364	0.00047
6-1B	0.2032	0.0000	0.20369	0.00049
7-1B	0.2032	0.0000	0.20358	0.00051
8-1B	0.2032	-0.0001	0.20356	0.00061
9-1B	0.2034	-0.0002	0.20374	0.00061
10-1B	0.2032	0.0000	0.20349	0.00056
1-3T	0.2011	0.0000	0.20214	0.00210
2-3T	0.2011	0.0000	0.20203	0.00234
3-3T	0.2010	0.0000	0.20175	0.00175
4-3T	0.2009	0.0001	0.20195	0.00226
5-3T	0.2011	0.0000	0.20199	0.00185
6-3B	0.2011	0.0000	0.20205	0.00200
7-3B	0.2011	0.0000	0.20210	0.00183
8-3B	0.2012	-0.0001	0.20223	0.00205
9-3B	0.2010	0.0000	0.20210	0.00198
10-3B	0.2011	0.0000	0.20216	0.00194
1-5T	0.1991	-0.0001	0.20046	0.00364
2-5T	0.1991	0.0000	0.20026	0.00375
3-5T	0.1991	0.0000	0.20033	0.00383
4-5T	0.1991	0.0000	0.20025	0.00369
5-5T	0.1991	-0.0001	0.20029	0.00404
6-5B	0.1992	-0.0001	0.20048	0.00380
7-5B	0.1991	0.0000	0.20059	0.00354
8-5B	0.1991	0.0000	0.20054	0.00392
9-5B	0.1991	0.0000	0.20074	0.00364
10-5B	0.1991	-0.0001	0.20054	0.00386

Ambient temperature for gauge pin measurements: 69°F

*Visible oxidation on the steel hub's inner surface was found and contributed to the inability to insert the same pre-test gauge pin used prior to creation of the micro-coupling interference joint.

Section 5 – Findings and Conclusions

The threshold objective was achieved and data acquired in an attempt to answer the additional goals of the test. Traditional press-fit equations were used as a tool to try to predict the coupling strength of the SMA interference joint. These equations appear sufficient to yield the initial static friction coupling force. The variable that is critical to a prediction of micro-coupling strength is the coefficient of friction between the SMA and case hardened steel. Once the SMA cylinder slips and begins extraction from the micro-coupling, the coefficient of static friction changes to kinetic friction, a lower value. The change in static to kinetic frictional coefficient leads to an expected static friction coupling force peak followed by a reduced coupling force as the SMA is pulled free. The expected initial static friction peak can be seen in experimental data found in the appendix, but unexpected static to kinetic friction transitions are found after the initial static friction peak followed by increasing coupling strength as the SMA is extracted. Ultimately, a smooth roll off in resistance with continued extraction was observed due to the decreased interference joint surface area contact as the SMA separated from the steel hub. Referencing the following figures:

Figure 4.1: First, the easiest trend to draw conclusions against is there appears to be no difference if the micro-coupling is created from the top-down or bottom-up. The red and green colors are evenly distributed. Second, it appears that the coefficient of friction is not consistent between the two materials used in the interference joint. Materials usually maintain a constant coefficient of friction and the normal forces imparted upon the materials directly result in increased frictional forces. There is not a linear increase in the trend of static friction peaks. It appears the assumed coefficient of friction of 0.13 was too small for the 1-mil interference and too large for the 5-mil inference. Finally, maximum coupling forces were achieved by the 3-mil interference micro-couplings. It is believed that a combination of SMA phase change caused by over-pressurization and column buckling of the SMA cylinder within the interference joint contributed to this effect.

Figure 4.2: There was no plastic deformation of the SMA beyond a visible surface texture change. The SMA's surface now had visible polished rings on both ends of the SMA cylinder; areas of highest pressure within the interference joint. At the 3 & 5-mil interferences, the upper third of the SMA cylinder showed surface scraping down the long axis. The inside of the casehardened steel hubs showed similar surface polishing and scraping. Martensitic de-stressing can be seen to be approximately 1-mil less than the nominal interference. The elasticity of the SMA can be seen by a diameter increase or "spring-back" upon being freed from the interference joint. This spring-back increased slightly as the interference increased, but does not point to an obvious conclusion relating to other test data.

Appendix Figures: The pseudoelastic properties of SMA within an interference joint yield exciting results. Initial static friction peaks are seen initially and then coupling strength increases with data plots accentuated by static to kinetic friction transitions. These transitions or "vibrations" are not believed to be the cause of increasing coupling strength because in preliminary sample tests not shown in this report, these vibrations appeared without an associated coupling strength increase. In an attempt to eliminate the tensile test machine motor's drive as the cause, three samples were extracted at 3 mm/min rather than the established 1 mm/min. These samples were: #10-3B, #5-5T and #10-5B (note: data sample rate was not increased). The same static to kinetic vibrations were observed now as a sign wave response.

Across most test specimens, maximum coupling strength was achieved when approximately one third of the SMA's length was exposed outside the steel hub. Ultimate peak strength of the interference joint could be investigated, but the SMA would have to be inserted significantly deep within the steel hub to achieve maximum strength before any exposure of the SMA's length from the steel hub. More testing is needed for any definitive conclusions about the cause for increasing coupling strength and the exact interaction between the hub/shaft interface within the micro-coupling. Prediction of these maximum values was not anticipated and atomic interactions between the SMA and case hardened steel need to be investigated further.

The micro-coupling design for the SMA²C EDU provides sufficient coupling strength for many applications, but most likely its 5-mil nominal interference is too aggressive. A smaller interference would provide similar initial static friction strengths, but a larger ultimate strength providing an increased factor of safety against involuntary forced decoupling under load. In addition, the fully de-stressed austenitic (small diameter) phase of the SMA would have greater separation from the larger inner diameter of the steel hub upon HTR yielding a higher probability of successful decoupling upon commanded micro-coupling release.

Appendix

Supporting Graphs & Diagrams

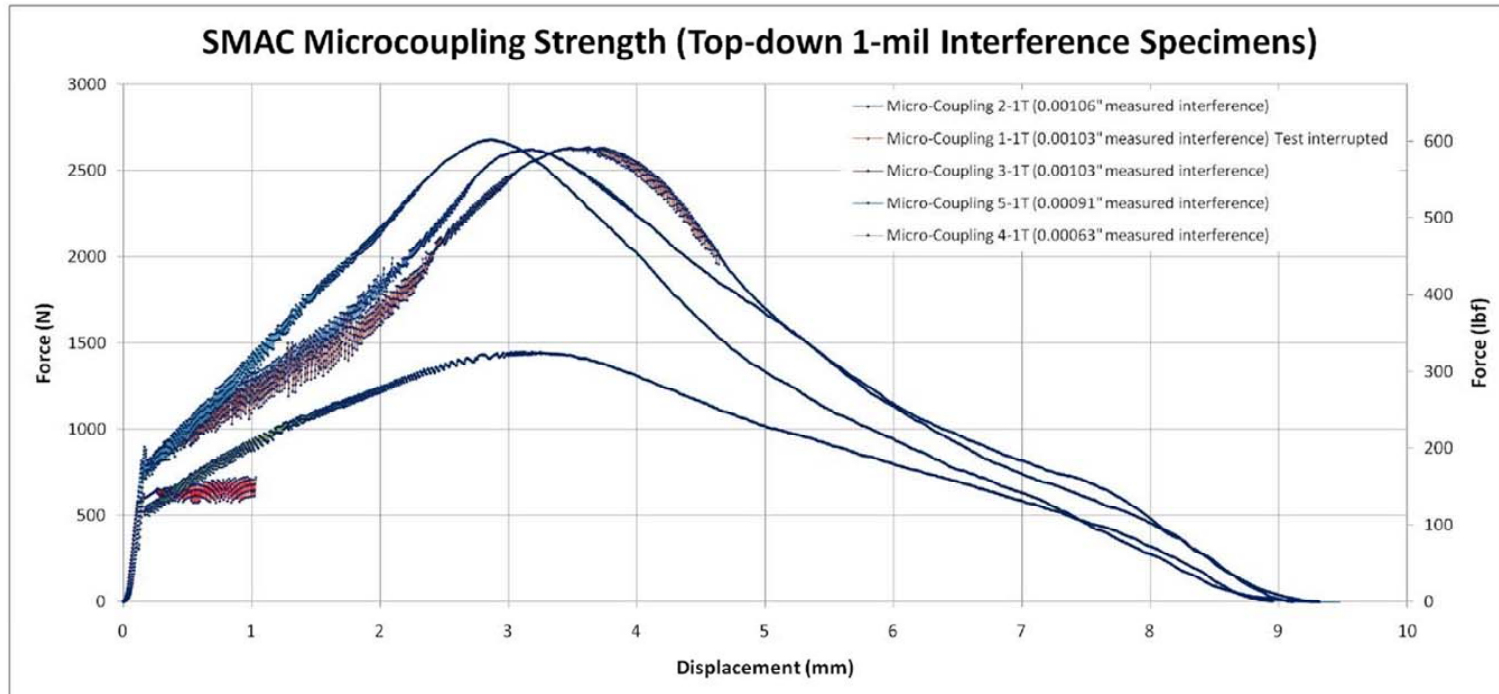


Figure A1 SMA²C Micro-Coupling Interference Joint Forced Removal: Top-down Specimens in Lot 0.001" Nominal Interference

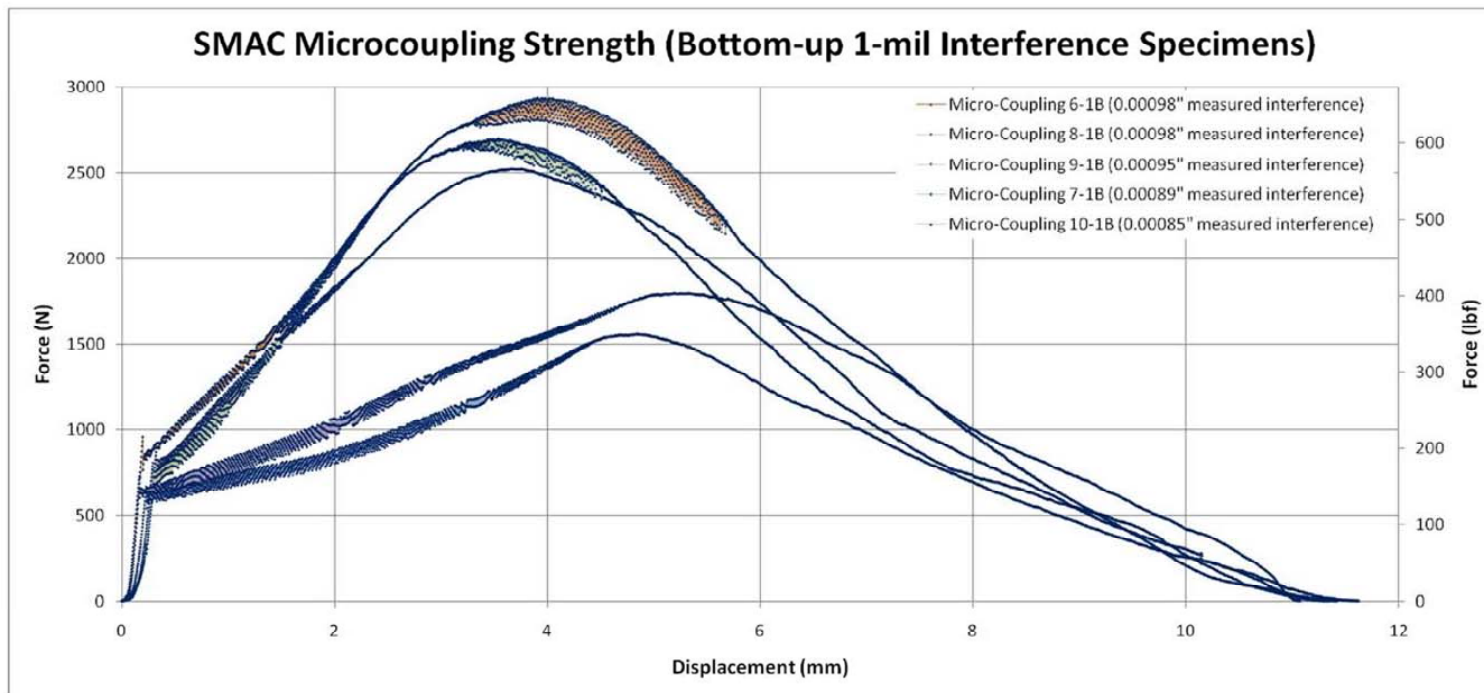


Figure A2 SMA²C Micro-Coupling Interference Joint Forced Removal: Bottom-up Specimens in Lot 0.001" Nominal Interference

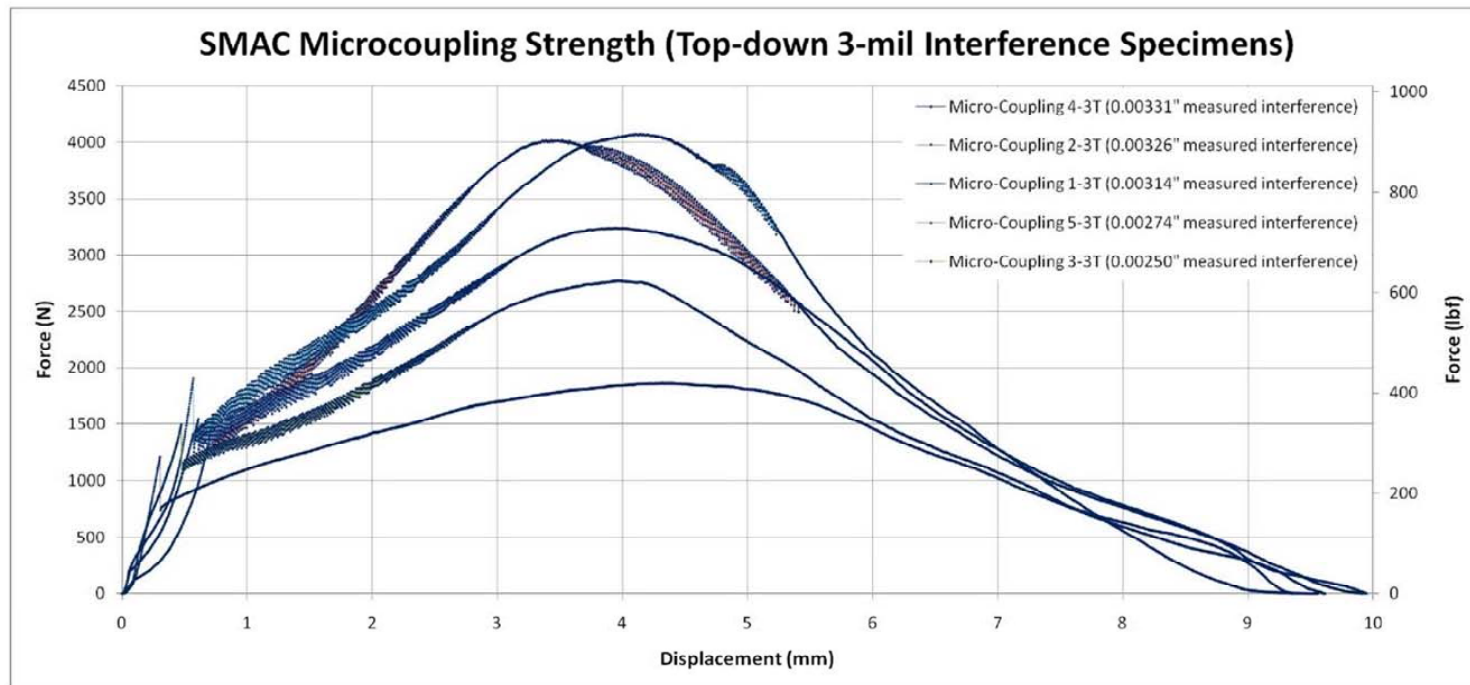


Figure A3 SMA²C Micro-Coupling Interference Joint Forced Removal: Top-down Specimens in Lot 0.003" Nominal Interference

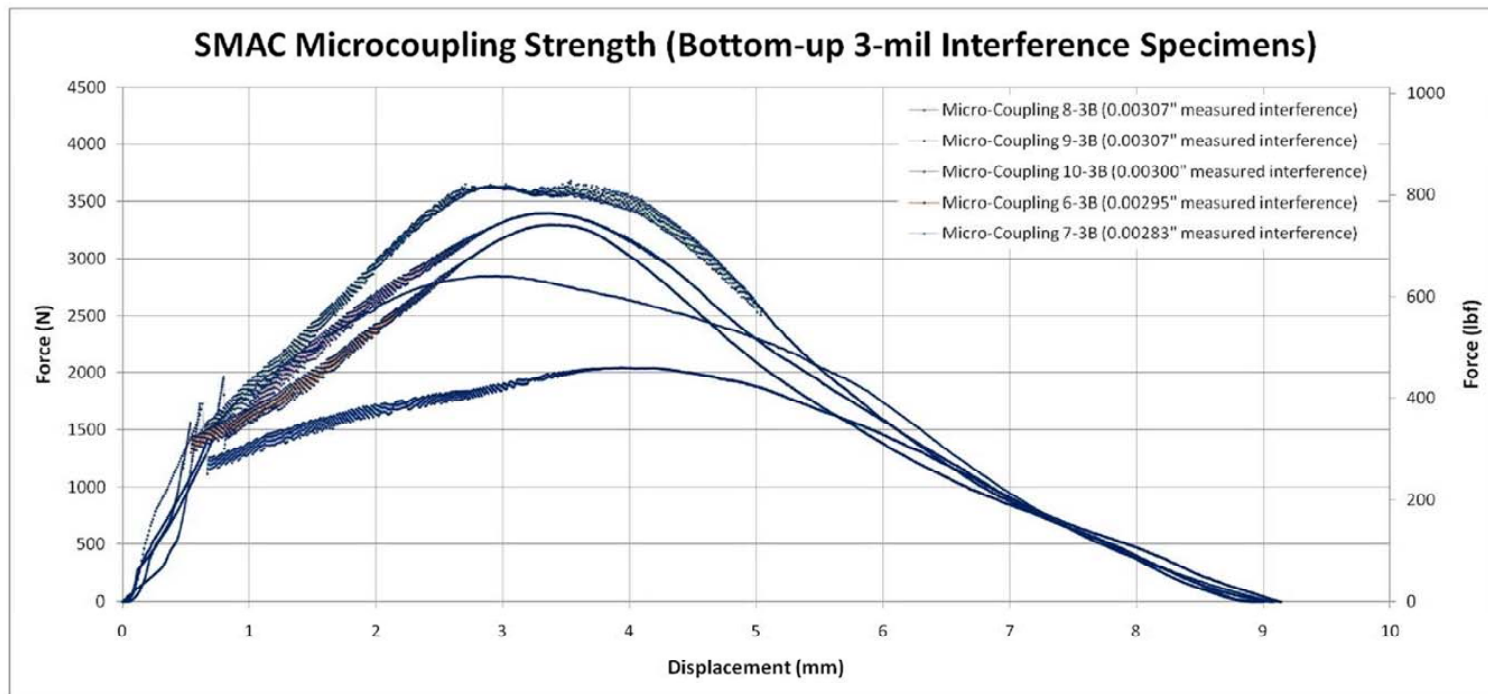


Figure A4 SMA²C Micro-Coupling Interference Joint Forced Removal: Bottom-up Specimens in Lot 0.003" Nominal Interference

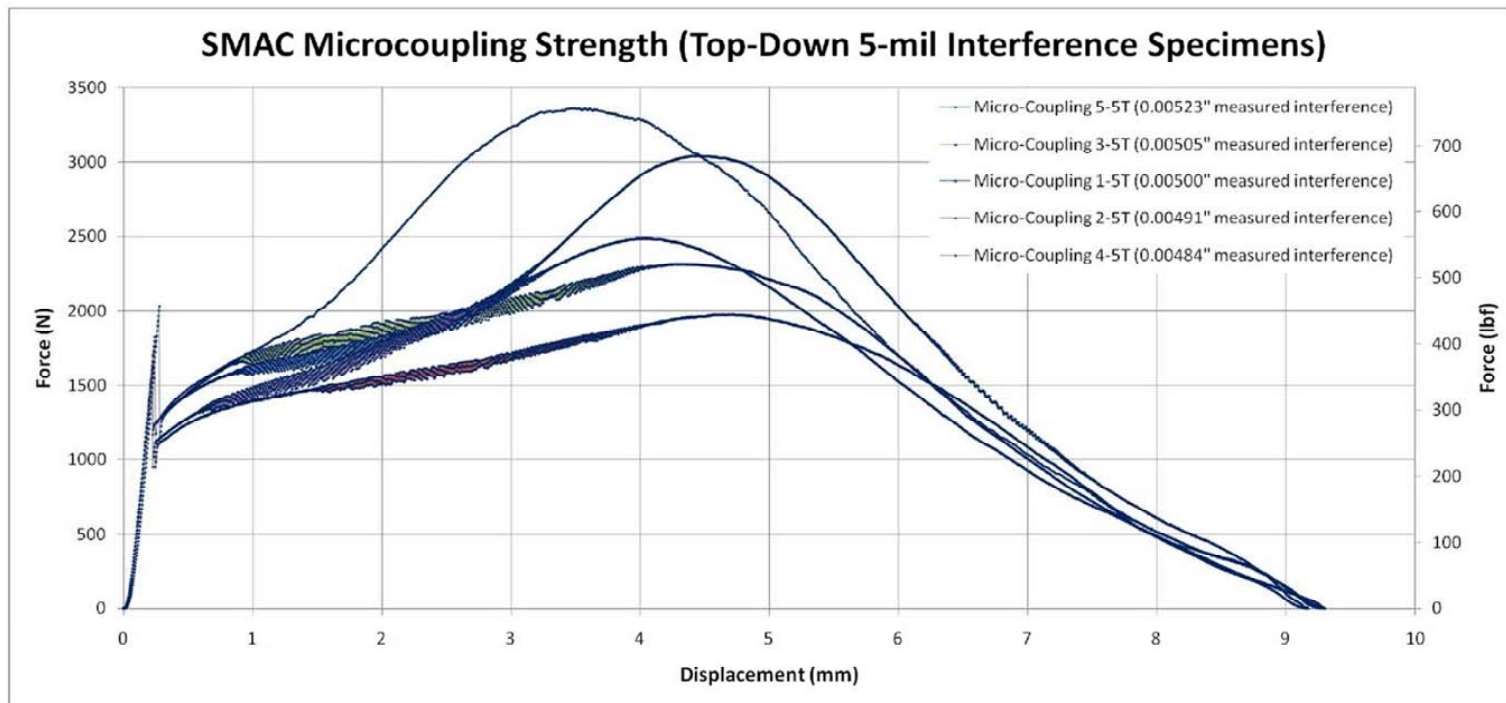


Figure A5 SMA²C Micro-Coupling Interference Joint Forced Removal: Top-down Specimens in Lot 0.005" Nominal Interference

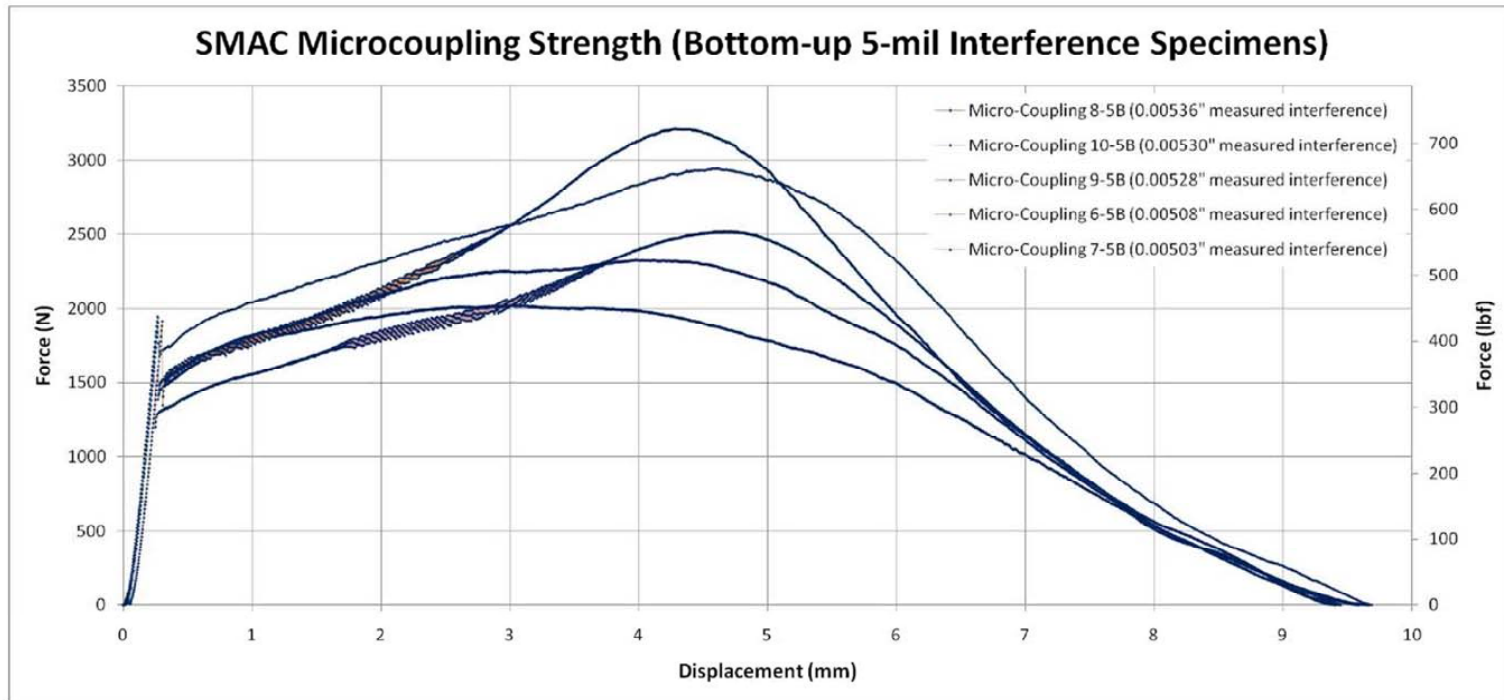


Figure A6 SMA²C Micro-Coupling Interference Joint Forced Removal: Bottom-up Specimens in Lot 0.005" Nominal Interference

Test Equipment and Instrumentation

Instrument or Equipment	Manufacturer	Model	Serial Number	Calibration Date
Micrometer	Mitutoyo	0-1" +/-0.0005"	293-832	Unknown
Gauge Pins	Deltronic	TP25: 0.1980" to 0.2045"; (+0.00004")	N/A	As manufactured 2009
Press-Fit Cradle Load Cell	Cooper Instruments	LKCP 474 2000lbf	162641 2K	28 October 2009
Load Cell Digital Readout	Cooper Instruments	DFI 3900-03	09492669	CH #1 match to above load cell
Tensile Machine Load Cell	Instron	8500 (2518-103)	uk193 USN 62271A4547	24 June 2009

CERTIFICATE OF TEST

DATE OF ISSUE: 24-Jun-09

Order/RMA Number:

RP0905080003

Page 1 of 2 pages

Instron - A Division of ITW

Customer

Naval Postgraduate School
Tested at Instron
825 University Ave
Norwood, MA 02062

Date of Verification: 24-Jun-09

Ambient Temperature: 70.8 °F

Machine

Manufacturer: Instron
Model: 8500
Serial No.: LCR8500

Transducer

Manufacturer: Instron
Model: 2518-103
Serial No.: uk193
Capacity: 1124 lbf
Type: Tension/Compression

Certification Statement

The forces verified with machine indicator GPIB (lbf) are WITHIN $\pm .5\%$ accuracy.

Data - Indicator 1. - GPIB (lbf)

TENSION

% of Range	Run 1			Run 2		
	Indicated (lbf)	Applied (lbf)	Error %	Indicated (lbf)	Applied (lbf)	Error %
100% Range (Full Scale: 1124 lbf)						
1	9.97063	9.9952	-.25	9.97680	9.9952	-.18
2	19.98225	19.9905	-.04	19.97875	19.9905	-.06
4	49.95650	49.9762	-.04	49.97527	49.9762	.00
7	69.98941	69.9667	.03	70.01316	69.9667	.07
10	99.93680	99.9524	-.02	99.94745	99.9524	.00
20	199.92344	199.9048	.01	199.95081	199.9048	.02
40	399.88571	399.8096	.02	399.94960	399.8096	.04
70	699.89311	699.6668	.03	699.95482	699.6668	.04
100	1099.94474	1099.4764	.04	1099.58252	1099.4764	.01
0 Return	.20745			.22839		

CERTIFICATE OF TEST

Order/RMA Number:
RP0905080003

Page 2 of 2 pages

Data - Indicator 1, - GPIB (lbf)

COMPRESSION

% of Range	Run 1			Run 2		
	Indicated (lbf)	Applied (lbf)	Error %	Indicated (lbf)	Applied (lbf)	Error %
100% Range (Full Scale: 1124 lbf)						
1	10.03311	9.9952	.38	10.03622	9.9952	.41
2	20.07612	19.9905	.43	20.07076	19.9905	.40
4	50.19003	49.9762	.43	50.18948	49.9762	.43
7	70.25068	69.9667	.41	70.24840	69.9667	.40
10	100.31668	99.9524	.36	100.31369	99.9524	.36
20	200.56665	199.9048	.33	200.58381	199.9048	.34
40	401.27921	399.8096	.37	401.20518	399.8096	.35
70	702.13059	699.6668	.35	702.14504	699.6668	.35
100	1101.31939	1099.4764	.17	1101.84541	1099.4764	.22
0 Return	.07426			.07473		

Verification Equipment

Make/Model	S/N	Description	Calibration Agency	Capacity	Cal Date	Cal Due
N/A	5	Set of Masses - U.S.	Instron	N/A	27-Apr-07	27-Apr-12

The value of acceleration due to gravity used to calculate the force exerted by the mass was 9.80349 m/s².

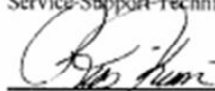
Verification Equipment Usage

Range F. S. (lbf)	Standard S/N	Mode	Percent(s) of Range	Uncertainty of Calibration (% of capacity)	Lower Limit (lbf) Standard Class A / A1
1124	5	T	1, 2, 4, 7, 10, 20, 40, 70, 100	.1	N/A
	5	C	1, 2, 4, 7, 10, 20, 40, 70, 100	.1	N/A

Comments:

Date: 24-Jun-09

Verified by: Brian Krim
Service Support Technician



APPENDIX D. MICRO-COUPLING ACTIVE RELEASE MECHANISM PATENT PENDING #12/878,760

Atty. Dkt. No. 20090003

MICRO-COUPLING ACTIVE RELEASE MECHANISM

William Mike Crane
Paul Michael Oppenheimer
Marcello Romano
James Hansen Newman

CROSS-REFERENCE TO RELATED APPLICATIONS

[0001] This application claims the benefit of U.S. Provisional Patent Application No. 61/242,637, filed September 15, 2009, which is hereby incorporated in its entirety by reference.

BACKGROUND OF THE INVENTION

1. Field of the Invention

[0002] The present invention relates generally to release mechanisms. More specifically, the present invention relates to actively commanded release mechanisms.

2. Description of the Related Art

[0003] The ability to deploy or release connected parts of a device or machine by a mechanism that is secure under extreme forces, yet will reliably actuate when commanded to do so, is extremely useful in situations where a latch or fastener is needed. Additionally, in many design situations, constraints of small size, mass, and operating power make use of several existing actuators impractical due to their complexity and inability to scale to the required size.

[0004] Many existing release mechanisms use moving parts and have the need for lubrication. For example, the SQUIGGLE®

Motor developed by New Scale Technologies consists of several piezoelectric ceramic actuators that change shape when electrically excited. These actuators are then attached to a threaded nut with a mating screw threaded inside that nut. Applying power to the actuators creates ultrasonic vibrations causing the nut to vibrate in an orbit. The nut's rotation moves the threaded mating screw in-and-out with a linear motion. For this example, both the micro-parts and lubrication needs of the mechanism lead to the possibility of binding and failure.

[0005] Some other existing release mechanisms are Non-Explosive Actuators (NEAs). Three NEA designs commonly used for actuation needs are: the Qwknut[®] designed by Starsys or NEA Split Spool Actuator by NEA Electronics Inc. used on the Cal Poly P-Pod (Poly Pico-satellite Orbital Dispenser); the FRANGIBOLT[®] actuator model FC2-16-31SR2; and the TiNi Pinpuller[®] both produced by TiNi Aerospace. The aforementioned NEAs are proven and reliable, but some may be too large for installation within small devices or could impart actuation shock to the system causing damage. In addition, some NEAs can be complex or draw excessive power leading to an increase in the number of failure modes for the actuator and the system using it.

SUMMARY OF THE INVENTION

[0006] In accordance with one embodiment, a micro-coupling active release mechanism includes: a bushing connectable to a first component, the bushing having a recess for receiving a shape memory alloy (SMA) cylindrical ring; a shape memory alloy (SMA) cylindrical ring connectable to a second component, wherein the SMA cylindrical ring is fit into the

recess of the bushing to form an interference joint that is releasable when the SMA cylindrical ring is heated to a transformation temperature that causes it to reduce in size. In one embodiment, the active release mechanism further includes a heating device for heating at least the SMA cylindrical ring to the transformation temperature. In one embodiment, the SMA cylindrical ring is made of a material that transforms at the transformation temperature from a larger martensitic phase diameter to a smaller austenitic phase diameter when heated at or above the transformation temperature.

[0007] In accordance with a further embodiment, a method for releasably coupling a first component to a second component includes: fitting a shape memory alloy (SMA) cylindrical ring into a bushing to create an interference joint; passing a bolt shaft of retaining bolt through an interior diameter of the SMA cylindrical ring, a portion of the bolt shaft extending out and from the SMA cylindrical ring, a bolt head of the retaining bolt catching on the SMA cylindrical ring and not passing through the SMA cylindrical ring; attaching the bushing to the first component; and attaching the SMA cylindrical ring to the second component using the portion of the bolt shaft extending out and from the SMA cylindrical ring; wherein heating the SMA cylindrical ring at or above a transformation temperature causes the SMA cylindrical ring to transform from a larger martensitic phase diameter to a smaller austenitic phase diameter and to release the interference joint allowing the first component to separate from the second component.

[0008] Embodiments in accordance with the invention are best understood by reference to the following detailed description when read in conjunction with the accompanying drawings.

BRIEF DESCRIPTION OF THE DRAWINGS

[0009] Figure 1A is a perspective view of the assembly of a micro-coupling interference joint in accordance with one embodiment;

[0010] Figure 1B is a top view of the micro-coupling interference joint assembled according to Figure 1A;

[0011] Figure 1C is a bottom view of the micro-coupling interference joint assembled according to Figure 1A;

[0012] Figure 2A is a perspective view of the assembly of a micro-coupling active release mechanism in accordance with one embodiment;

[0013] Figure 2B is a perspective view of the assembled micro-coupling active release mechanism of Figure 2A;

[0014] Figure 2C is a perspective view of the assembled micro-coupling release mechanism of Figure 2B with heat applied thereto;

[0015] Figure 2D is a perspective view of the micro-coupling release mechanism of Figure 2B after application of heat and release thereof;

[0016] Figure 3A is a back end view of an assembled micro-coupling active release mechanism in accordance with one embodiment;

[0017] Figure 3B is a front end view of the assembled micro-coupling active release mechanism of Figure 3A;

[0018] Figure 3C is a side view of the assembled micro-coupling active release mechanism of Figure 3A;

[0019] Figure 3D is a bottom view of the assembled micro-coupling active release mechanism of Figure 3A;

[0020] Figure 4 is a perspective view of one example of a micro-coupling active release mechanism assembled in a nano-satellite and used as the door release mechanism in accordance with one embodiment;

[0021] Figure 4A is a close-up view of the micro-coupling active release mechanism of Figure 4; and

[0022] Figure 5 is a graph showing coupling strength test data for the micro-coupling active release mechanism in accordance with one embodiment.

DETAILED DESCRIPTION OF THE INVENTION

[0023] Broadly viewed, embodiments in accordance with the micro-coupling active release mechanism include a shape memory alloy (SMA) cylindrical ring that is press-fit into a bushing or other mating attachment and held in place by frictional forces between the SMA cylindrical ring and the bushing or other mating attachment. Upon heating of the SMA cylindrical ring, the SMA cylindrical ring reduces in diameter and releases from the bushing or other mating attachment. More specifically, the press-fit SMA cylindrical ring creates an interference joint between the bushing or other mating attachment. This interference joint is releasable upon activation of the SMA cylindrical ring via conductive or direct current thermal heating which shrinks the press-fit SMA cylindrical ring. When the press-fit SMA cylindrical ring shrinks, the frictional force is relieved allowing the SMA cylindrical ring to separate from the bushing or other mating attachment. As can be understood by

those of skill in the art from the following description, embodiments in accordance with the micro-coupling active release mechanism can be adapted to accommodate the available volume of a given environment.

[0024] Embodiments in accordance with the micro-coupling active release mechanism provide a simple and reliable release mechanism having a minimal number of parts. In some embodiments, the release mechanism can be used to release components with a simple, single-motion actuation. In some embodiments, the micro-coupling active release mechanism can have a small size, small mass and small actuation power requirements. This allows for use of the micro-coupling active release mechanism in very small devices while minimizing the possibility of failure by reducing the number and complexity of the parts. Some embodiments of the micro-coupling active release mechanism can be useful for many applications in system design, such as safety devices, tamper locks, robotics, aeronautics, military, marine and spacecraft systems.

[0025] Referring to Figures 1A, 1B and 1C, one exemplary embodiment of a method for press-fitting a SMA cylindrical ring 10 into a bushing 14 to create an interference joint 12 is described. In one embodiment, SMA cylindrical ring 10 has an inner diameter and an outer diameter, as well as a wall thickness and a length. In one embodiment, SMA cylindrical ring 10 is formed of a shape memory alloy (SMA) material capable of having both an austenitic phase and a martensitic phase.

[0026] In one embodiment, SMA cylindrical ring 10 is press-fit into bushing 14 using a cold-press method. For example, in one embodiment, SMA cylindrical ring 10 is inserted into

bushing 14 in a cold twinned or cold de-twinned martensitic phase. This cold-press method forms a stronger interference joint 12, keeps the outer diameter of SMA cylindrical ring 10 small, and achieves a greater reduction in the outer diameter of SMA cylindrical ring 10 upon heating to ensure successful decoupling from bushing 14.

[0027] In another embodiment, SMA cylindrical ring 10 is press-fit into bushing 14 using a shrink-fit method. For example, in one embodiment, SMA cylindrical ring 10 is heated to its austenitic phase, inserted into bushing 14, and allowed to cool and expand into its martensitic phase, thereby creating interference joint 12. As illustrated in Figure 1A, an insertion tool 16 can be used to insert SMA cylindrical ring 10 into bushing 14 using either the cold-press or shrink-fit method.

[0028] In one embodiment, bushing 14 has an inner diameter for receiving SMA cylindrical ring 10. When SMA cylindrical ring 10 is press-fit into bushing 14, frictional forces between the outer diameter of press-fit SMA cylindrical ring 10 against the interior wall of bushing 14 create the holding power of interference joint 12. To effect release of interference joint 12, SMA cylindrical ring 10 is heated to its austenitic phase and reduces in outer diameter. This reduction in outer diameter relieves the frictional forces between SMA cylindrical ring 10 and bushing 14 allowing release of SMA cylindrical ring 10 from bushing 14.

[0029] In one embodiment, interference joint 12 is utilized as part of a micro-coupling active release mechanism; interference joint 12 provides the frictional holding force to allow two components, i.e., a first component and a second component, to be coupled together until the activation of the

micro-coupling active release mechanism effected by shrinking SMA cylindrical ring 10 on application of heat. In one embodiment, SMA cylindrical ring 10 can be formed of a pseudoelastic alloy, such as a "G" type nickel titanium (NiTi) alloy, such as one provided by Intrinsic Devices, Inc., that has activation "Heat to Recover" (HTR) temperatures of 95-105°C, e.g., transformation temperatures of 95-105°C. Heating of the pseudoelastic alloy to a temperature within the associated HTR temperature range initiates a phase change in which the larger martensitic phase diameter of SMA cylindrical ring 10 is reduced to its smaller austenitic phase diameter.

[0030] In one embodiment, a relatively high onset activation temperature, e.g., relatively high onset transformation temperature, is utilized to be high enough to prevent unintentional activation of SMA cylindrical ring 10, yet require little power to actuate. The change in the inner and outer diameters of SMA cylindrical ring 10 upon heating results from a change in the atomic positions within the NiTi alloy when transitioning from martensite to austenite. In various embodiments, SMA cylindrical ring 10 can be formed using one or more substances having different material properties allowing for a wide range of micro-coupling actuation characteristics.

[0031] In one embodiment, SMA cylindrical ring 10 can be press-fit into bushing 14 in accordance with a specified set of interference values used to create a needed coupling force in resulting interference joint 12. In one embodiment, the inner diameter of bushing 14 can be set to be greater than the recovered or reduced (memory) size of SMA cylindrical ring 10, thereby allowing SMA cylindrical ring 10 to free

itself from bushing 14 upon activation, i.e., heating of SMA cylindrical ring 10 to a transformation temperature, e.g., HTR. SMA cylindrical ring 10 can be manufactured with a pre-determined thickness and length sufficient to yield enough change in diameter upon activation to ensure release from bushing 14 and also have enough strength to avoid failure in tension, compression and/or shear when placed under load.

[0032] Referring to Figures 2A through 2D, one embodiment of a micro-coupling active release mechanism 22 is described. In the present embodiment, for purposes of description it can be assumed that micro-coupling active release mechanism 22 is for coupling a first component (not shown) to a second component (not shown). Further, for purposes of description, bushing 14 is attachable to a first component and SMA cylindrical ring 10 is attachable to a second component.

[0033] In one embodiment, SMA cylindrical ring 10 is press-fit into bushing 14 as earlier described with reference to Figures 1A, 1B and 1C. In one embodiment, SMA cylindrical ring 10 can be actively actuated by a heating device 18, such as a resistive heater, that can be conductively coupled to SMA cylindrical ring 10 or to bushing 14. For example, heating device 18 can be connected directly to SMA cylindrical ring 10 or wrapped around bushing 14 (as shown in Figures 2C and 2D).

[0034] In one embodiment, a retaining bolt 20 is passed through the interior diameter of SMA cylindrical ring 10 to secure SMA cylindrical ring 10 to the second component. In one embodiment, retaining bolt 20 includes a bolt shaft 23 having a first diameter, i.e., a bolt shaft diameter, and a bolt head 24 having a second diameter, i.e., a bolt head diameter. In one embodiment, the bolt shaft diameter of bolt

shaft 23 is sized to pass through (e.g., within) the inner diameter of SMA cylindrical ring 10, but the bolt head diameter of bolt head 24 is larger than the inner diameter of SMA cylindrical ring 10 and smaller than the inner diameter of bushing 14 in austenitic phase. In this way bolt head 24 "catches" on SMA cylindrical ring 10 and cannot pass through SMA cylindrical ring 10. As seen in Figure 2B, this allows a portion of bolt shaft 23 to extend out and from SMA cylindrical ring 10 for attachment to the second component. Thus in Figure 2C, assuming bushing 14 is attached to the first component and SMA cylindrical ring 10 is attached to the second component (via retaining bolt 20), the first and second components are releasably coupled. In Figure 2D, heating SMA cylindrical ring 10 results in the atomic transformation of SMA cylindrical ring 10 from its larger martensitic phase into its smaller diameter ("memory shape") austenitic phase. Once heated, SMA cylindrical ring 10 shrinks and releases from its press-fit to bushing 14, thereby allowing SMA cylindrical ring 10, along with retaining bolt 20, to slide out of bushing 14, releasing the coupling of the first and second components.

[0035] In one embodiment, if the material into which SMA cylindrical ring 10 is press-fit, i.e., the material of bushing 14, is not electrically conductive, direct electrical current can be passed through SMA cylindrical ring 10 to induce resistive heating and subsequent SMA cylindrical ring 10 activation. Passive SMA actuation techniques of SMA cylindrical ring 10, such as exposure to an intense indirect heat source, can also be used to actuate the release of the micro-coupling active release mechanism 22, i.e., release of the interference joint, in addition to adjusting the alloy's

metal composition characteristics of SMA cylindrical ring 10 to change desired actuation temperatures.

[0036] Referring to Figures 3A through 3D, in one embodiment, a micro-coupling active release mechanism 30 including SMA cylindrical ring 10 and bushing 14 is positioned inside a mountable mechanism, housing 32. In one embodiment, the design of housing 32 can be adapted to accommodate the particular application of SMA micro-coupling active release mechanism 30. In one embodiment, housing 32 is utilized to attach to one of a coupled pair of components (not shown) while holding interference joint 12. In one embodiment, interference joint 12 is formed between SMA cylindrical ring 10 and bushing 14 as earlier described. Housing 32, for example, can be used to attach to a first component (not shown) while holding interference joint 12.

[0037] In one embodiment, retaining bolt 20 passes through SMA cylindrical ring 10, catching bolt head 24 such that a portion of bolt shaft 23 extends from SMA cylindrical ring 10 for attachment to a second component (not shown). In one embodiment, retaining bolt 20 can be made of titanium or a strong stainless steel alloy for high strength and low coefficient of thermal expansion. In one embodiment, the diameter of bolt shaft 23 is less than the inside diameter of SMA cylindrical ring 10 in its austenitic phase (i.e., less than the austenitic "memory" shape diameter) so as not to constrain the shrinkage of SMA cylindrical ring 10 upon actuation. In one embodiment, on release actuation, heating device 18 is activated and both bushing 14 and SMA cylindrical ring 10 are heated to a transformation temperature, e.g., an HTR temperature.

[0038] In one embodiment, a thermal isolation ring 34 can be used to isolate housing 32 from heating device 18 and heated bushing 14. Heating of bushing 14 and SMA cylindrical ring 10 together takes advantage of the thermal expansion of the inner diameter of bushing 14 and also the subsequent reduction of the outer diameter of SMA cylindrical ring 10 upon reaching the transformation temperature, e.g., HTR. The resulting differences in diameter release SMA cylindrical ring 10 from its assembled press-fit in bushing 14, thereby releasing retaining bolt 20 and SMA cylindrical ring 10 from bushing 14 and allowing separation of the first and second components (see Figure 2D).

[0039] In some embodiments, a pusher plate 36 and an attached spring 38 can be included in micro-coupling active release mechanism 30. Pusher plate 36 and spring 38 can aid in separation of SMA cylindrical ring 10 and retaining bolt 20 by applying a pre-load to micro-coupling active release mechanism 30.

[0040] Referring to Figures 4 and 4A, in one embodiment a micro-coupling active release mechanism 40 is illustrated installed in a nano-satellite 42. In one embodiment, micro-coupling active release mechanism 40 is microcoupling active release device such as microcoupling active release mechanism 30. In this embodiment, micro-coupling active release mechanism 40 is employed to releasably hold a retaining door 44 in place on nano-satellite 42 throughout launch and for at least a portion of a time while in orbit.

[0041] In one embodiment, for purposes of description, microcoupling active release mechanism 40 is installed on nano-satellite 42 such that bushing 14 together with housing 32, heating device 18, push plate 26 and spring 38 are

attached to nano-satellite 42 and SMA cylindrical ring 10 is attached to the interior side of retaining door 44 by retaining bolt 20. In Figures 4 and 4A, SMA cylindrical ring 10 and retaining bolt 20 of micro-coupling active release mechanism 40 are not shown, however it is understood that that these portions of micro-coupling active release mechanism 40 are present in the embodiment.

[0042] Initially, when retaining door 44 of nano-satellite 42 is closed, SMA cylindrical ring 10 is coupled with bushing 14 forming interference joint 12. On activation of micro-coupling active release mechanism 40, retaining door 44 separates from nano-satellite 42 allowing a smaller interior satellite 46 to be released. More specifically, on activation of micro-coupling active release mechanism 40, heating device 18 is activated such that SMA cylindrical ring 10 is heated to a transformation temperature, e.g., HTR, allowing SMA cylindrical ring 10 to release from the press-fit in bushing 14. SMA cylindrical ring 10 (with retaining bolt 20) and retaining door 44 then release from nano-satellite 42. In some embodiments, pusher plate 36 and spring 38 aid in separation of SMA cylindrical ring 10 with retaining door 44 by applying a pre-load to interference joint 12. With retaining door 44 removed, the smaller interior satellite 46 can be released.

[0043] Referring to Figure 5, coupling strength data is shown in a graph derived from a single micro-coupling test article when subject to forces great enough to forcefully extract SMA cylindrical ring 10 from its interference joint 12 in accordance with one embodiment. Coupling strength static friction peaks, maximum coupling strength, and kinetic friction slip transitions can be seen. The test data in the

graph of Figure 5 may be representative of multiple test articles.

[0044] In some applications, it may be desirable to form interference joint 12 without the use of a separate mountable bushing, e.g., bushing 14, and instead form a bushing-like recess, or other receiving space, in two components to be releasably coupled. Thus in another embodiment of micro-coupling active release mechanism, a first component and a second component to be coupled are releasably joined by forming a first hole in the first component and a second hole in the second component.

[0045] In one embodiment, the first hole and the second hole are formed to meet the tolerances needed to press-fit opposite end portions of SMA cylindrical ring 10 into each of the first hole and the second hole. In one embodiment, a first end portion of SMA cylindrical ring 10 is press-fit into the first hole of the first component, thereby leaving a second end portion of SMA cylindrical ring 10 exposed and available for press-fit into the second hole of the second component. In this embodiment, the material that SMA cylindrical ring 10 is press-fit into, i.e., material within which the first hole and second hole are formed, is of sufficient strength, has the proper surface finish for effective frictional coefficients, and has low thermal conductivity for implementation. In this embodiment, heating device 18 or other heat source is used to actuate SMA cylindrical ring 10 and decouple the first and second components. More specifically, as earlier described, SMA cylindrical ring 10 is heated to a specified HTR temperature or within a specified HTR temperature range causing SMA

cylindrical ring 10 to shrink in diameter and release from the press-fit in the first hole and the second hole.

[0046] Embodiments in accordance with the micro-coupling active release mechanisms described herein are composed of few parts and can be formed to have small size and small mass. The design allows for large coupling strength and requires little power to actuate release. Those of skill in the art can understand that embodiments in accordance with the invention can also be scaled up in size to accommodate larger applications, but that accordingly more power may be needed to actuate release.

[0047] This disclosure provides exemplary embodiments of the invention. The scope of the invention is not limited by these exemplary embodiments. Numerous variations, whether explicitly provided for by the specification or implied by the specification or not, may be implemented by one of skill in the art in view of this disclosure.

CLAIMS

We claim:

1. An active release mechanism comprising:
a bushing connectable to a first component, the bushing having a recess for receiving a shape memory alloy (SMA) cylindrical ring; and
a shape memory alloy (SMA) cylindrical ring connectable to a second component, wherein the SMA cylindrical ring is fit into the recess of the bushing to form an interference joint that is releasable when the SMA cylindrical ring is heated to a transformation temperature that causes it to reduce in size.
2. The active release mechanism of Claim 1, wherein the SMA cylindrical ring is made of a material that transforms at the transformation temperature from a larger martensitic phase diameter to a smaller austenitic phase diameter when heated at or above the transformation temperature.
3. The active release mechanism of Claim 2, wherein the SMA cylindrical ring is formed of a pseudoelastic alloy that has an associated transformation temperature.
4. The active release mechanism of Claim 2 further comprising:
a heating device for heating at least the SMA cylindrical ring to the transformation temperature.

5. The active release mechanism of Claim 1 further comprising:

a retaining bolt for attaching the SMA cylindrical ring to the second component, the retaining bolt comprising:

a bolt shaft having a bolt shaft diameter; and

a bolt head having a bolt head diameter;

wherein the bolt shaft diameter is smaller than an inner diameter of the SMA cylindrical ring; and

wherein the bolt head diameter is larger than the inner diameter of the SMA cylindrical ring;

wherein the bolt shaft passes through the inner diameter of the SMA cylindrical ring and extends out from the SMA cylindrical ring for attachment to the second component; and

further wherein the bolt head does not pass through the inner diameter of the SMA cylindrical ring.

6. The active release mechanism of Claim 4, wherein the heating device heats both the SMA cylindrical ring and the bushing.

7. The active release mechanism of Claim 4, wherein the heating device is an electrically resistive heater.

8. The active release mechanism of Claim 4, wherein the heating device includes direct electrical current applied to the SMA cylindrical ring.

9. The active release mechanism of Claim 4 further comprising:

a housing connecting the bushing to the first component.

10. The active release mechanism of Claim 9, further comprising:

a pusher plate; and

a spring;

wherein the pusher plate and the spring are arranged to aid in the separation of the SMA cylindrical ring and the retaining bolt from the bushing.

11. The active release mechanism of Claim 1, wherein the SMA cylindrical ring is press-fit into the recess of the bushing.

12. The active release mechanism of Claim 1, wherein the SMA cylindrical ring is press-fit using a cold-press method.

13. The active release mechanism of Claim 1, wherein the SMA cylindrical ring is press-fit using a shrink-fit method.

14. A method for releasably coupling a first component to a second component, the method comprising:

fitting a shape memory alloy (SMA) cylindrical ring into a bushing to create an interference joint;

passing a bolt shaft of retaining bolt through an interior diameter of the SMA cylindrical ring, a portion of

the bolt shaft extending out and from the SMA cylindrical ring, a bolt head of the retaining bolt catching on the SMA cylindrical ring and not passing through the SMA cylindrical ring;

attaching the bushing to the first component; and
attaching the SMA cylindrical ring to the second component using the portion of the bolt shaft extending out and from the SMA cylindrical ring;

wherein heating the SMA cylindrical ring at or above a transformation temperature causes the SMA cylindrical ring to transform from a larger martensitic phase diameter to a smaller austenitic phase diameter and to release the interference joint allowing the first component to separate from the second component.

15. The method of Claim 14, wherein fitting a shape memory alloy (SMA) cylindrical ring into a bushing to create interference joint comprises:

press-fitting the SMA cylindrical ring into the bushing to form the interference joint.

16. The method of Claim 14, wherein fitting a shape memory alloy (SMA) cylindrical ring into a bushing to create interference joint comprises:

obtaining the SMA cylindrical ring in a cold twinned martensitic phase; and

inserting the SMA cylindrical ring into the bushing while in the shape memory alloy is in the cold twinned martensitic phase to form the interference joint.

17. The method of Claim 14, wherein fitting a shape memory alloy (SMA) cylindrical ring into a bushing to create interference joint comprises:

obtaining the SMA cylindrical ring in a cold de-twinned martensitic phase; and

inserting the SMA cylindrical ring in the cold de-twinned martensitic phase into the bushing to form the interference joint.

18. The method of Claim 14, wherein fitting a shape memory alloy (SMA) cylindrical ring into a bushing to create interference joint comprises:

obtaining the SMA cylindrical ring in a martensitic phase;

heating the SMA cylindrical ring to a temperature at or above the transformation temperature to transform the SMA cylindrical ring to an austenitic phase;

inserting the SMA cylindrical ring in the austenitic phase into the bushing; and

cooling the SMA cylindrical ring to a temperature below the transformation temperature to transform the SMA cylindrical ring to a martensitic phase and form the interference joint.

19. An active release mechanism comprising:

a first component, the first component having a first hole for receiving a first end portion of a shape memory alloy (SMA) cylindrical ring;

a second component, the second component having a second hole for receiving a second end portion of the shape memory alloy (SMA) cylindrical ring; and

a shape memory alloy (SMA) cylindrical ring connectable to the first component at a first end portion and to the second component at a second end portion,

wherein the first end portion of the SMA cylindrical ring is press-fit into the first hole to form a first interference joint and press-fit into the second hole to form a second interference joint,

and further wherein the first interference joint and the second interference joint are releasable when the SMA cylindrical ring is heated to a transformation temperature that causes it to reduce in size.

20. The active release mechanism of Claim 19 further comprising:

a heating device for heating at least the SMA cylindrical ring to the transformation temperature.

ABSTRACT OF THE DISCLOSURE

A micro-coupling active release mechanism including a shape memory alloy (SMA) cylindrical ring that is fit into a bushing or other mating attachment creating an interference joint held in place by frictional forces. The interference joint can be released upon actuation in which the SMA cylindrical ring is heated causing it to shrink in size, relieving the frictional forces of the interference joint thereby releasing the SMA cylindrical ring from the bushing or other mating attachment.

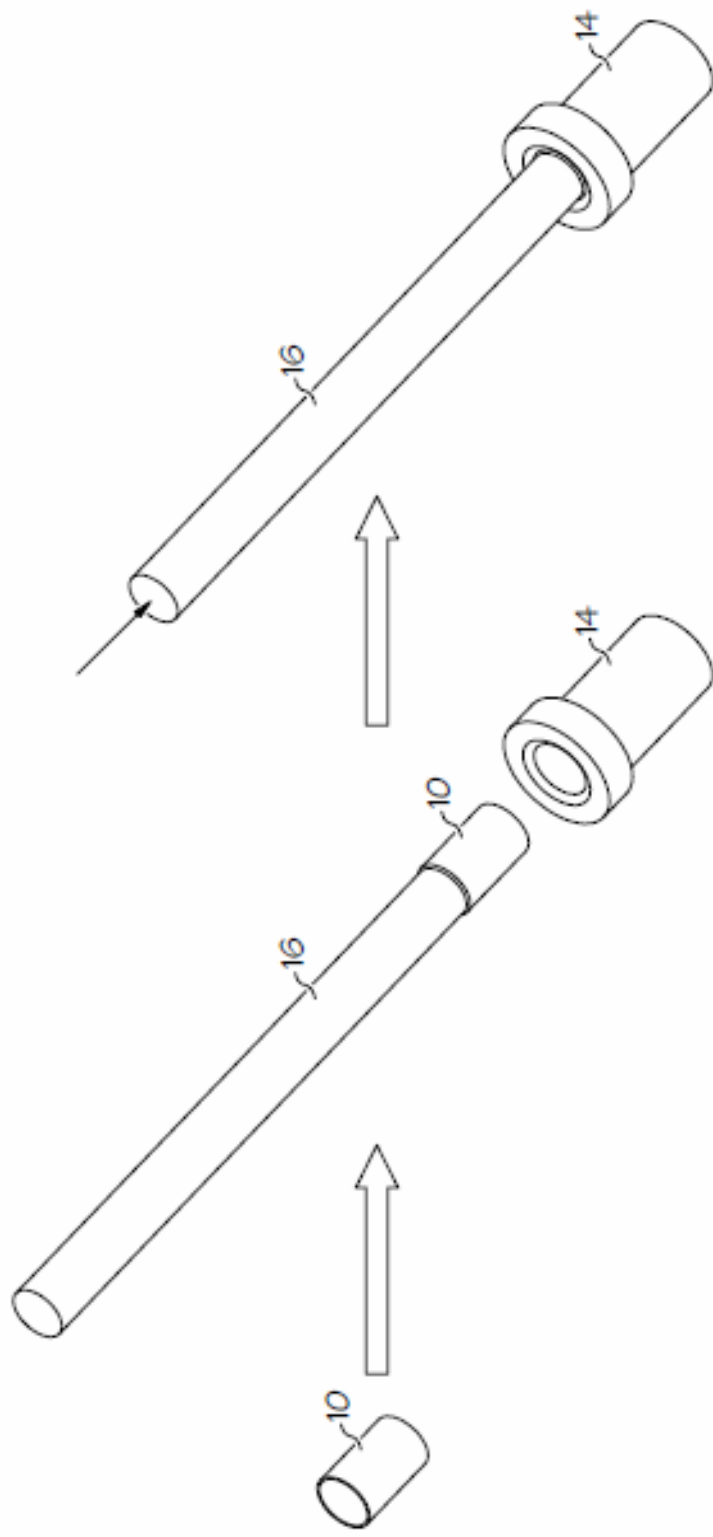


FIG. 1A

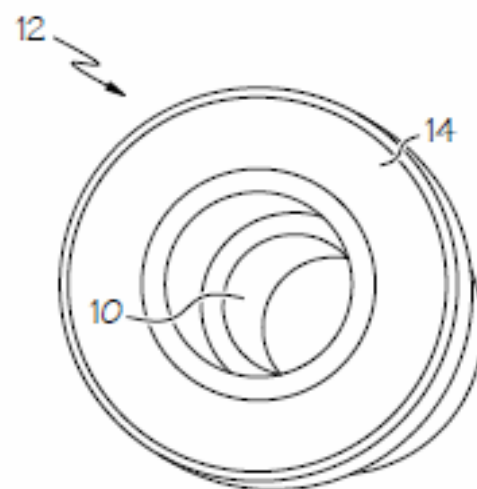


FIG. 1B

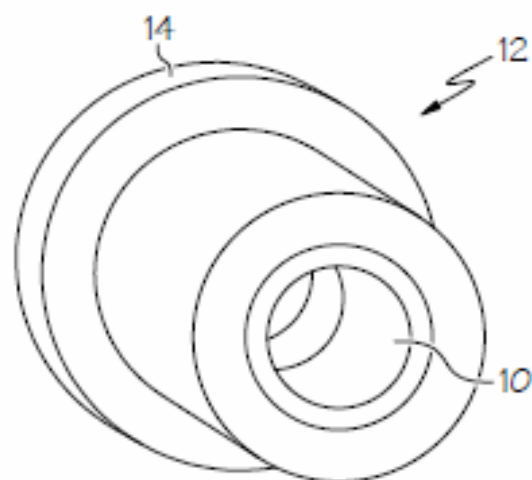


FIG. 1C

3/8

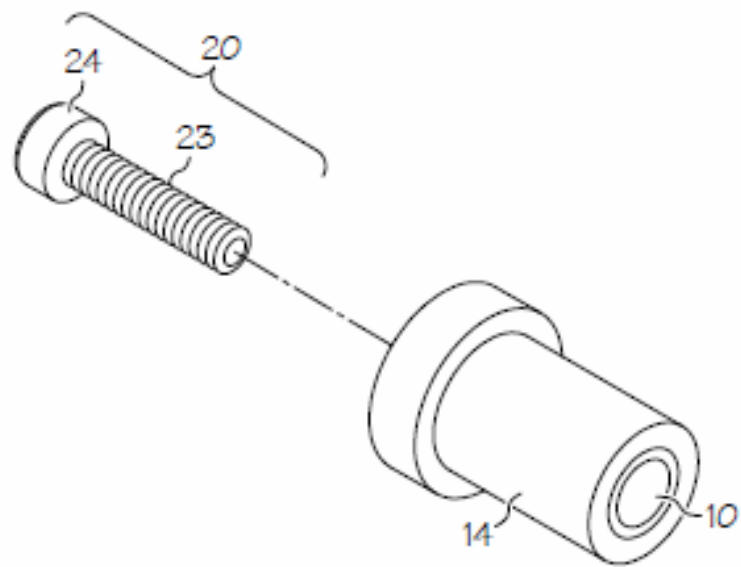


FIG. 2A

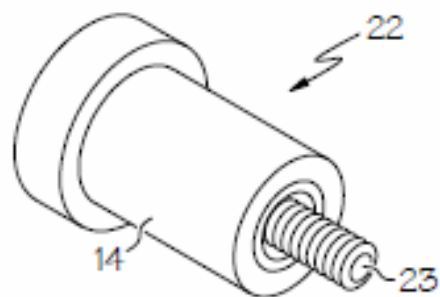


FIG. 2B

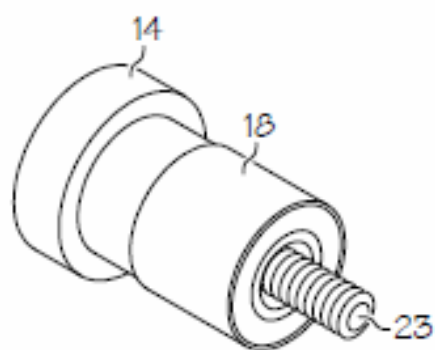


FIG. 2C

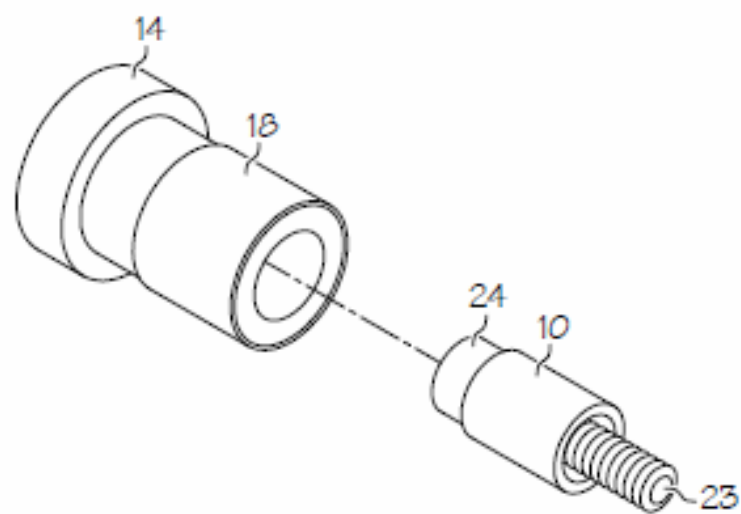


FIG. 2D

5 / 8

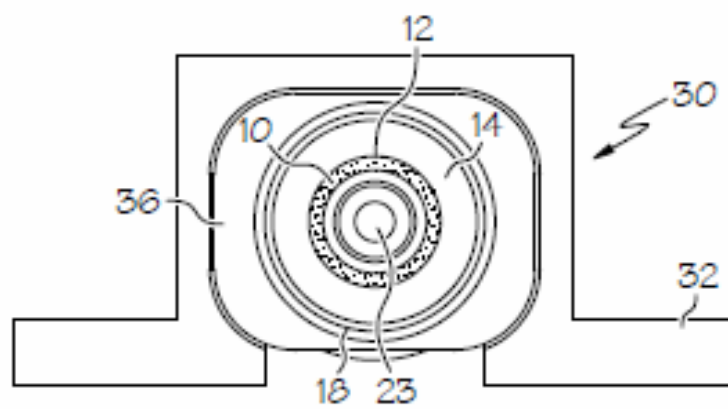


FIG. 3A

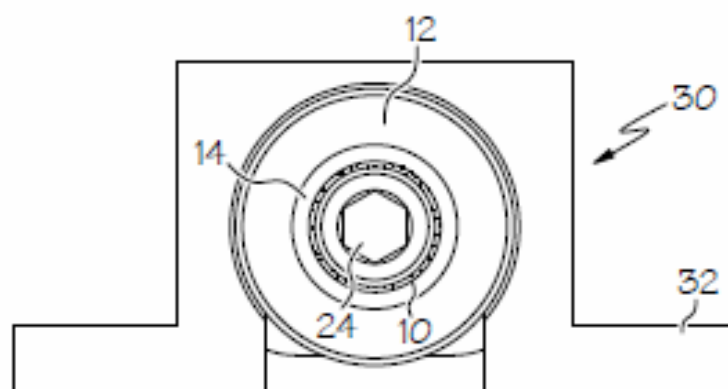


FIG. 3B

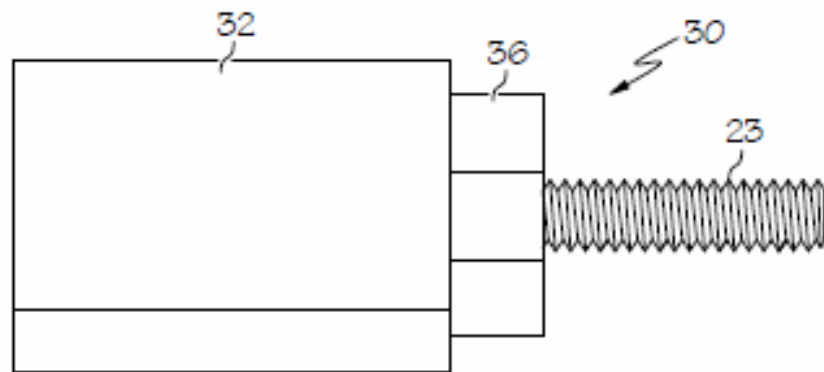


FIG. 3C

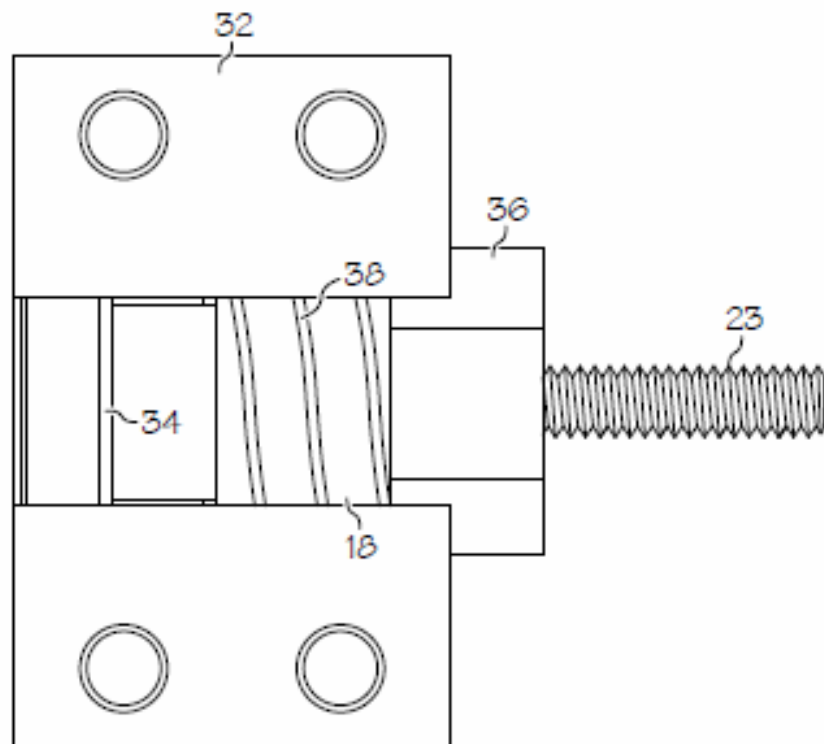
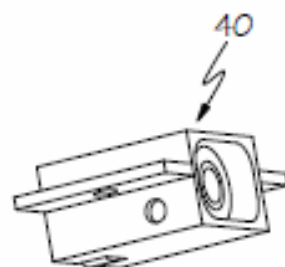
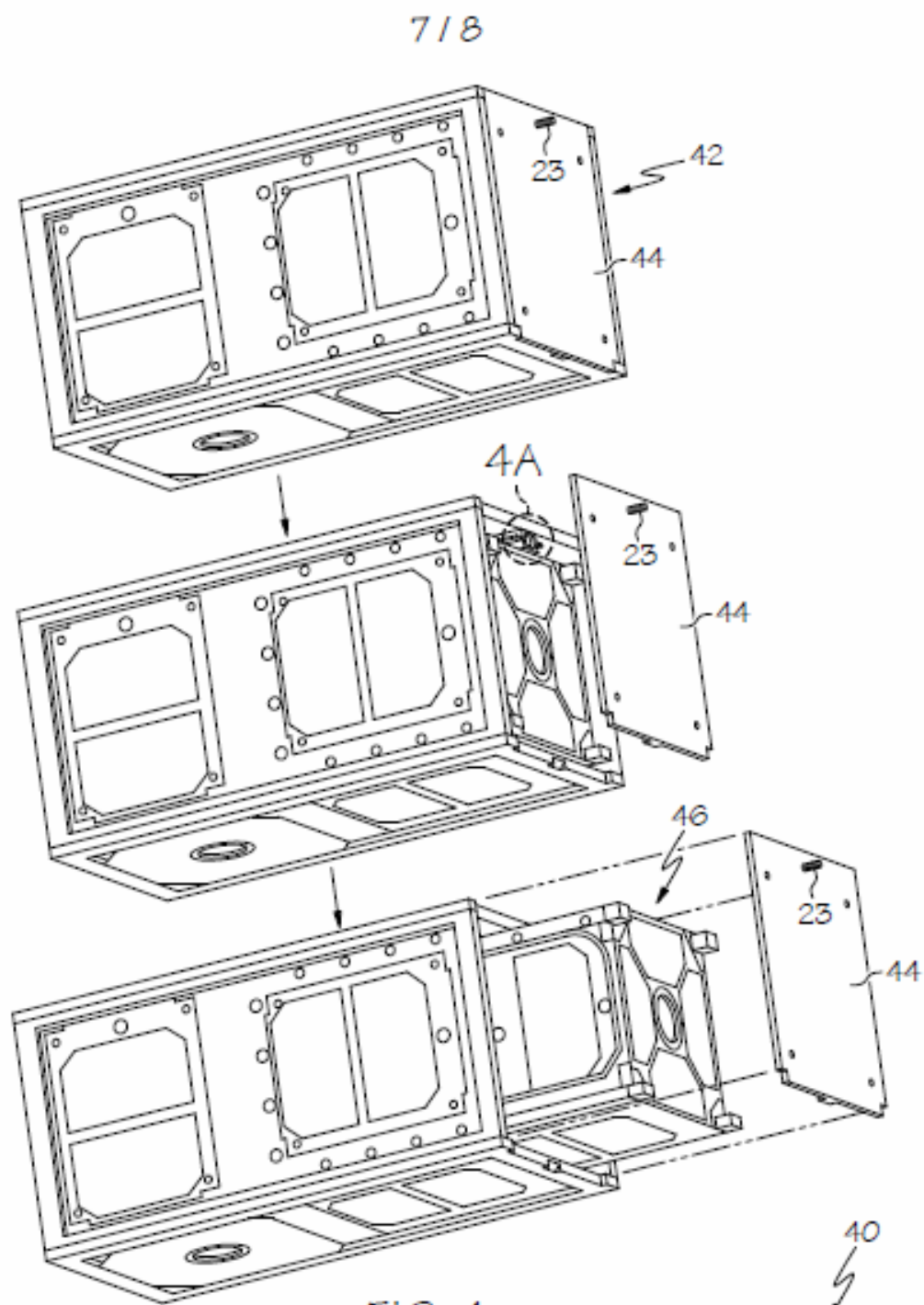


FIG. 3D



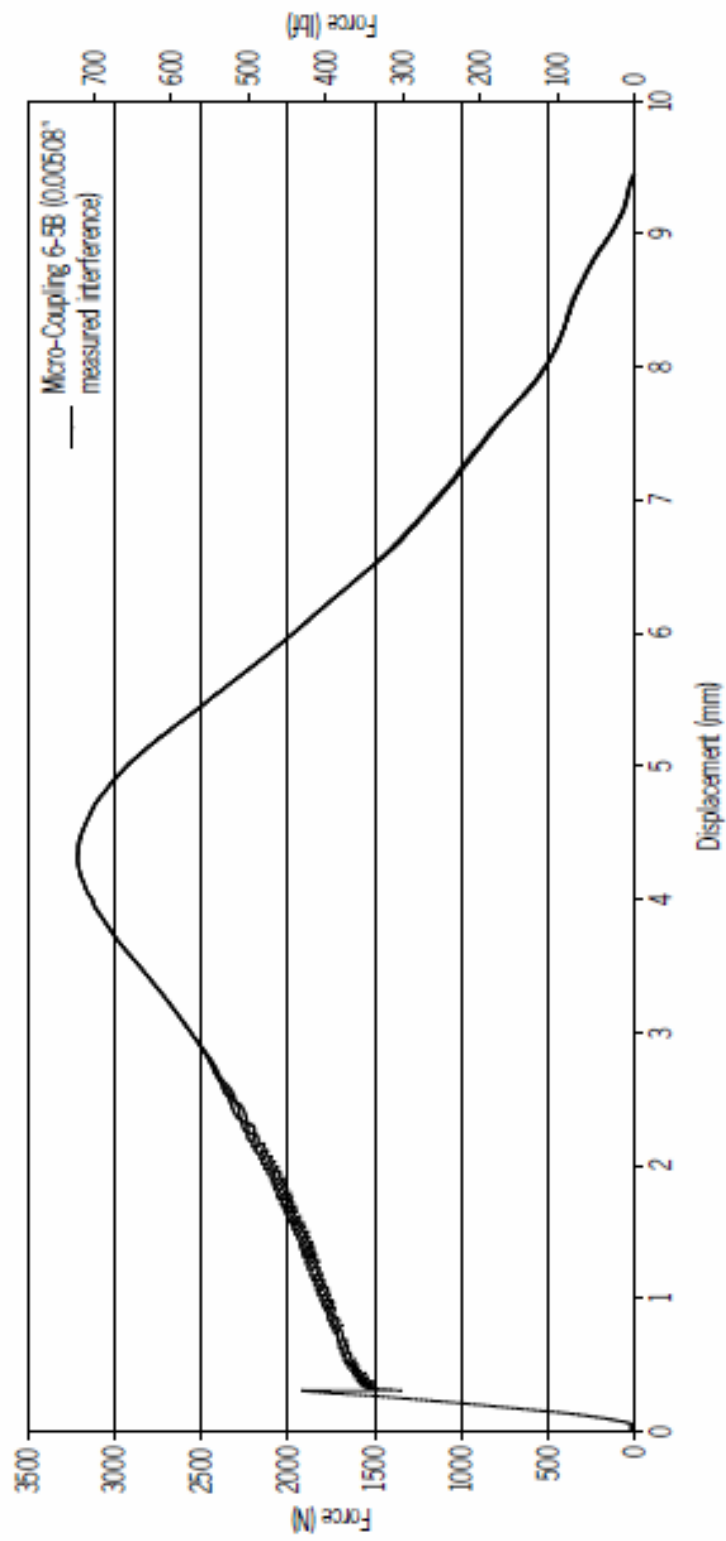


FIG. 5

APPENDIX E. SMA²C ACTUATION PREDICTED POWER CONSUMPTION CALCULATIONS (SPACE)

SMAC (Shape Memory Alloy Coupling) EDU Actuation Power Consumption Calculations						
Dimention of SMA	Metric	English	Notes / Sources			
Diameter - inner:	3.9942 mm	0.1573 in				
Diameter - outer:	5.1892 mm	0.2043 in				
Length:	7.7978 mm	0.3070 in				
Volume:	67.2136 mm ³	0.0041 in ³				
NiTi Specific Density:	0.0065 g/mm ³	0.2348 lbm/in ³	SMA Modeling & Eng Applications (Lagoduas) pg 105 table 2.5			
Dimention of Bushing						
Diameter - inner:	5.0571 mm	0.1991 in				
Diameter - outer:	7.1438 mm	0.2813 in				
Oveall length:	16.2408 mm	0.6394 in				
Head length:	3.2296 mm	0.1272 in				
Head Diameter - outer:	10.7950 mm	0.4250 in				
Volume:	490.8748 mm ³	0.0300 in ³				
Case-hardended Steel Specific Density:	0.0078 g/mm ³	0.2801 lbm/in ³	Engineer's Edge http://www.engineersedge.com/properties_of_metals.htm			
Equation Constants and Variables (needed for Minco white paper equations):						
SMA mass	0.437 g	0.0010 lbm				
Bushing mass	3.806 g	0.0084 lbm				
Total Mass to be heated:	4.243 g	0.0094 lbm				
SMA Specific Heat (Cp)	0.200 Cal/g*°C	0.125 BTU/lb*°F	Intrinsic Devices Inc.			
Bushing Specific Heat (Cp)	0.486 J/g*°C	0.116 BTU/lb*°F	Engineer's Edge http://www.engineersedge.com/properties_of_metals.htm			
Tf (C)	100.0 C	212.0 F				
Ti (C)	-45.0 C	-49.0 F				
Ta (C)	-45.0 C	-49.0 F				
t (hrs)	0.017 hrs	60 sec				
Heater Coverage Area:	7.44 mm ²	0.293 in ²	Heater dimensions = .3125x.9375"			
SMA Thermal Conductivity	0.867 BTU*in/ft ² /F/hr		10.4 BTU/hr*ft*°F Intrinsic Devices Inc.			
Bushing Thermal Conductivity	1.750 BTU*in/ft ² /F/hr		21.0 BTU/hr*ft*°F The engineering toolbox			
Length of Loss Conductive Path (Polythermide insulation washer)	1.00 mm	0.039 in	http://www.engineeringtoolbox.com/thermal-conductivity-metals-d_858.html			
Emissivity of Bushing	0.700		1 Btu/(hr °F ft ² /ft) = 1 Btu/(hr °F ft) = 1.731 W/(m °K) = 1.488 kcal/(h m °K)			
Tf (absolute)	672.000 R					
Ta (absoute)	411.000 R					
Conductive Loss Area Bushing	0.0797 in ²	0.00055 ft ²	Contact area to Polythermide = Circumfrence under brim of bushing			
Conductive Loss Area SMA	0.0134 in ²	0.00009 ft ²	Contact area to retaining bolt = Top of SMA cylinder			
Radiative Loss Surface Area	0.9061 in ²	0.00629 ft ²	Total surface area of bushing			
Power Required Estimate:						
Heater Power Minimum (No Loss) Thermo Calc:	5.366 Watts		P_heater = m_total*Cp(Tf-Ti)/3.412t			
+ 20% estimated heat losses =	6.439 Watts		Initial Estimate!			
Power Required Detailed Calculations:						
	Steady State Heat Losses					
Conduction Loss (P_cd) =	1.883 Watts	Bushing	See Minco White Paper for Formula			
	1.562 Watts	SMA	See Minco White Paper for Formula			
Radiation Loss =	0.388 Watts	Bushing	See Minco White Paper for Formula			
Steady State Loss (Space):	3.833 Watts					
	Warmup Power Calculations					
Warmup Coefficient =	0.01469		Hw = Steady State Loss/(Tf-Ta)			
Warmup Power (Space):	7.324 Watts		See Minco White Paper for Formula			
Total Power Required (Space) =	11.157 Watts		Steady State Losses + Warmup Power			
+ 10% =	12.273 Watts		10% Margin			
Required Power Calculations (SPACE):						
Supplied Bus Voltage	12.00	10.00	5.00	Volts		
EDU Foil Heater Resistance	12.6	12.6	12.6	Ohms		
Amperage	0.952	0.794	0.397	Amps	i = V/R	
Available Power	11.429	7.937	1.984	Watts	P = V ² /R	
Total Power Required for HTR	12.273 Watts				As calculated from above	
	1.07	1.55	6.19	min	Power Required/Available Power	
Time required by foil Heater Type	64	93	371	sec		

THIS PAGE INTENTIONALLY LEFT BLANK

APPENDIX F. SMA²C ACTUATION PREDICTED POWER CONSUMPTION CALCULATIONS (LABORATORY)

SMAC (Shape Memory Alloy Coupling) EDU Actuation Power Consumption Calculations									
Dimintions of SMA	Metric		English		Notes / Sources				
Diameter - inner:	3.9942	mm	0.1573	in					
Diameter - outer:	5.1892	mm	0.2043	in					
Length:	7.7978	mm	0.3070	in					
Volume:	67.2136	mm ³	0.0041	in ³					
NiTi Specific Density:	0.0065	g/mm ³	0.2348	lbm/in ³	SMA Modeling & Eng Applications (Lagoduas) pg 105 table 2.5				
Dimintions of Bushing									
Diameter - inner:	5.0571	mm	0.1991	in					
Diameter - outer:	7.1438	mm	0.2813	in					
Oveall length:	16.2408	mm	0.6394	in					
Head length:	3.2296	mm	0.1272	in					
Head Diameter - outer:	10.7950	mm	0.4250	in					
Volume:	490.8748	mm ³	0.0300	in ³					
Case-hardended Steel Specific Density:	0.0078	g/mm ³	0.2801	lbm/in ³	Engineer's Edge				
					http://www.engineersedge.com/properties_of_metals.htm				
Equation Constants and Variables (needed for Minco white paper equations):									
SMA mass	0.437	g	0.0010	lbm					
Bushing mass	3.806	g	0.0084	lbm					
Total Mass to be heated:	4.243	g	0.0094	lbm	Power Requirements:				
SMA Specific Heat (Cp)	0.200	Cal/g*°C	0.125	BTU/lb*°F	Intrinsic Devices Inc.				
Bushing Specific Heat (Cp)	0.486	J/g*°C	0.116	BTU/lb*°F	Engineer's Edge				
Tf (C)	100.0	°C	212.0	°F	http://www.engineersedge.com/properties_of_metals.htm				
Ti (C)	18.7	°C	65.7	°F					
Ta (C)	18.7	°C	65.7	°F					
t (hrs)	0.017	hrs	60	sec					
Heater Coverage Area:	7.44	mm ²	0.293	in ²	Heater dimensions = .3125x.9375"				
SMA Thermal Conductivity	0.867	BTU*in/ft ² /F/hr			10.4 BTU/hr*ft*°F Intrinsic Devices Inc.				
Bushing Thermal Conductivity	1.750	BTU*in/ft ² /F/hr			21.0 BTU/hr*ft*°F The engineering toolbox				
Length of Loss Conductive Path					http://www.engineeringtoolbox.com/thermal-conductivity-metals-d_858.html				
(Polythermide insulation washer)	1.00	mm	0.039	in	1 Btu/(hr *°F ft ² /ft) = 1 Btu/(hr *°F ft) = 1.731 W/(m *°K) = 1.488 kcal/(h m *°C)				
Emissivity of Bushing	0.700								
Tf (absolute)	672.000	R							
Ta (absoute)	525.660	R							
Conductive Loss Area Bushing	0.0797	in ²	0.00055	ft ²	Contact area to Polythermide = Circumfrence under brim of bushing				
Conductive Loss Area SMA	0.0134	in ²	0.00009	ft ²	Contact area to retaining bolt = Top of SMA cylinder				
Radiative Loss Surface Area	0.9061	in ²	0.00629	ft ²	Total surface area of bushing				
T_avg	138.83	°F			Red Text Denotes Laboratory Environment with Convection				
Convection Factor H	2.195137								
Power Required Estimate:									
Heater Power Minimum (No Loss) Thermo Calc:		3.009	Watts		P_heater = m_total*Cp*(Tf-Ti)/3.412t				
+ 20% estimated heat losses =		3.610	Watts		Initial Estimate!				
Power Required Detailed Calculations:									
Steady State Heat Losses:									
Conduction Loss (P_cd) =	1.056	Watts	Bushing	See Minco White Paper for Formula					
	0.876	Watts	SMA	See Minco White Paper for Formula					
Radiation Loss =	0.282	Watts	Bushing	See Minco White Paper for Formula					
Convection Losses =	0.575	Watts		See Minco White Paper for Formula					
Steady State Loss (Lab) =	2.789	Watts							
Warmup Power Calculations:									
Warmup Coefficient:	0.01906			Hw = Steady State Loss/(Tf-Ta)					
Warmup Power:	4.515	Watts		See Minco White Paper for Formula					
Total Power Required (Lab) =	7.303	Watts		Steady State Losses + Warmup Power					
+ 10% =	8.034	Watts		10% Margin					
Required Power Calculations (LAB):									
Supplied Bus Voltage	12.00	10.00	7.00	Volts					
EDU Foil Heater Resistance	12.6	12.6	12.6	Ohms					
Amperage	0.952	0.794	0.556	Amps	i = V/R				
Available Power	11.429	7.937	3.889	Watts	P = V ² /R				
Total Power Required for HTR	8.034	Watts			As calculated from above				
	0.70	1.01	2.07	min	Power Required/Available Power				
Time required by foil Heater Type	42	61	124	sec					

THIS PAGE INTENTIONALLY LEFT BLANK

LIST OF REFERENCES

- [1] D. C. Lagoudas, Ed., Department of Aerospace Engineering Texas A&M, *Shape Memory Alloys Modeling and Engineering Applications*. Springer Science + Business Media, LLC 2008.
- [2] T. W. Duerig, *Engineering Aspects of Shape Memory Alloys*. Contributors: K. N. Melton, D. Stockel, C. M. Wayman. Published by Butterworth-Heinemann, 1990.
- [3] T. Borden, “Shape-memory alloys: forming a tight fit,” *Mechanical Engineering*, October 1991, vol. 113, no. 10; with additional consultation from author at Intrinsic Devices, San Francisco, CA, 2009.
- [4] B. J. Hamrock, S. R. Schmid, and B. O. Jacobson, *Fundamentals of Machine Elements* (2nd ed.), New York: McGraw Hill, 1999.
- [5] T. A. Philpot, *Mechanics of Materials*. Hoboken: John Wiley and Sons, 2008.
- [6] K. Bramble, “Press fit engineering design equations and calculator,” Engineer's Edge, Copyright 2000 - 2010, by Engineers Edge, LLC.
<http://www.engineersedge.com/calculators/machine-design/press-fit/press-fit-equations.htm>.
- [7] S. Chatterjee and G. P. Carman, “High friction interface with pseudoelastic NiTi,” *Journal of Applied Physics Letters*, no. 91, 024104 (2007).
- [8] M. Abedini, H. M. Ghasemi, and M. N. Ahmadabadi, “Tribological behavior of NiTi alloy in martensitic and austenitic states,” *Journal of Materials and Design*, vol. 30, no. 4493–4497, 2009.
- [9] R. Liu and D. Y. Li, “Experimental studies on tribological properties of pseudoelastic NiTi alloy with comparison to stainless steel 304,” *Metallurgical and Materials Transactions*, vol. 31A, no. 2773, Nov. 2000.
- [10] J. D. Booker and C. E. Truman, “A statistical study of the coefficient of friction under different loading regimes,” *Journal of Applied Physics*, no.41 (174003), 2008.
- [11] T. Borden (private consultation), Intrinsic Devices Inc., San Francisco, CA, 2009.

- [12] Intrinsic Devices Inc., *Material Properties Product Document*; San Francisco, CA, <http://www.intrinsicdevices.com>.
- [13] M. Palmer, "Propagation of uncertainty through mathematical operations," in Massachusetts Institute of Technology Web Modules. http://web.mit.edu/fluids-modules/www/exper_techniques/2.Propagation_of_Uncertaint.pdf.
- [14] W. M. Crane, P. M. Oppenheimer, M. Romano, and J. H. Newman, "Micro-coupling active release mechanism," United States Patent and Trade Office, Patent Pending 12/878,760, Sep. 09, 2010.
- [15] MINCO Inc. "*Estimating power requirements of etched-foil heaters*," white paper, 2008, <http://www.minco.com>.
- [16] National Aeronautics and Space Administration, "Design criteria for controlling stress corrosion cracking," *MSFC-SPEC-522B*, Jul. 1987.
- [17] C. Melone, "Preliminary design, simulation, and test of the electrical power subsystem of the TINYScope nano-satellite," M.S. thesis, Naval Postgraduate School, 2009.

INITIAL DISTRIBUTION LIST

1. Defense Technical Information Center
Ft. Belvoir, Virginia
2. Dudley Knox Library
Naval Postgraduate School
Monterey, California
3. Naval Research Laboratory
SW Washington, DC
4. Air Force Research Laboratory
Space Vehicles Directorate
Kirtland Air Force Base, New Mexico
5. Professor Marcello Romano
Naval Postgraduate School
Monterey, California
6. Professor James Newman
Naval Postgraduate School
Monterey, California
7. Mr. Paul Oppenheimer
Naval Research Laboratory
SW Washington, DC